UNIVERSITÀ DEGLI STUDI DI TRIESTE

XXXIII CICLO DEL DOTTORATO DI RICERCA IN

SCIENZE DELLA RIPRODUZIONE E DELLO SVILUPPO

Hidradenitis suppurativa: identification of the main cellular and molecular pathways involved in immune and cutaneous cell biology.

Settore scientifico-disciplinare: MED/05

DOTTORANDA
Rossella Gratton

COORDINATORE
PROF. Paolo Gasparini

SUPERVISORE DI TESI
PROF. Sergio Crovella

ANNO ACCADEMICO 2019/2020

UNIVERSITÀ DEGLI STUDI DI TRIESTE

XXXIII CICLO DEL DOTTORATO DI RICERCA IN

SCIENZE DELLA RIPRODUZIONE E DELLO SVILUPPO

Hidradenitis suppurativa: identification of the main cellular and molecular pathways involved in immune and cutaneous cell biology.

Settore scientifico-disciplinare: MED/05

DOTTORANDA
Rossella Gratton

COORDINATORE
PROF. Paolo Gasparini

SUPERVISORE DI TESI
PROF. Sergio Crovella

ANNO ACCADEMICO 2019/2020

RIASSUNTO

L'idrosadenite suppurativa (HS) è una patologia infiammatoria cutanea altamente debilitante caratterizzata dalla presenza di lesioni profonde, ascessi, noduli infiammati, lesioni purulente e cicatrici nelle regioni inverse del corpo ricche di ghiandole apocrine.

La patogenesi dell'HS è complessa e multifattoriale e in essa è stata identificata una stretta interazione tra fattori genetici, immunologici, infettivi e ormonali, sebbene i meccanismi molecolari alla base di questi fenomeni non sono stati ancora completamente caratterizzati.

Un ulteriore livello di complessità è dato dal fatto che comunemente l'HS può manifestarsi anche in combinazione con altre comorbidità che coinvolgono più apparati dando luogo a varianti sindromiche in cui l'HS rappresenta un segno distintivo.

Nonostante siano state di recente identificate delle varianti genetiche possibilmente associate alla patogenesi di tali condizioni cutanee, la diagnosi di questi disordini è ancora esclusivamente basata su osservazioni cliniche poiché spesso i casi non condividono le stesse mutazioni e comunemente le mutazioni identificate non sono informative dei processi biologici che risultano essere alterati nei pazienti. Tenendo conto di questi aspetti, nell'affrontare patologie complesse che presentano un'eziologia genetica altamente eterogenea, studi genetici e genomici basati su famiglie supportati da saggi funzionali, costituiscono uno strumento necessario e rilevante per identificare nuovi meccanismi patogenetici potenzialmente coinvolti nell'insorgenza, nella progressione e nella gravità delle patologie in analisi. Lo scopo di questo lavoro, infatti, è stato quello di aumentare le conoscenze relative all'eziopatogenesi dell'HS e di una sua variante sindromica, la sindrome PASH, che presenta un coinvolgimento sia cutaneo che articolare ed è caratterizzata dalla manifestazione contemporanea di pioderma gangrenoso, acne e HS. A tal fine sono stati eseguiti studi su famiglie per identificare varianti genetiche e descriverne l'impatto sul fenotipo HS e PASH. Per questi studi sono state reclutate e sottoposte ad analisi genetiche due famiglie affette da una forma familiare di HS (una famiglia sarda e una friulana) e una famiglia con un paziente PASH. In ciascuna famiglia sono state identificate mutazioni private che sono state ulteriormente caratterizzate sia *in silico* che *in vitro*. In aggiunta, i risultati ottenuti dai saggi funzionali costituiscono un importante punto di partenza per lo sviluppo di trattamenti personalizzati che possono essere somministrati a gruppi selezionati di pazienti che presentano una specifica mutazione.

Nella famiglia sarda una rara variante missenso (MAF<0.01) (rs767801219; g. 43322952T>A; NM_014345:exon4:c.A2120T; p.K707I) è stata rilevata nell'esone 4 del gene *ZNF318* in 17

membri della famiglia. Tra questi sono presenti tutti gli 11 individui che hanno dichiarato di essere affetti da HS all'inizio dello studio. La possibilità che questa variante giochi un ruolo cruciale nello sviluppo della malattia non è inficiata dalla presenza degli altri 6 soggetti della famiglia che possiedono la variante e che hanno riportato di essere sani, infatti il tratto genetico presenta un *pattern* di ereditarietà autosomica dominante con penetranza incompleta, alcuni membri adulti mutati potrebbero aver deliberatamente nascosto di essere affetti dall'HS a causa del forte senso di vergogna e di disagio che spesso porta i pazienti a rifiutare la malattia, in alcuni casi la mancata segnalazione potrebbe essere associata a diagnosi errate e alcuni membri hanno da poco raggiunto la pubertà e potrebbero non aver ancora manifestato l'HS. Predire gli effetti della variante identificata è estremamente complesso: essa è rara e non è mai stata precedentemente correlata a nessuna malattia, inoltre ZNF318 non è mai stata cristallizzata e non è dunque possibile prevedere l'impatto della variante sulla struttura della proteina. Nonostante ciò abbiamo proposto un possibile ruolo causativo della variante nel fenotipo HS della famiglia: è possibile che la variante missenso comprometta l'attività di co-repressore di ZNF318 sul recettore degli androgeni (AR) causando lo sviluppo di una risposta potenziata, continua e deregolata a questi ormoni. Questo evento si potrebbe trovare alla base di alterazioni che si ripercuotono sulla funzionalità delle ghiandole sebacee e nel processo della sebogenesi, nella progressione del ciclo vitale del capello, nella guarigione delle ferite, nella costituzione di una barriera cutanea integra e funzionale e nelle eccessive risposte infiammatorie indotte da un'up-regolazione AR-dipendente del TNF-α. Nel loro complesso, i risultati ottenuti hanno ulteriormente evidenziato l'impatto cruciale degli ormoni nella patogenesi dell'HS e hanno permesso di ipotizzare che i membri affetti, in particolare le donne, potrebbero beneficare dalla somministrazione di terapie ormonali anti-androgeniche.

Nel caso di una famiglia friulana affetta da HS, è stata identificata una rara (MAF<0.01) variante frameshift (rs538180888; g.54645236_54645237insT; NM_053283.4:c.225dup; NP_444513.1:p.Ala76Fs) nell'esone 4 del gene *DCD* negli individui manifestanti la patologia. *DCD* codifica per la dermicidina (DCD), un peptide antimicrobico (AMP) noto per espletare efficaci attività antimicrobiche contro batteri Gram-positivi e Gram-negativi, e contro *Candida albicans*. Esperimenti *in silico* hanno permesso di evidenziare che la variante rende la struttura del peptide mutato più rigida, meno stabile e meno compatta, e che conferisce all'AMP una carica netta positiva. Da ciò si è ipotizzato che le alterazioni strutturali e di carica possano indurre una perdita della natura anfipatica di DCD, condizione che è stata vista essere necessaria per lo svolgimento del meccanismo d'azione di antimicrobicità del peptide. La nostra ipotesi è stata confermata dal fatto che la forma mutata di DCD non è in grado né di espletare la sua funzione battericida contro *S. aureus*, *S. epidermidis* e *S. lugdunensis*, né di limitare la formazione di biofilm di *S. aureus*, né di

eradicare biofilm preformato di *S. aureus*. Considerando che i malati della famiglia hanno riportato di essere spesso soggetti a lesioni ricorrenti e suppurative nelle zone inguinali e ascellari, la variante frameshift nel gene *DCD* potrebbe, almeno parzialmente, giustificare la maggiore suscettibilità alle infezioni osservata nei casi. La caratterizzazione degli effetti della variante nei membri della famiglia potrebbe porre le basi per lo sviluppo di opzioni terapeutiche personalizzate rappresentate per esempio dalla supplementazione e dall'attivazione di AMP naturali, specificatamente di DCD, grazie allo sviluppo di sistemi avanzati di *drug delivery* topici.
Nel caso del paziente PASH, è stata identificata una variante missenso (rs17604693; g.7565494 A>T; c.913A>T; p.Ile305Phe) in eterozigosi nell'esone 7 del gene *DSP*, codificante la desmoplachina (DSP) che è una componente cruciale dei desmosomi. Saggi *in silico* hanno confermato che la variante rende i dimeri DSP più compatti e stabili, mentre studi *ex vivo* e *in vitro* hanno evidenziato che la variante missenso può danneggiare il reclutamento di DSP verso il desmosoma favorendo quindi una distribuzione citosolica della desmoplachina, alterare la struttura generale del desmosoma che appare più allungato e flesso, mentre non sembra avere un effetto sulla proliferazione e il differenziamento cellulare. In aggiunta, nel paziente PASH sono stati rilevati elevati livelli di perdita di acqua transepidermica (TEWL) rispetto ad un controllo sano. Questi risultati suggeriscono che la variante studiata possa causare una perdita della funzione di barriera della cute piuttosto che essere associata a difetti di cheratinizzazione e di proliferazione.

Nel contesto di disordini complessi con una eziologia genetica eterogenea, il nostro studio evidenzia la primaria importanza di effettuare studi genetici e genomici basati su famiglie, ulteriormente implementati da saggi funzionali, con lo scopo di identificare potenziali nuovi geni e vie cellulari coinvolte nella patogenesi di HS e della sindrome PASH. Abbiamo confermato che nel contesto di queste malattie la valutazione di potenziali alterazioni a livello ormonale, un'aumentata suscettibilità alle infezioni batteriche e della barriera cutanea, costituiscono meccanismi altamente patogenetici che dovrebbero essere inizialmente vagliati e descritti. In aggiunta, il vantaggio diretto derivante dallo studio di varianti genetiche private, che sono cioè ristrette solo a certe famiglie, danno la possibilità di proporre e sviluppare interventi terapeutici personalizzati che possano essere somministrati a gruppi di pazienti che portano specifiche mutazioni.

Questo lavoro di tesi è stato svolto presso il laboratorio di Genetica Immunologica dell'IRCCS Burlo Garofolo di Trieste.

ABSTRACT

Hidradenitis suppurativa (HS) is a highly debilitating inflammatory skin disease presenting deep-seated lesions, abscesses, inflamed nodules, pus-discharging tunnels and scars, typically occurring in intertriginous apocrine gland-bearing regions.

The pathogenesis of HS is complex and multifactorial in which a strict interplay between genetic, immunologic, infectious and hormonal factors have been identified, though the precise molecular mechanisms underlying these aspects have not yet been fully characterised.

A further level of complexity is given by the fact that commonly HS may also occur in combination with other comorbidities involving multiple organ systems, that give rise to syndromic variants in which HS represents a distinctive hallmark.

In spite of recently identified genetic variants potentially underlying the pathogenesis of these skin diseases, the diagnosis of these disorders is still based on clinical observations due to the fact that most patients do not share the same mutations and since commonly mutations themselves are not informative of the biological pathways that result to be disrupted in cases. So said, while dealing with these complex disorders in which the genetic aetiology is highly heterogeneous, the assessment of family-based genetic and genomic studies, further supported by functional assays, appears as a necessary and powerful tool for the identification of novel pathogenic mechanisms potentially involved in the onset, progression and severity of disorders. Indeed, the aim of this work was to augment the knowledge of the etiopathogenesis of HS and of a syndromic variants of HS manifesting a cutaneous and articular involvement given by the simultaneous occurrence of pyoderma gangrenosum, acne and HS, namely PASH syndrome, by performing family-based studies aimed at retrieving genetic changes and in defining their possible impact in HS and PASH phenotype for each tested family. To this aim, two families presenting a familiar form of HS (a Sardinian and a Friulian family) and one family with one PASH patient were recruited and subjected to genetic analysis. These assays allowed the identification of private variants in each family that were further characterised *in silico* and *in vitro*. In addition, results obtained in the functional studies critically constitute a crucial starting point for the development of tailored and personalised treatments to be administered successfully to selected patients carrying specific mutations.

In the case of the Sardinian family affected by HS, a rare (MAF<0.01) variant in heterozygosis (rs767801219; g. 43322952T>A; NM_014345:exon4:c.A2120T; p.K707I) was retrieved in exon 4

of *ZNF318* gene in 17 family members comprising all of the 11 individuals who initially declared to be affected by HS and in additional 6 family members that haven't mentioned to possess any sign of the disease. The fact that the variant was also detected in individuals who declared not be affected by HS does not deny the possible causality of the identified SNV in the family; indeed, the trait presents an autosomal dominant inheritance pattern with incomplete penetrance, some adult mutated family members might have deliberately confirmed not to possess the disease because of the sense of shame and discomfort that commonly lead patients to reject HS, in some cases a failure to report the disease is possibly associated to misdiagnosis, and some family members have only just passed puberty, suggesting that they haven't manifested HS yet. Even if predicting the effects of the identified SNV is extremely hard since the variant is rare, few references are available, it has never been previously correlated to any disease and it is not currently possible to predict its impact on protein structure, due to the fact that ZNF318 has never been crystallised, we have proposed a possible causative role of the SNV in HS phenotype. It is possible that the variant might impair the co-repressor activity of ZNF318 that causes in turn an androgen receptor (AR)-mediated enhanced, continuous and deregulated response to circulating androgens. This event might stand at the basis of alterations occurring in sebaceous glands and sebogenesis, progression of the hair cycle, wound healing, skin barrier function and to an abnormal inflammatory responses driven by an AR-dependent up-regulation of TNF-α. Collectively, obtained results further corroborated the crucial impact of hormonal influence in the pathogenesis of HS and allowed to speculate that affected family members, especially females, might benefit from the administration of anti-androgenic hormonal therapies.

In the case of a Friulian family affected by HS, a rare (MAF<0.01) frameshift insertion (rs538180888; g.54645236_54645237insT; NM_053283.4:c.225dup; NP_444513.1:p.Ala76Fs) occurring on exon 4 of *DCD* gene in affected family members was identified. This gene encodes for dermcidin (DCD), an antimicrobial peptide (AMP) known to exert well defined antimicrobial activities against both Gram-positive and Gram-negative bacteria, as well as against *Candida albicans*. *In silico* studies revealed that the identified variant renders the mutated peptide more rigid, less stable and less compact in structure, and confers to the AMP an overall positive net charge. We have hypothesised that the resulting structural and charge changes detected in the mutated peptide might directly impact its antimicrobial activity due the loss of the amphiphilic nature of DCD, condition seen to be crucial for the antimicrobial mechanism of action of the AMP. Our hypothesis was confirmed by the fact that mutated DCD is not able to exert a bactericidal effect neither on planktonic *S. aureus*, *S. epidermidis* and *S. lugdunensis*, nor is able to limit biofilm formation or to eradicate pre-formed biofilm by *S. aureus*. Bearing in mind that affected cases lamented the

development of recurrent suppurating lesions predominantly in the inguinal and axillary regions, the frameshift variant in *DCD* might, at least partially, explain the major susceptibility to bacterial infections observed in cases. The characterisation of the effect of the identified variant in family members might lay the foundation for the development of personalized treatment options given for instance by the supplementation and activation of natural AMPs, specifically of DCD, by developing advanced topical drug delivery systems.
In the case of a PASH patient, a missense exonic variant (rs17604693; g.7565494 A>T; c.913A>T; p.Ile305Phe) was identified in homozygosis in exon 7 of *DSP* gene, encoding for desmoplakin (DSP) defined as a crucial component of desmosomes. *In silico* assays confirmed that the SNV renders DSP dimers more compact and stable, while *ex vivo* and *in vitro* studies highlighted that the missense variation might potentially impair the recruitment of DSP on membrane-bound desmosomal structures hence favouring a cytoplasmic distribution, alter the general structure of desmosomes that appear as majorly stretched out and flexed, but seems not to impact cellular proliferation and differentiation. Additionally, in the PASH case elevated levels of transepidermal water loss (TEWL) were registered when compared to healthy controls. Collectively these results possibly indicate that the identified *DSP* SNV is potentially associated to a disruption in skin barrier function rather than being linked to keratinisation or proliferation defects.

In the context of complex disorders presenting a heterogeneous genetic aetiology, our study highlights the crucial importance in performing family-based genetic and genomic studies, further implemented by functional assays, aimed of identifying potential novel genes and cellular routes involved in the pathogenesis of HS and PASH syndrome. We have confirmed that, while dealing with these disorders, the evaluation of potential disruptions in hormonal imbalance, an augmented susceptibility to bacterial infections and skin barrier function, constitute highly pathogenic mechanisms that need to be initially addressed and further envisaged. Moreover, the direct advantage deriving from the study of a genetic variant that is private and therefore restricted only to certain families, lies in the possibility to propose and develop tailored therapeutic interventions to be applied to clusters of patients carrying specific mutations.

This PhD dissertation has been conducted in the immunology genetics laboratories of the IRCCS Burlo Garofolo of Trieste.

INDEX

1. **INTRODUCTION**
1.1 Hidradenits Suppurativa 1
1.2 Diagnosis and staging of Hidradenitis Suppurativa 2
1.3 Phenotypic classification of patients affected by Hidradenitis Suppurativa. 4
1.4 Skin 5
1.4.1 Epidermis. 5
1.4.2 The pilosebaceous unit. 9
1.5 Pathogenesis of Hidradenitis Suppurativa 12
1.5.1 Genetics 13
1.5.2 Aberrant immune responses. 22
1.5.3 Hormonal influence 26
1.5.4 Bacterial infections. 27
1.5.5 Environmental risk factors 29
1.6 Syndromic variants of Hidradenitis Suppurativa 29
1.6.1 PASH syndrome 30
1.6.2 PAPASH, PsAPASH and PASS syndromes 33
1.7 Therapy 33
2. **AIM**. 36
3. **MATERIALS AND METHODS**
Part 1: the case of a PASH patients
3.1 Patients. 40
3.2 Genetic tests 40
3.2.1 Genomic DNA extraction from saliva. 40
3.2.2 Whole exome sequencing (WES) and data analysis. 40
3.2.3 Sanger sequencing for the confirmation of the selected variants identified by WES. . . 43
3.3 *In silico* studies 43
3.3 Molecular dynamics for the evaluation of *DSP* SNV on protein structure and stability. . 43
3.4 Skin features of the PASH patient 44
3.4.1 Immunohistochemistry (IHC) 44
3.4.2 Transmission Electron Microscopy (TEM) 45
3.4.3 Transepidermal water loss (TWEL) 46
3.5 *In vitro* assays. 46
3.5.1 Cell culture. 46
3.5.2 Genome editing of *DSP* gene with CRISPR-Cas9 technology. 47
3.5.3 Western Blot. 54

3.5.4 RNA isolation and semi-quantitative real-Time PCR. 54
3.5.5 Immunocytochemistry (ICC) for the detection of hyper-adhesive desmosomes. 55
3.5.6 Transmission Electron Microscopy (TEM) 56
3.5.7 Proliferation assay. 57
3.6 Statistical analysis. . . . . .. .57
Part 2: the case of a Sardinian family
3.7 Patients. 58
3.8 Genetic tests 60
3.8.1 Genomic DNA extraction from saliva. 60
3.8.2 Sanger sequencing for the identification of mutations in *NCSTN*, *PSENEN* and *PSEN-1* ……..60
3.8.3 Whole exome sequencing (WES) and data analysis. 61
3.8.4 Sanger sequencing for the screening of selected variants identified by WES. 61
3.9 *In vitro* assays. 63
3.9.1 Cell culture. 63
3.9.2 Genome editing of *ZNF318* with CRISPR-Cas9 technology. 63
3.9.3 Western Blot. 64
3.9.4 RNA isolation and semi-quantitative real-Time PCR. 64
3.10 Statistical analysis. 65
Part 3: the case of a Friulian family
3.11 Patients. 65
3.12 Genetic tests. 66
3.12.1 Genomic DNA extraction from saliva. 66
3.12.2 Whole exome sequencing (WES) and data analysis. 66
3.12.3 Sanger sequencing for the confirmation of the selected variants identified by WES. . 66
3.13 *In silico* studies. 67
3.13.1 Comparative modeling. 67
3.13.2 Molecular dynamics. 68
3.13.3 Principal component analysis (PCA) 68
3.14 *In vitro* antimicrobial studies. 69
3.14.1 Peptides. 69
3.14.2 Bacterial strains and culture conditions. 69
3.14.3 *In vitro* activity of DCD peptides against planktonic bacteria. 70
3.14.4 *In vitro* activity of DCD peptides against biofilm formation. 70
3.14.5 *In vitro* activity of DCD peptides against pre-formed biofilm. 71
3.15 Statistical analysis. 71

4. **RISULTS AND DISCUSSION**

Part 1: the case of the PASH patient

4.1 Identification of a missense exonic variant in *DSP* gene in a PASH patient. 73

4.2 *In silico* studies: *DSP* (rs17604693) increases protein stability and compaction. 79

4.3 Generation of *DSP* clones using CRISPR-Cas9 and ssODN-mediated genome editing. . . .83

4.4 Intracellular distribution of DSP. 85

4.5 Desmosome morphology. 89

4.6 Differentiation and proliferation of keratinocytes. 93

4.7 Barrier function of the skin and TEWL. 97

Part 2: the case of the Sardinian family

4.8 Identification of a missense exonic variant in *ZNF318* gene in the affected family members 104

4.9 Generation of *ZNF318* knock-in clones using CRISPR-Cas9 and ssODN-mediated genome editing. 117

4.10 ZNF318 protein levels and *ZNF318*gene expression levels . . .. .118

Part 3: the case of the Friulian family

4.11 Identification of a missense exonic variant in *DCD* gene in affected family members. . 120

4.12 *In silico* studies: Comparative modeling for the prediction of the 3D structure of DCD mutant peptide. 126

4.13 *In silico* studies: DCD (rs538180888) decreases the peptide's stability and compaction, and increases its rigidity. 128

4.14 Principal component analysis. 130

4.15 *In vitro* growth inhibition of planktonic bacterial cells by DCD AMPs. 131

4.16 *In vitro* activity of DCD against biofilm formation and eradication. 133

5. **CONCLUSION**. 138

6. **BIBLIOGRAPHY**. 142

INTRODUCTION

1.1 Hidradenits Suppurativa

Hidradenitis Suppurativa (OMIM#142690; HS), also known as acne inversa, is a recurrent, chronic, debilitating and inflammatory follicular occlusive disorder affecting the epidermis and the dermis (Vossen et al., 2018). HS patients possess a heterogeneous phenotype and clinical manifestations include painful and deep-seated lesions, abscesses, inflamed nodules, pus-discharging tunnels and scars, which typically occur in intertriginous apocrine gland-bearing regions such as the axillae, the inguinal and ano-genital regions, the perineum and the infra-mammary folds in female patients (Sabat et al., 2020; Napolitano et al., 2017).

The prevalence of HS is estimated to range between 0.05-4% in Europe, shows a female predominance with a female-to-male ratio of 3:1 (Deckers et al., 2014) and one-third of HS patients possess a positive family history (Elkin et al. 2020). HS generally occurs after puberty, during the second or third decade of life, although prepubertal infants and post-menopausal women presenting a novel-onset of the disease have also been reported in literature (Seyed Jafari et al., 2020; Seyed Jafari et al., 2018).

The diagnosis of HS is still problematic primarily due to the absence of specific pathognomonic tests and to many possible differential diagnoses with other skin diseases possessing similar clinical manifestations (Lindhardt Saunte and Jemec, 2017). As a consequence, patients bear an improper management of the disease that ultimately results in the development of recurrent lesions, secondary infections and chronic pain that have a huge negative impact on the patient's quality of life (Elkin et al., 2020; Lindhardt Saunte and Jemec, 2017). Indeed, although the skin is the primary affected site, HS is known to lead to the emergence of severe psychological and physiological complications. Psychological comorbidities, including depression and anxiety, have been seen to be common amongst HS cases and generally stem from chronic pain, movement limitations and malodour due to purulent secretions (Elkin et al., 2020; Sabat et al., 2020; Vossen et al., 2018). Moreover, HS patients are frequently affected by other health conditions such as metabolic syndromes, androgen dysfunction and auto-inflammatory disorders (Frew et al., 2019). These aspects strongly suggest the existence of a connection between the disease, metabolic and hormonal issues, and inflammatory pathways, therefore indicating that a deep characterisation of the mechanisms underlying these

complex cross-talks is of pivotal importance in order to successfully monitor the onset, progression and severity of the disease.

HS patients are not subjected to a standard therapy and therapeutic interventions are strongly influenced by the severity of the disease. Furthermore, even if HS is classified as an inflammatory disorder, the majority of the patients don't respond to non-steroidal anti-inflammatory drugs (NSAIDs), suggesting that there is the necessity to counteract different responses other than the sole inflammatory phenotype (Ingram et al., 2015).

1.2 Diagnosis and staging of Hidradenitis Suppurativa

The diagnosis of HS is still very critical due to the presence of multiple differential diagnoses with other common skin disorders that possess extremely similar phenotypic features if compared to those exhibited by HS cases (Lindhardt Saunte and Jemec, 2017).

Specifically, in the daily clinical practice HS might be misdiagnosed with the following skin diseases (Lindhardt Saunte and Jemec, 2017):

- Acne: also defined as an inflammatory dermatological disorder centred on hair follicles, characterised by the presence of open or closed comedones, inflamed lesions, suppurating cysts and scars, which however present a differential distribution (upper torso and face) if compared to the typically affected body areas in HS (Pink et al., 2018);
- Cutaneous Crohn's disease: an extension of inflammatory bowel disease (IBD), showing perianal and inguinal abscesses, tunnels and scars (van der Zee et al., 2016);
- Pilonidal sinus disease: inflammatory dermatosis exhibiting genital and intergluteal abscesses, sinus tracts, and painful and inflamed lesions (Frew and Navrazhina, 2019; Benhadou et al., 2019);
- Granuloma inguinale: ulcers and granulations of tissue in the genital and inguinal folds caused by *Klebsiella granulomatis* infectious agent (Lindhardt Saunte and Jemec, 2017);
- Cutaneous tuberculosis: caused by a chronic infection by *Mycobacterium tuberculosis* that leads to the development of abscesses, purulent drainage and fistulas (Dos Santos et al., 2014);
- Follicular pyoderma: given by an infection of the follicular ostium by *Staphylococcus aureus* resulting in nodules, abscesses and purulent skin lesions occurring on the scalp, face, limb and also at inverse body sites (Edlich et al., 2005);
- Actinomycosis: rare chronic condition caused by *Actinomyces* spp. characterised by fistulas, sinus tracts and abscesses in the mouth, gastrointestinal tract, lungs and breasts (Valour et al., 2014);

- Lymphogranuloma venereum: ulcerative disease of the inguinal and genital folds caused by infections by *Chlamydia trachomatis* (Rawla et al., 2020);
- Steatocystoma multiplex: follicular tumours possessing inflamed draining nodules (Lindhardt Saunte and Jemec, 2017);
- Metastasis: given by inflamed nodules (Lindhardt Saunte and Jemec, 2017).

Only if physicians are sure to exclude their presence, HS can be considered as a possible diagnosis.

Moreover, due to the absence of pathognomonic tests, a key necessity is to dispose of fixed and well-defined diagnostic criteria. To date, patients strictly need to fulfil all the features listed in the following 3 criteria based on clinical observations (Vekic et al., 2018):

1. presence of typical lesions: deep-seated painful nodules, abscesses, tunnels (sinus tracts and fistulas), scars;
2. localisation of lesions in specific body areas: typical lesions must occur in one or more of the predilection areas such as the axillae, the inguinal and ano-genital regions, the perineum and the infra-mammary folds in female patients;
3. relapsing and chronicity of lesions: chronicity is a relevant aspect. Lesions should present at least two recurrences within 6 months or be persistent and/or chronic for more than 3 months (Lindhardt Saunte and Jemec, 2017).

It is crucial to recall that on average HS cases experience a 7.2 years delay between the initial presentation of symptoms and the final establishment of the diagnosis (Saunte et al., 2015). In this critical context, the assessment of robust diagnostic guidelines seems to be promising in providing an early recognition of HS, thus promptly overcoming a series of limitations and unsolved issues that have for long affected patients and the clinics.

The severity of the disease can be evaluated using various scoring systems including: Hurley staging, used to stratify cases into three groups of increasing severity based on the evaluation of the presence of abscesses and the absence of sinus tracts (Hurley I), the presence of multiple abscesses and confirmation of sinus tract formation (Hurley II), and the existence of multiple abscesses, sinus tracts and scars affecting widespread skin partitions (Hurley III) (Wieczorek and Waleka, 2018); modified Sartorius score (MSS), takes into account the number, type and distance between lesions, the anatomical affected sites and the presence of normal skin (Sartorius et al., 2003); Physician Global Assessment (PGA), a six-stage scale commonly employed during clinical trials that allows an efficient follow-up of patients by evaluating the clinical improvement of abscesses, inflammatory nodules, and draining fistulas (Kimball et al., 2012); Hidradenitis Suppurativa

Clinical Response (HiSCR), is considered as a valuable tool to determine treatment effects and also to study inflammatory manifestations (Tzanetakou et al., 2016); Dermatology Life Quality Index (DLQI), usually achieved through self-compiled questionnaires that patients use to report the impact of HS on their quality of life by considering aspects such as the number of flares, the degree of pain and the impact of the disease in every day life (Finlay and Khan, 1994); International Hidradenitis Suppurativa Severity Score System (IHS4), most recent and dynamic approach that takes into account the degree of inflammation and the number of inflammatory lesions and of affected areas (Shanmugam et al., 2017; Zouboulis et al., 2017).

1.3 Phenotypic classification of patients affected by Hidradenitis Suppurativa

HS patients can be stratified into different groups in relation to the presence of comorbidities and to the type and localisation of lesions (van der Zeer and Jemec, 2015):

- Regular type: group encompassing the majority of HS cases that satisfy all the fixed diagnostic criteria;
- Frictional furuncle type: classification that comprehends regular type HS patients that are overweight and therefore prone to the development of abscesses and deep-seated nodules in body areas subjected to enhanced mechanical friction (buttocks, abdomen and thighs);
- Scarring folliculitis type: group comprehending regular type HS patients who are commonly smokers and overweight, manifesting in addition pustules, superficial nodules, cysts, cribriform scarring and double-ended comedones. Lesions are usually superficial, scarring is frequent and body areas including the pubic region, the buttocks and the groins are affected;
- Conglobata type: category that includes moderate and severe HS cases bearing a positive family history of the disease that are characterised by cysts and acne conglobata lesions primarily localised on the face and on the back;
- Ectopic type: group of HS patients showing phenotypic manifestations in unusual locations;
- Syndromic type: class of patients presenting the simultaneous manifestation of HS together with other pathologic conditions. In this context, it is possible to identify a spectrum of syndromes associated with HS including: PASH syndrome, given by the combination of **P**yoderma gangrenosum (PG), **A**cne (A) and **HS**; PsAPASH syndrome, deriving from the association between **Ps**oriatic **A**rthritis, **P**G, **A** and **HS**; PAPASH syndrome, defined by the concomitant manifestation of **P**G, **A**, **P**yogenic **A**rthritis and **HS**; PASS syndrome, given by the simultaneous diagnosis of **P**G, **A**, H**S** and Ankylosing **S**pondylitis.

While dealing with HS, a particular discussion must be dedicated to the skin, the primary affected site in HS.

1.4 Skin

The intricate structure of the skin encompasses a complex composition suitable for the accomplishment of diverse functions including: initial barrier against pathogens, mechanical injury, UV radiations and chemicals; regulation site of the amount of water released in the environment and of the temperature (Yousef et al., 2020).

The skin is partitioned in three layers (Gilaberte et al., 2016): the epidermis is the uppermost layer and is defined as a squamous stratified epithelium composed predominantly by keratinocytes and also by dendritic cells; the dermis is the middle layer bearing a matrix of amorphous connective tissue and collagen, a nervous and vascular network, resident fibroblasts, mast cells and macrophages; the hypoderm, the lowest level, is a subcutaneous vascularised tissue exerting an endocrine role and composed by lobules of adipocytes separated by collagen fibres.

The skin presents several appendages, defined as epidermal and dermal-derived structures, that possesse unique functional, histological and structural characteristics. Skin appendages include sweat glands, nails and the pilosebaceous unit (Yousef et al., 2020).

1.4.1 Epidermis

The epidermis is a multi-layered epithelium, comprising the interfollicular epidermis (IFE) and associated skin appendages including hair follicles, sebaceous glands and apocrine glands. The major functions of the epidermis encompass innate immunity activities through the constitution of a protective barrier against pathogens and other environmental noxae, the lubrication of the skin through lipid synthesis, the constitution of a barrier aimed at limiting transepidermal water loss, and thermoregulatory activities induced by the presence of hair and sweat (Watt, 2014).

The IFE is composed by both proliferating and progressively differentiating keratinocytes, organised in four layers that, from the deepest to most superficial one, are represented by the basal layer, spinous layer, granular layer and the stratum corneum (Gratton et al., 2020).

The basal layer is formed by a single sheet of proliferating cells that directly rest on the basement membrane and that are strictly involved in maintaining the homeostasis, integrity and functionality of the epidermis. Epidermal stem cells (ESCs) reside in the basal layer and are represented by mitotically active cells that at every division cycle either yield other stem stems that self-renew or

transient amplifying cells, progenitor cells that undergo progressive terminal differentiation through a process that is strictly driven and regulated by specific local signals, thus ultimately generating the IFE and the skins' appendages (Gratton et al., 2020; Gilaberte et al., 2016).

During terminal differentiation, transient amplifying cells stop proliferating, lose their ability to adhere to the basement membrane and progressively ascend upwards through the various layers of the epidermis towards the stratum corneum. During the migration, keratinocytes undergo an extensive remodelling of keratin intermediate filaments and begin the synthesis of other layer-specific markers, thus acquiring the characteristics of fully differentiated corneocytes through a process known as keratinization (Gilaberte et al., 2016).

Keratinocytes of the basal layer are mitotically active cells, distinguished by the presence of dispersed keratin intermediate filaments originated by the heteropolimerisation between the type I acidic cytokeratin (K) 5 and the type II basic K14 (Sanghvi-Shah and Weber, 2017).

The spinous layer is a 4-8 sheet of post-mitotic but metabolically active keratinocytes possessing a variable morphology ranging from polyhedral in the suprabasal region to flat in the upper partitions. In these cells, the K5 is substituted by the production of type I acidic K1 and K14 by the synthesis of type II basic K10, and these newly polimerised keratin intermediate filaments aggregate into thin bundles (Fuchs, 2008). Cells also start to produce precursors of the cornified envelope, such as involucrin, and express the transglutaminase enzyme that is responsible for the ε-(γ-glutamyl) lysine cross-linking of involucrin into the insoluble cornified envelope (Bikle, 2011).

An additional hallmark of the basal layer and the spinous layer are desmosomes, defined as highly specialised adhesive intercellular junctions tied to the keratin intermediate filament network, that convey resistance to mechanical stress, promote tissue integrity and strictly regulate differentiation and proliferation (Dubash and Green, 2011).

The granular layer is composed of flattened and still living cells that stop producing keratins and express abundant basophilic keratohyalin granules resulting from the accumulation of the newly synthesised profilaggrin and loricrin proteins. Cells also possess lamellar cytoplasmic bodies, vesicles containing free sterols, phospholipids, glycolipids, glycoproteins and acid hydrolases, that progressively fuse with the cell membrane hence releasing their content in the extracellular space where lipids contribute to the constitution of the permeability barrier of the skin (Gilaberte et al., 2016; Bikle, 2011).

As the cells progressively transit from the granular layer to the stratum corneum, organelles are destroyed and the final maturation of the cornified envelope occurs. Specifically, pro-filaggring is cleaved into its active moiety filaggrin, protein known to possess a strong binding affinity for keratin; indeed, filaggrin crosslinks keratin intermediate filaments causing their tight aggregation

into microfibrils organised in parallel arrays, that ultimately result in the formation of highly insoluble keratin (Gratton et al., 2020). Next, proteins such as involucrin and loricrin are covalently cross-linked by the transglutaminase. At this point corneocytes possess an insoluble and highly resistant cornified envelope that replaces the plasma membrane. Corneocytes are principally held together by the extracellular lipid matrix, and are gradually shed in the environment through the desquamation process (Bikle, 2011; Wikramanayake, 2014) (Figure 1).

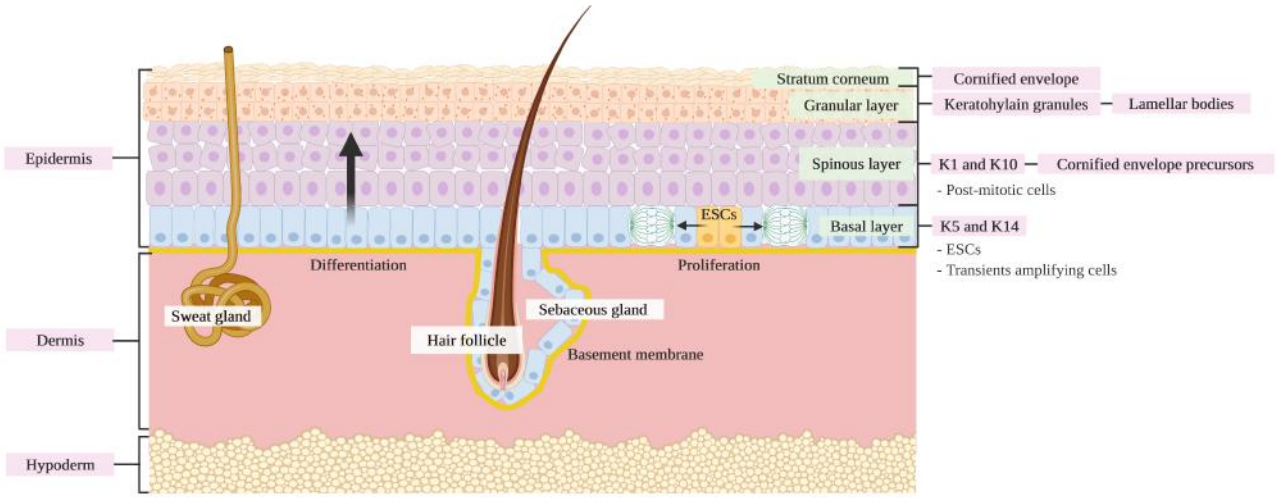

Figure 1. Schematic representation of the skin. The skin is composed of three layers: the epidermis, the dermis and the hypoderm. The epidermis, the uppermost portion, is a stratified squamous epithelium comprising the interfollicular epidermis (IFE) and associated skin appendages including hair follicles, sebaceous glands and apocrine glands. The IFE is formed by progressively differentiating keratinocytes organised in different layers in which cells possess specific markers of differentiation that, from the deepest to most superficial one, are given by: the basal layer, a single sheet of proliferating cells that directly rest on the basement membrane in which both epidermal stem cells and transient amplifying cells reside, the latter express high levels of cytokeratin (K14) and K10 and are committed to terminal differentiation; the spinous layer, multilayer of post-mitotic and metabolically active keratinocytes that express K1, K10 and precursors of the cornified envelope; granular layer, given by flattened but still living cells characterised by the accumulation of keratohyalin granules and lamellar bodies; stratum corneum, formed by corneocytes possessing an insoluble and highly resistant cornified envelope that replaces the plasma membrane.

The skin barrier functionally resides in the most superficial layer of the epidermis composed by the corneocytes of the stratum corneum that are interspersed in an abundant extracellular lipid matrix (van Smeden and Bouwstra, 2016). This layer possesses various barrier properties that comprise regulatory and defensive mechanism aimed at maintaining the cutaneous homeostasis through the constitution of (Berardesca et al., 2018; Del Rosso and Levin, 2011): epidermal permeability barrier, aimed at preventing an excessive epidermal water loss (TEWL), retention of moisture for enzymatic desquamation and providing selective permeability of exogenous and endogenous substances; immunity barrier, involved in the protection against numerous external stressors, hence

impeding the permeation of compounds from the environment into the viable epidermal and dermal layers thereby limiting the onset of immune responses; antioxidant barrier, counteracting damaging effects induced by reactive oxygen species; antimicrobial barrier, due to the presence of antimicrobial peptides in the sweat and sebum, and to lipid moieties expressed in croneocytes; photoprotection barrier, against UV radiations thanks to the photoprotective properties of molecules such as melanin.

Several parameters can be measured in order to assess the barrier function of the skin and include TEWL, stratum corneum hydration (SCH), skin surface pH, elasticity and temperature.
In particular, the maintenance of cutaneous hydration, gained by limiting the loss of water and electrolytes from the internal environment, is of crucial importance in order to strictly maintain the mechanical and physical properties of the skin, regulate drug penetration and desquamation (Berardesca et al., 2018).
The presence of a decreasing water gradient between the deeper dermal layers and the most superficial partitions of the epidermis, induce a passive diffusion of water from the inner layers to the stratum corneum (Merk, 2018), in which corneocytes possess the ability to retain water. Indeed, during the process of terminal differentiation these cells progressively acquire natural hygroscopic agents and are immersed into a multi-lamellar lipid matrix principally composed by cholesterol, cholesterol sulphate, free fatty acids and ceramides (Mojumdar et al., 2017). Specifically, in this layer water is bound both to the polar heads of the intercellular lipids, and inside corneocytes where water is efficiently ligated to the natural hygroscopic moisturising factor molecule originated from the breakdown of filaggrin during the process of terminal differentiation (Schleusener et al., 2021). In the stratum corneum, an appropriate water content seems to primarily affect the flexibility and the viscoelastic properties of the epidermis through the plasticization of keratin filaments by water, induce resistance to shearing forces, favour the desquamation of individual corenocytes, regulate the pH of the skin and promote the formation of the cornified envelope (Mojumdar et al., 2017; Del Rosso and Levin, 2011). In addition, adequate water levels are strictly required since different enzymes involved in the maintenance of the functional and structural integrity of the stratum corneum are hydrolytic and are not efficient when water is present below a threshold concentration (Del Rosso and Levin, 2011).
A common general characterisation of the skin barrier function *in vivo,* both in healthy and disease states, is the evaluation of TEWL through an indirect biophysical non-invasive approach based on the usage of open or closed chambers that measure the amount of unbound water that passively evaporates through the skin to the external environment due to water vapour pressure gradient on

both sides of the skin barrier (Rogiers and EEMCO Group, 2001; Schleusener et al., 2021). Notably, the accuracy of TEWL measurements can vary considerably according to different factors including age, sex, diurnal hour, season, climate, skin site, skin depth and body mass index (Das et al., 2009).

In healthy skin, increments in TEWL values induce signalling cascades that are directed at restoring the permeable capability of the stratum corneum, initially by rapidly incrementing the secretion of lipids that compose the multi-lamellar lipid matrix. In various inflammatory skin diseases, including psoriasis, atopic dermatitis and other eczematous dermatitis, different studies confirmed the presence of an incremented TEWL accompanied by a low water content of lesional-skin and to a reduced lipid content that collectively leads to a defective water retention capacity of the stratum corneum (Montero-Vilchez et al., 2021; Qingyang et al., 2019). In this context, when TEWL becomes deregulated and exceeds the ability to restore the permeability function of the stratum corneum, the degradation of corneodesmosomes by hydrolytic enzymes is impaired and results in the shedding in clumps of corneocytes, event that causes the skin to acquire the features of xerotic skin, and also elicit a progressive damage of protein and lipid components of the stratum corneum. The maintenance of xerotic changes progressively lead to the development of inflammatory responses driven by cytokine release, that are commonly associated to the development of erythema and pruritus. Moreover, another possible response to a prolonged disruption of the permeability barrier is epidermal hyperplasia, typically associated to the formation of hyperkeratotic eczema (Del Rosso and Levin, 2011).

1.4.2 The pilosebaceous unit

The pilosebaceous unit is a dynamic structure distributed all over the skin, showing the highest levels of diffusion on the scalp, while it is absent in a limited number of districts including the plantar and palmar surfaces and the lips. This skin appendage is composed by structures comprehending the hair shaft, the hair follicle, sebaceous glands and an arrector pili muscle (Yousef et al., 2020).

The hair shaft is defined as the portion of the hair that protrudes from the skin's surface, while the hair follicle represents the primary structure implied in hair growth. Specifically, the hair follicle is divided into three segments (Veijouye et al., 2017; Yousef et al., 2020): infundibulum, the most superficial section encompassing the region spanning from the invagination of the epidermis to the level of the ductal opening of the sebaceous gland, and represents the area in which the sebum is expressed; isthmus, short middle section that originates from the opening of the sebaceous gland's

duct to the insertion site of the arrector pili muscle, and is the site containing the bulge region composed by a niche of hair follicle multipotent and highly proliferative stem cells able to generate all the epithelial lineages of the skin including keratinocytes, sebocytes and hair; inferior segment, functionally representing the growing part of the follicle, is given by the remainder of the deep hair follicle and begins from the site of insertion of the arrector pili muscle and expands at the base to form the hair bulb. The hair bulb is coated by epithelial-derived proliferative germ cells, namely the matrix cells, whose function is to promote the growth of the hair follicle and secondarily of the hair shaft (Morgan, 2014). At the base of the bulb is the dermal papilla, invagination composed by loose vascularised connective tissue that provides blood to the growing hair follicle. Surrounding the dermal papilla is the dermal sheath containing progenitors cells involved in the maintenance and regeneration of the dermal papilla, while also possessing wound healing functions (Jahoda and Reynolds, 2001).

In addition, in response to signals deriving from the dermal papilla, matrix cells rapidly divide, ascend upwards and progressively differentiate into the various layers that constitute the hair follicle and hair shaft (Vidal et al., 2005).

The hair follicle is further divided histologically in the inner root sheath (IRS) and outer root sheath (ORS), collectively defined as concentric cylindrical epithelial structures encircling the hair shaft originating from progressively differentiating and ascending matrix cells. Structurally the IRS lies in between the ORS (externally) and the hair (centre), and expands from the isthmus to the lower part of the bulb where it generates a rigid channel that directly encloses and protects the growing hair. Functionally, in addition to serving as a protective covering, the IRS is also involved in the regulation of the moulding, adherence and keratinization of the growing hair (Joshi, 2011; Wang et al., 2020).

The ORS represents a direct continuation of the basal layer of the epidermis that completely circumscribes the entire hair follicle. This region surrounds the IRS, and is constituted by the multipotent stem cells of the bulge region, keratinocytes and melanocytes. During hair growth, stem cells residing in the bulge are thought to leave this district and migrate towards the matrix in order to then initiate the proliferation/differentiation processes required to form a novel hair shaft. Stem cells seem to migrate across the ORS, suggesting that this cell layer might originate crucial signals able to direct the movement of these cells towards the bulb through mechanisms that are yet not fully characterised (Vidal et al., 2005). In addition, ORS cells are thought to progressively provide replacement cells for the epidermis (Jahoda and Reynolds, 2001).

The strict balance existing between proliferation, regeneration and differentiation within the hair follicle, actively contributes to the progression of the hair cycle which comes in specific phases

known as: anagen or growth phase, characterised by high proliferation rates of matrix cells that leads to a progressive extension of the hair follicle deep into the dermis and to the growth of the hair; catagen or regression phase, dominated by apoptotic processes starting from the lower partition of the follicle that cause follicular retraction and degeneration; telogen or rest phase, followed by the shedding of the hair shaft (Won Oh et al., 2016).

Other crucial components of the pilosebaceous unit comprise the arrector pili muscle and the sebaceous gland. The arrector pili muscle is a bundle of smooth muscular fibres arising from the uppermost portion of the dermis, right beneath the epidermis, that converge at the level of the upper isthmus of each follicular unit in correspondence of the bulge area, while at a lower level of the isthmus the muscle divides into branches that encircle the various lobules of the sebaceous gland. The principle function of the arrector pili muscle is the promotion of hair erection, a mechanism known to promote the retention of heat. Nevertheless, novel additional functions associated to this structure have recently been unravelled and include the induction of sebum secretion, protection of the stem cell niche located in the bulge region, and contribution to the structural integrity of the pilosebaceous unit (Deconinck and Blanpain, 2019). The sebaceous gland is an exocrine gland constituted by lobules and a keratinised duct, structure that is connected to the distal portion of the hair follicle through which sebum is constitutively released by holocrine secretion. The principle cell type of sebaceous glands is given by sebocytes that are differentiated epithelial cells involved in the synthesis of sebum, a mixture of lipids and cellular debris that is released in the gland's ductal opening following cellular disruption. The principle functions of sebum include waterproofing of the skin, preservation of the skin barrier function, protection against UV radiations and regulation of body temperature (Clayton et al., 2020). Nevertheless, recent evidences highlighted that sebaceous glands possess functions that are far beyond the sole production of sebum. Indeed, this exocrine compartment has been defined as the neuroendocrine organ of the skin that responds to circulating hormones and that is also involved itself in hormone production. In addition, sebaceous glands are responsible for the production of anti-microbial peptides and lipids, pro-inflammatory cytokines and chemokines, and also take part in wound healing processes (Clayton et al., 2020; Kamp et al., 2012; Deconinck and Blanpain, 2019) (Figure 2).

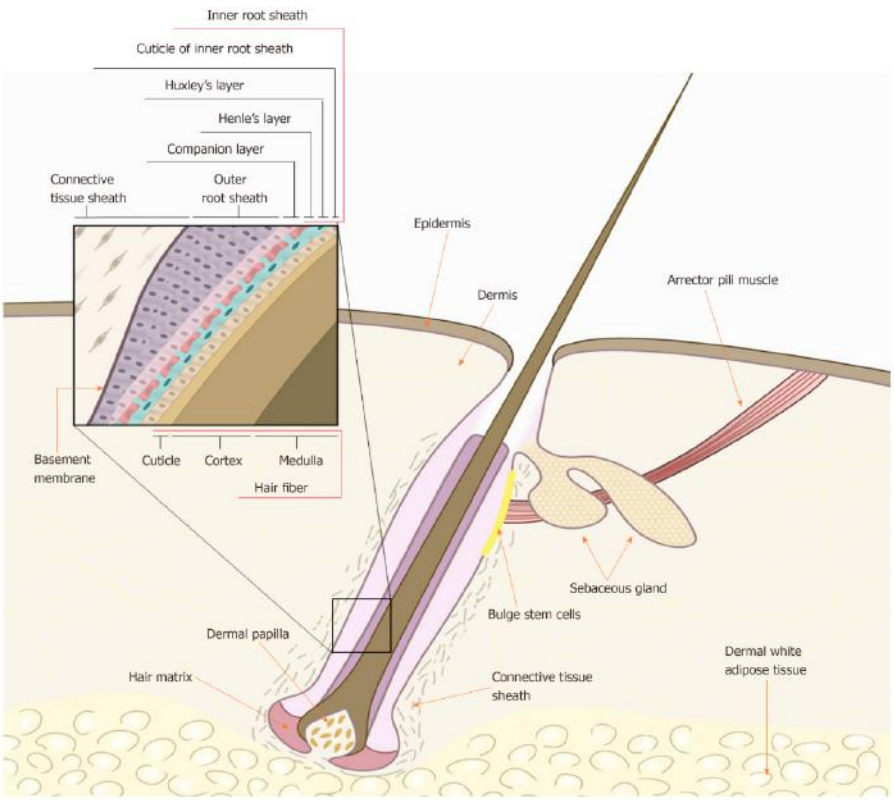

Figure 2. The pilosebaceous unit. An intact human pilosebaceous unit is composed by the hair shaft, the hair follicle, sebaceous glands and an arrector pili muscle. The bulge region is composed by a niche of hair follicle multipotent and highly proliferative stem cells able to generate all the epithelial lineages of the skin including keratinocytes, sebocytes and hair. At the base of the bulb is the dermal papilla, invagination composed by loose vascularised connective tissue that provides blood to the growing hair follicle. Surrounding the dermal papilla is the dermal sheath containing progenitors cells involved in the maintenance and regeneration of the dermal papilla.
The hair follicle is further divided histologically in the inner root sheath (IRS) and outer root sheath (ORS), collectively defined as concentric cylindrical epithelial structures encircling the hair shaft originating from progressively differentiating and ascending matrix cells (Wang et al., 2020).

1.5 Pathogenesis of Hidradenitis Suppurativa

Current evidences suggest that the pathogenesis of HS is complex and multifactorial showing a strict interplay between genetic, immunologic, hormonal, infectious and environmental factors (Sabat et al., 2020); nevertheless, the mechanisms at the basis of these events are not yet fully characterised. To date, the most accredited hypothesis asserts that the pathogenesis of HS can be restricted to a three-stage sequence of events occurring in intertriginous body areas in proximity of the pilosebaceous unit (Vossen et al., 2018).

The first stage is characterised by follicular occlusion and subsequent dilation. In this context, the occlusion of the hair follicle is mainly induced by hyperkeratosis and hyperplasia of the infundibular region of the piloseabaceous unit.
The second event comprises the disruption of the dilated follicle with the subsequent scattering of follicular contents (keratin fibres, pathogen associated molecular patterns (PAMPs), danger associated molecular patterns (DAMPs) and commensal flora) in the surrounding dermis, therefore triggering a massive inflammatory response (Vossen et al., 2018; Kathju et al. 2012; Vekic et al., 2018).
The third event is characterised by the onset of traits typical of chronic HS such as a chronic inflammatory state accompanied by scarring, abscesses and tunnel or sinus tract formation. The latter are defined as partially intra-cutaneous epithelialized cavities presenting optimal habitat conditions for biofilm-producing bacteria, whose presence might also contribute in sustaining inflammation in association with purulent drainage (Vossen et al., 2018).

1.5.1 Genetics

The first genetic study performed on HS was conducted by Fitzsimmons and colleagues in 1984 on a total of 21 members deriving from 3 UK families showing a transmission of the skin disorder through three generations (Fitzsimmons et al., 1984). The next year, the study was extended to other 23 families that allowed authors to conclude, based on the familiar aggregation and on the number of affected individuals, that the disease's transmission is possibly indicative of a single gene disorder inherited as an autosomal dominant trait (Fitzsimmons et al., 1984).

Still, their observations were not strictly consistent with the designed inheritance pattern since the frequency of affected first-degree relatives was found to be of 34% against the expected 50% for a dominant disease. In addition, some of the analysed families revealed that more women were affected than man, recapitulating the 3:1 female-to-male ratio that is currently confirmed by diverse epidemiological studies (Garg et al., 2017), while in other families a male-to-male transmission resulted to be favoured. Taken together, these aspects seemed to strongly suggest the unfeasibility of defining HS as a "one-gene-one trait" disease.
The observed discrepancies in the genetic transmission pattern gave inevitably rise to alternative conclusions to the study, or else that either the pathology presents incomplete penetrance of the dominant trait, or that these inconsistencies might be deriving from a combination of different factors including lacking diagnosis, the inclusion in the study of healthy children that would have probably manifested HS once the study was already concluded, and to the strong feeling of shame

related to the disorder that cause relatives to hide their condition to the other family members (Fitzsimmons et al., 1984).

However, recent studies conducted on HS patients have confirmed that one third of them possess a positive family history with an autosomal dominant pattern of inheritance in most cases albeit with an incomplete penetrance (Ingram, 2016; van Straalen et al., 2020).

Furthermore, these analyses allowed the identification of susceptibility genes involved in the pathogenesis of the disease, including those encoding for various subunits of the γ-secretase complex and others associated to innate immunity and fibroblast homeostasis (Tricarico et al., 2019) (Figure 3).

Gene	Encoding protein	Function	Mutation category
PSENEN	Presenilin enhancer protein 2	Essential subunit of the gamma-secretase complex, an endoprotease complex that catalyzes the intramembrane cleavage of integral membrane proteins such as Notch receptors, and Amyloid-beta Precursor Protein	Frameshift, nonsense, splicing, missense
PSEN1	Presenilin 1	Catalytic subunit of the gamma-secretase complex, an endoprotease complex that catalyzes the intramembrane cleavage of integral membrane proteins such as Notch receptors, and Amyloid-beta Precursor Protein	Frameshift
NCSTN	Nicastrin	Essential subunit of the gamma-secretase complex, an endoprotease complex that catalyzes the intramembrane cleavage of integral membrane proteins such as Notch receptors, and Amyloid-beta Precursor Protein	Missense, nonsense, frameshift, splice site
GJB2	Gap junction protein beta 2, Connexin-26	Member of the gap junction protein family specialized in cell-cell contacts that provide direct intracellular communication.	Missense
FGFR2	Fibroblast growth factor receptor	Member of the fibroblast growth factor receptor family that plays an essential role in the regulation of cell proliferation, differentiation, migration, and apoptosis, and in the regulation of embryonic development	Missense
OCRL1	Inositol polyphosphate 5-phosphatase	Involved in regulating membrane trafficking and primary cilium formation	Missense
TNF	Tumor necrosis factor	Multifunctional proinflammatory cytokine involved in the regulation of a wide spectrum of biological processes including cell proliferation, differentiation, apoptosis, lipid metabolism, and coagulation	Non coding variant that is associated with gene expression
IL-12Rb1	Interleukin-12 Receptor Subunit Beta-1	IL-12/IL-23 pathway. IL-12 is implicated in the differentiation of the Th-1 immune response and IL-23 is mediating T17 response, the latter priming chronic neutrophils influx	Missense
DEFB103	Defensin beta 3 (hBD3)	Play an important role in innate epithelial defense	Copy number variation
DEFB4	Defensin beta 2 (hBD2)	Play an important role in innate epithelial defense	Copy number variation
MYD88	Myeloid differentiation primary response protein MyD88	Plays a central role in the innate and adaptive immune response and it is involved in the Toll-like receptor and IL-1 receptor signaling pathways	Nonsense

Figure 3. Summary of the genes involved in HS pathogenesis including their encoding protein product, functions and the type of mutation category (Tricarico et al., 2019).

The first discovered typical pool of mutations occurring in familiar forms of HS comprehends mutations in presenilin enhancer-2 (*PSENEN),* nicastrin (*NCSTN*) and presenilin 1 (*PSEN-1*) genes. Interestingly, these genes encode for the various components of the γ-secretase complex, a transmembrane protease composed by four subunits comprising: presenilin 1 and 2 (PSEN1-2), the catalytic subunit, encoded respectively by *PSEN-1* and *PSEN-2* genes; three cofactor subunits involved in the stabilisation of the complex represented by presenilin enhancer-2 (PSENEN) encoded by *PSENEN* gene, nicastrin (NCSTN) encoded by *NCSTN* gene, and anterior pharynx defective-1 (APH1) encoded by *APH1A*/*APH1B* genes (Carroll and Li, 2016; Zhang et al., 2014).

Notably, 41 unique mutations typical of familial or sporadic HS have been found in these genes and encompass splice-site, frameshift and missense mutations and 19 variants that determine the onset of a premature stop codon (Frew et al., 2017; Li et al., 2019). The major limitation encountered in these findings is that not all identified genetic variants underwent functional studies, thus their effects cannot be predicted; nevertheless, the characterised ones are loss of functions mutations (Frew et al., 2017).

γ-secretase and Notch signaling

The γ-secretase is a protease that catalyses the cleavage of single-pass transmembrane proteins including Notch receptors, amyloid precursor protein, members of the cadherin family and Toll-like receptors (De Strooper et al., 1999).

Notch signalling is an evolutionary conserved intracellular cascade involved in the regulation of a vast variety of cellular processes including cell proliferation, migration, differentiation, cell fate and death, both during development and pathological conditions, through a simple signal transduction route involving the transmission of signals from the cell surface to the transcriptional machinery (Gratton et al., 2020; Siebel and Lendahl, 2017).

In mammals, four different Notch receptors (Notch1-4) and five functional Notch ligands (Serrate ligands -Jagged1, Jagged2-, Delta-like family of ligands (DLL)1, DLL3, DLL4) have been described (Gratton et al, 2020; Bray, 2016).

Notch signalling cascade is triggered following the binding of a Notch receptor to a ligand expressed on a juxtaposed cell. These interactions lead to a progressive proteolytic processing of the receptor, firstly by ADAM disintegrin and metalloprotease and ultimately by the γ-secretase, the latter promotes the final releases of the intracellular active fragment of Notch, namely the C-terminal Notch intracellular domain (NICD) (Gratton et al., 2020). Once released, the NICD translocates to the nucleus and binds to the conserved DNA binding transcription factor recombination signal binding protein for immunoglobulin kappa J region (RBP-Jκ), which progressively recruits transcription factors that are required for both repression and activation of Notch target genes (Figure 4) (Gratton et al., 2020).

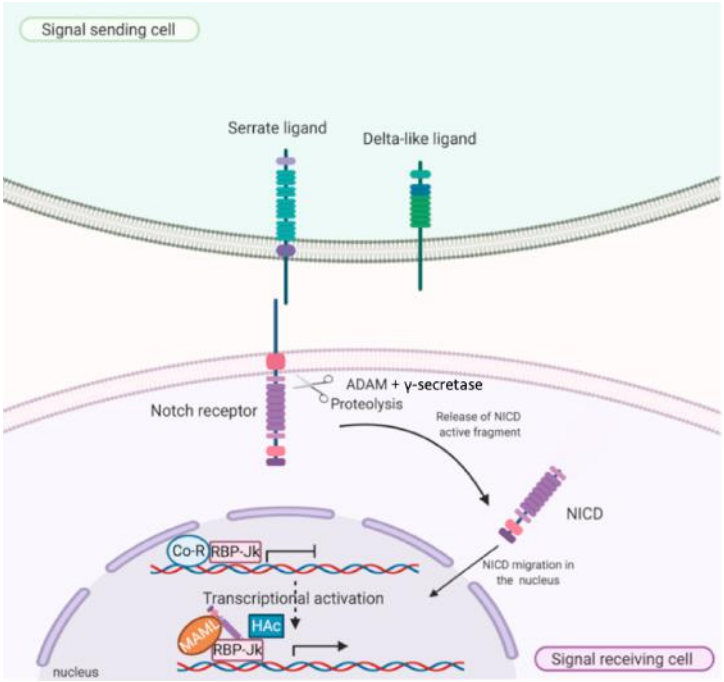

Figure 4. Notch signaling. Notch receptor binds to a Notch ligand on a juxtaposed cell. Upon binding Notch receptor is proteolytically cleaved by ADAM disintegrin and metalloprotease and ultimately by the γ-secretase, cleavage that results in the release of the intracellular active fragment, the NICD. Once releases in the cytoplasm, the NICD migrates to the nucleus where it binds to the conserved DNA binding transcription factor recombination signal binding protein for immunoglobulin kappa J region (RBP-Jκ), which progressively recruits transcription factors that are required for both repression and activation of Notch target genes (Gratton et. al, 2020).

Notch signalling in the skin

Notch signalling has been proven to exert fundamental functions in the skin primarily by mediating the correct maintenance of epidermal homeostasis by strictly regulating the balance between cellular differentiation and proliferation programs in epidermal cells (Rangarajan et al., 2001; Gratton et al., 2020). Indeed, Notch 1-4 receptors and functional ligands (Jagged 1, Jagged 2 and DDL1) possess a differential distribution throughout the layers of the skin, thus strongly indicating that their distinctive localisation pattern is specifically linked to the expression of layer-specific genes (Watt et al., 2008). The binding of Notch receptors to Jagged 1 and Jagged 2 promotes keratinocyte terminal differentiation (Blanpain et al., 2006), while interactions between Notch and DLL1 occur in the basal layer and are involved in the maintenance of ESCs in an undifferentiated state (Blanpain et al., 2006).

Notch signalling has also been reported to play a primary role in maintaining the homeostasis of skin appendages. Specifically, in hair follicles high expression levels of Notch receptors (Notch1-3) and ligands (Jagged 1 and Jagged 2) are retrieved primarily at the base of the follicle in clusters of cells that are subjected to active proliferation and more distally in cells committed to terminal differentiation (Watt et al., 2008).

Functional alterations in the γ-secretase in the skin district have been seen not to impair Notch signalling during early embryonic morphogenesis, while in post-natal skin a loss of function of this complex showed a direct impact on cellular proliferation and growth, ultimately leading to hyper-proliferation of epidermal cells, absence of mature sebocytes and conversion of hair follicles into cysts (Watt et al., 2008; Pan et al., 2004). Collectively these features strongly resemble the phenotypic manifestation occurring in HS patients, thus strongly corroborating the hypothesis that interactions between the γ-secretase and Notch transduction might shed light on crucial pathogenic mechanisms involved in HS. The patterns of mutations found in *NCSTN*, *PSEN-1* and *PSENEN* genes strongly indicates that a loss of function of the components of the γ-secretase, that establish a haploinsufficiency of the complex, are to be considered as putative genetic targets while dealing with familial HS.

Indeed, at least in a subset of familial HS cases, the γ-secretase-Notch signalling axis appears as a convincing route involved in the diseases' pathogenesis, as suggested by results obtained in mice skin in which the disruption of *NCSTN*, *PSEN-1* and *PSENEN* leads to the onset of common clinical features of HS including follicular keratinization, epidermal hyperplasia and formation of extensive epidermal cysts (Pink et al., 2013) (Pan et al., 2004). Interestingly, the γ-secretase is known to be involved also in the processing of cytokine receptors (e.g. IL-6R and IL-1β R1/R2), therefore insufficiencies in the activity of this complex might deregulate inflammatory responses and could explain, at least partially, the inflammatory nature of HS (Haapasalo and Kovacs, 2011).

Notably, two different studies conducted on groups of patients that did not report a family history of HS, highlighted that only a limited number of these sporadic cases actually carried pathogenic variants in *NCSTN*, *PSEN-1* and *PSENEN* morbid genes (Pink et al., 2012; Ingram and Piguet, 2013). Furthermore, the deep sequencing of *NCSTN* gene performed on European and African-American HS cases enrolled in the Pioneer I and II clinical trials, the majority of which possessed a familial form of the disease, revealed that only one patient presenting a family history of HS carried a non-sense mutation in the gene, while in only one sporadic case a missense variant was identified in the targeted genetic locus (Liu et al., 2016). These results are highly impacting since they strengthen the hypothesis that variants in the γ-secretase genes take into account only a restricted portion of HS patients and are therefore not sufficient alone to describe the wide phenotypic spectrum of the disease.

As shown in Figure 3, other 8 genes have been linked to the susceptibility and progression of HS.

GJB2 gene encoding for connexin-26 (Cx-26) protein is well known to carry mutations that are associated to both autosomal dominant and recessive sensorineural hearing loss (Rabionet et al., 2000) and also to syndromes that present simultaneously neurosensory deafness and skin

manifestations (erythrokeratodermia), namely the Vohwinkel's syndrome (Maestrini et al., 1999) and keratitis-ichthyosis-deafness (KID) syndrome (Montgomery et al., 2004; Lazic et al., 2012). Mutations in *GJB2* disrupt the activity of Cx-26 that is normally involved in the formation of cell-to-cell specialised cytoplasmic channels that favour the selective transport of ions and small molecules between adjacent cells, hence strictly regulating intercellular communication and a vast variety of cellular activities including the maintenance of tissue homeostasis by regulating proliferation and differentiation programs, organised cellular responses to extrinsic stimuli, development and growth control (Richard, 2001). Cx-26 is one of the most expressed connexins in human skin and shows a predominant localisation pattern in correspondence of the eccrine sweat glands and hair follicles (Lucke et al., 1999). Not surprisingly, recently mutations in *GJB2* gene have been registered in HS cases and, although the exact correlations between HS and Cx-26 dysfunction are yet to be fully understood, it is thought that they might lead to epidermal hyperproliferation, follicular plugging and rupture, spillage of cellular debris, keratins and glandular secretion in the subcutaneous district and to cyst formation, hence triggering inflammatory responses (Montgomery et al., 2004; Lazic et al., 2012).

FGFR2 gene, encoding for the fibroblast growth factor receptor (FGFR2), is expressed in keratinocytes, sebaceous glands and hair follicles, and is known to mediate specific epidermal-dermal signalling pathways that regulate cell proliferation, differentiation, apoptosis, migration, the formation of skin appendages, the proliferation and lipogenesis of sebaceous glands, and to maintain the homeostasis of the pilosebaceous unit (Melnik, 2009). Lately, a rare and damaging germ line missense variant was identified in exon 5 on *FGFR2* gene (c.G492C, pK164N) in a HS case following whole exome sequencing on blood-derived DNA. The variant is thought to possess a pathological consequence linked to the resulting impairment of the tyrosine-kinase activity of the fibroblast growth factor receptor (Higgins et al., 2017). Even though to date no functional studies are available on this mutation, an important aspect to consider is the involvement of FGFR2 in the activation of MAPK/ERK and PI3K/Akt-signal transduction pathways; indeed, the activation of PI3K/Akt axis, caused by mutations in the γ-secretase complex, is defined as HS-related and leads to aberrant keratinocyte proliferation and differentiation (Xiao et al., 2016).

Mutations in HS patients have been also identified in *OCRL1* gene encoding for inositol polyphosphate 5-phosphatase (OCRL1), a lipid phosphatase that catalyses the hydrolysis of the membrane phospholipid phosphatidylinositol 4,5-bisphosphate (PIP2) which is critically involved in membrane trafficking, membrane/cytoskeletal interface, polarisation of epithelial cells and cell signalling (Cui et al., 2010; Czech, 2000). Mutations in *OCRL1* gene are known to be associated to a X-linked disorder characterised by proximal tubule dysfunction, namely the Dent Disease 2

(DD2). In this context, Marzuillo et al. conducted a study on 5 DD2 cases possessing mutations in *OCRL1* gene, 4 of which were histologically diagnosed with HS during follow-up, hence suggesting a novel possible association between DD2 and HS (Marzuillo et al., 2018). Specifically, *OCRL1* mutations induce a decrement in OCRL1 activity ultimately resulting in a progressive accumulation of PIP2 substrate in the plasma membrane. The accumulation of PIP2 in fibroblasts seems to promote *Staphylococcus spp*. driven-aggression, therefore suggesting that in HS cases these variants might, at least partially, explain the observed increased susceptibility to cutaneous infections (Marzuillo et al., 2018).

A particular attention should be focused on the growing evidences that indicate the pivotal role exerted by deregulated immune responses in the onset, severity and progression of HS. Notably, various studies have been conducted with the aim of unravelling the potential role in the pathogenesis of HS of variants in genes encoding for proteins involved in immune responses.

Savva et al. conducted the first study aimed at evaluating the presence of single nucleotide polymorphisms (SNPs) alleles in genes related to immune responses in HS cases. Their work was performed on 190 HS patients and 84 healthy controls, to investigate the potential role of SNPs in tumor necrosis factor (*TNF*) and in Toll-like receptor-4 (*TLR-4*) genes in HS progression. Their results revealed the presence of only one relevant SNP occurring in the promoter region of *TNF* gene (-238 *TNF* SNP) that acts as a moderator for the course of the disorder; indeed, it is related to a grater predisposition to develop exacerbations and to the occurrence of more severe forms of the disease (Savva et al., 2013).

Dysregulations in antigen presentation often occurs in the pathogenesis of diverse chronic skin disorders including HS, in which this event results prominent in skin lesions, principally through the IL-12/IL-23 signalling route. Both IL-12 and IL-13 receptors share the IL-12Rβ1 subunit encoded by the *IL-12Rb1* gene. Previous genetic studies defined an association between *IL-12Rb1* and inflammatory and auto-immune disorders in which the presence of missense SNP alleles determine an altered function of the encoded subunit that presumably results in an aberrant antigen presentation, hence rendering this locus particularly attractive as a causative candidate also for HS. Giatrakos et al. conducted a study on 139 HS patients and 113 healthy controls and their results indicate that the SNPs identified in the *IL-12Rb1* gene do not convey genetic predisposition; however, they observed that the registered SNPs possess a direct association with the disease's phenotype since they are associated to severe outcomes and to the involvement of a greater number of skin areas (Giatrakos et al., 2013).

Antimicrobial peptides (AMPs) constitute a class of crucial mediators that are known to take part to inflammatory responses occurring in the skin. Specifically, these molecules are expressed by

diverse skin cells, including keratinocytes, and represent a fundamental component of the innate immunity responses activated to counteract skin pathogens and commensals. The study of these peptides appears as particularly intriguing in the context of HS; indeed, a deregulated growth of the skin's microflora together with pathogen colonization of the skin of patients, constitute major issues supported by the usage of antibiotics as a first line therapeutic approach (Ingram et al., 2015; Orenstein et al., 2020). Considering the role of microbial infections in HS, one would expect to register a decrement in the expression of antimicrobial peptides to explain the increased susceptibility of patients to develop bacterial infections. Nevertheless, a study conducted by Giamarellos-Bourboulis et al. gave rise to an unexpected outcome. Human β-defensins (hBD)-2 and hBD-3, expressed respectively by the *DEFB4* and *DEFB103* genes located in a β-defensin cluster, are well established peptides whose expression is associated with the severity of skin infections by *Staphylococcus aureus* (Zanger et al., 2010; Giamarellos-Bourboulis et al., 2016). Authors observed and increment in the number of *DEFB4* and *DEFB103* genes that is found to be associated to increased levels of hBD-2 and hBD-3, identifying this aspect as a factor that conveys genetic susceptibility while conferring a protection towards the development of a severe phenotype (Giamarellos-Bourboulis et al., 2016).

Myeloid differentiation primary response protein MyD88 gene (*MYD88*) encodes for a cytosolic adaptor protein exerting fundamental functions both in innate and adaptive immune response by acting as a signal transducer in the Toll-like receptors and IL-1 signalling route, that result in the induction of several pro-inflammatory genes. Defects related to this gene are commonly associated to an increased susceptibility to develop pyogenic bacterial infections. By studying a cohort of 101 HS cases, Agut-Busquet and colleagues observed that a polymorphism in the *MYD88* gene (GG genotype of rs6853) is associated to an increased risk in developing a severe form of the disease (Agut-Busquet et al., 2018).

The impact of genetics in the susceptibility, progression and aggravation of hereditary and sporadic forms of HS, should not only be limited to the evaluation of single mutations that impact the functionality of proteins that are potentially associated to the disease. Indeed, other genetic variations, related for instance to transcriptomic signatures or epigenetic changes, need to be considered in order to provide novel insights into which genes (and therefore proteins) are possibly involved in HS and in the wide spectrum of the disease's phenotype.

Coates et al. performed the analysis of the skin transcriptome in HS uncovering gene signatures that collectively indicate that the pathogenesis of HS might be driven by changes in the expression of AMPs, altered sweat gland function and share similar routes activated in chronic wounds. Indeed, the top differentially expressed genes between lesional and non-lesional areas of HS skin

encompass: increased expression of diverse AMPs, being *S100A7A* together with *DEFB4* the most significantly up-regulated ones in lesional skin, probably due both to a generic over-activation of the innate immune system towards microorganisms or to a reaction to an altered microbiome in lesional areas; increased expression profile of epidermal differentiation complex (EDC) cluster of genes that encode for proteins involved in the terminal differentiation of keratinocytes, that might possibly suggest the presence of high levels of terminally differentiated keratinocytes in lesions hence possibly leading to a decreased regenerative capacity; decreased expression in lesions of genes associated with sweat-gland function, district known to be directly involved in the regulation of sweat generation, epidermal homeostasis, wound-healing, re-epithelialization and cutaneous immunity, therefore indicating an overall loss of normal skin architecture and function due to a decreased number of sweat glands (Coates et al., 2019).

Moreover, whole-tissue-whole-transcriptome-sequencing (RNA-seq) assays conducted on lesional and non-lesional samples of HS cases indicate that skin lesions in HS possess a unique heterogeneous and complex inflammatory signature enriched in genes involved in complement activation, B cell signalling, phagocytosis-associated pathways, neutrophil recruitment, macrophage activation, wound healing, chronic inflammation, TNF-α secretion, lipopolysaccharide (LPS) signalling, IL-12 production and T-cell recruitment. Noteworthy, also the non-lesional skin in HS presents defects in immune regulatory pathways when compared to the skin transcriptome of healthy controls, highlighting a significant reduction in immune regulatory pathways and activation of specific pro-inflammatory routes. When compared to healthy skin, both lesional and non-lesional HS skin present significantly differentially expressed genes involved in homeostatic processes (e.g. cell division, metabolism, respiration, apoptosis and DNA damage repair) and immune pathways involving components of B-cells and myeloid compartment and their activation (Lowe et al., 2020). Single-cell RNA-seq (scRNA-seq) technique has been widely assessed to outline the cellular composition of HS. These assays confirmed that myeloid cells and B cells are the major contributors to the HS transcriptome profile as skin lesions progress, further indicating that myeloid cells seem to adopt a strong inflammatory phenotype driven by the activation of IL-1 signalling, while an augmentation of B cells further differentiated memory B cells, plasma cells, and plasmablasts persist (Lowe et al., 2020). Furthermore, scRNA-seq assays further outlined the cellular composition (keratinocytes, endothelial cells, smooth muscle cells, melanocytes, fibroblasts and T-cells), the specific signature genes and crucial cell-to-cell communication pathways between different cell types in HS pathogenesis. In a study conducted by Gudjonsson et al., authors observed extensive interactions amongst all the principle cellular types in HS, such as interactions amongst B

cells and plasma cells with stromal tissue cells and other immune cell components. In addition, endothelial and keratinocyte populations resulted to present extensive interactions with members of the Notch signalling pathway. Both *IL17A*- and *IFNG*-expressing T cells were registered in HS skin. *IL18*, a promoter of IFN-γ responses, was primarily derived from keratinocytes (Gudjonsson et al., 2020).

The genes that have been so far identified as frequently altered in different cohorts of HS cases might contribute to the assessment of genetic analysis in which a gene panel for the most common variants are employed. Nevertheless, considering the highly complex and variable genetic background in HS cases, the analysis of gene panels based on previously identified susceptibility genes for HS, usually results as unsuccessful in the determination of causative variants in the majority of patients. Indeed, cases with a clear HS phenotype but presenting no association with a known disease gene, might present novel gene associations or express a combination of variants in several genes (complex genetic trait). In this critical context, technologies such as whole exome sequencing (WES), constitute a revolutionary approach that allows the concurrent analysis of multiple genomic coding regions. This experimental approach permits a broader screening in patients presenting specific disease patterns, and potentially leads to the identification of causative variants underlying the pathogenesis of the disease (Kosukcu et al., 2021; Luo et al., 2021; Li et al., 2017).

1.5.2 Aberrant immune responses

As previously reported, the development of aberrant immune responses in HS is thought to be tightly associated to the occurrence of mutations in susceptibility genes associated to innate and adaptive immune responses. Moreover, specific transcriptomic signatures in lesional skin that comprise an enrichment of genes involved in AMPs production, altered sweat gland function, complement activation, neutrophil recruitment, phagocyte-associated pathways, macrophage activation, TNF-α secretion, B-cell signalling and T-cell activation have been registered (Lowe et al., 2020; Gudjonsson et al., 2020).

The major pathogenic feature in HS is a deregulated immune activation and a gradual progression towards a chronic inflammatory state. These responses seem to exhibit classical features of a neutrophilic dermatosis (inflammasome-driven predominance of interleukin (IL)-1β), to be characterised by a strong anti-inflammatory response dominated by IL-10, and to elicit a clear contribution of T_H-17 and T_H-1 lymphocytes (Sabat et al., 2020).

Cutaneous immune responses

Early pathogenic events in HS are thought to be triggered by local cellular damage induced by enhanced mechanical friction in intertriginous body sites, that leads to the release of DAMPs and promote the transfer of microbial components in the skin, thus inducing the activation of resident immune cells, primarily of macrophages, that produce cytokines and chemokines that ultimately favour perivascular and perifollicular immune cell infiltration (Sabat et al., 2020). In this context, a further intensification of the inflammatory response is primarily given by an augmented bacterial sensing exerted by local macrophages and dendritic cells (DCs) due their increased expression of Toll-like receptor (TLR) 2 (Hunger et al., 2008), and to the activation of the inflammasome platform following the recognition of DAMPs that promotes the activation and secretion of IL-1β (Witte-Handel et al., 2019). A high expression of both TLR2 and of the inflammasome complex have been detected in HS skin (Sabat et al., 2020).

The principal secreted pro-inflammatory cytokines include IL-1β and TNF-α and these mediators collectively possess diverse effects including: IL-1β induction of the production of chemokines (e.g. CXCL6 and CXCL1) that promote the recruitment of neutrophilic granulocytes; TNF induction of the synthesis of a wide range of chemokines (e.g. CXCL2, CXCL8 and CXLCL10 in keratinocytes) that attract in the skin monocytes that locally differentiate in macrophages and DCs, neutrophils, T_H-17 and T_H-1 cells, activate endothelial cells, and promote the synthesis of the anti-inflammatory cytokine IL-10 by macrophages. As a direct consequence, HS developing lesions are characterised by massive perifollicular immune cell infiltrates, thought to produce mediators that seem to favour hyperkeratosis and hyperplasia of the infundibular epithelium, hence leading to the subsequent follicular occlusion (Sabat et al., 2020).

Amongst the immune cell infiltrates found in HS lesions, the role exerted by T_H-17 and T_H-1 lymphocytes seems to be of crucial importance for the intermediary pathogenic stages. IL-23 and IL-12 secreted by macrophages and DCs seem to be the main drivers eliciting the activation of T_H-1 and T_H-17 cells.

Interferon-γ (INF- γ), the principal cytokine produced by T_H-1 lymphocytes, exerts several critical functions including: further activation of endothelial cells thereby additionally favouring the infiltration of immune cells in the lesional area; induction of the production of T_H-1 attracting chemokines; activation of tissue-resident macrophages (Schroder et al., 2003; Sabat et al., 2020).

IL-17, the main cytokine secreted by T_H-17 lymphocytes, is also known to possess several functions such as: stimulate the production of chemokines that prompt the recruitment of neutrophils; induce

the synthesis of cytokines that primarily sustain IL-17-mediated inflammatory responses; stimulate the production of antimicrobial peptides (AMPs) (Albanesi et al., 1999).

Interestingly, the levels of IL-22 found in HS skin are low and this might be due both to the lack of TH-22 infiltrates and/or to the high expression of IL-22 inhibitors. In the presence of IL-17, IL-22 cytokine is one of the major inductors of AMPs synthesis, thus low levels of IL-22 might at lest partially explain the insufficient blockade of bacterial propagation in the inflamed skin. Furthermore, IL-22 is also involved in counteracting tissue damage and metabolic alterations during inflammatory processes (Sabat et al., 2020). Indeed, diminished quantities of this cytokine might partially justify tissue destruction and the onset of systemic metabolic alterations registered in HS cases (Figure 5).

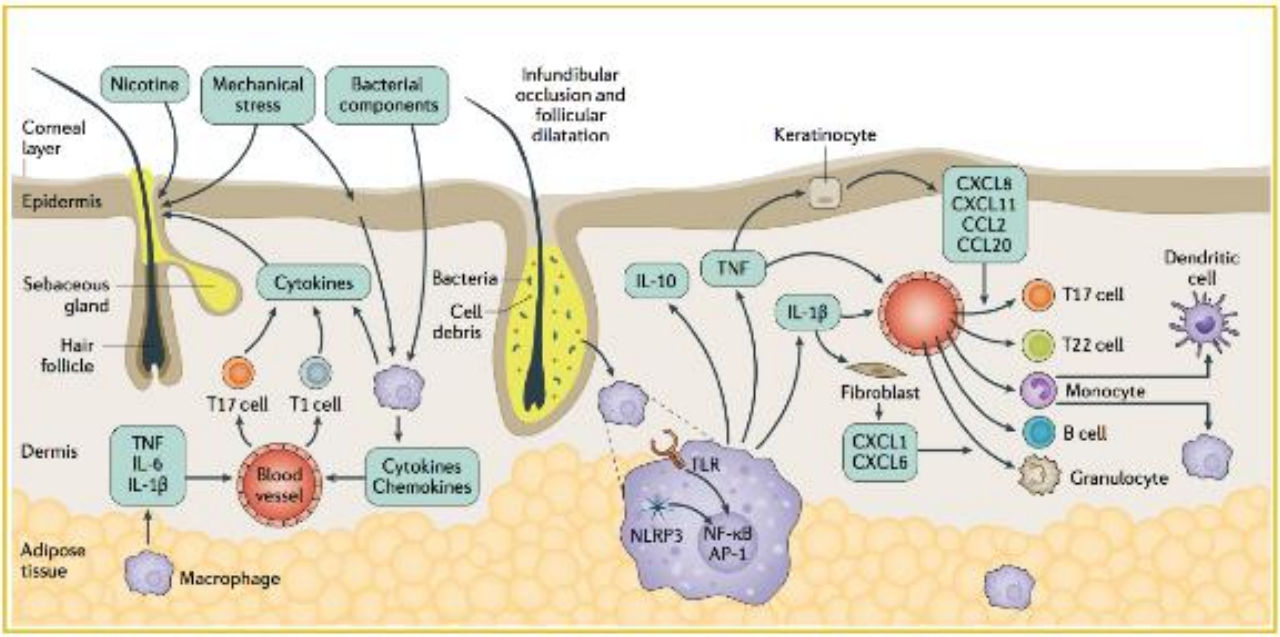

Figure 5. Initial and intermediate events involved in the pathogenesis of HS. In HS, skin alterations occur in intertriginous body sites around the pilosebaceous unit. Local cellular damage induced by enhanced mechanical friction leads to the release of danger associated molecular patterns (DAMPs), and promote the transfer of microbial components in the skin, thus inducing the activation of resident immune cells that produce cytokines and chemokines that ultimately favour a massive perivascular and perifollicular infiltration of immune cells that are thought to produce mediators that favour hyperkeratosis and hyperplasia of the infundibular epithelium, hence leading to the subsequent follicular occlusion. In the intermediary pathogenic stages IL-17-producing TH-17 cells and interferon-γ (INF- γ)-producing TH-1 lymphocytes are abundant in HS lesions and further sustain the development of inflammatory responses (Sabat et al., 2020).

Both massive cell infiltration and microbial propagation in the perifollicular lesional areas cause a dilation and further rupture of the hair follicle, leading to a subsequent scattering of the follicular content in the surrounding dermis, event that additionally boosts the inflammatory response.

During the final pathogenic events, a further immune cell infiltration mediated by a high cytokine and chemokine production around the ruptured hair-follicle, contributes to the formation of abscesses and intra-cutaneous inflammatory nodules. Next, under the stimulation of high levels of cytokines including IL-1β, IL-6 and IL-32, fibroblasts are activated and produce elevated levels of extracellular matrix-degrading enzymes that might ease the rupture of adjacent dilated follicles and are directly involved in tissue destruction (Sabat et al., 2020; Witte-Handel et al., 2019; Nomura, 2020).

At this stage, a great neutrophilic infiltration and activation occurs in HS skin, and these cells further contribute to the secretion of pro-inflammatory cytokines and to pus formation. The accumulation of pus and the progressive tissue destruction might lead to the production of pus-discharging sinus tracts and fistulas (Nomura, 2020; Sabat et al., 2020) (Figure 6).

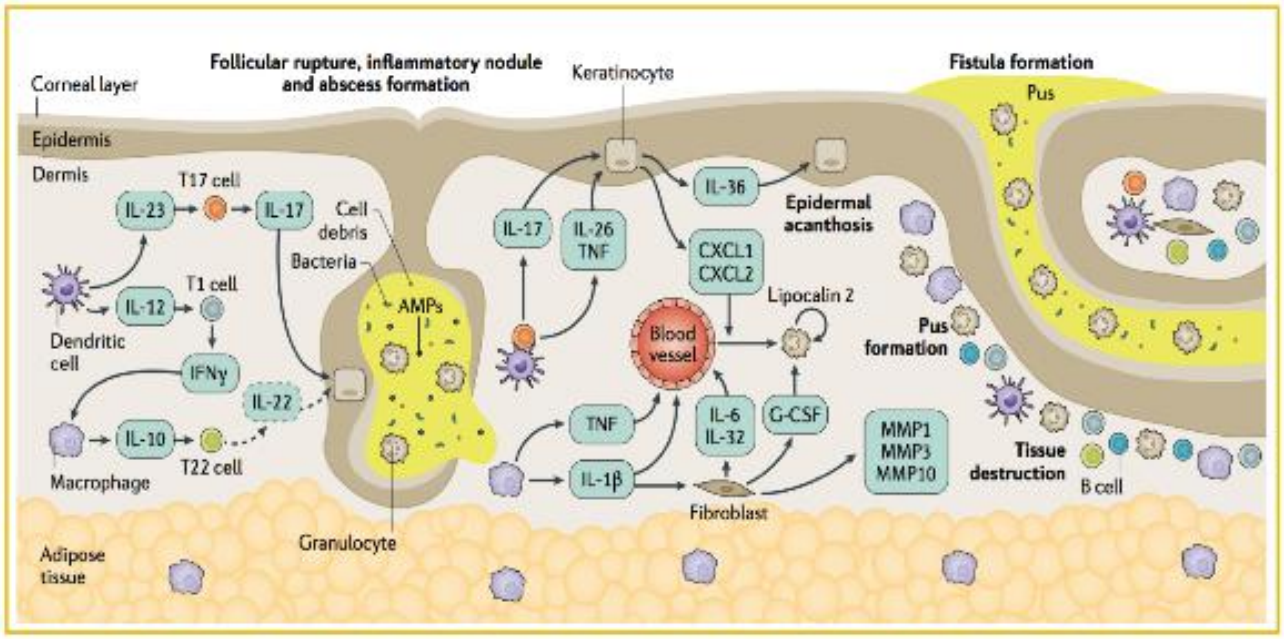

Figure 6. Final events involved in the pathogenesis of HS. Bacterial propagation and massive immune cell infiltration in the perifollicular lesional areas determine follicular rupture, leading to the scattering of follicular contents in the surrounding dermis that additionally boost the inflammatory response. The further production of chemokines and cytokines in this area favour the formation of abscesses and intra-cutaneous inflammatory nodules. In this context, the production of extracellular matrix-degrading enzymes by activated fibroblasts might ease the rupture of adjacent dilated follicles. A high neutrophilic infiltration and activation contributes to the additional secretion of pro-inflammatory cytokines and to pus formation. The progressive tissue destruction and the development of pus induce the formation of pus-discharging sinus tracts and fistulas (Sabat et al., 2020).

All of these factors strongly suggest that the aberrant inflammatory responses in HS skin are critical in defining the pathogenesis of the disease by directly affecting: antimicrobial responses that result to be insufficient; progressive tissue destruction; pus formation.

Systemic immune responses

Due the enhanced and persistent inflammatory response in HS skin, not surprisingly different cytokines and mediators might reach the bloodstream and contribute to the onset of systemic inflammatory episodes and comorbidities (Sabat et al., 2020).
Augmented IL-32 levels in inflammatory chronic conditions are known to represent a risk factor for the development of cardiovascular diseases (Damen et al., 2017), while high IL-1β and IL-6 circulating levels promote the production of the acute-phase protein serum amyloid A that might lead to severe outcomes such as amyloid A amyloidosis and atherosclerosis (Shridas and Tannock, 2019). Furthermore, elevated circulating levels of IL-17 and TNF might be linked to the onset of HS-associated Crohn's disease, spondyloartropathy or spondyloartrthritis (Sabat et al., 2020; Nomura, 2020).
While considering the onset of systemic immune responses in HS, an extremely useful approach is given by the application of WES technology, procedure that presents the advantage of being a non-invasive methodology that analyses DNA extracted from saliva. Indeed, WES can deal with the high complexity of the molecular effectors and signalling pathways potentially impacted in these responses and therefore promote the identification of the molecular actors possibly contributing to the development of exaggerated systemic immune responses in HS.

1.5.3 Hormonal influence

The role of sex hormones (progestogens, androgens and oestrogens) in the pathogenesis of HS has for long been debated and the outcomes of diverse clinical studies still appear to be contrasting. Nevertheless, female predominance, post-pubertal onset, worsening of clinical symptoms during the premenstrual period and an overall improvement of flares during pregnancy and post-menopause, strongly corroborate the involvement of hormones in HS (Riis et al., 2016). Moreover, the appearance of similar phenotypic features between HS and acne vulgaris, a well established androgen-dependent disorder, have suggested that at least partially overlapping pathogenic patterns involving androgen dysfunction might occur also in HS. The major events underlying this possible association include: pre-menstrual exacerbations; most severe cases are commonly recorded in

males; augmented keratinization of the skin, event that is known to be mainly driven by androgens (Riis et al., 2016).

HS female patients often report to suffer from flares in the pre-menstrual period when the levels of progesterone is high and are generally more prone to develop androgen-related consequences such as irregular menstruations, acne and hirsutism (Mortimer et al., 1986). Moreover, the prevalence of polycystic ovary syndrome (PCOS), a hyper-androgenic disorder, amongst HS cases is 9% against 2,9% registered in non-affected females (Garg et al., 2018). Furthermore, *in vivo* studies assessed in mouse models showed that androgens induce an incremented pro-inflammatory response driven by augmented levels of TLR-mediated monocyte expression of TNF-α, thus also strongly suggesting a possible correlation between androgenic imbalance and inflammatory phenotypes (Lai et al., 2009).

Considering therapeutic interventions, different case reports underlined that the administration of progestogen-based oral contraceptives in female cases leads to the onset of exacerbated HS clinical manifestations (Jemec, 1988).

Nevertheless, the fact that the levels of plasma testosterone, dehydroepiandrosterone and apocrine gland androgen converting enzymes are no different in HS patients if compared to controls (Barth and Kealey, 1991), that the disease commonly manifests many years after puberty (Seyed Jafari et al., 2020), and that anti-androgen therapies combined with oestrogens do not result to be more beneficial than the administration of sole oestrogens (Mortimer et al., 1986), need to be taken into serious account as they represent factors that are not strictly consistent with a possible androgenic involvement in HS.

Confirming the important role played by hormones in the HS pathogenesis, in a recent article Buonomo et al. observed the development or exacerbation of HS in two transgender man following the administration of testosterone therapy (Buonomo et al., 2021).

So said, the overall impact of hormones on the pathogenesis of HS remains unclear but the mechanisms relative to hormonal imbalances is appealing and requires further clarifications.

1.5.4 Bacterial infections

The contribution of bacterial infections in HS pathogenesis has for long been debated and still needs to be fully defined. Even if the clinical presentation of HS strongly resembles the one of infectious processes, it is still unclear whether microbial infections constitute a primary or secondary event in the development of HS lesions. Nevertheless, to date the major accredited hypothesis suggests that HS should not be considered as a primary infectious disease but rather as an inflammatory skin condition predisposing cases to develop self-infections (Nikolakis et al., 2015). These aspects underline the presence of strict interplays between microbial dysbiosis, defined as a pathogenic

imbalance in the composition of commensal bacteria, and aberrant immune responses. The mechanisms at the basis of these interactions are still not clear and are currently under investigation. Different findings support the assumption that commensal bacteria act as secondary colonisers and not as primary initiators of inflammatory responses in HS. It is presumable that during the initial pathogenic stages, the enhanced mechanical friction in intertriginous body sites promotes the spilling of commensal flora in the progressively occluding follicle. Upon follicular rupture, commensal bacteria scatter in the surrounding dermis and are recognised by pathogen-recognition receptors (PRRs) thus further sustaining the ongoing inflammatory response in the skin (Vossen et al., 2018).

Next, one of the major signatures of aberrant innate immune responses in HS skin is given by an insufficient infiltration of TH-22 cells resulting in low levels of IL-22, a potent inducer of AMPs production. Indeed, low levels of AMPs are thought to lead to an insufficient blockade of bacterial propagation in the inflamed skin (Wolk et al, 2011).

Crucial aspects regarding the microbiological composition of HS skin and lesions currently needs to be unravelled since they are suggested to mediate, at last to some extent, the propensity of HS cases to develop suppurating and inflammatory lesions and may drive the selection of targeted therapeutic interventions (Nikolakis et al., 2015). Recently, a case-control study highlighted the presence of a dysbiosis in both lesional and non-lesional skin of HS patients if compared to healthy controls (Vossen et al., 2018). This condition might induce a shift of harmless microorganisms to pathogenic, a change that can dominate and drive inflammation as shown in various chronic inflammatory conditions (Naik et al., 2018). Furthermore, considerable variations in microbiome composition have also been observed amongst HS patients and seem to correlate with the severity of the disease (Guet-Revillet et al., 2017).

Moreover, chronic HS lesions are rarely sterile and are characterised by an incremented polybacterial colonization. In the majority of cases, the microbiological profile of HS lesions is given by the combination between normal skin commensals including anaerobic cocci, and a polymorphous anaerobic microbiota comprising microbial commensals typically residing in different mucosal body sites including genital, gut and oropharyngeal districts (Guet-Revillet et al., 2017).

Nevertheless, even if these features might invite to reconsider a primary role of bacteria in HS pathogenesis, the great inter-individual variability in the composition and relative abundance of commensal opportunistic flora in HS lesions in which no single common culprit organism can be found, variations in microbiome arrangement, together with the lacking development of infectious

complications in HS cases, still strongly supports a secondary rather than primary role of bacterial infections in HS pathogenesis (Naik et al., 2018).

1.5.5 Environmental risk factors

To date, the impact of environmental factors in the onset, progression and severity of HS are well defined. Cigarette smoking is recognised as a triggering factor for HS, and approximately 85% of HS cases are current or former smokers (Konig et al., 1999). Indeed, nicotine is thought to negatively impact the diseases' outcome through various mechanisms. Nicotine is a cholinergic agonist that has been seen to act as a potent inducer of epidermal hyperplasia following the binding to non-neuronal nicotinic acetylcholine receptors (nAChRs), molecules that have been seen to be expressed in HS skin and in particular to be accentuated in the infundibular region of the pilosebaceous unit (Hana et al., 2007). Thus, the induction of an increase in the number of cells in the infundibular epithelia might enhance follicular plugging. Moreover, *in vivo* studies conducted on mice highlighted that nAChR activation by nicotine is able to suppress antimicrobial responses in the skin primarily by reducing AMPs production (Radek et al., 2010). These findings suggest that nicotine exposure might be linked, at least partially, with a major susceptibility to bacterial propagation and biofilm formation. Furthermore, nicotine stimulates the production of IL-10 by activated immune cells, a cytokine that is known to be tightly involved in HS pathogenesis (Sabat et al., 2020).

Notably, a significant association between HS and metabolic disorders have been identified; indeed, about 50% of HS cases are found amongst the obese population (Sabat et al., 2020). Obesity is thought to worsen HS outcome by enhancing the mechanical friction and subsequent cellular damage at inverse body sites, and also by promoting a constant state of subclinical inflammation. Specifically, the presence of exceeding quantities of macronutrients in the adipose tissue stimulates adipocytes to produce pro-inflammatory mediators such as TNF-α and IL-6 as well as adiponectin and leptin, that collectively contribute to the onset of continuous inflammation and oxidative stress (Ellulu et al., 2017).

1.6 Syndromic variants of Hidradenitis Suppurativa

The term syndromic HS is used to define a heterogeneous group of inherited or immune-mediated diseases in which the manifestation of HS is recognised as a common feature. Even if syndromic HS occurs in a minority of patients, there is a great interest in unravelling the principal molecular and cellular mechanisms involved in their onset since they are still largely neglected.

PASH, PaAPASH, PAPASH and PASS syndromes encompass a continuous clinical spectrum of auto-inflammatory syndromic variants of HS manifesting cutaneous and articular involvement, in which the presence of HS represents a distinctive hallmark. These syndromes are characterised by an enhanced infiltration of mature neutrophils in the skin in the absence of infectious stimuli, known as neutrophilic dermatosis, and by a hyper-production of IL-1 family of cytokines. Indeed, as in HS, psoriasis, A, arthritis and PG, the main common characteristic that seems to be involved in their pathogenesis is a neutrophilic activation by the TH-17/TNF-α axis (Cugno et al., 2017).

1.6.1 PASH syndrome

PASH syndrome possesses an auto-inflammatory nature that primarily affects young adults who very precociously exhibit the typical clinical manifestations (Cugno et al., 2017). Three main patterns of skin lesions have so far been identified is PASH cases and include: abscesses and fistulas that ultimately progress in pus-discharging sinuses and scars; mild to severe facial acne; papulopostular lesions, ulcers and ulcerated nodules (Marzano et al., 2014). PASH cases are often characterised by the persistence of chronic lesions (Zagaria et al., 2020; Ead et al., 2018) presenting exudation of fibrin and leucocytes with an elevated neutrophilic activation caused by the induction of TH-17/TNF-α axis (Cugno et al., 2017). In addition, the chronicity of lesions highly suggest that wound healing processes are deregulated in PASH patients. Moreover, the histopathological features of PASH skin are typically characterised by neutrophilic dermatosis that are consistent with bacterial super-infections, therefore creating a potential link between PASH syndrome and the expanding spectrum of bacterial biofilm disorders and wound healing alterations (Ead et al., 2018). Host immune responses towards chronic wounds promote the development of a specific microenvironment characterised by low oxygen tension, necrotic debris and slough formation, that collectively favour bacterial growth; in fact, not surprisingly about 78.2% of chronic wounds contain biofilm formations (James et al., 2008). In response to biofilm, the host induces the release of inflammatory cytokines and growth factors, including TNF-α, IL-6, CXCL8/IL-8 chemokine, epidermal growth factor (EGF), platelet-derived growth factor and VEGF that increases vascular permeability (Prabhakara et al., 2011). Specifically, TNF-α pro-inflammatory cytokine released by leukocytes, fibroblasts, and keratinocytes, is highly expressed in chronic wounds and is associated to persistent and perpetuating inflammatory responses (Kalliolias and Ivashkiv, 2016). The resulting enhanced inflammatory response increases the production of exudative byproducts that induce the further production of necrotic tissue and slough (Ead et al., 2018). Noteworthy, the administration

of anti-TNF agents, including neutralising antibodies, have been shown to induce wound healing responses in mouse models (Ashcroft et al., 2012).

The concomitant presence of IBD (Crohn's disease and ulcerative colitis) and rheumatologic features, have also been registered in patients (Marzano et al., 2014). PASH cases are subjected to a strong psychological burden that is mainly due to the extensive, painful, malodorous and chronic skin lesions, and in addition to the current lack of available therapeutic interventions.

The genetic basis of PASH syndrome is only partially known and seems to be variable; nevertheless, pathogenic variants in recognised auto-inflammatory genes including proline-serine-threonine phosphatase interacting protein 1 (*PSTPIP1*) gene (Garcovich et al., 2020; Braun-Falco et al., 2012), pyrin (*MEVF)* gene (Garcovich et al., 2020), *NLRP3* (Marzano et al., 2014) gene and nucleotide-binding oligomerization domain-containing protein-2 (*NOD2*) gene (Marzano et al., 2014) have been identified.

Inflammasomes are multiprotein complexes involved in the activation of caspase-1 and caspase-5 proteases that ultimately catalyse the cleavage and activation of pro-inflammatory cytokines IL-1β and IL-18, and the induction of pyroptosis (Kummer et al., 2007).

To date, NLR family pyrin domain containing 3 (NALP3), encoded by *NLRP3* gene is the most studied inflammasome since it has been found to be associated to various inflammatory, metabolic and neurological diseases. NALP3 is characterised by a confined tissue distribution and is predominantly localised in non-keratinising squamous epithelium, immune blood cells (monocytes, dendritic cells, neutrophils, B and T cells), peripheral blood mononuclear cells and microglia cells (Kummer et al., 2007).

The activation of NALP3 promotes the recruitment of the adaptor apoptosis-associated speck-like protein containing a CARD (ASC), protein that binds to NALP3 and that recruits and activates caspase-1 (Ferrero-Miliani et al., 2007). It is currently suggested that the recruitment of pro-caspase-1 to the inflammasome platform induces an auto-proteolytic cleavage of the enzyme into an active caspase-1, that ultimately leads to the cleavage and release pro-inflammatory cytokines IL-1β and IL-18 (Walsh et al., 2014).

The core of the pyrin inflammosome is given by the cytoplasmic PRR pyrin protein, encoded by the *MEVF* gene. The assembly and activation of pyrin inflammasome requires the binding of pyrin to the homotrimeric proline-serine-threonine phosphatase interacting protein 1 (PSTPIP1), encoded by *PSTPIP1* gene, a cytoskeleton-associated adaptor protein. The ligation of PSTPIP1 to pyrin induces a conformational change that unmasks its domain involved in the binding with ASC, and less frequently with NALP3 (Yu et al., 2007). Subsequently, pro-caspase-1 is recruited to the complex,

thus ultimately resulting in enzymatic activation, followed by the processing and secretion of the pro-inflammatory cytokines IL-1β and IL-18 (Schnappauf et al., 2019). Pathogenic variants found in these genes seem to promote a major affinity (stronger and longer) binding between pyrin and PSTPIP1 and an augment recruitment of ASC by pyrin. Furthermore, pyrin is also known to act as a negative regulator of inflammasome activity, therefore an augmented binding affinity between pyrin and PSTPIP1 is thought to impair pyrin's regulatory effect on inflammasome activity thus further enhancing the inflammatory cascade (Heymann and Rosen-Wolff, 2013).

Mutations in *NOD2* gene, encoding for nucleotide-binding oligomerisation domain-containing protein-2 (NOD2), have also been retrieved in PASH cases and are additionally known to be associated with an augmented risk for the development of Crohn's disease (CD) (Hampe et al., 2002). NOD2 is a cytoplasmic Nod-like receptor (NLR) constitutively expressed in immune cells (neutrophils, dendritic cells, macrophages), in the epithelial Paneth cells of the small intestine and in epithelial cells and is involved in mediating inflammatory responses against bacterial antigens (Ferrero-Miliani et al., 2007). Following the detection of bacterial muramyl dipeptide (MDP), NOD2 activates different transduction routes such as inflammatory transcriptional programs driven by the activation of NF-kB signaling cascade, the autophagic route, and endoplasmic reticulum stress, as strategies converging towards intracellular bacterial clearance (Negroni et al., 2018).

Pathogenic variants in *NOD2* might result in both loss-of-function or gain-of function mutations inducing respectively a defect in limiting inflammatory responses or a hyper-activation of inflammatory pathways (Eckmann and Karin, 2005; Negroni et al., 2018). Nevertheless, the true outcome of the so far identified *NOD2* variants on PASH phenotype still needs to be clarified.

Though the precise pathogenic mechanisms underlying PASH syndrome have not been yet fully elucidated, it is possible to hypothesise that along with neutrophilic activation driven by the TH17/TNF-α axis (Cugno et al., 2017), pathogenic mutations in auto-inflammatory genes might significantly contribute to an aberrant deregulation of inflammatory signaling pathways, therefore sustaining the exaggerated inflammatory response observed in neutrophilic dermatoses.

Mutations in HS-specific genes (*NCSTN*, *PSENEN*, *PSEN1*, *APH1*) have also been identified in PASH cases. Specifically, a loss-of-function mutation in *NCSTN* gene has been recently registered in one patient (Duchatelet et al., 2015). This finding strongly underlines a potential connection between HS, PASH and impaired Notch signaling (Marzano et al., 2014; Cugno et al., 2017).

1.6.2 PAPASH, PsAPASH and PASS syndromes

Other auto-inflammatory HS-related clinical variants of PASH syndrome have been described and are represented by PAPASH, PsAPASH and PASS conditions.
PAPASH is characterised by the manifestation of pyogenic arthritis together with the triad of PG, A and HS; in PAPASH a missense variant was registered in *PSTPIP1* gene (Marzano et al., 2013).
PsAPASH is given by the simultaneous diagnosis of psoriatic arthritis together with PG, A and HS; nonetheless, the genetic defects underlying this disease are yet unknown (Saraceno et al., 2015).
PASS comprises a very rare condition in the broad phenotypic spectrum of syndromic HS and is given by the simultaneous presence of PG, acne conglobata, HS and seronegative spondyloartrhtitis (Bruzzese, 2012), and cases present elevated serum levels of IL-1β and IL-1 Receptor antagonist (IL-1Ra) (Leuenberger et al., 2016). Also in this case, the genetic background of PASS cases is largely neglected.
It is important to note that in two recent clinical studies conducted on a total of 10 patients affected by PASH, PAPASH, PsAPASH and PASS, no pathogenic variants were registered neither in auto-inflammatory genes (*PSTPIP1*, *MEVF*, *NLRP3*, *NOD2*) nor in HS-specific genes (*NCSTN*, *PSENEN*, *PSEN1*, *APH1*) thus indicating that dealing with auto-inflammatory HS syndromic variants opens an extremely complex scenario (Gottlieb et al., 2019).

1.7 Therapy

To date, no standard therapies have yet been designed to treat HS patients, being that therapeutic interventions are primarily selected based on the severity of the disease and on the clinical features expressed by patients. Furthermore, even if HS is classified as an inflammatory disease, the majority of the cases don't respond to non-steroidal anti-inflammatory drugs (NSAIDs), suggesting that there is the necessity to counteract different responses other than the sole inflammatory phenotype.
Generally, the management of HS is extremely complex and requires an individualised approach that takes into account activities directly managed by patients aimed at modifying specific lifestyle habits (e.g. smoking cessation, reduction of body weight, pain management, psychological support, rigorous skin hygiene practices, loose clothing to avoid excessive friction with the skin) and medical and surgical treatments (Jafari et al., 2020). Some commonly employed medical and surgical treatments include (Ingram et al., 2015; Orenstein et al., 2020): oral or topical administration of antibiotics, with the aim of counteracting bacterial infections that often colonise

lesions; disinfectant and bacteriostatic topical treatments, that rarely result to be effective due to the fact that lesions are commonly deep-seated; hormonal therapies, based on the assumption that HS has been frequently associated to androgenic dysfunction; anti-hyperglycemic treatments, bearing in mind that HS cases might develop metabolic syndrome characterised by hyper-insulinism and insulin resistance; immunomodulators and biologics might be undertaken with the aim of obtaining strong immunosuppressive effects when the first line of therapy, given by antibiotics and topical agents, results to be ineffective; surgical treatments are performed only when medical interventions fail since surgery is commonly associated to a high probability of relapses and/or of skin retraction (Figure 7).

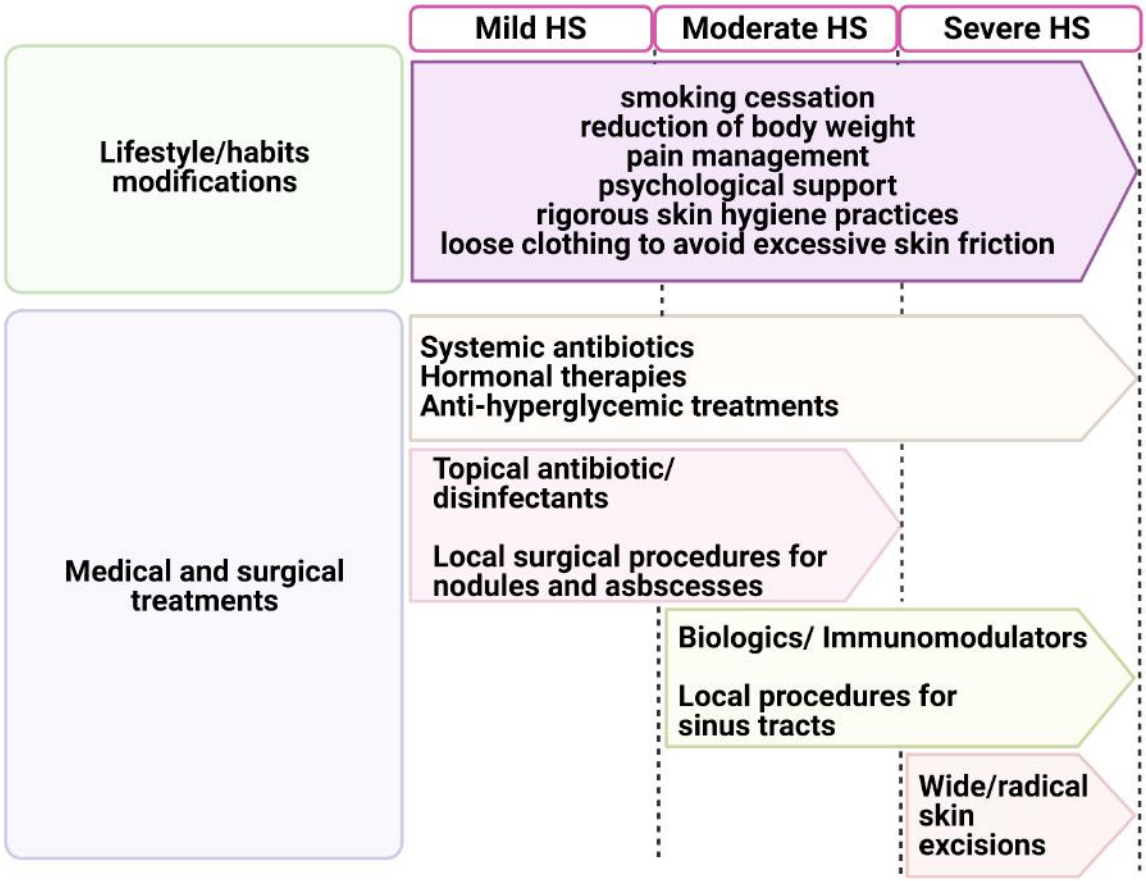

Figure 7. Clinical practice recommendations for the treatment of HS. In mild, moderate and severe HS, patients are invited to modify their lifestyle and habits such as cessing with smoking, reduce body weight, proceed with a proper pain management, seek for psychological support, undergo rigorous skin hygiene practices and wear loose clothing to avoid excessive skin friction. The administration of systemic antibiotics, hormonal therapies and anti-hyperglycemic treatments are commonly employed in mild to severe cases. In mild and moderate HS patients topical antibiotic and disinfectants are commonly employed, and local surgical procedures to remove nodules or abscesses can occur. In

moderate to severe patients the administration of biologics and immunomodulators, and the local removal of sinus tracts is common. In severe cases, the performance of wide skin excisions might be necessary.

2. AIM

Hidradenitis suppurativa (HS) and syndromic variants of HS, the latter defined as a spectrum of disorders involving multiple organ systems in which HS represents a distinctive hallmark, are highly debilitating inflammatory diseases presenting a multifactorial pathogenesis in which a strict and complex interplay between genetic, immunologic, infectious and hormonal factors have been identified, though the precise molecular mechanisms underlying these aspects have not yet been fully characterised.

Interestingly, in HS and in syndromic variants of HS, some mutations are found to be recurrent and to primarily occur in susceptibility genes encoding for various subunits of the γ-secretase complex and others associated to innate immunity and fibroblast homeostasis. However, it is clear that most patients do not share the same mutations and that commonly mutations themselves are not informative of the biological pathways that result to be disrupted in cases. While dealing with these complex disorders in which the genetic aetiology is highly heterogeneous, the assessment of family-based genetic and genomic studies, further supported by functional assays, appears as a powerful tool for the identification of novel pathogenic mechanisms potentially involved in the onset, progression and severity of the disorder. Nevertheless, this approach presents a limitation linked to the fact that the study is focused on a genetic variant that is private and therefore restricted only to certain families. On the other hand, a relevant advantage related to this approach is given by the possibility to develop tailored and personalised treatments to be administered successfully to selected patients carrying specific mutations.

Part 1: The case of a PASH patient

Whole exome sequencing (WES) allowed the identification of a A>T missense exonic variant (rs17604693; g.7565494 A>T; c.913A>T; p.Ile305Phe) in exon 7 of *DSP* gene in a PASH patient (HSM5). *DSP* encodes for desmoplakin (DSP) a fundamental component of desmosomes. WES results for HSM5, together with the evaluation of the family segregation of the variant in F_HSM5 (father) and M_HSM5 (mother), were confirmed in Sanger sequencing (Figure 8).

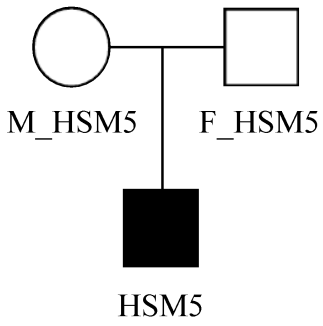

Figure 8. Pedigree of the family of HSM5.

Following genetic studies, the initial experimental setting was aimed at performing *in silico* molecular dynamic studies to determine the impact of the SNV on protein structure. Next, spontaneously immortalised human keratinocytes (HaCaT) cells were genome edited with CRISPR-Cas9 technology in order to generate an *in vitro* genetic model in which cellular clones carry the *DSP* variant of interest. Next, the study of the effect of the *DSP* SNV on the intracellular distribution of DSP, on the morphology of desmosomal structures, on differentiation and proliferation processes were performed both on skin biopsies deriving from the PASH patient and healthy controls matched per age and sex, and *in vitro* on genome edited HaCaT cells. Finally, in order to determine the potential role of *DSP* missense variant on skin barrier function, TEWL was measured in the PASH case, his mother and father, and healthy controls matched per age and sex.

Part 2: the case of the Sardinian family

Genetic tests, performed on 47 members of a Sardinian family affected by a familial form of HS, allowed the identification of a rare (MAF<0.01) missense SNV in *ZNF318* (rs767801219; g. 43322952T>A; NM_014345:exon4:c.A2120T; p.K707I) in 17 family members comprising all of the 11 individuals who initially declared to be affected by HS and in additional 6 family members that haven't mentioned to possess any sign of the disease (Figure 9).

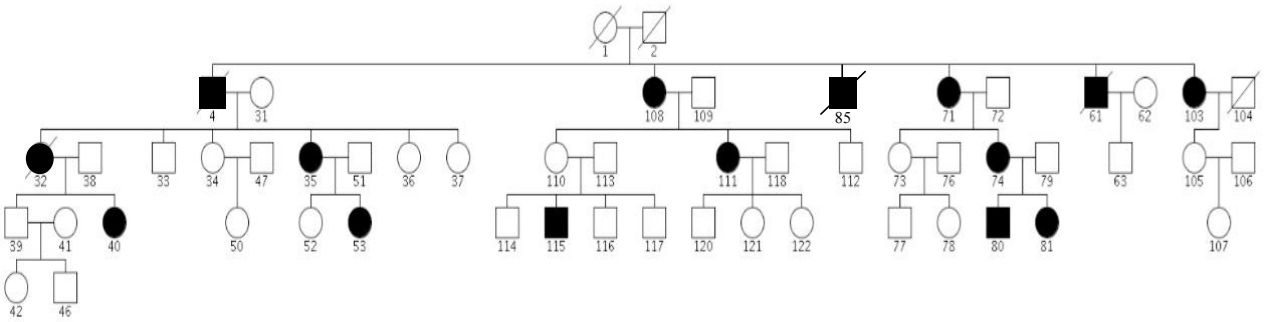

Figure 9. Pedigree of the Sardinian family. 47 individuals adhered to the study, 11 of which declared to be affected by the diseases and 4 of which were reported to have been affected by HS (deceased cases).

Following genetic analysis, mutated individuals were subjected to a questionnaire that takes into account age, sex, body mass index (BMI), everyday habits (smoke, diet), the history of the disease, the presence of other correlated pathologies and therapies, in order to search for potential causative links between the registered SNV and HS progression in the family. Next, HaCaT cells were genome edited with CRISPR-Cas9 technology in order to retrieve an *in vitro* genetic model in which clones carry the designated *ZNF318* SNV that might contribute to better characterise the impact of the missense variant.

Part 3: the case of a Friulian family

WES analysis lead to the identification of a rare (MAF<0.01) frameshift insertion (rs538180888; g.54645236_54645237insT; NM_053283.4:c.225dup; NP_444513.1:p.Ala76Fs) in *DCD* gene in HS affected family members of a Friulian family. This gene encodes for dermcidin (DCD), an AMP exerting a well established antibacterial activity (Figure 10).

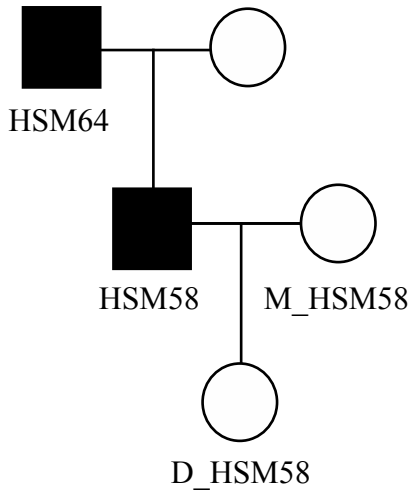

Figure 10. Pedigree of the Friulian family.

After genetic analysis, the effect of the frameshift insertion in *DCD* gene on protein structure was assessed *in silico* through comparative modelling and molecular dynamic procedures. Next, *in vitro* antimicrobial studies were performed in order to measure the antimicrobial activity of the mutated DCD peptide on planktonic bacteria, on biofilm deposition and on biofilm eradication.

The aim of this work was to augment the knowledge of the pathogenic mechanisms at the basis of HS and syndromic variants of HS, specifically of PASH syndrome, by performing family-based studies aimed at identifying genetic changes and in defining their putative impact in HS and PASH phenotype. The assessment of functional studies aimed at characterising the potential role of identified genetic variants in the pathogenesis of these diseases, also constituted a crucial starting point for the development of personalised therapeutic interventions.

3. MATERIALS AND METHODS

Part 1: The case of a PASH patient

3.1 Patients

Thanks to a cooperation with the Dermatology Department of the Fondazione IRCCS Ca' Granda Ospedale Maggiore Policlinico of Milan, a PASH patient (HSM5) was enrolled in this study. His father (F_HSM5), mother (M_HSM5), and healthy controls matched per age and sex for HSM5, F_HSM5 and M_HSM5 were also recruited. All the enrolled individuals signed a written informed consent previously approved by the Comitato Etico Unico Regionale (CEUR) of Friuli Venezia Giulia (FVG) (RC 16/18, Prot. N.0001094 (14/01/2019), CEUR-2018-Sper-127-BURLO).

3.2 Genetic tests

3.2.1 Genomic DNA extraction from saliva

Genomic DNA from enrolled patients was extracted from saliva. Briefly, saliva samples were obtained using an all-in-one kit for the collection, stabilisation and transportation of DNA (Oragene DNA OG 500, DNAGenotek, Ottawa, CA). DNA extraction was then performed assessing an ethanol precipitation using the prepIT-L2P2 kit (Oragene and ORAcollect® collection kit, Genotek, Canada) following the manufactures' protocol.

3.2.2 Whole exome sequencing (WES) and data analysis

The concentration and purity of extracted DNA samples was assessed with the Qubit assay (Invitrogen, Oregon, USA) and by agarose gel. Samples were then subjected to whole exome sequencing (WES) with 100X of expected coverage, in outsourcing by Macrogen (Seoul, Korea). Briefly, DNA exome sequencing reactions were executed through Illumina® HiSeq 2500 System, following library preparation (SureSelect Human all exons V6 kit).
The global coverage was re-calculated through Picard tool and recovered an average of 93.9%, 36.0% and 9.3% for 10, 50, 100X coverage respectively. Adapters were trimmed using the Trim Galore tool, searching and removing Illumina adapters, reads with length below 15 base pairs, and low quality ends from reads with Phred score below 20 (http://www.bioinformatics.babraham.ac.uk/projects/trim_galore/).

The FASTQ file containing the raw reads was aligned employing the Burrows-Wheeler Aligner (BWA) Software Package (H. Li, R. Durbin, Fast and accurate long-read alignment with Burrows-Wheeler Transform, Bioinformatics 26 (5) (2010) 589–595), specifically the bwa-mem tool was assessed using the Human Genome version 38 (GRCh.38) as the selected reference. Next, Picard tools (https://broadinstitute.github.io/picard/) were used to remove and mark duplicate reads, and GATK v. 4.1.2.0 (https:// software.broadinstitute.org/gatk/) permitted base recalibration and variant calling by excluding those variants having low genotyping and mapping quality (GQ < 20 and MQ<40). Assurance and quality control were displayed with FastQC.

Variant annotation was performed with ANNOVAR software (K. Wang, M. Li, H. Hakonarson, ANNOVAR: functional annotation of genetic variants from high-throughput sequencing data, Nucleic Acids Res. 38 (16) (2010) e164) using databases relative to the GRCh.38 reference genome (dbSNP 151, CADD; GERP++, SIFT, PolyPhen2, FATHMM, MutationTaster, MutationAssessor, COSMIC70, ClinVar, 1000 Genomes Project, ExAC 03, genomicsSuperDups, wgRNA, GWAS Catalog, and Interpro).

All retrieved variants from WES analysis were screened in order to recover the SNVs that are most likely to be deleterious or pathogenic or functional, variants were ranked according to the Combined Annotation Dependent Depletion (CADD) based on the PHRED-like score with a cut-off of 25. Next, selected variants were progressively screened according to gene function and those genes found to exert functions related to HS etiopathogenesis were selected and subjected to further analysis (Figure 11).

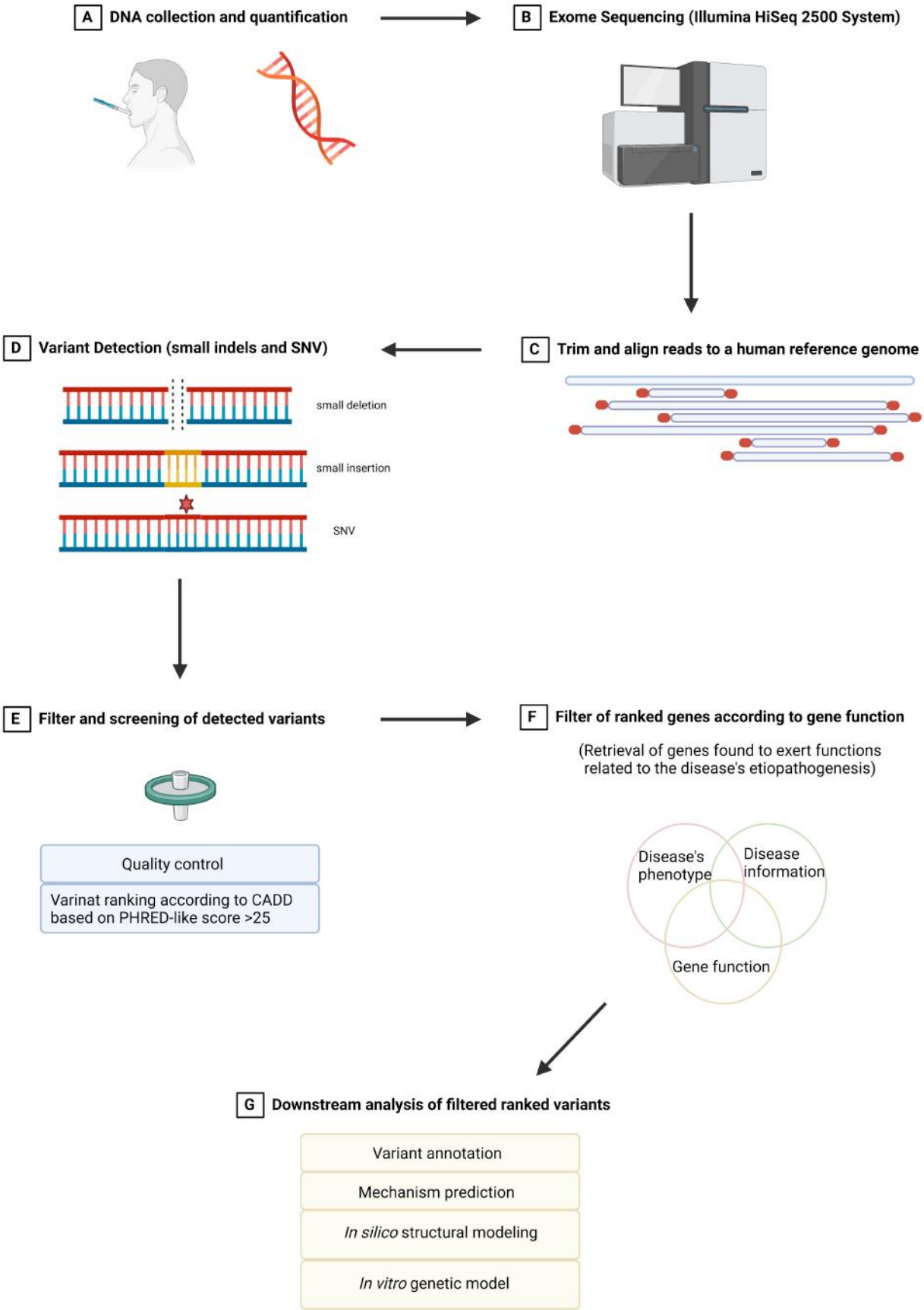

Figure 11. Whole exome sequencing (WES) pipeline.

WES analysis were performed by Dr. Ronald Moura (IRCCS Burlo Garofolo, Trieste) and by Prof. Lucas Andrè Cavalvanti Brandao (IRCCS Burlo Garofolo, Trieste). The PhD student, was involved in the screening phase to recover potentially deleterious or pathogenic or functional SNVs, and in the screening of selected variants based on gene function.

3.2.3 Sanger sequencing for the confirmation of the selected variants identified by WES

Genomic DNA samples were amplified using the KAPA2G Fast HotStart Ready Mix (KAPA Biosystems) using primers for *desmoplakin (DSP)* gene (*DSP*_forward primer: 5'-TCCAGGGAGATCATGTGGAT-3', *DSP*_reverse primer 5'-GGAAGGATTTTTCACGACCA-3') (Eurofins Genomics, Germany).
The following protocol and PCR program were employed:

KAPA2G Fast HotStart Ready Mix	6,25 µL
*DSP*_forward primer (10 µM)	0,625 µL
*DSP*_reverse primer (10 µM)	0,625 µL
H2O	4,25 µL
Genomic DNA (50 ng)	0,75 µL
Final volume of reaction	12,5 µL

Step	Temperature	Time (min.)	Number of cycles
Initial denaturation	95 °C	3:00	1
Denaturation	95 °C	0:10	
Annealing	55 °C	0:10	40
Extension	72 °C	0:05	
Final extension	72 °C	1:00	1
	4 °C	Hold	

Sanger sequencing of DNA amplification products was performed by Eurofins Genomics (Eurofins, Germany). The obtained chromatograms were analysed using the CodonCode Aligner Software (Version 8.0.2, LJ-COR Inc.).

3.3 *In silico* studies

3.3 Molecular dynamics for the evaluation of *DSP* SNV on protein structure and stability

Desmoplakin (DSP) structure was downloaded from Protein Data Bank (PDB: 3R6N) and non-residue elements including water, sulphate or other molecules, were removed from the file. Next, the mutagenesis tool from PyMOL (pymol.org) was used in order to change the relevant amino acids and generate the mutant heterozygous and homozygous form of the protein.
The dimer was then inserted in a 0.7 nm cubic box, filling the voided space with SPC-E water molecules. Calcium and sodium ions were added with the aim of reaching the system electronic equilibrium. Energy minimisation was carried out using default parameters. The equilibrium phase for temperature and pressure was carried out during 10 ns, while the production phase lasted 100 ns. Also, these steps were performed using default parameters. In order to investigate the stability and compaction of the complexes, Root-mean square deviation (RMSD), Radius of gyration (Rg) and Solvent accessible surface area (SASA) parameters were evaluated. All molecular dynamics simulations were performed using the GROMACS 2020.2 (Abraham et al., 2015).
Molecular dynamics simulations were performed thanks to a cooperation with Dr. Ronald Moura (IRCCS Burlo Garofolo, Trieste). The PhD student was directly involved in the analysis and interpretation of retrieved data.

3.4 Skin features of the PASH patient

Skin biopsies deriving from an ulcerative lesional area of the left armpit of HSM5 and form the same body site of a healthy control matched per age and sex, were kindly provided by the Dermatology Department of the Fondazione IRCCS Ca' Granda Ospedale Maggiore Policlinico of Milan.

3.4.1 Immunohistochemistry (IHC)

Sections of 5-7 µm thickness were cut from the paraffin-embedded skin biopsies, deparaffinised in xylol solution, rehydrated in decreasing concentrations of ethanol (100% (v/v), 96% (v/v)), and briefly washed in distilled water. Next, immunostaining for DSP (desmoplakin I/II cloneA-1, Santa Cruz Biotechnology, Inc. Dallas, Texas 75220 U.S.A.), ki67 (clone MIB-1 M7240, Dako Glostrup, Denmark), K14 (Cytokeratin 14 (LL001) Santa Cruz Biotechnology, Inc. Dallas, Texas 75220 U.S.A.) and K10 (Cytokeratin 10 (RKSE60), Santa Cruz Biotechnology, Inc. Dallas, Texas 75220 U.S.A.) was performed.
Briefly, heat-induced antigen retrieval was assessed using pressure-cooking in 0,5 mM EDTA pH 8.0 solution, followed by 1 hour incubation at room temperature with the primary antibody. Next, for the chromogenic enzyme-mediated detection of antigens, samples were incubated with a

primary antibody enhancer (secondary anti-mouse IgG (H+L) antibody, kit UltraVision Quanto Detection System HRP Polymer, Thermo Fisher Scientific), followed by the addition of the polymer (kit UltraVision Quanto Detection System HRP Polymer, Thermo Fisher Scientific) and of the diaminobenzidine (DAB) chromogen (DAB Quanto Chromogen, Thermo Fisher Scientific) (DAB Quanto substrate, Thermo Fisher Scientific) following the manufactures' protocol.
Samples were then counterstained with Carazzi hematoxylin and sections were mounted on positively charged glass histological slides using a permanent mounting media (Eukitt® Quick Hardening Mounting Medium, Sigma-Aldrich).
Samples were scanned using the Aperio ScanScope XT system (Aperio Technologies, Leica Micorsystems) and images at 60x magnification in bright field were acquired using the Olympus BX63 with DP80 camera (Olympus-Lifescience) and analysed using the cellSens software (Olympus-Lifescience). IHCs were performed thanks to a collaboration with the Department of Medical and Surgical Health Sciences of the University of Milan (Bicocca).

3.4.2 Transmission Electron Microscopy (TEM)

Skin biopsies were fixed using a primary glutaraldehyde fixative solution (2% glutaraldehyde and 4% paraformaldehyde) in sodium cacodylate buffer for 4 hours at room temperature, followed by three time washing in sodium cacodylate buffer. Samples were then incubated in a secondary oxium tetroxide fixative solution (oxium tetroxide 2% diluted in sodium cacodylate buffer) for 1 hour at room temperature followed by three times washing with sodium cacodylate buffer. Specimens were dehydrated using increasing concentrations of ethanol (50% (v/v), 70% (v/v), 95% (v/v), 100% (v/v)) and embedded in 100% epoxy resin (epon 812 kit, Sigma-Aldrich) at 60 °C for 24 hours. Next, ultrathin sections (60-80 nm) were cut using an ultramicrotome, stained with 2% aqueous uranyl acetate and lead citrate (Leica) and mounted on Pioloform-filmed copper grids. Sections were analysed using a CM 10 transmission electron microscope (Philips) and digital images were collected using the Megaview III camera (Emsis).
From acquired images the length of desmosome was measured manually, while the degree of flexion and the diameter of desmosomes was directly determined using the AnalySIS software. TEM was performed thanks to a collaboration with the Department of Medical and Surgical Health Sciences of the University of Milan (Bicocca). The IRCCS Burlo Garofolo of Trieste requested the implementation of these analyses since the required tools are not available in the Institute.

3.4.3 Transepidermal water loss (TWEL)

Transepidermal water loss (TEWL) measures were conducted on HSM5, F_HSM5, M_HSM5 and on healthy controls matched to each family member per age and sex. In addition, TEWL values were also acquired on HS patients matched per age and sex to HSM5. At the time of TEWL measurements, HSM5 did not present active flares.
TEWL measurements were performed using the Tewameter™ 210 open-chamber device (Courage and Kahazaka electronic GmbH, Germany) following the EEMCO guidelines for *in vivo* measurements of water in the skin (Berardesca et al., 2018). The Tewameter™ 210 open chamber device consists of a hollow cylinder placed in contact with the skin so that the water vapour directly diffuses from the skin surface to the ambient atmosphere through the chamber. The device is able to detect the humidity gradient thanks to two set of sensors, one for the detection of relative humidity and the other for the retrieval of temperature values, properly set up in the cylinder. Readings are converted by a microprocessor into a single TEWL value by calculating the diffusion rate in $g/m^2/h$. On all recruited individuals, TEWL readings were performed in triplicate on the face (forehead and/or cheeks), left fingertip and right fingertip, the predilection anatomical sites reported in EEMCO guidelines (Berardesca et al., 2018). TEWL was performed thanks to a collaboration with the Dermatology Department of the Fondazione IRCCS Ca' Granda Ospedale Maggiore Policlinico of Milan.

The immune genetic laboratory of the IRCCS Burlo Garofolo of Trieste required to execute IHC, TEM and TEWL analysis to collaborators due to the absence of the required experimental tools in the Institute. The staff of the immune genetic laboratory of the IRCCS Burlo Garofolo of Trieste, together with the PhD student, actively coordinated the execution of experimental procedures and were directly involved in the interpretation of acquired data and in the assessment of statistical analysis.

3.5 *In vitro* assays

3.5.1 Cell culture

In vitro functional studies were performed on spontaneously immortalised human keratinocyte line (HaCaT cells), that were chosen since they represent a widely accepted model mimicking human keratinocytes, frequently employed for the study of skin biology, differentiation, immunologic and inflammatory responses and possess a normal epithelial phenotype (Wilson, 2014).

HaCaT cells grow as adherent cells and were cultured in 5% CO_2 at 37 °C in low-calcium complete growth medium prepared with:

- Dulbecco's Modified Eagle Medium with no calcium chloride (DMEM, Gibco, ThermoFisher Scientific);
- 2% L-glutamine 2 mM and 1% penicillin-streptomycin amphotericin B 1X solution (Sigma Chemical Co. Aldrich, St. Louis, CA);
- 10% low calcium foetal bovine serum. Foetal bovine serum (FBS, Euroclone, Italy) was calcium-depleted by incubation with Chelex® 100 sodium form 50-100 mesh (dry) resin (Sigma Chemical Co. Aldrich, St. Louis, CA) and incubated for 1 hour at 4 °C under agitation. The Chelex was subsequently removed using a Millipore 0.22 μm filter unit system (Merk);
- 0,03 mM calcium chloride (Sigma Chemical Co. Aldrich, St. Louis, CA).

Under low calcium conditions (0,03 mM), HaCaT cells are maintained in a fully basal state, widely recognised to be optimal for the study of basic processes related to the skin biology (Wilson, 2014). For the study of hyper-adhesive calcium independent desmosomes (Kurinna et al., 2014) and for the differentiation of HaCaT keratinocytes (Wilson, 2014), complete growth medium was supplemented with calcium chloride (99.99% anhydrous powder, Sigma-Aldrich), in order to obtain a high-calcium complete growth medium with a final calcium concentration of 2.8 mM.

3.5.2 Genome editing of *DSP* gene with CRISPR-Cas9 technology

The progressive development of genome-editing technologies, primarily based on the usage of engineered or bacterial nucleases, gave the opportunity to target and directly modify virtually any genomic sequence in almost all eukaryotic cells, enabling the formation of isogenic cell lines and animal models suitable for the study of gene function and of cellular behaviours and activities. These editing tools have so far shown remarkable potentials in a vast number of fields including applied biotechnology, biomedical research and basic research (Li et al., 2020).

To date, the core genome editing technologies contemplate the usage of programmable nucleases such as zinc-finger nucleases (ZFNs), transcription activator-like effector nucleases (TALENs) and clustered regularly interspersed short palindromic repeat (CRISPR)-Cas9 associated nuclease (CRISPR-Cas9). Editing procedures can be performed both *in vivo* and *in vitro* by directly conveying the editing machinery *in situ*, therefore performing permanent site-specific changes to the genome of cells and organisms (Li et al., 2020). Site-specific DNA modifications arise from the production of double-strand breaks (DSBs) induced by nucleases that trigger the activation of

highly efficient DNA-repair pathways that are known to be active in almost all cell types and organisms, namely homology-direct repair (HDR) and non-homologous end-joining (NHEJ). HDR results in gene integration or single-base pair corrections and requires the presence of a donor template sequence with homology sequences to the targeted chromosomal site. Alternatively, NHEJ elicits primarily gene disruptions/inactivation/knockouts through the formation of random insertions or deletions (indels) of diverse lengths in correspondence of the DSB site (Li et al., 2020; Zafar et al., 2020). Notably, the presence of indels in the coding region of a target gene typically induce the formation of a frameshift mutation that results either in RNA degradation through nonsense-mediate decay (NMD) or in the production of a non-functional truncated protein (Lieber et al., 2010).

CRISPR-Cas9 genome editing technology, first assessed by J.A Doudna and E. Charpentier (Jinek et al., 2012), exploits an adaptive immunity response of bacteria and archea against invading viruses and plasmids to direct the silencing of exogenous DNA through RNA-guided DNA cleavage (Wiedenheft et al., 2012; Maraffini, 2015; Nussenzweig and Maraffini, 2020).

When adapted to genome editing, the most frequently employed system is the type-II CRISPR-Cas9 machinery that depends on a single RNA-programmed Cas9 protein deriving from *Streptococcus pyogenes* (SpCas9) to target a specific DNA sequence.

The CRISPR-Cas9 system encompasses two components, a single-stranded guide RNA (sgRNA) and a Cas9 endonuclease. The sgRNA is composed by a highly specific and unique 20 nucleotide base-pair spacer designed in order to complement in a sequence-specific manner the genomic target (or protospacer) to be modified, and by a 3' end scaffold sequence (≈80 nucleotides) that is necessary for the recruitment and binding of the Cas9 to the sgRNA. At the 3' or 5' end of the protospacer is found a variable DNA region that is required to allow Cas9 protein binding to the DNA target identified as the protospacer adjacent motif (PAM), which is often given by a 5'-NGG-3' or 5'-NAG-3' sequence (Jiang and Doudna, 2017).

The assembly of the sgRNA with Cas9 determines a substantial structural rearrangement of the endonuclease that achieves an active DNA recognition-competent conformation that allows the complex to search for complementary target DNA sites. The recognition of the target site necessitates both complementary base pairing between the 20 nucleotide spacer sequence with the DNA protospacer, and the presence of a PAM sequence next to the targeted locus. Different experimental settings have highlighted that a necessary prerequisite is the initial recognition of the PAM by Cas9 in order to then allow the endonuclease to scan the adjoining DNA for putative target sequences complementary to the sgRNA. Indeed, in absence of PAM recognition, Cas9 immediately dissociates from DNA and is directed towards a novel site. The recognition of the PAM triggers a displacement of the DNA strand (R-loop) and promotes the invasion of the RNA

guide to form sgRNA-DNA hybrids. Upon the formation of a Cas9-sgRNA-target DNA complex, the endonuclease is ready to cleave the targeted genomic locus at a specific site at 3 base-pairs from the PAM sequence, hence inducing the generation of predominantly blunt-end DSBs (Jiang and Doudna, 2017; Pickar-Oliver and Gersbach, 2019).

The ligation of DSBs can rapidly occur through NHEJ, which is often error-prone and results in random insertions, deletions or inversions that typically alter open reading frames therefore disrupting a gene's function and generating a gene knock out. On the other hand, DSBs can be mended through HDR in presence of a donor DNA template that harbours homology arms flanking the genomic target, therefore acting as a template to repair the damaged DNA. HDR allows a high fidelity gene correction/replacement/insertion, the generation of desired point mutations, the acquisition of precise gene knockouts, introduction of tags or reporters, and gain of function mutations (Jiang and Doudna, 2017) (Figure 12).

To date, CRISPR-cas9 has become the most adopted genome editing tool due to its high efficiency, multiplexability and low costs.

An intriguing application of CRISPR-Cas9 is associated to the study of human diseases. Indeed, the ability to edit the genome, both *in vitro* and *in vivo*, permits the creation of more accurate cellular and animal disease models that are crucial to understand the impact of a genetic casual factor on a given disorder, favour the understanding of mechanisms associated to the disease and evaluate potential therapeutic strategies (Wu et al., 2020; Li et al., 2020; Riordan et al., 2015; Sakuma et al., 2014). Moreover, CRISPR-Cas9 has been seen to be suitable also for the constitution of disease models relative to disorders harbouring more mutations; in this context, simultaneous edits and repairs in multiple genes are possible by using plasmids containing numerous sgRNAs (Sakuma et al., 2014; Ousterout et al., 2015).

In addition, this technology also possesses a high clinical and therapeutic potential by promoting the modification of target genes *via* disruption, correction or replacement. Nevertheless, ethical and technical criticisms, including potential immunotoxicity, DNA-damage toxicity, precision of the editing due the low efficiency of HDR contrasted by the default activation of NHEJ pathway and delivery systems, need to be taken into serious account while considering the exploitation of this technique for clinical practice (Uddin et al., 2020). This gene editing approach can be applied both *ex vivo*, involving the genetic modification of cells outside the patient's body that are then reintroduced back, and *in vivo*, when CRISPR components are directly delivered into the patients for cell editing procedures. Ex vivo approaches are limited to a reduced number of cell types that can survive and be expanded in culture including T cells (Baylis and McLeod, 2017) and hematopoietic stem and progenitor cells (Yu et al., 2016), therefore showing great potentials for

haematological disorders and cancer immunotherapy. On the other hand, *in vivo* manipulations are strictly required to face a wide range of genetic disorders involving other tissue types and typically occur through systemic delivery or local injection in specific tissues (Uddin et al., 2020).

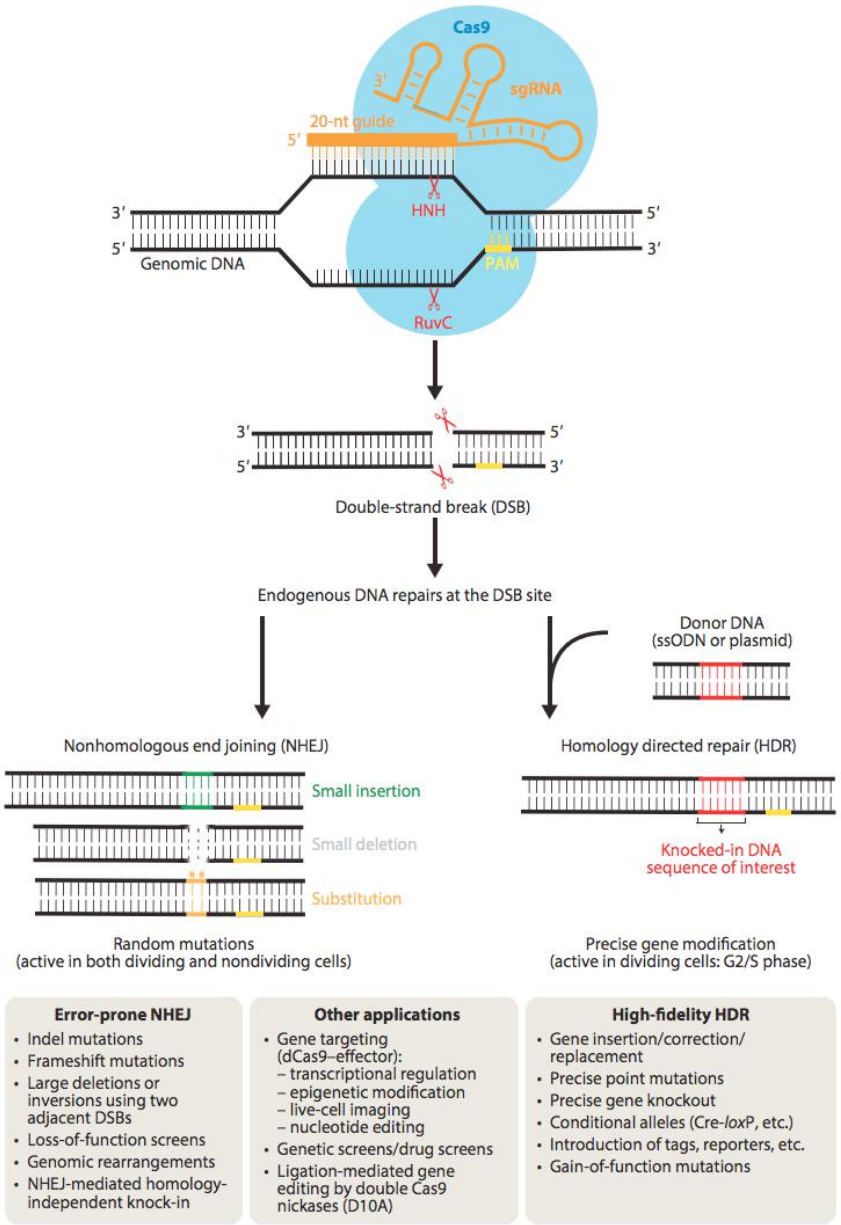

Figure 12. Mechanism of CRISPR-Cas9 technology. The synthetic sgRNA structure directs the Cas9 endonuclease to a DNA target sequence and further guides Cas9 to introduce a double-strand break (DSB) on a target genomic DNA locus. The DSB generated by two distinct Cas9 nuclease domains is repaired by host-mediated DNA repair mechanisms. In the absence of a repair template, the prevalent error-prone non-homologous end-joining (NHEJ) pathway is activated and causes random insertions and deletions (indels) or even substitutions at the DSB site, frequently resulting in the disruption of gene function. In the presence of a donor template containing a sequence of interest flanked by homology arms, the error-free homology directed repair (HDR) pathway can be initiated to create

desired mutations through homologous recombination, which provides the basis for performing precise gene modification, such as gene knock-in, deletion, correction, or mutagenesis (Jiang and Doudna, 2017).

CRISPR-Cas9 single guide RNAs (sgRNAs) targeting exon 7 of *DSP* gene were designed using the CRISPR design tool (http://crispr.mit.edu./) and cloned in the pX458 plasmid (pSpCas9(BB)-2A-GFP, Addgene plasmid # 48138). To perform genome editing, a suspension of $5x10^6$ HaCaT wild type cells were nucleofected using the Amaxa® Cell Line Nucleofector ® Kit V (Lonza) with 2,5 µg of pX458 plasmid containing the most efficient sgRNA (sgRNA_*DSP*: 5'-CACCAACATCGCTCAGAAAC-3'), 0,5 µM of single stranded oligo DNA nucleotide (ssODN) (ssODN_*DSP*: 5'-TGGATCAATGACTGCGAGGAGGAGGAGCTGCTGTACGACTGGAGCGACAAGAACACA AAC**T**TCGCTCAGAAACAGGAGGCCTTCTCCGTAAGTTCACCCCACGCGGCTGTAGATG CTTGT-3') using the 4D Nucleofector™ X Unit (Lonza, Italy) device following the manufactures' instructions. The employed sgRNA_*DSP* and ssODN_*DSP* sequences were kindly provided by Prof. Michele Boniotto (Insitute Mondor de Recherche Biomédicale, Cretéil, Paris, France).
Next, transfected HaCaT cells were seeded in a T75 culture flask and rescued for 2 days in low-calcium complete growth medium to allow cellular stabilisation. Cells were then detached using TrypLE™ Express (Gibco, ThermoFisher Scientific, Italy), centrifuged at 300 x g for 7 minutes and resuspended in 1 mL of Dulbecco's Phosphate Buffered Saline (DPBS, EuroClone, Italy). In order to study the genetic variant of interest, the mutant clones were isolated from the pool of nucleofected cells to isolate single-cell clones. Specifically to this end, single GFP-positive cells were dispensed in each well of fifteen 96 multi-well plates using the BDFACSAria™ III sorter (BD Biosciences-US).

Screening and selection of single cell-derived DSP clones

Single cell-derived *DSP* clones were passaged multiple times until sufficient cells were available for screening through the analysis of genomic DNA and RNA.
DNA was extracted with Yolk Sac Lysis Buffer (10 mM Tris-HCl pH 8.3, 50 mM KCl, 2 mM $MgCl_2$, 0,45% IGEPAL CA-630, 0,45% Tween-20) supplemented with 20 mg/mL of Proteinase-K (Promega). Briefly, samples were lysed with Yolk Sac Lysis Buffer, incubated at 60 °C for 4 hours and heated at 95 °C for 10 minutes to inactivate Proteinase-K. PCR amplification of extracted DNA was performed using the KAPA2G Fast HotStart Ready Mix (KAPA Biosystems) using primers encompassing the CRISPR-targeted region (*DSP*_forward primer: 5'-

TCCAGGGAGATCATGTGGAT-3'; *DSP*_reverse primer: 5'-GGAAGGATTTTTCACGACCA-3') (Eurofins Genomics, Germany).

The employed protocol and PCR program are reported below:

KAPA2G Fast HotStart Ready Mix	6,25 µL
*DSP*_forward primer (10 µM)	0,625 µL
*DSP*_reverse primer (10 µM)	0,625 µL
H2O	4,25 µL
Genomic DNA (50 ng)	0,75 µL
Final volume of reaction	12,5 µL

Step	Temperature	Time (min.)	Number of cycles
Initial denaturation	95 °C	3:00	1
Denaturation	95 °C	0:10	
Annealing	55 °C	0:10	40
Extension	72 °C	0:05	
Final extension	72 °C	1:00	1
	4 °C	Hold	

Sanger sequencing of DNA amplification products was performed by Eurofins Genomics (Eurofins, Germany). The obtained chromatograms were analysed using the CodonCode Aligner Software (Version 8.0.2, LJ-COR Inc.).

In addition, total RNA from selected CRISPR-edited single cell clones was extracted with TRIZOL Reagent (Invitrogen, Life Technologies, Carslbad USA) following the manufacturers' protocol. At the end of the procedure, RNA pellets were air-dried and dissolved in an appropriate volume of RNase-free water. The concentration and purity of each sample was assessed using the NanoDrop® ND-1000 (Celbio). 2 µg of total RNA per 20 µL reaction, were reverse transcribed into single-stranded cDNA using the High Capacity cDNA Reverse Transcription Kit with RNase inhibitor (Applied Biosystems® Thermo Fisher, Monza, Italy).

The following reverse transcription protocol and program were used:

10x RT-Buffer	2 µL
10x Random Primers	2 µL
25x dNTP Mix (100 mM)	0,8 µL
Oligo-d(T)	0,5 µL
Multiscribe™ Reverse Transcriptase	1 µL
RNase Inhibitor	1 µL
RNA (2 µg) diluted in RNase-free water	12,7 µL
Final volume of reaction mixture	20,0 µL

Step	Temperature	Time (min.)
Primer annealing	25 °C	10:00
DNA polymerization	37 °C	120:00
Enzyme deactivation	85 °C	5:00
	4 °C	Hold

Next, cDNA sequences were amplified using the KAPA2G Fast HotStart Ready Mix (KAPA Biosystems) and primers that recognise exons flanking the CRISPR-targeted exons (*DSP*_cDNA_forward primer: 5'-AAAGGGCGGAGATGGACA-3'; *DSP*_cDNA_reverse primer: 5'-AACTGAAAGTAGGCAGCATTTTCT-3') (Eurofins Genomics, Germany).

cDNA samples were amplified using the protocol and program reported below:

KAPA2G Fast HotStart Ready Mix	6,25 µL
*DSP*_cDNA_forward primer (10 µM)	0,625 µL
*DSP*_cDNA_reverse primer (10 µM)	0,625 µL
H2O	4,25 µL
cDNA (non-diluted)	0,75 µL
Final volume of reaction	12,5 µL

Step	Temperature	Time (min.)	Number of cycles
Initial denaturation	95 °C	3:00	1
Denaturation	95 °C	0:10	
Annealing	58 °C	0:10	40
Extension	72 °C	0:10	

Final extension	72 °C	1:00	1
	4 °C	Hold	

Sanger sequencing of cDNA amplification products was performed by Eurofins Genomics (Eurofins, Germany). The obtained chromatograms were analysed using the CodonCode Aligner Software (Version 8.0.2, LJ-COR Inc.).

3.5.3 Western Blot

HaCaT wild type and HaCaT *DSP* genome-edited clones were cultured at a density of $2x10^5$ cells/well in 6 well plates. 24 hours after seeding, cells were washed briefly in PBS and lysed on ice with RIPA buffer (Pierce™ RIPA Buffer, Thermo Scientific) and protease inhibitor cocktail (Halt™ Protease Inhibitor Cocktail, Thermo Scientific). Lysates were centrifuged at 14,000 x g for 10 minutes at 4 °C to eliminate cell debris and quantified using Bradford assay (Biorad, Hercules, USA) following the manufactures' protocol.
30 µg of protein extracts were loaded on 4-20% Tris-Tricine gels (BioRad) and separated by SDS-PAGE. Proteins were transferred on a nitrocellulose membrane (Nitrocellulose Blotting membrane, Amersham™ Protran™ Premium 0,2 µm NC, GE Healthcare Life Sciences) by performing a wet transfer in ice cold transfer buffer (0,25 M Trisbase, 1,92 mM glycine, 20% methanol, pH 8.3) for 90 minutes at 0,30 mA at 4 °C.
Membranes were probed with primary antibodies and were developed with HRP-conjugated secondary antibodies and Clarity™ substrate (BioRad, Hercules, USA).
The primary antibodies used to assess DSP expression levels include: anti-DSP (MABT1492, Millipore); anti-Hsp90 (Santa Cruz Biotechnologies, Dallas, USA).
Protein signals from membranes were acquired using the ChemiDoc™ Imaging system (BioRad) and data were analysed using the Quantity One software (version 4.6.6, BioRad).

3.5.4 RNA isolation and semi-quantitative real-Time PCR

HaCaT wild type and HaCaT *DSP* genome-edited clones were cultured at a density of $2x10^5$ cells/well in 6 well plates. 24 hours after seeding, total RNA was extracted and reverse transcribed in single stranded cDNA using the reagents, protocols and programs reported in section 3.5.2 *Screening and selection of single cell-derived DSP clones*.
Next, semi-quantitative real-time PCR was performed using the Taqman Gene Expression assay for human *DSP* (HS00950591_m1) gene and human *ACTB* (HS99999903_m1), used as endogenous control (Applied Biosystems® Thermo Fisher, Monza, Italy). The PCR amplification cycle was

performed with the ABI 7500 Real-Time PCR platform (Applied Biosystems® Thermo Fisher, Monza, Italy).

The protocol and program used to perform the semi-quantitative Real-Time PCR reaction is reported below:

cDNA diluted in water	2 µL
Taqman Gene Expression Master Mix (Applied Biosystems)	5 µL
Assay	0,5 µL
H_2O	3,5 µL
Final volume of reaction	11 µL

Step	Temperature	Time	Number of cycles
Denaturation	95 °C	10:00	1
Denaturation	95 °C	0:15	40
Annealing/elongation	60 °C	1:00	
	4 °C	Hold	

Results are indicated as the fold increase of the relative quantitative values (RQ) where RQ= $2^{(-\Delta\Delta Ct)}$. All samples were analysed in triplicate using the SDS 1.4 software (Applied Biosystems® Thermo Fisher, Monza, Italy).

3.5.5 Immunocytochemistry (ICC) for the detection of hyper-adhesive desmosomes

In order to evaluate hyper-adhesive calcium independent desmosomes, HaCaT wild type and HaCaT *DSP* genome-edited clones were seeded at $3x10^5$ cells/well in 6 well plates in low-calcium complete growth medium and grown on sterile glass coverslips coated with poly-L-lysine. Once cells reached 95% confluency, low-calcium complete growth medium was replaced by high-calcium calcium complete growth medium over night. Next, cells were incubated for 90 minutes in low-calcium complete growth medium supplemented with 3 mM EGTA (Sigma-Aldrich) to retrieve only hyper-adhesive desmosomes (Kurinna et al., 2014). Cells were then fixed using a mixture with an equal ratio of ice-cold methanol and acetone (1:1) for 10 minutes at room temperature, washed in PBS, permeabilized for 20 minutes at room temperature with 0,5% TritonX100 (Sigma Aldrich) diluted in PBS and blocked in blocking buffer (3% bovine serum albumin (BSA) dissolved in PBS) for 1 hour at room temperature. Coverslips were incubated 3 hours at 37 °C with anti-DSP (MABT1492, Millipore) and anti-phalloidin (DyLightTM 554 Phalloiding #13054, Cell Signaling

Technologies) primary antibodies diluted in blocking buffer, followed by 1 hour incubation at room temperature with anti-mouse Alexa Fluor 488 secondary antibody (A11029, Invitrogen, Thermo Fisher Scientific, Waltham, Massachusetts) and anti-mouse Alexa Fluor 568 secondary antibody (A11004, Invitrogen, Termo Fisher Scientific, Waltham, Massachusetts). A mounting medium with 4',6-diamidino-2-phenylindole (DAPI) (H1300, Vectashield, Burlingame, California) was employed to seal coverslips on glass slides (Superfrost, 10143560, Thermo Fisher Scientific).
In order to quantify hyper-adhesive calcium independent desmosomes, DSP *puncta*/cell were counted. Images were acquired using the Cytation 5 Cell Imaging Multi-Mode Reader (BioTek): 10 random fields of view were counted for each sample with a 60x objective and acquired as a stack of 10-15 images with a depth field of 10 µm and each image was separated by 0.5 µm. Using the instruments' 'Z-stack Projection' plugin, image stacks were averaged to a single two-dimensional image.

3.5.6 Transmission Electron Microscopy (TEM)

HaCaT wild type and HaCaT *DSP* genome-edited clones were cultured in T75 culture flasks until a confluence of 95-100% was reached. For the differentiation of HaCaT keratinocytes, the complete growth medium was supplemented with calcium chloride (99.99% anhydrous powder, Sigma-Aldrich), in order to obtain a high-calcium complete growth medium with a final calcium concentration of 2.8 mM. The HaCaT cells are maintained in a high-calcium complete growth medium for 10 days, replacing the growth medium every day. Next, high-calcium complete growth medium was removed and cells were washed twice in 0.12 M phosphate buffer solution pH 7.4 (monobasic sodium dihydrogen orthophosphate NaH_2PO_4 0.24 M solution, dibasic disodium hydrogen orthophosphate Na_2HPO_4 0.24 M solution). Cells were then fixed using a primary glutaraldehyde fixative solution (2% glutaraldehyde and 4% paraformaldehyde diluted in 0.12 M phosphate buffer solution pH 7.4) for 10 minutes at room temperature, washed twice in 0.12 M phosphate buffer solution pH 7.4, scraped free using a rubber-policeman and centrifuged at 10,000 x g for 10 minutes at room temperature. Next, the supernatant was discarded and fresh primary glutaraldehyde fixative solution was added to pellets overnight. Afterwards, the primary glutaraldehyde fixative solution was removed and cells were washed twice in 0.12 M sodium cacodylate buffer solution pH 7.4 (Sodium Cacodilate, Sigma-Aldrich). Samples were then subjected to a further fixation using the secondary oxium tetroxide fixative solution (oxium tetroxide 1% diluted in 0.12 M sodium cacodylate buffer solution pH 7.4) and washed two times in 0.12 M sodium cacodylate buffer solution pH 7.4. Dehydration of samples was performed using increasing concentrations of ethanol (50% (v/v), 70% (v/v), 90% (v/v), 100% (v/v)) and specimens

were then embedded in 100% epoxy resin (epon 812 kit, Sigma-Aldrich) for 48 hours. Next, samples were placed in the tip of Beem capsule filled with 100% fresh epossidic resin, and polimeryzed in an oven at 70 °C for 12-24 hours. At the end of the incubation period, the block was trimmed and ultrathin sections (0.5-1.5 μm) were cut using an ultramicrotome and collected on a grid. Grids were stained with 5% uranyl acetate solution, washed, stained in Reynolds lead citrate solution and washed.
High resolution TEM images were acquired by Media System Lab using a low voltage electron microscope (LVEM 25, Delong instruments) through the usage of a low-noise and high sensitivity 5.5MP scientic CMOS camera for imaging.

The staff of the immune genetic laboratory of the IRCCS Burlo Garofolo of Trieste, together with the PhD student, actively coordinated the execution of the experimental procedure and were directly involved in the interpretation of acquired data.

3.5.7 Proliferation assay

Proliferation assay was performed using the carboxyfluorescein succinimidyl ester (CFSE, 21888, Sigma-Aldrich, Saint Louis, Missouri) following the manufactures' instructions. Briefly, before plating, cells were counted so as to obtain $2x10^5$ cells/well to be subsequently seeded in 6-well plates. Next, counted cells were washed in PBS and centrifuged at 300 x g for 7 minutes. At the end of the centrifugation, cell pellets were thoroughly dried and incubated at room temperature for 10 minutes in the dark with 5 μM of CFSE dissolved in PBS. At the end of the incubation period, an equal volume of low-calcium complete growth medium was added for other 5 minutes. Then, cells were washed in PBS, resuspended in low-calcium complete growth medium and seeded in 6-well plates. After 24, 48 and 72 hours from plating, cells were harvested, fixed with 4% paraformaldehyde and the fluorescent signal was acquired using the MACSQuant® Analyzer 10 cytofluorimeter (Miltenyi Biotec). Results are expressed as the mean fluorescent intensity (MFI) of CFSE probe (λ_{EM}525nm) and collected data were analysed with the FlowLogic software (version 7.2.1, Inivai Technologies). Each condition was analysed in triplicate.

3.6 Statistical analysis

The Prism 6.0 software (GraphPad Software, La Jolla, California, USA) was used to perform statistical analysis. All statistical assessments were two-sided, and a p value < 0.05 was used for the rejection of the null hypothesis. The Mann–Whitney *U test* was employed to evaluate differences amongst all the analysed samples.

Part 2: The case of a Sardinian family

3.7 Patients

A Sardinian family affected by a familiar form of HS was recruited thanks to a cooperation with the Dermatology Department of the Fondazione IRCCS Ca' Granda Ospedale Maggiore Policlinico of Milan. All the enrolled individuals signed a written informed consent previously approved by the Comitato Etico Unico Regionale (CEUR) of Friuli Venezia Giulia (FVG) (RC 16/18, Prot. N.0001094 (14/01/2019), CEUR-2018-Sper-127-BURLO). A total of 47 family members were enrolled in the study, 11 of which decleared to be affected by HS (HS35, HS40, HS53, HS71, HS74, HS80, HS81, HS103, HS108, HS111, HS115) (Table 1).

HS	Age	Sex
35	50	F
40	36	F
53	24	F
71	81	F
74	48	F
80	24	M
81	22	F
103	80	F
108	85	F
111	50	F
115	24	M
31	83	F
33	60	M
34	57	F
36	51	F
37	47	F
38	67	M
39	41	M
41	43	F
42	13	F
46	10	M

47	58	M
50	21	F
51	52	M
52	30	F
62	82	F
63	60	M
72	84	M
73	55	F
76	52	M
77	37	M
78	24	F
79	50	M
105	47	F
106	54	M
107	24	F
109	87	M
110	58	F
112	47	M
113	65	M
114	28	M
116	22	M
117	19	M
118	26	F
120	22	M
121	26	F
122	15	F

Table 1. Sardinian family. List of the 47 family members that were enrolled in the study reporting age and sex. In orange are indicated those family members who declared to be affected by HS at the beginning of the study.

In addition, affected family members, together with individuals resulting positive for genetic testing, were subjected to a questionnaire that takes into account age, sex, body mass index (BMI), everyday habits (smoke, diet), the history of the disease, the presence of other correlated pathologies and therapies.

3.8 Genetic tests

3.8.1 Genomic DNA extraction from saliva

Genomic DNA from enrolled individuals was extracted from saliva following the same procedure reported in the section 3.2.1.

3.8.2 Sanger sequencing for the identification of mutations in *NCSTN, PSENEN* and *PSEN-1*

NCSTN, PSENEN and *PSEN-1* genes were amplified using the KAPA2G Fast HotStart Ready Mix (KAPA Biosystems) using the primers indicated in Table 2 (Eurofins Genomics, Germany).

Gene	Exon	Forward primer	Reverse primer	Annealing (°C)
NCSTN	1	5'-ACACGAACTTCCGGTCTCTTAG-3'	5'-GAAAGAGGATTTACAGGGTGGG-3'	60
NCSTN	2	5'-AGTGTGTGCCCAAGAAATCAG-3'	5'-ATCTTGCCTAGCTTGACAGACG-3'	60
NCSTN	3	5'-CTAGAGGTGCCTGTATTCACCC-3'	5'-CTTTCCTTCTGAGGACCACCC-3'	61
NCSTN	4	5'-TAAGTCAACAGTTTGATTCCCC-3'	5'-TGAGCAGCAAAGACAAATAAACAC-3'	59
NCSTN	5	5'-TTGAGTCACCACCTCCTTTTG-3'	5'-GCCTCAAGTGATCCTCCTGTC-3'	60
NCSTN	6 to 7	5'-GGATAAATGTCTCCGAAAAGGG-3'	5'-AAGAGAATATACCTGTCCTGTGGC3'	60
NCSTN	8	5'-TAAATTGGGAAGCCTCAAATG-3'	5'-TGGAGGAATCTAAAGGGGAGAC-3'	60
NCSTN	9 to 10	5'-GCTGACTAGCAGTTGAGGTGAC-3'	5'-TCCAATCCTGTCTCTTACCCTG-3'	59
NCSTN	11	5'-AAAGGCTTGAGGGATAAAGGTC-3'	5'-GATGGACCTGAAGTTCTGGAG-3'	59
NCSTN	12 to 13	5'-CTCTCACCCCTTTCTTCTGATG-3'	5'-ATTCTCACCGGCATCAACAGTC-3'	61
NCSTN	14 to15	5'-TCTCCCAACTCCAGTCTATCTG-3'	5'-CTGAGGACTGCATCTCTCCAC-3'	59
NCSTN	16	5'-TAAAGGGACAGCAGCCAGTTAG-3'	5'-CAGGGACAGATTTGCAGTAGG-3'	60
NCSTN	17	5'-GGAGACAAAGTCTGTAGGCTGG-3'	5'-GGCTCAATGTAGTTTGACCCTG-3'	60
PSENEN	1 to 2	5'GCTCTTTAATCCAGCCAGCTTAC-3'	5'CTCTCTTGGGATCCAGAAATTG-3'	60
PSENEN	3 to 4	5'- CAGAAATCTCCATTTGAACTTG-3'	5'GGGACATGAAAACAAGTCTTAGG-3'	59
PSEN-1	1	5'-AGGTGGAGCTCTGGGTTCTCC-3'	5'-ATCTTTTAGGACACCGGCTTCG -3'	63
PSEN-1	2	5'CTTATTGCTAAAGAGGTCTACCTTGAG-3'	5'-GTAGAGAAAGCCTGCCTAGCCC-3'	60
PSEN-1	3	5'-GAAAGGTTTGTTTCTGCTTAATG -3'	5'-AAAGTAGAGAAAGCCTGCCTAGC -3'	58
PSEN-1	4	5'-AAGACCCAGGTAAAAGAGAGGAC-3'	5'- AACATGAAGTAATAACCCCTCGC-3'	59
PSEN-1	5	5'-TGAAGCAATTTTAGAGTGTAGCTG-3'	5'- ATTACACATGCACCTGGCTTC-3'	59

PSEN-1	6	5'- ACCAATATCTAGGTAAAGCCATTC-3'	5'-TTATAAGCAAGGAGCAACAGAAG-3'	57
PSEN-1	7	5'-AATAGCACAGTTGATATAGGTTATGG-3'	5'- TGAAGAGTTATGGGATGTACACG-3'	58
PSEN-1	8	5'-TCACCTGCCATTTATTTCATATTC-3'	5'-AGAGATCTGCAGGAGTTCCAGG-3'	60
PSEN-1	9	5'- CTTAAGGCAGCATTAGGAAGAC-3'	5'-TGACTGTATTGTTGGGTTTTGAG-3'	58
PSEN-1	10	5'-AGCTTTTGTTAGGAAGAGGCTTG-3'	5'- CCAAAAGGTCAGGCTGTAAAATG-3'	61
PSEN-1	11	5'-AACACAGCTGAAGCCTAATTTTG-3'	5'CAGATAGCTGGAATATTTAACCCAC-3'	59
PSEN-1	12	5'-TTCTTCCAGATTGAATGAACGTC-3'	5'- ATAGTGCAAGGTGGTCAGGAAG-3'	60

Table 2. List of primers used to amplify *NCSTN, PSENEN* and *PSEN-1* genes, including the name of the gene, the targeted exonic regions, the sequences of the forward and reverse primers, and the temperature of annealing (Annealing (°C)) for each set of primers.

The PCR protocol and program employed for the amplification of target sequences using each set of primers, followed the same protocol described in section 3.2.3.

Sanger sequencing of DNA amplification products was performed by Eurofins Genomics (Eurofins, Germany). The obtained chromatograms were analysed using the CodonCode Aligner Software (Version 8.0.2, LJ-COR Inc.).

3.8.3 Whole exome sequencing (WES) and data analysis

Whole exome sequencing analysis was performed using the same procedure described in section 3.2.2.

3.8.4 Sanger sequencing for the screening of the selected variants identified by WES

Genomic DNA samples were amplified using the KAPA2G Fast HotStart Ready Mix (KAPA Biosystems) using the primers (Eurofins Genomics, Germany) reported below (Table 3):

Gene	Forward primer	Reverse primer	Annealing (°C)
NEB	5'- CAATGAGCCAAAACTGATGC-3'	5'-ACATGCAAAAACCACAGAGC-3'	55
ANKAR	5'- CTTGCTCCCTCCCTTACAGA-3'	5'- CCACCAGTGTTTGTTGCATT-3'	55
FAM126B	5'-CAACCCCAATGCTGGTACTT-3'	5'- GGATTTTCATCAGGGGCTTC-3'	58
DNAH6	5'-TTTCAGGAACAAACAAAATTGA-3'	5'-ACTGGGAGAGGGCTCCTAA-3'	55

PDE11A	5'-CCCTGGAAATGTCTCCTCAA-3'	5'-TTGATTGTGATTTGCGAAGG-3'	55
SCN7A	5'-CGGCGCTGATTTACTTCCT-3'	5'- GTCCCAAAGGACACAATGGA-3'	55
IL18RAP	5'- AGCAGGAGGCATAACAGTGG-3'	5'- GCCCAACAATAAGGCAGAAC-3'	58
LRIG1	5'-CTCCCAACCCACCTGTTAGA-3'	5'- TGTTACTCCAGGGGACAAGC-3'	58
IBSP	5'-CGCCAATGAATACGACAATG-3'	5'-GATGCAAAGCCAGAATGGAT-3'	55
ALB	5'-GGAGGTTCTGGGGAGAATGT-3'	5'-TTTTGACCATGTCGGAAAGTT-3'	55
ARHGEF37	5'-GTCCGTGACATCCACTTTCC-3'	5'-TTCCCAGCACCTCAATCTCT-3'	58
HDDC2	5'-CTTTGGGGATGTTATCTGCTG-3'	5'-ACTCTGTGAGGGTGGAGAAAAA-3'	58
ZNF318	5'-AACATGCACCTGACTGCAAC-3'	5'-AGGAACGACTTCATGGCAAG-3'	58
FAM26F	5'- TTGGGCTGGATCTTGATAGC-3'	5'-GGCCCTTCGGATTGAAAGTA-3'	58
NDUFAF6	5'-AACTGCTGGTGTTGCTTTCA-3'	5'-TGCAAAGTCCGTGCTAAAAA-3'	55
PRUNE2	5'-CCCTCACTTCTTCGATCAGG-3'	5'- AACACATCCACGGGAACAAT-3'	55
DMRT3 g. 977056	5'- AAGGGAGCTGGAGAGACGAC-3'	5'-TCGATGATGAGGATGCACTT-3'	60
DMRT3 g.111956226	5'- CCCAGACACGTTGAGGTTTT-3'	5'- ACTGGCTTCTCGCCAAAGTA-3'	58
ATXN2	5'- TCGGGTTGAAATCTGAAGTG-3'	5'- GATGAGAATGAGCACGCATC-3'	55
FOXM1	5'- GCAAGCTGAAGGTCCAACAT-3'	5'- CACCTCAAAGGGATCTGAGC-3'	58
KIAA1033	5'- CAATGGAGGAGTATCTGTGTCA-3'	5'- TGCAATCTTTTTAATCTGCTCA-3'	55
DOCK9	5'- AAGATAGCCCGAAGGAAGGT-3'	5'- ACGGTTTTACATTGGCTTGC-3'	55
MMP15	5'- GGTACGAGTGAAAGCCAACC-3'	5'- TGGTCTCATCAGCGTGAAAG-3'	58
LLGL1	5'- GCCTCAAGTCATCCACCTATG-3'	5'- AAGTCATCAGCCCCTACCAG-3'	58
SDK2	5'- CCCAGGACATTGGAGAGAAC-3'	5'- GGTGGAGGTGGAGAAGTTGA-3'	59
SPAG5	5'- CCTCCTGAGAGAGCCACACT-3'	5'- TGGTTTGCTTTTGTTCACCA-3'	55
CD3EAP	5'- AAAAGGGACAGATGGCAATG-3'	5'- GGCAGTTCAGGCTCTAGTGG-3'	55
KIF16B	5'- GACTTTCCAGATCCAGTTTGC-3'	5'- AGAGGATGGGGCTGCTTT-3'	56
TSHZ2	5'- AAAGTCGTGAAAAGCGAGGA-3'	5'- CTTTGTTGATGGCTGTGGTG-3'	55

Table 3. List genes deriving from WES analysis, including the name of the gene, the primer sequences and the temperature of annealing (Annealing (°C)) for each set of primers.

The PCR protocol and program employed for the amplification of target sequences using each set of primers, repeated the procedures described in section 3.2.3.
Sanger sequencing of DNA amplification products was performed by Eurofins Genomics (Eurofins, Germany). The obtained chromatograms were analysed using the CodonCode Aligner Software (Version 8.0.2, LJ-COR Inc.).

3.9 *In vitro* assays

3.9.1 Cell culture

In vitro functional studies were performed on spontaneously immortalised human keratinocyte line, HaCaT cells, that were cultured in low-calcium complete growth medium as described in section 3.5.1.

3.9.2 Genome editing of *ZF318* gene with CRISPR-Cas9 technology

CRISPR-Cas9 single guide RNAs (sgRNAs) targeting exon 4 of *ZF318* gene were designed using the CRISPR design tool (http://crispr.mit.edu./) and cloned in the pX458 plasmid (pSpCas9(BB)-2A-GFP, Addgene plasmid # 48138). To perform genome editing, a suspension of $5x10^6$ HaCaT wild type cells were nucleofected using the Amaxa® Cell Line Nucleofector ® Kit V (Lonza) with 2,5 µg of pX458 plasmid containing the most efficient sgRNA (sgRNA_*ZNF318*: 5'-GGTCAGACTTTAGGAATGGA-3'), 0,5 µM of ssODN (ssODN_*ZNF318*: 5'-CTCTCCAGAGGTGTCCCATCCACACCCACCTTCTCCTGTGGATCCTTACCTGCTCACAA**T**AAACTCTCCTCCATTCCTAAAGTCTGACCATCCAGTGGGTCATATTTCAGGACCA-3') using the 4D Nucleofector™ X Unit (Lonza, Italy) device following the manufactures' instructions. The employed sgRNA_*ZNF318* and ssODN_*ZNF318* sequences were kindly provided by Prof. Michele Boniotto (Insitute Mondor de Recherche Biomédicale, Cretéil, Paris, France).

Next, single GFP-positive cells were dispensed in each well of fifteen 96 multi-well plates using the BDFACSAria™ III sorter (BD Biosciences-US) following the protocol described in section 3.5.2.
Screening and selection of single cell-derived ZNF318 clones.

Single cell-derived *ZNF318* clones were passaged multiple times until sufficient cells were available for screening through the analysis of genomic DNA and RNA.
DNA was extracted with Yolk Sac Lysis Buffer by performing the same procedure reported in section 3.5.2. PCR amplification of extracted DNA was performed using the KAPA2G Fast HotStart Ready Mix (KAPA Biosystems) using primers encompassing the CRISPR-targeted region

(*ZNF318*_forward primer: 5'-AACATGCACCTGACTGCAAC-3'; *ZNF318*_reverse primer: 5'-AGGAACGACTTCATGGCAAG-3') (Eurofins Genomics, Germany). The PCR protocol and program employed for the amplification of target sequences using each set of primers, repeated the procedures described in section 3.5.2, using an annealing temperature of 60 °C.

Sanger sequencing of DNA amplification products was performed by Eurofins Genomics (Eurofins, Germany). The obtained chromatograms were analysed using the CodonCode Aligner Software (Version 8.0.2, LJ-COR Inc.).

In addition, total RNA from selected CRISPR-edited single cell clones was extracted with TRIZOL Reagent (Invitrogen, Life Technologies, Carslbad USA) following the manufacturers' protocol. RNA was quantified and reverse transcribed into single-stranded cDNA using the same protocol and program applied in section 3.5.2.

Next, cDNA sequences were amplified using the KAPA2G Fast HotStart Ready Mix (KAPA Biosystems) using primers that recognise exons flanking the CRISPR-targeted exons (*ZNF318*_cDNA_forward primer: 5'-ATGCGAAGATCCATGACTTG-3'; *ZNF318*_cDNA_reverse primer: 5'-TTCAATAACCTTTTGCTTCTGG-3') (Eurofins Genomics, Germany). cDNA samples were amplified using the protocol and program described in section 3.5.2, using an annealing temperature of 58 °C and an extension phase of 15 seconds.

Sanger sequencing of cDNA amplification products was performed by Eurofins Genomics (Eurofins, Germany). The obtained chromatograms were analysed using the CodonCode Aligner Software (Version 8.0.2, LJ-COR Inc.).

3.9.3 Western Blot

Western Blot assay on HaCaT wild type and HaCaT *ZNF318* genome-edited clones, followed the same methods reported in section 3.5.3.

The primary antibodies used to assess ZNF318 expression levels include: anti-ZNF318 (Sigma-Aldrich); anti-Hsp90 (Santa Cruz Biotechnologies, Dallas, USA).

3.9.4 RNA isolation and semi-quantitative real-Time PCR

HaCaT wild type and HaCaT *ZNF318* genome-edited clones were cultured at a density of $2x10^5$ cells/well in 6 well plates. 24 hours after seeding, Total RNA was extracted and reverse transcribed in single stranded cDNA using the protocols and programs reported in section 3.5.2.

Next, semi-quantitative real-time PCR was performed using the Taqman Gene Expression assay for human *ZNF318* (HS00204987_m1) gene and human *ACTB* (HS99999903_m1), used as endogenous control (Applied Biosystems® Thermo Fisher, Monza, Italy). The platform, protocol

and program assessed to perform the semi-quantitative Real-Time PCR reaction is described in section 3.5.4.

Results are indicated as the fold increase of the relative quantitative values (RQ) where RQ= $2^{(-\Delta\Delta Ct)}$. All samples were analysed in triplicate using the SDS 1.4 software (Applied Biosystems® Thermo Fisher, Monza, Italy).

3.10 Statistical analysis

The Prism 6.0 software (GraphPad Software, La Jolla, California, USA) was used to perform statistical analysis. All statistical assessments were two-sided, and a p value < 0.05 was used for the rejection of the null hypothesis. The Mann–Whitney *U test* was employed to evaluate differences amongst all the analysed samples.

Part 3: The case of a Friulian family

3.11 Patients

Thanks to the Biomolecular Analyses for Tailored Medicine in AcneiNversa (BATMAN) project, funded by ERA PerMed and by a grant from the Institute for Maternal and Child Health IRCCS 'Burlo Garofolo' (RC 16/18), a Friulian family affected by HS was recruited. HSM58 is a 50 year old male with a diagnosis of HS and Hurley stage I disease, who was also diagnosed with other comorbidities including celiac disease and dyslipidemia, who developed the first clinical signs of HS at 22 years of age. HSM64, the father of HSM58, is a 77 year old man affected by HS, who further reported to be subjected to the onset of relapsing furuncles and to have undergone two surgical treatments for the removal of dermal abscesses during his adolescence. D_HSM58, the daughter of HSM58, is 11 years old and her parents revealed she is starting to manifest relapsing inguinal furuncles. M_HSM58, the mother of D_HSM58, was also recruited in the study and she reported not to be affected by any known pathology (Table 4). All participating individuals signed a written informed consent previously approved by the Comitato Etico Unico Regionale (CEUR) of Friuli Venezia Giulia (FVG) (RC 16/18, Prot. N.0001094 (14/01/2019), CEUR-2018-Sper-127-BURLO).

HSM	Age	Sex	Age of onset	Severity	Associated diseases
HSM58	50	M	22	Hurley satge I	Celiac disease and dyslipidemia
HSM64	77	M	Puberty	Hurley satge I	
D_HSM58	11	F	Started to manifest inguinal furuncles, not diagnosed yet		None
M_HSM58	47	F			None

Table 4. Table reporting the age, sex, age of onset of HS, the severity of the disease and the presence of associated disorders in the members of the Friulian family who adhered to the study.

3.12 Genetic tests

3.12.1 Genomic DNA extraction from saliva

Genomic DNA from enrolled individuals was extracted from saliva following the same procedure reported in the section 3.2.1.

3.12.2 Whole exome sequencing (WES) and data analysis

WES and data analysis was performed following the protocol described in section 3.2.2

3.12.3 Sanger sequencing for the confirmation of the selected variants identified by WES

Genomic DNA samples were amplified using the KAPA2G Fast HotStart Ready Mix (KAPA Biosystems) using the primers reported in Table 5 (Eurofins Genomics, Germany).

Gene	Forward primer	Reverse primer	Annealing (°C)
CDC42BPG	5'-ATCTCATCCCAGGCACTCAC-3'	5'-TCACCTCATCCACCTTCTCC-3'	59
TGM5	5'-GGCCGAGACATTTCAGAGAG-3'	5'-AAGAGTCAACCCCCATCCTT-3'	58
BNC1	5'-TTCTGGCTGTGTCTGTTTCG-3'	5'-TTCCGTGCAGCTTACCTTCT-3'	57
DCD	5'-CAACCTCTCTTCCCCACCTT-3'	5'-ACCAACCTTCCCATGACAGA-3'	59
LYSMD4	5'-TAGGACATCGCCAGTGACAG-3'	5'-ATCCTGATGGAGACCCACAA-3'	58

FGF22	5'-CGTGGTCATCAAAGCAGTGT-3'	5'-TCCCCAACTCAGGATTGAAC-3'	57

Table 5. List genes deriving from WES analysis, including the name of the gene, the primer sequences and the temperature of annealing (Annealing (°C)) for each set of primers.

The PCR protocol and program employed for the amplification of target sequences using each set of primers, is the same reported in section 3.2.3.
Sanger sequencing of DNA amplification products was performed by Eurofins Genomics (Eurofins, Germany). The obtained chromatograms were analysed using the CodonCode Aligner Software (Version 8.0.2, LJ-COR Inc.).

The first genetic variant addressed in the study is the one occurring in *DCD* gene, encoding for dermcidin (DCD) AMP. This AMP is found in human sweat where it exerts well established antimicrobial activities against both Gram-positive (*Staphylococcus aureus, Staphylococcus epidermidis, Staphylococcus lugdunensis, Enterococcus faecalis, Listeria monocytogenes*) and Gram-negative bacteria (*Escherichia coli, Pseudomonas putida, Salmonella typhimurium*), as well as *Candida albicans* (Burian and Schittek, 2015).

3.13 *In silico* studies

3.13.1 Comparative modelling

For three-dimensional (3D) modeling purposes, an alignment of each sequence was made against the Protein Data Bank (PDB) using the BLASTp tool to find the best template protein for constructing comparative models, where the dermcidins with the highest sequence identity and complete coverage of the conserved domain were selected. Using Modeller 10.1 Webb and Sali, 2014), one hundred models were constructed for each dermcidin sequence. The best model was chosen according to the discrete optimized protein energy (DOPE) score that accesses the model's energy and indicates the most probable structure. Finally, a further validation of the models was performed by analysing the quality of the folding and the stereochemistry of the models. Structural features of dermcidin, based on conserved sites, were accessed comparing 3D models using PyMOL software.

3.13.2 Molecular dynamics

The dermcidin peptides modelled in the previous step (3.13.1), were inserted in a 0.7 nm cubic box, filling the voided space with SPC-E water molecules. Calcium and sodium ions were added with the aim of reaching the system electronic equilibrium. Energy minimisation was carried out using default parameters. The equilibrium phase for temperature and pressure was carried out during 10 ns, while the production phase lasted 100 ns. Also, these steps were performed using default parameters. Molecular dynamics trajectories were performed unrestrained at constant pressure and temperature of 1 atm and 300 K. The LINCS method (Hess et al., 2008) was employed to constrain bonds involving hydrogen atoms. Integration analysis was carried out using the leapfrog algorithm with a 2-fs integration time step. Analysed systems were initially optimized for energy using 50,000 steps of the steepest descent algorithm. All atomistic simulations were performed for 100 ns using the force fields and periodic boundary conditions in the x, y, and z directions.
In order to investigate the stability and compaction of the complexes, Root-mean square deviation (RMSD), Root-mean square fluctuation (RMSF), B-factor, Radius of gyration (Rg) and Solvent accessible surface area (SASA) parameters were evaluated. All molecular dynamics simulations were performed using the GROMOS 53A6 (Oostenbrink et al., 2004).

3.13.3 Principal component analysis (PCA)

In order to define the main conformational changes of analysed systems during the simulation of molecular dynamics trajectories, the Principal component analysis (PCA) was performed. PCA studies were assessed using the trajectories previous simulations with the GROMACs package (anaeig). The technique was performed for α-carbon atoms during 100 ns, period of the dynamics simulation. The Cartesian coordinates of such atoms were used to generate the covariance matrix and the first two components were used to generate the graphic result.

In silico studies were performed thanks to a collaboration with Dr. Rodrigues de Moura (IRCCS Burlo Garofolo, Trieste). The PhD student was directly involved in the analysis and interpretation of retrieved data.

3.14 *In vitro* antimicrobial studies

3.14.1 Peptides

DCD wild type (DCD_WT) and DCD mutated (DCD_MT) peptides at >95% purity purchased from NovoPro Bioscience Inc. (Shangai, China), were resuspended in HCl 10 mM, vacuum-dried three times from HCl 10 mM, and resuspended in H_2O. The quality and purity of peptides was verified by ESI-MS (API 150 EX Applied Biosystems). The Concentration of each stock solution was assessed by spectrophotometric determination of tryptophan ($\epsilon_{280} = 5500\ M^{-1}\ cm^{-1}$) by measuring the differential absorbance at 215 nm and 225 nm (Waddell, 13346201), and by spectrophotometric determination of peptide bonds (ϵ_{214} calculated as described by Kuipers and Gruppen) (Kuipers and Gruppen, 2007).
In addition, DCD-1 and DCD1-L dermcidin-derived peptides, already available in the laboratory of Prof. Schittek (Department of Dermatology, University of Tübingen, Germany), were initially tested to compare their activity with DCD_WT custom peptide (Table 6).

Peptide	Sequence
DCD_WT	N-SSLLEKGLDGAKKAVGGLGKLGKDAVEDLESVGKGAVHDVKDVLDSV-C
DCD_MT	N-SSLLEKGLDGAKKSCGGTRKTRKRCSRRSRKRG-C
DCD-1	N-SSLLEKGLDGAKKAVGGLGKLGKDAVEDLESVGKGAVHDVKDVLDSV-C
DCD-1L	N-SSLLEKGLDGAKKAVGGLGKLGKDAVEDLESVGKGAVHDVKDVLDSVL-C

Table 6. Sequence of DCD_WT and DCD_MT custom peptides, together with DCD-1 and DCD-1L dermcidin-derived peptide controls.

3.14.2 Bacterial strains and culture conditions

Staphylococcus aureus (*S. aureus*, ATCC 25923), *Staphylococcus epidermidis* (*S. epidermidis*, ATCC 14990) and *Staphylococcus lugdunensis* (*S. lugdunensis*, ATCC 43809) were preserved in 1 mL cryovials containing 40 % glycerol and 60 % Luria Bertani broth (LB broth, Sigma-Aldrich) and stored at -20 °C. Two days before the assessment of the antimicrobial activity of peptides on planktonic bacteria, on the formation of biofilm and on pre-formed biofilm, bacterial strains were seeded on LB agar (Sigma-Aldrich) plates and grown at 37 °C overnight. The day before antimicrobial testing, for each strain one colony was withdrawn from LB agar plates using a sterile

10 µL microloop and resuspended in 5 mL of LB broth. Bacterial strains were incubated at 37 °C overnight under shaking conditions.

3.14.3 *In vitro* activity of DCD peptides against planktonic bacteria

For each bacterial strain, an initial standardised inoculum with a final test concentration of 1 x 10^8 CFU/mL was incubated with DCD_WT or DCD_MT or DCD-1 or DCD-1L peptides at 2 µM (20 µg/mL) final concentration. Following 3 hour incubation, 10-fold serial dilutions of bacterial suspensions were seeded on Tryptic Soy Broth (TSB, Sigma-Aldrich) plates and the number of colony forming units (CFU) was counted after incubation at 37 °C overnight.
DCD-1 and DCD-1L dermcidin-derived peptides were employed as positive controls to compare and validate the activity of the customised DCD_WT peptide.
The assay was performed by Prof. Schittek (Department of Dermatology, University of Tübingen, Germany) thanks to an on going cooperation on this topic.

3.14.4 *In vitro* activity of DCD peptides against biofilm formation

Inhibition of biofilm formation was evaluated against *S. aureus* in wells of a 96-well flat-bottom non-treated tissue-culture microtiter plate (Sarstedt, Germany), by adding 10 µl of a standardized inoculum, with a final concentration of 1-5 × 10^7 CFU/mL, to 100 µl of Brain Heart Infusion (BHI) broth (Sigma-Aldrich) supplemented with 2% sucrose containing DCD_WT or DCD_MT peptide at a 2 µM (20 µg/mL) final concentration. After incubation at 37°C for 24 h, non-adherent bacteria were removed by washing twice each well with 100 µl of sterile PBS (pH 7.2; Sigma-Aldrich S.r.l.). Incubation with methanol (Sigma-Aldrich) for 15 minutes at room temperature was performed to fix slime and adherent cells, that were then stained for 5 min at room temperature with 100 µl of 0,1% crystal violet solution (Sigma-Aldrich). The wells were then rinsed with distilled water and crystal violet solution was solubilised by adding 200 µl of 95% ethanol at room temperature for 30 minutes under shaking conditions. The absorbance reads were measured at 560 nm using the GloMax® Discover Microplate Reader (Promega). The low cut-off was represented by approximately 3 standard deviations above the absorbance mean of control wells (containing medium alone without bacteria).

3.14.5 *In vitro* activity of DCD peptides against pre-formed biofilm

Biofilms were allowed to form in each well of a 96-well flat-bottom non-treated tissue-culture microtiter plates as described in section 3.14.4. After 24 hours, biofilms were exposed to 100 µl of BHI broth supplemented with 2% sucrose containing DCD_WT or DCD_MT peptide at a 2 µM (20 µg/mL) final concentration. After incubation for 24 hours at 37 °C, biofilms were washed, stained with crystal violet solution and absorbance reads were acquired as previously reported in section 3.14.4.

3.15 Statistical analysis

Data analysis was performed by ordinary one-way analysis of variance (ANOVA) followed by Dunnett's multiple comparisons test (*$P < 0.05$; **$P < 0.01$; ***$P < 0.001$; ****$P < 0.0001$), comparing non treated (control) cells with the other experimental conditions. Results represent three independent experiments with at least four technical replicates ± SD. Statistical analysis has been conducted with Prism 6.0 software (GraphPad Software, La Jolla, California, USA).

4. RESULTS AND DISCUSSION

Part 1: The case of a PASH patient

1 **Genetic studies**

WES: Identification of a A>T missense exonic variant (rs17604693; g.7565494 A>T; c.913A>T; p.Ile305Phe) in exon 7 of *DSP* gene in homozygosis in HSM5.

Segregation of the variant in the family: evaluation of the segregation of the variant in F_HSM5 and M_HSM5, with Sanger sequencing. The proband was ultimately validated as homozygous for the SNV in *DSP*, while it was found in heterozygosis in F_HSM5 and in M_HSM5.

2 ***In silico* studies**

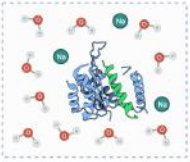

Study of the impact of the identified *DSP* variant (rs17604693) on protein structure.

Molecular dynamic (MD) procedures were performed in order to reproduce realistic behaviours of wild type DSP dimers, and of those carrying the variant in heterozygosis and in homozygosis, with the aim of retrieving detailed information relative to molecular movement and particle motion in function of time.

3 ***In vitro* and *ex vivo* functional studies**

A. **HaCaT *DSP* clones**

Generation of HaCaT *DSP* cellular clones using CRISPR-Cas9 and ssODN-mediated genome editing.

B. **Study of the impact of *DSP* SNV on the intracellular distribution of DSP**

IHC assays on skin biopsies derived from HSM5 and a healthy control matched per age and sex.

ICC for the detection of hyper-adhesive desmosome in HaCaT *DSP* clones.

C. **Study of the impact of *DSP* SNV on the morphology of desmosomes**

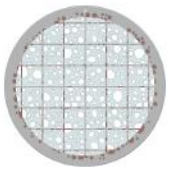

TEM on skin biopsies derived from HSM5 and a healthy control matched per age and sex, to measure the lenght and degree of flexion of desmosomes.

TEM on HaCaT *DSP* clones to qualitatively determine the morphology of desmosomes.

D. **Study of the impact of *DSP* SNV on differentiation and proliferation**

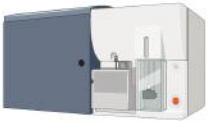

IHC on skin biopsies derived from HSM5 and a healthy control matched per age and sex, to evaluate the levels of markers of cutaneous differentiation and proliferation.

Cytofluorimetric proliferation assay in HaCaT *DSP* clones with CFSE staining.

4 ***In vivo* determination of the skin's permeability barrier function**

TEWL assay on HSM5, F_HSM5 and M_HSM5 and healthy controls matched per age ans sex, to evaluate the impact of the identified *DSP* variant in the maintenance of the skin permeability barrier function.

Figure 13. Schematic pipeline of the experimental procedures that were employed to study the impact of the identified *DSP* SNV.

4.1 Identification of a missense exonic variant in *DSP* gene in a PASH patient

The PASH patient (HSM5) enrolled in this study is followed-up since 2009 by the Dermatology Department of the Fondazione IRCCS Ca' Granda Ospedale Maggiore Policlinico of Milan. HSM5 is a 31 year old male diagnosed with PASH syndrome and also possessing different associated comorbidities including Crohn disease (CD), vertebral osteoporosis, metasteroid cataract, arterial hypotension, iatrogenic hypoadrenalism and paroxysmal supraventricular tachycardia. HSM5 possess the common CD-associated mutation, given by a frameshift variation caused by a duplication of a C in the coding sequence of *NOD2* autoinflammatory gene (rs2066847; c.2938dup; p.Leu1007fsins). This variant has been identified as a marker of severe clinical phenotype and to be associated with a complicated CD course (Schnitzler et al., 2014).

The father (F_HSM5) and mother (M_HSM5) of HSM5 were also recruited in this study. F_HSM5 reported not to be affected by any known pathology, while M_HSM5 decleared to be affected by inflammatory disorders such as rheumatoid arthritis and psoriasis (Figure 14).

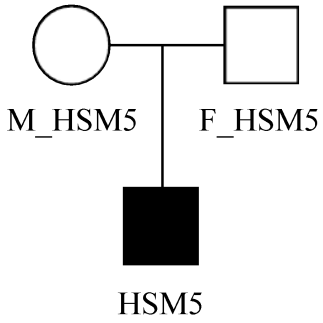

Figure 14. Pedigree of the family of HSM5.

Yet, bearing in mind that the genetic basis of PASH syndrome is only partially known and seems to be highly variable, HSM5 was subjected to WES analysis in order to identify other potentially recurrent deleterious single nucleotide variations (SNVs) that might be associated to PASH phenotype.

In the overall analysis, a total of 184 different variants were retrieved, and in order to recover the SNVs that are most likely to be deleterious or pathogenic or functional, variants were ranked according to the Combined Annotation Dependent Depletion (CADD) based on the PHRED-like score with a cut-off of 25 (Table 7).

Chr	Position	Gene	SNV	Variant effect	HSM5
1	g.16130268 C>T	*EPHA2*	rs35903225	Missense	C/T
1	g.95027223 C>T	*ALG14*	.	Missense	C/T
1	g.149021033 C>A	*PDE4DIP*	rs140993521	Missense	A/A
1	g.151000537 C>T	FAM63A	rs145467872	Missense	C/T
2	g.140541066 C>T	*LRP1B*	rs146867394	Missense	C/T
2	g.151527007 C>T	*NEB*	rs35625617	Missense	C/T
3	g.53179610 C>G	*PRKCD*	.	Missense	C/G
3	g.193314086 C>T	*ATP13A5*	rs78188075	Missense	C/T
5	g.80960922 C>G	*RASGRF2*	.	Missense	C/G
5	g.140841658 C>T	*PCDHA8*	rs146047089	Missense	C/T
6	g.7565494 A>T	*DSP*	rs17604693	Missense	T/T
7	g.25142754 C>T	*C7orf31*	.	Missense	C/T
7	g.128841524 A>C	*FLNC*	rs34972246	Missense	A/C
9	g.5656610 G>C	*RIC1*	rs12686794	Missense	G/C
10	g.76058743 C>T	*LRMDA*	rs1171639192	Missense	C/T
11	g.85709355 T>C	*SYTL2*	rs1429198700	Missense	T/C
11	g.107504696 C>A	*ALKBH8*	.	Missense	C/A
11	g.108486410 G>A	*KDELC2*	rs74911261	Missense	G/A
12	g.57254861	*R3HDM2*	rs78607331	Missense	C/T

	C>T				
13	g.24294839 C>T	*SPATA13*	rs140467795	Missense	C/T
14	g.93951044 C>T	*ASB2*	rs142812400	Missense	C/T
16	g.29996838 G>C	*INO80E*	.	Missense	G/C
16	g.84222522 C>T	*KCNG4*	rs140124801	Missense	C/T
19	g.10637706 G>C	*SLC44A2*	rs142741358	Missense	G/C
20	g.38554042 C>T	*RALGAPB*	.	Missense	C/T

Table 7. List of the single nucleotide variations (SNV) identified in HSM5 through WES analysis. For each variant is provided the chromosome, the genomic position including the reference allele and the alternate allele, the name of the gene, the locus accession for the variant type assigned by dbSNP (rs), mutation category and the genotype found in HSM5. When not available, the rs is indicated with a dot (.). Retrieved variants were ranked according to the Combined Annotation Dependent Depletion (CADD) based on the PHRED-like score with a cut-off of 25.

Next, selected genes were further investigated with the aim of creating a prioritization amongst the determined variants according to gene function. This approach led to the selection of a gene considered as highly appealing in the context of dermatologic disorders, *DSP* gene.

Specifically, results identified in HSM5 a A>T missense exonic variant (rs17604693; g.7565494 A>T; c.913A>T; p.Ile305Phe) in homozygosis in exon 7.

WES results for HSM5, together with the evaluation of the family segregation of the variant in F_HSM5 and M_HSM5, were confirmed in Sanger sequencing. The proband was ultimately validated as homozygous for the SNV in *DSP*, while it was found in heterozygosis in F_HSM5 and in M_HSM5 (Figure 15).

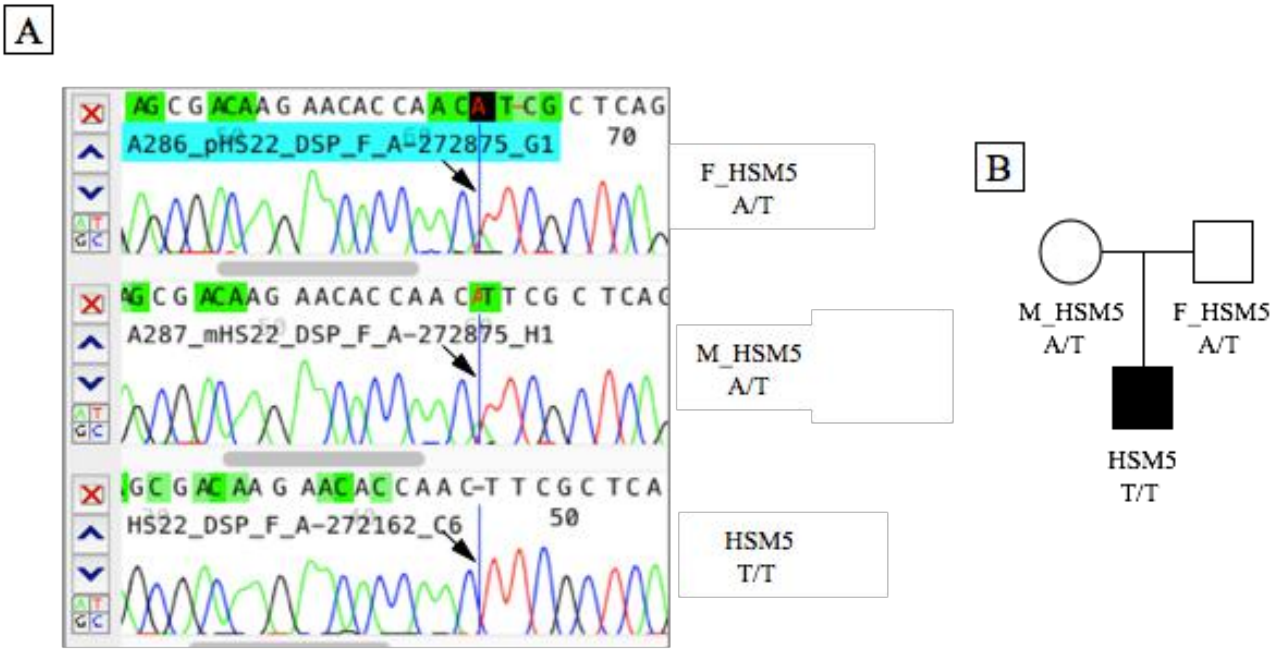

Figure 15. Validation of *DSP* (rs17604693; c.913A>T; p.Ile305Phe) variant in all family members. WES results identified in HSM5 a A>T missense exonic variant (rs17604693; g.7565494 A>T; c.913A>T; p.Ile305Phe;) in homozygosis on exon 7 of *DSP* gene. (A) Confirmation in Sanger sequencing of WES results for HSM5 together with the evaluation of the family segregation of the variant in F_HSM5 and M_HSM5. HSM5 was ultimately validated as homozygous for the SNV in *DSP*, while it was found in heterozygosis in F_HSM5 and in M_HSM5. (B) Schematic representation of the pedigree of the family of HSM5. Identified genotypes for *DSP* (rs17604693; g.7565494 A>T; c.913A>T; p.Ile305Phe) variant are reported under each family member.

DSP (NC_000006.12) is a 45098 bp long protein coding gene, mapping on the long arm of chromosome 6 (6p24.3), consisting of 14 exons and encoding for DSP, an obligate and the most abundant component of functional highly specialised adhesive intercellular junctions known as desmosomes.

Desmosomes exert their functions by providing both intermediate filament linkage and cell-to-cell adhesion, therefore conferring strong mechanical strength to tissues and contributing to the maintenance of tissue architecture and cohesiveness. Not surprisingly, these structures are abundant in districts that are continuously subjected to mechanical solicitations such as the epidermis, hair follicles and the myocardium (Garrod and Chidgey, 2008). Nevertheless, different studies highlighted novel additional functions of desmosomes that include the regulation of a vast variety of signalling pathways including skin barrier functionality, cell proliferation, differentiation, migration, apoptosis and cytoskeletal remodelling, events considered as potentially crucial for the onset and progression of disorders possessing dermatologic phenotypes including PASH syndrome (Dubash and Green, 2011; McAleer et al., 2015).

Desmosomes are defined as modular structures in which it is possible to recognise three major classes of components: adhesion molecules that interact in the extracellular space to connect adjacent cells; intermediate filament cytoskeleton; cytoplasmic plaque, comprehending proteins that mediate a direct linkage between adhesion molecules and cytoskeletal elements (Garrod and Chidgey, 2008).

In desmosomes the adhesion molecules are represented by desmosomal cadherins, desmogleins (Dsgs 1-4) and desmocollins (Dscs 1-3), transmembrane glycoproteins belonging to the superfamily of cadherin calcium-dependent adhesion molecules. The binding between desmosomal cadherins of neighbouring cells is predominantly heterophilic, however recent evidences strongly suggest that a homophilic adhesion is also possible (Chitaev and Troyanovsky, 1997). The cytoplasmic tails of desmosomal cadherins interact with the intracellular desmosomal plaque proteins. The outer portion of the plaque is composed by the intracellular tails of Dsgs and Dscs that bind to the armadillo family of linker proteins, namely plakoglobin (PG) and plakophilins (PKP 1-3). The inner portion of the desmosomal plaque is composed by DSP, member of the plakin family, that functions as a cytoskeletal adaptor protein that binds to PG, PKPs and intermediate filaments. The binding of DSP to intermediate filaments guarantees the ultimate tethering of the cytoskeletal elements to the desmosomal plaque (Dubash and Green, 2011) (Figure 16).

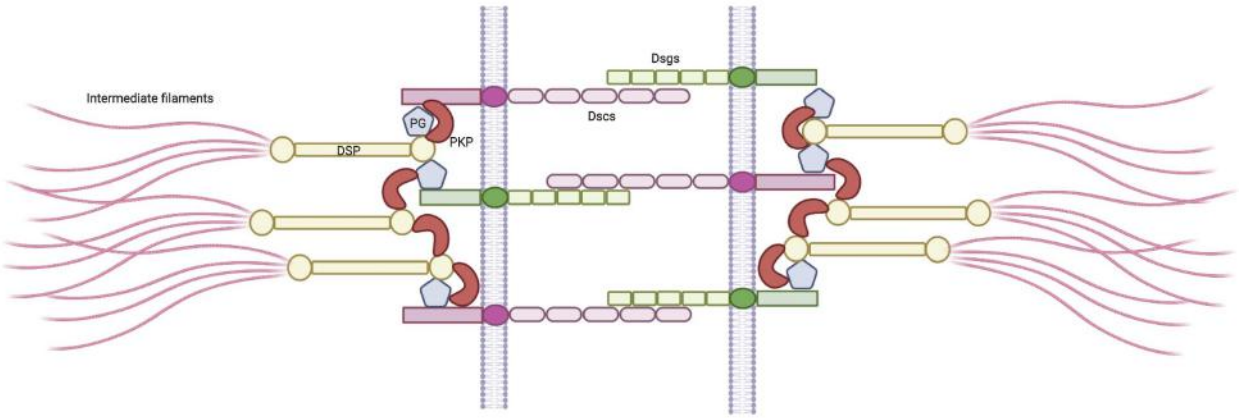

Figure 16. Architectural organisation of desmosomes. In desmosomes, the adhesion molecules are represented by desmosomal cadherins, desmogleins (Dsgs) and desmocollins (Dscs), that bind primarily through homophilic interactions with cadherins located on a neighbouring cell. The cytoplasmic tails of Dsgs and Dscs interact with intracellular proteins that constitute the desmosomal plaque that are collectively represented by the armadillo family of linker proteins, namely plakoglobin (PG) and plakophilins (PKPs), and by DSP, member of the plakin family, that functions as a cytoskeletal adaptor protein that binds to PG, PKPs and intermediate filaments.

Desmosomes are widely expressed in stratified epithelia in which mechanical strength together with the necessity to maintain tissue architecture and cohesiveness are of crucial importance.

Specifically, in the skin the genes encoding for the various components of desmosomes are differentially expressed in order to allow keratinocytes to proliferate and undergo terminal differentiation. Indeed, while DSP, PG and PKP are evenly expressed throughout the four layer of the epidermis, Dsgs and Dscs present layer-specific expression patterns. In the lower layers Dsg2 and Dsg3 are highly expressed, while Dsg1 is found to be localised in the upper partitions of the skin. Next, Dsg4 represents the dominant desmoglein in the granular layer. Dsc2 and Dsc3 are prevalently located in desmosomes of the basal and spinous layer, while Dsc1 is primarily found in the stratum granulosum (Holthöfer et al., 2007; Delva et al., 2009) Different desmosomal composition convey to these structures different biochemical and functional properties.

Desmosomes are known be also critically involved in the maintenance of the architecture, of the functions of the hair follicle and to withstand mechanical stress. Dsg4 is the main desmoglein expressed in hair follicles and is crucial for differentiation processes. Dsg3 is expressed in the ORS, in matrix cells and in the medulla, and DSG3 knockout mice display hair loss and failure to anchor telogen hair (Chidgey et al., 2001). Dsc1, expressed in the IRS and the upper ORS, and Dsc3, found in all the cells of the hair follicle, possesses a fundamental role in maintaining the structural integrity and control of proliferation and differentiation processes in this skin appendage. Indeed, in mice presenting a conditional ablation Dsc1 and Dsc3 display hair follicle degeneration (Chidgey et al., 2001) and hair loss respectively (Chen et al., 2008). Also, PKPs, primarily expressed in the ORS region, are crucial in defining the various proliferation/differentiation/adhesion processes occurring in hair follicles during hair cycle progression. Indeed, overexpression of PKPs in mice hair follicles result in decreased keratinocyte proliferation and in a shortening of the anagen phase (Charpentier et al., 2000). Moreover, though no human pathologies are associated to mutations in *PKP3* gene, the ablation of PKP3 in mice results in defective hair follicle morphogenesis and DSP delocalisation (Sklyarova et al., 2008). DSP together with PGs are defined as desmosomal hallmarks in hair follicles since they are localised in all cells types (Kurzen et al., 1998).

Interestingly, mutations in all three families of desmosomal proteins have been identified in various human diseases, including skin keratinisation disorders and cardiomyopathies, principally inducing either abnormalities in tissue morphogenesis and differentiation, or the disruption of tissue integrity as a direct consequence of the loss of adhesion properties (Garrod and Chidgey, 2008).

Specifically, mutations in *DSP* have been found to be associated with autosomal recessive and dominant disorders characterised by alopecia, palmo-plantar keratoderma, skin fragility woolly-hair syndrome, erythrokeratodermia, dilated cardiomyopathy, arrhythmogenic right ventricular cardiomyopathy/dysplasia (Paller et al., 2018).

Yermakovich and collaborators, identified two novel missense variants on exon 24 of *DSP* gene in two sisters affected by Carvajal syndrome, characterised by palmo-plantar keratoderma, skin fragility woolly-hair syndrome and ventricular dilated cardiomyopathy (Yermakovich et al., 2018).
In a study conducted by Norgett et al., a recessive mutation in *DSP* gene (7901delG) has been linked to the emergence of woolly hair syndrome, generalised striate keratoderma and ventricular cardiomyopathy. The identified genetic variant has been hypothesised to induce defects in cellular adhesion caused by the reduced ability of the C-terminal region of mutated DSP to interact with intermediate filaments. Further corroborating cell-adhesion defects are the results of IHC assays performed on skin samples of cases that revealed the presence of large intercellular spaces in the suprabasal layers (Norgett et al., 2000).
One case report presenting a *DSP* mutation that completely truncated the C-terminal region of the protein was affected by severe acantholytic epidermolysis bullosa and was characterised by lack of hair (alopecia), nail loss, and death at 10 days post-partum due to excessive TEWL (Jonkman et al., 2005).
Recently, a novel missense variant in *DSP* was identified by McAleer et al. in a patient affected by severe dermatitis, multiple allergies, and metabolic wasting (SAM) syndrome. Results obtained on skin biopsies, suggest that the identified mutation might induce aggregates and accumulation of DSP in the cytoplasm and a dissociation between keratin filaments and desmosomal structures, thus resulting in hyperkeratosis, hyperplasia and compromised skin barrier possibly associated with enhanced immune cell infiltrates (McAleer et al., 2015).
Furthermore, experiments conducted on *DSP*-null mice by Vasioukhin and collaborators, revealed that desmosomes lacked in the attachment of keratin filaments in the inner plaque of the junctional complex, resulted in aberrations in actin reorganisation and in an impairment in membrane sealing that has been seen to affect epithelial sheet formation, and possessed an overall failure in the stabilisation of adherens junctions (Vasioukhin et al., 2001).
All these findings further support the selection of *DSP* variant amongst the retrieved genes as potentially intriguing in the context of PASH syndrome.
In this study the impact of the A>T missense exonic variant (rs17604693) was evaluated with the aim of clarifying its potential impact in the skin and of shedding light on possible novel mechanisms involved in the progression of the disease in HSM5.

4.2 *In silico* studies: *DSP* (rs17604693) increases protein stability and compaction

DSP is organised in a tripartite structure in which it is possible to recognise globular heads and tails separated by a central α-helical coil-coiled rod domain. The N-terminal domain is involved in

targeting DSP to the cadherin-armadillo complexes of the desmosomal plaque by mediating the direct binding of DSP to PG and PKPs. Indeed, at the N-terminal end of the head is located the plakin domain comprising residues 180-1022, organised in six spectrin repeats (SRs 3-8) and a Src homology 3 domain (SH3), containing targeting consensus sequences to direct the association of DSP with the components of the desmosomal plaque during junction assembly (Choi and Weis, 2016). The central rod region mediates self-dimerization by inducing the formation of a parallel coil-coiled dimer with a parallel orientation on the forming junctional complex (Godsel et al., 2005). The C-terminal domain consists of three homologous plakin repeat domains (PRDs A, B, C), defined as specialised linkers and regulatory regions that facilitate the binding to intermediate filaments (epidermal keratins, epithelial keratins, desmin and vimentin) (Al-Jassar et al., 2011) (Figure 17).

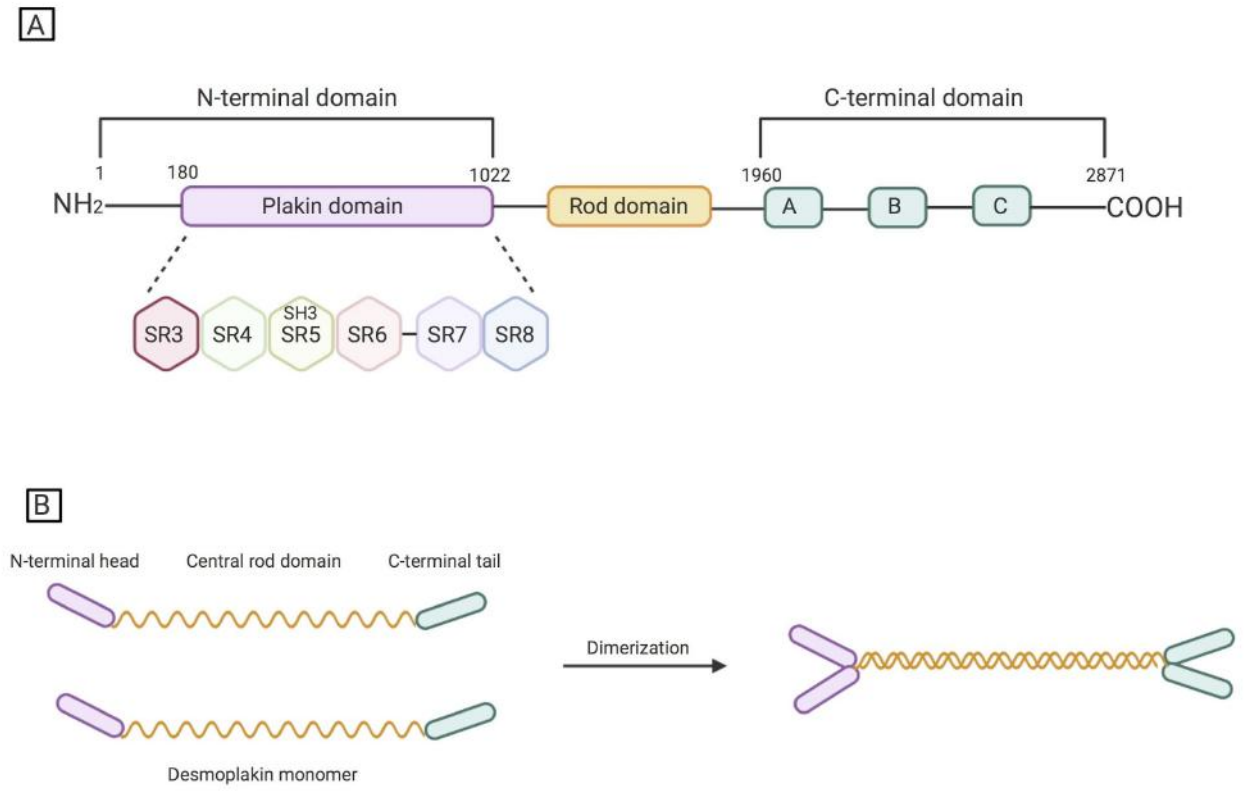

Figure 17. Structural organisation of DSP. (A) DSP is organised in a tripartite structure in which it is possible to recognise: a N-terminal globular head comprising the plakin domain (residues 180-1022) organised in six spectrin repeats (SRs 3-8) and a Src homology 3 domain (SH3); a central α-helical coil-coiled rod domain; a C-terminal globular region consisting of three homologous plakin repeat domains (PRDs A, B, C). (B) DSP undergoes a self-dimerization mediated by the central rod region in order to generate a dimer that is recruited on the forming junctional complex.

The identified *DSP* missense variant (rs17604693) leads to the amino acid substitution p.Ile305Phe, occurring in the plakin domain. In order to determine the impact of the amino acid change on

protein structure, molecular dynamic (MD) procedures were performed in order to reproduce realistic behaviours of wild type DSP dimers, and of those carrying the variant in heterozygosis and in homozygosis, with the aim of retrieving detailed information relative to molecular movement and particle motion in function of time.

MD assays were performed for 100 ns in order to study the stability and the conformational changes on DSP structure upon mutation.

RMSD of the backbone atoms is defined as crucial parameter to evaluate the stabilisation and equilibration of MD trajectories. As shown in Figure 18 A, the backbone atoms of wild-type DSP did not show a significant stabilisation in the selected time interval, thus suggesting that MD simulations should be performed for times greater than 100 ns to truly define the wild-type's trajectory. The mutant DSP dimer carrying the variant in heterozygosis stabilised at 1,5 nm after 20 ns and did not show any significant change after that, thereby suggesting that the modelled protein is stable throughout the simulation. The DSP dimer carrying the variant in homozygosis stabilised after the first 11 ns, with an average RMSD of 1,2 nm, and kept constant until 80 ns, following which an increment in RMSD value was observed and possessed an average of 2 nm. The RMSD analysis collectively indicate that the presence of the variant, both in heterozygosis and homozygosis, affects protein stability ultimately resulting in an increased stability of the protein complex.

The Rg analysis was employed to determine the level of compaction and the overall dimensions of DSP wild-type and mutated DSP dimers. As shown in Figure 18 B, in the wild-type dimer an initial stabilisation was registered at 5,25 nm at 15 ns was followed by an increment in Rg values that further stabilise at an average Rg value of 5 nm around 70 ns that were then maintained until the end of the stimulation. The mutant DSP dimer carrying the variant in heterozygosis stabilised at an average Rg value of 5,1 nm at about 10 ns but was subjected to a slightly decreased throughout the simulation. The mutant DSP dimer carrying the variant in homozygosis stabilised at an Rg value of 5,2 nm around 10 ns and did not show any significant variations after that. These results suggest that the variant, both in heterozygosis and homozygosis, affect the dimer's level of compaction by increasing it if compared to the wild-type protein.

SASA is a parameter widely employed for the evaluation of the surface area of the protein accessible to the solvent, and in which high SASA values are indicative of a relative expansion. Results highlighted that in the DSP wild-type dimer starts with a SASA value of 575 nm^2 that progressively decreases over time reaching a minimum average value of 525 nm^2 at the end of the trajectory. A similar trend was observed in the DSP dimer carrying the variant in heterozygosis, in which a starting SASA average value of 570 nm^2 gradually decrements reaching an average SASA

final value of 525 nm^2 at the end of the simulation. On the contrary, in the case of DSP dimer carrying the mutation in homozygosis, average SASA values of 570 nm^2 are maintained throughout the trajectory (Figure 18 C). Results indicate an increment in the accessible surface of the mutant dimers, particularly relevant in the homozygote, if compared to the wild-type protein.

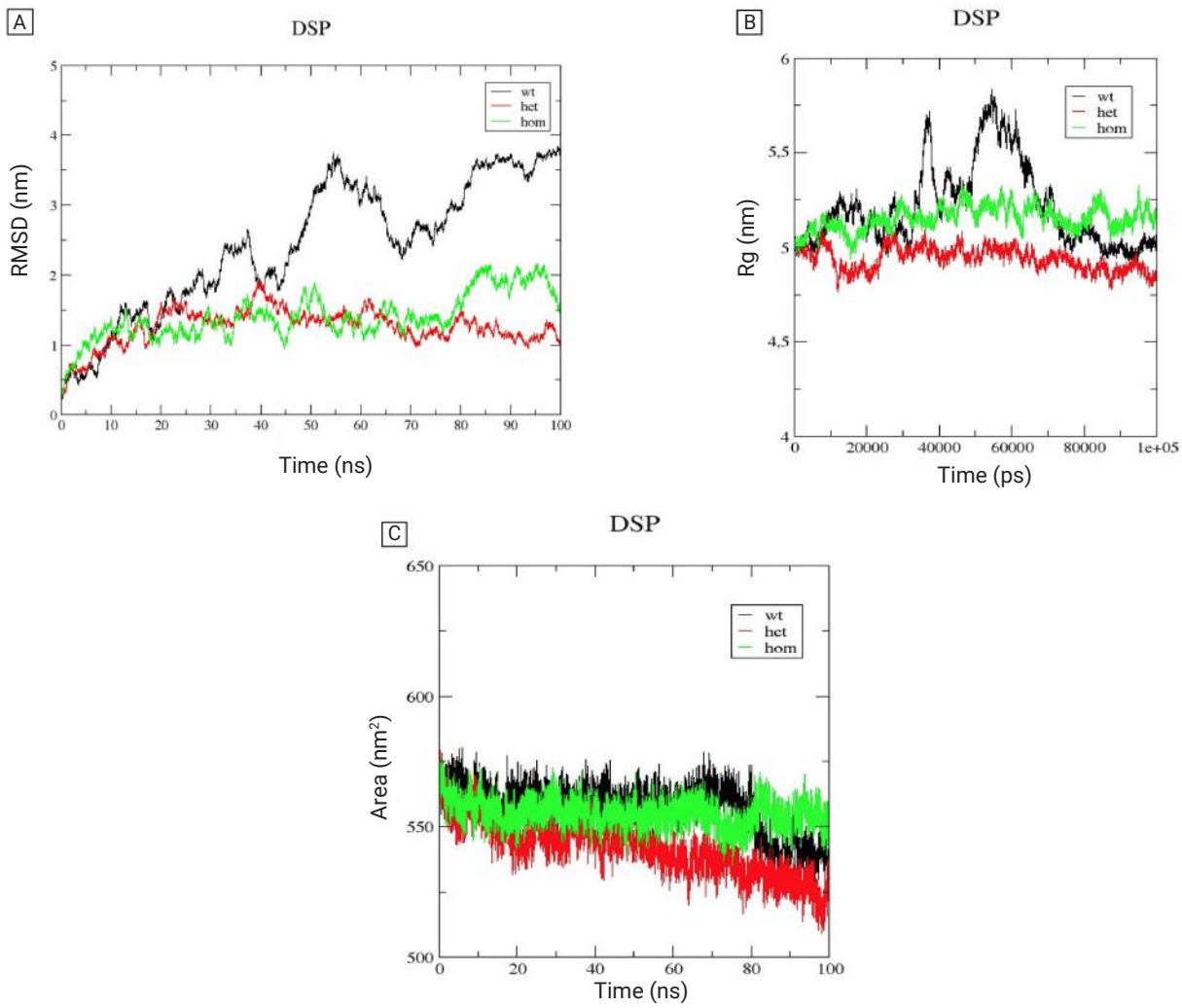

Figure 18. Molecular dynamics of wild type and mutated DSP dimers. (A) Backbone Root-mean square deviation (RMSD) for the backbone atoms of the wild-type DSP dimer (black), of the DSP dimer carrying the variant in heterozygosis (red) and of the dimer presenting the variant in homozygosis (green) are shown as a function of time (ns). (B) Radius of gyration (Rg) of Cα atoms in the molecular dynamics trajectory for the wild-type DSP dimer (black), of the DSP dimer carrying the variant in heterozygosis (red) and of the dimer presenting the variant in homozygosis (green) are shown as a function of time (ps). (C) Solvent accessible surface area (SASA) of the wild-type DSP dimer (black), of the DSP dimer carrying the variant in heterozygosis (red) and of the dimer presenting the variant in homozygosis (green) are shown as a function of time (ns).

Overall, results suggest that both mutated DSP dimers possess a major level of stability and compaction if compared to the wild-type condition. It is possible to speculate that the presence of a non-polar amino acid containing an aromatic side chain might affect the overall conformation of the

protein by principally altering the formation hydrogen-bonds and the overall flexibility of the dimers. Both parameters are currently under investigation.

4.3 Generation of *DSP* clones using CRISPR-Cas9 and ssODN-mediated genome editing

In order to strictly determine the effects, contributions and implications of *DSP* variant in the skin, CRISPR-Cas9 and ssODN-mediated genome editing was used to obtain HaCaT cells carrying the point mutation of interest (rs17604693; g.7565494 A>T; c.913A>T, p.Ile305Phe).

The generation of *DSP* clones was achieved using a CRISPR-Cas9 editing system that combines the pSpCas9 endonuclease with a sgRNA and a ssODN, the latter acts as a donor template for DNA repair via the high fidelity HDR mechanism.

The progressive screening through Sanger sequencing of genomic DNA derived from *DSP* genome-edited HaCaT clones allowed the identification of three cellular lineages of interest:

- clone possessing one wild-type allele and one carrying the desired base edit (WT/KI) (figure 19 A);
- clone presenting one allele carrying the chosen nucleotidic substitution and the other presenting an insertion resulting in a *DSP* knock-out (KI/KO);
- clone possessing one wild-type allele and the other exhibiting a deletion leading to a *DSP* knock-out (WT/KO).

Next, Sanger sequencing was performed on cDNA amplicons deriving from all three selected clones. Results confirmed that the single base substitution determines the desired base change also at the cDNA level.

In the case of the KI/KO clones only the cDNA carrying the nucleotidic substitution was present (Figure 19 B), while in the WT/KO clones only the wild-type cDNA sequence was recovered (Figure 19 C). Taken together, these results suggest that the transcript deriving from the *DSP* KO allele undergoes non-sense mediated decay (NMD).

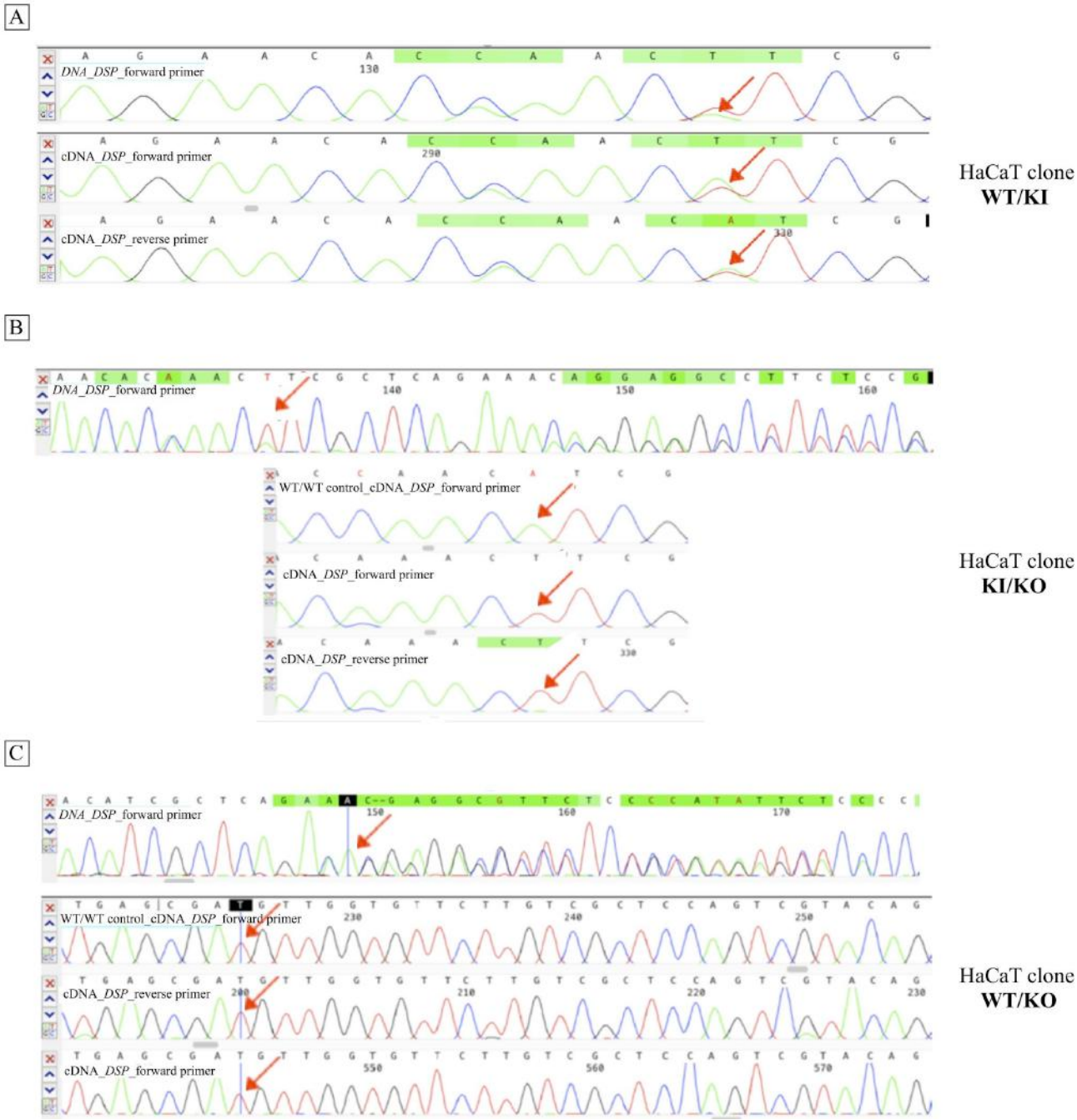

Figure 19. Screening of HaCaT *DSP* genome-edited clones. The generation of *DSP* clones carrying the point mutation of interest (rs17604693; g.7565494 A>T; c.913A>T, p.Ile305Phe) was obtained through CRISPR-Cas9 and ssODN-mediated genome editing in HaCaT cells. Genomic DNA and cDNA deriving from clones were progressively screened through Sanger sequencing that allowed the identification of three cellular lineages of interest. (A) HaCaT WT/KI clones: Sanger sequencing of genomic DNA showed that the clone possesses one wild-type allele and one carrying the desired base edit. Sanger sequencing of cDNA confirmed that both the wild-type and mutated sequences are present. (B) HaCaT KI/KO clone: Sanger sequencing of genomic DNA highlighted that the clone presents one allele carrying the chosen nucleotidic substitution and the other presenting an insertion resulting in a *DSP* knock-out. Sanger sequencing of cDNA confirmed that the single base substitution determines the desired base change also at the cDNA level. (C) HaCaT WT/KO clone: Sanger sequencing of genomic DNA verified that the clone presents one wild-type

allele and the other exhibiting a deletion leading to a *DSP* knock-out. Sanger sequencing of cDNA confirmed the sole expression of the wild-type sequence.

No clones possessing the patient's genotype were found. Nevertheless, although aware of the limitations of this model, KI/KO and WT/KO cells were considered as appropriate candidates since they respectively only express the mutated allele, as in the case of HSM5, or the wild-type allele, as in the case of a healthy control. On the other hand, WT/KI clones were selected since they recapitulate the genotype found in F_HSM5 and M_HSM.

4.4 Intracellular distribution of DSP

DSP is known to play a central role in desmosome function, while its dynamics during junction assembly is still not fully characterised but seems to be primarily regulated by cell-to-cell contacts, actin cytoskeleton and interactions with intermediate filaments that collectively lead to a rapid local gathering of DSP on newly forming membrane-bound junction complexes (Godsel et al., 2015).
During the early stages of cell contact-initiated desmosome assembly, DSP appears to be located in precursor cytoplasmic granular aggregates associated with intermediate filament bundles, PKPs and also with cortical actin (Green, 1987). The binding of DSP to PKPs appears to be tightly linked to the assembly competence since PKPs favour the cytoplasmic clustering and aggregation of DSP and promote its association to the cytoskeletal components (Godsel et al., 2015).
During the later stages of desmosome assembly, intermediate filaments and microfilaments are thought to promote the translocation of DSP particles towards the assembling desmosomes on cell borders. Specifically, actin is thought to mediate the reorganization of DSP-associated intermediate filament bundles and/or to escort DSP particles to sites of desmosome formation more directly. Recent evidences suggest that the absence of the intermediate filament-binding domain determines a more rapid recruitment of DSP to cell-to-cell contacts sites if compared to when DSP is tethered to intermediate filaments (Godsel et al., 2015).
In Figure 20 are reported representative images resulting from DSP immunostaining of an ulcerative lesional area of the left armpit of HSM5 and from the same body site of a healthy control matched per age and sex (HSM5_healthy control). As shown in Figure 20 A, in HSM5 healthy control, despite a slight and widespread cytoplasmic signal, DSP is primarily localised in correspondence of cell borders, thus strongly suggesting that the protein is in large part recruited at the level of desmosome structures that are known to be highly expressed in keratinocytes (Dubash and Green, 2011). A significantly different distribution pattern is observed in the skin sample of HSM5 in which DSP signal is predominantly registered in the cytoplasm (Figure 20 B).

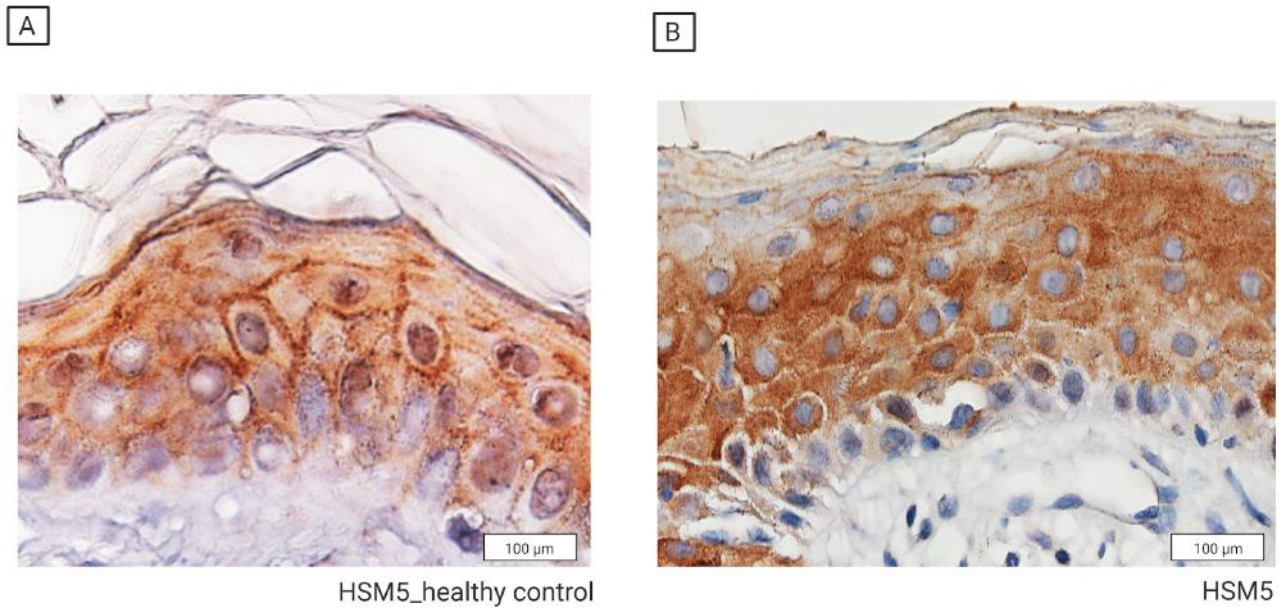

Figure 20. Intracellular localisation of DSP in skin biopsies. Immunostaining of DSP was performed on skin biopsies deriving from an ulcerative lesional area of the left armpit of HSM5 and from the same body site of a healthy control matched per age and sex (HSM5_healthy control). (A) In HSM5 healthy control, despite a slight and widespread cytoplasmic signal, DSP is primarily localised in correspondence of cell borders. (B) In HSM5, the intracellular distribution of DSP is predominantly registered in the cytoplasm. All images were acquired at 60x magnification (scale bar 100 µm).

In order to further endorse the impact of *DSP* variant on the cellular localisation of the protein, *in vitro* experiments on HaCaT *DSP* WT/WT, WT/KI, WT/KO and KI/KO cells were performed. In the experimental settings the number of DSP *puncta*/cells were counted in order to define the localisation of DSP on hyper-adhesive calcium-independent desmosomes.

Based on the structure of the extracellular domain of Dsgs and Dscs, calcium seems to play a fundamental role in cell-to-cell adhesion by supporting the acquisition of a rigid conformation. Nevertheless, recent findings suggest that desmosomes are able to assume two alternative adhesive states (Garrod, 2013; Garrod and Chidgey, 2008): a lower-affinity calcium-dependent adhesion, condition adopted by desmosomes during the initial stages of embryonic development and in cells on the edge of wounded epithelia that confers to desmosomes a junctional strength comparable to that of adherens junctions; a hyper-adhesive calcium-independent state that seems to be the normal condition adopted in tissues, including the intact epithelia *in vivo*, in which hyper-adhesion is thought to strongly counteract disruption by increased mechanical forces, thus strongly contributing to the maintenance of tissue integrity. Hyper-adhesive calcium-independent desmosomes have also been detected and described in cells in confluent sheets in culture (Kurinna et al., 2014).

As shown in Figure 21, a significant reduction in DSP *puncta*/cells was registered both in HaCaT WT/KI cells if compared to WT/WT condition (*DSP puncta*/cell: WT/KI 0,5228±0,08521, p<0.0001; WT/WT 0,8593±0,1069) and in KI/KO clones in comparison with the WT/KO lineage (*DSP puncta*/cell: KI/KO 0,1695±0,07785, p<0.0005; WT/KO 0,3041±0,07488). In all tested conditions, an average 58% reduction in the number of DSP *puncta*/cells were registered in mutated clones if compared to the respective control. The fact that some DSP+ structures encircled in red appear as intracellular has to be attributed to the experimental procedure. Indeed, they can be considered as desmosomal structures since their disconnection from the neighbouring cells is due to the loss of the adjoining cell, containing the remaining portion of the junction, as a consequence of the particularly rough experimental settings required for the retrieval of only hyper-adhesive desmosomes and of fixing procedures.

These results strongly suggest that the presence of the *DSP* variant might negatively impact the recruitment of DSP on the desmosomal plaque, thus further corroborating the outcomes registered in IHC experiments.

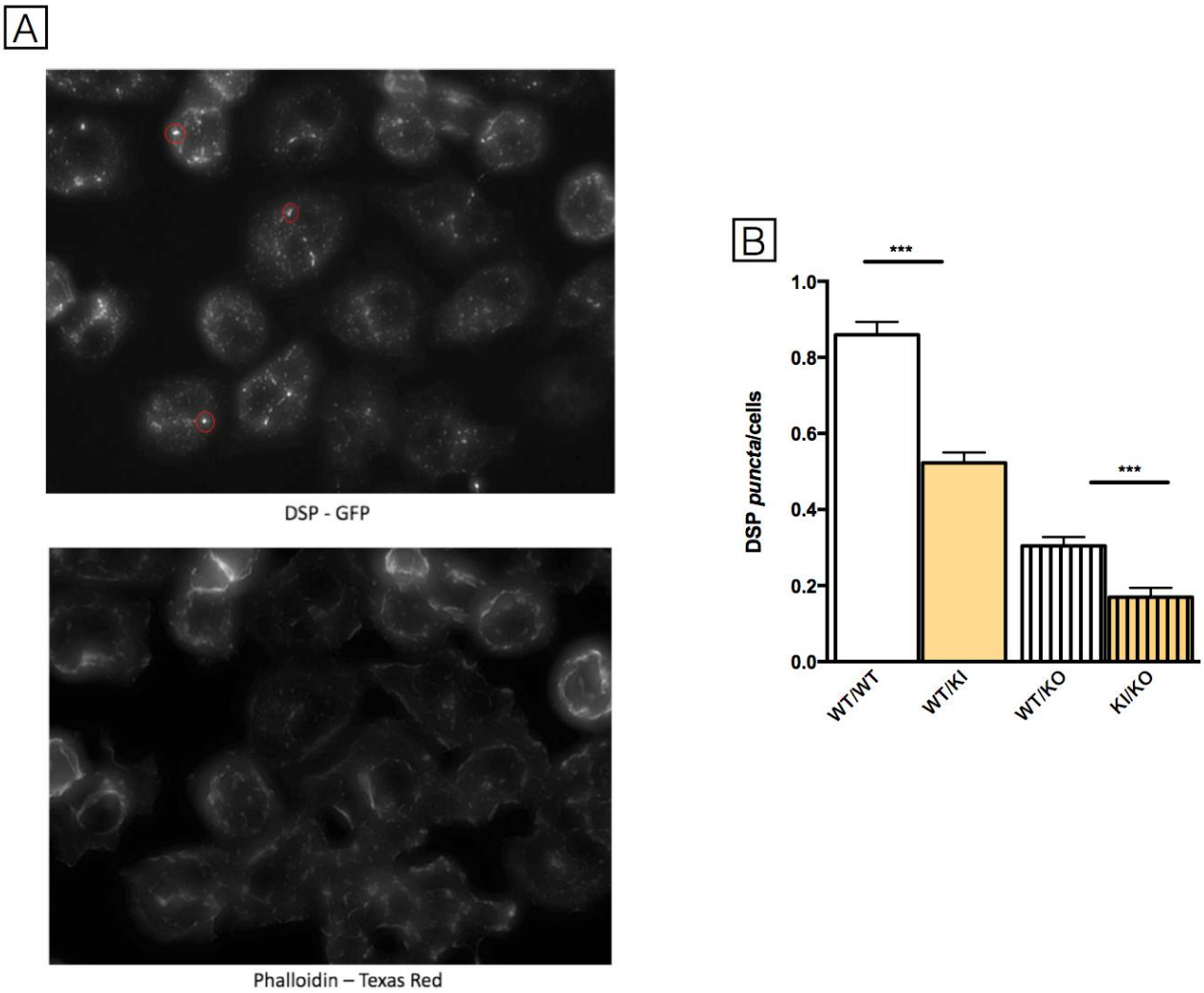

Figure 21. Hyper-adhesive calcium-independent desmosomes in HaCaT *DSP* clones. HaCaT *DSP* clones were incubated over-night in high calcium complete growth medium to induce the formation of desmosomes. Next, cells were incubated 90 minutes in low-calcium complete growth medium supplemented with 3 mM EGTA to retrieve only hyper-adhesive desmosomes. The remaining calcium-independent hyper-adhesive desmosomes were stained with DSP antibody. (A) Representative image of *DSP* WT/WT keratinocytes stained with a DSP antibody in which DSP in hyper-adhesive desmosomes (DSP *puncta*) are included in the red circles. (B) The number of DSP *puncta*/cell were counted in 10 random fields of view for each sample. Results are representative of three independent experiments. Data analyses were performed with Mann-Whitney *U test* by comparing *DSP* WT/WT cells with *DSP* WT/KI cells and WT/KO clones with KI/KO clones; ***p<0.0001; ***p< 0,0005.

Next, DSP protein levels and gene expression levels were evaluated. As represented in Figure 22 A no significant variations in DSP protein levels were registered neither in WT/KI cells when compared to WT/WT cells nor in KI/KO cells with respect to WT/KO clones. Conversely, a significant increment in *DSP* gene expression was observed in KI/KO cells when compared to the control (Fold increase *DSP*: KI/KO 2,043±0,3285, p<0,01; WT/KO 1), while no significant variations were determined in the other two tested cell lineages (Figure 22 B).

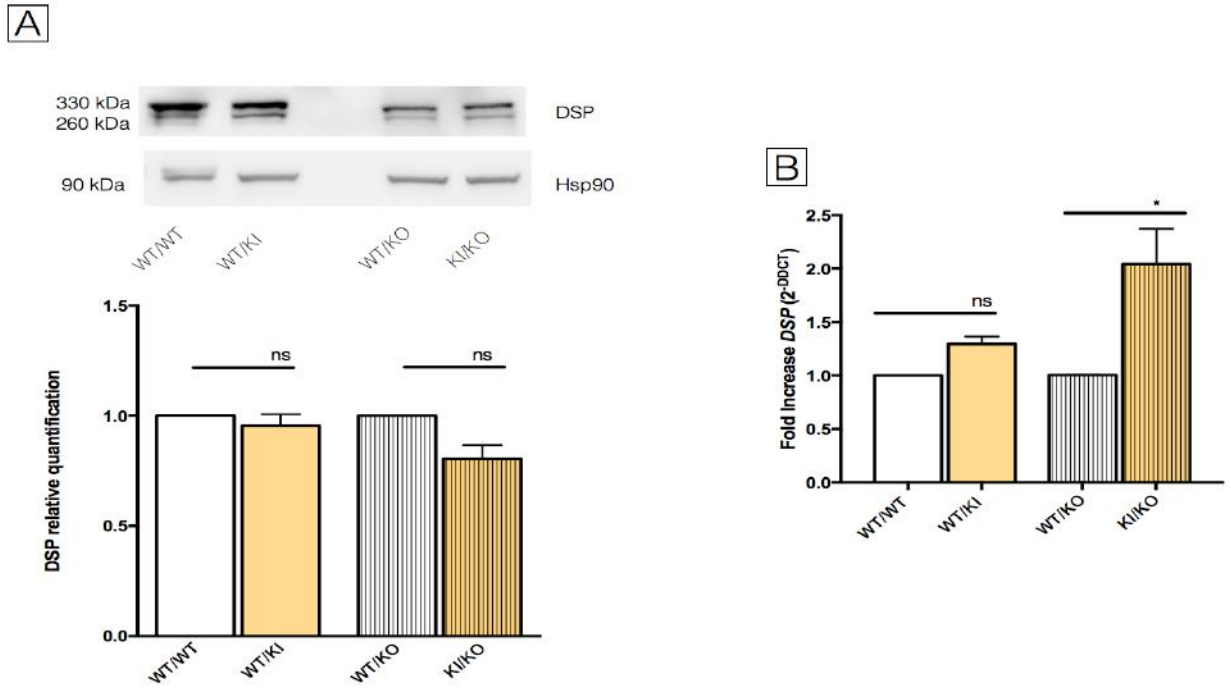

Figure 22. DSP protein levels and *DSP* gene expression in HaCaT *DSP* clones. (A) Representative Western blot image showing protein levels of DSP and Hsp90, the latter used as the reference protein (top). Quantification of DSP increase normalised to Hsp90 optical density (bottom). (B) Real time quantitative polymerase chain reaction (PCR) and results normalised to *ACTB* expression. Expression of *DSP* WT/WT and *DSP* WT/KO clones was normalized to 1. Expression data for three experiments are reported as $2^{-\Delta\Delta Ct}$ average ± SD. Results are representative of three independent experiments. Data analyses were performed with Mann-Whitney *U test* by comparing DSP WT/WT cells with DSP WT/KI cells and WT/KO clones with KI/KO clones; ns: not significant; *p< 0,01.

These results might suggest the presence of mechanisms aimed at compensating (Garrod and Chidgey, 2008) the insufficient recruitment of DSP in proximity of hyper-adhesive desmosomes, condition that becomes particularly relevant in the case of KI/KO cells. In addition, a consistent number of literature findings have reported that alterations in protein conformation might determine its premature or rapid degradation in different subcellular districts (Waters, 2001). It is possible to hypothesise that the mutated DSP protein undergoes an enhanced degradation therefore possibly resulting in a reduction in the protein's steady-state concentration within the cell; bearing in mind that DSP is an obligate component of desmosomes, necessary for the complex to exert its function, it is plausible that augmented gene expression levels of *DSP* might counteract the degradation of the mutated protein hence contributing to the maintenance of basal levels of DSP in the cell. Clearly, these are only postulations that need to be verified.

Collectively, these results suggest the inability of mutated DSP to be recruited on the cell membrane in correspondence of desmosome assembly sites. Since the amino acid substitution p.Ile305Phe occurs in the N-terminal plakin domain, it is possible to speculate that the binding affinity of DSP for the cytoskeletal adaptor proteins PG and PKPs might be reduced, ultimately rendering the mutated protein unable to stably associate to the outer portion of the desmosomal plaque.

Moreover, a possible consequence might also reside in the fact that altered interactions with PKPs might limit the cytoplasmic clustering and aggregation of DSP in discrete cytoplasmic aggregates and interfere with its association to the cytoskeletal components (Godsel et al., 2015).

In addition, as suggested by molecular modelling assays, the homozygous form of the protein appears to be more compact if compared to the wild-type one, thus possibly resulting in an altered protein conformation that might lead to substantial differences in the overall structure and exposition of its domains therefore altering the binding with components involved in mediating its gathering, chaperoning and ultimate recruitment to desmosomes, hence potentially interfering with DSP particle assembly, positioning and dynamics.

4.5 Desmosome morphology

Desmosomes possess a highly organised, characteristic and well conserved electron dense structure. Under physiological conditions desmosomes appear as complexes possessing an overall diameter that ranges between 0.2-0.5 μm, are composed by two intracellular electron-dense plaques in each of the two joining cells which are separated by an intercellular cleft and show a length ranging from 100-300 nm. These specific and unique structural characteristics are considered as strictly necessary

to guarantee the correct organisation and function of mature desmosomes (Garrod and Chidgey, 2008; Hino et al., 1991).

The study of desmosome morphology was performed by conventional TEM on samples deriving from an ulcerative lesional area of the left armpit of HSM5 and from the same body site of HSM5 healthy control.

No significant variations in the diameter of desmosomes were registered in HSM5 if compared to the healthy control; indeed, acquired measurements ranged between the physiological 0.2-0.5 µm values. Nevertheless, defects in desmosome ultrastructure were reported in terms of length and degree of flexion of the junctional complex. In HSM5 desmosomes appeared to be significantly longer when compared to those observed in the healthy control sample, which instead presents normal physiological values (Desmosome length (nm): HSM5 473±152,7, p<0,0001; HSM5_healthy control 280,5±53,62) (Figure 23).

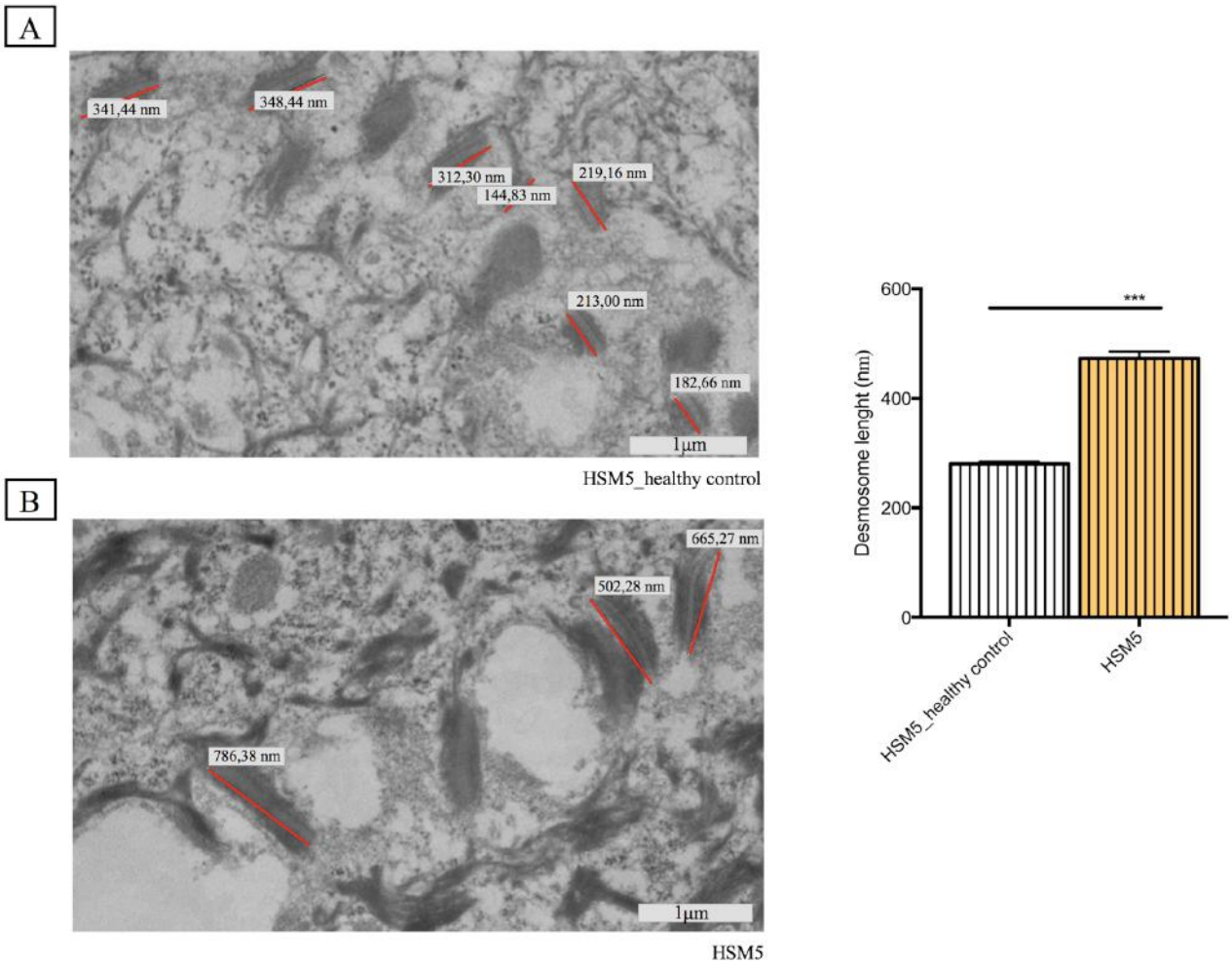

Figure 23. Transmission electron microscopy (TEM) for the determination of the length of desmosomes. TEM analysis shows an increment in the length of desmosomes in HSM5 if compared to HSM5 healthy control. The study of

desmosome length was performed on skin biopsies deriving from an ulcerative lesional area of the left armpit of HSM5 and from the same body site of the HSM5 healthy control. Representative image of desmosomes measured in HSM5_healthy control (A) and in HSM5 (B). Results are expressed as average length (nm) ± SD of 180 independent measurements. Data analyses were performed with Mann-Whitney *U test* comparing HSM5_healthy control with HSM5; ***p< 0,0001. All images were acquired at 19k x magnification (scale bar 1 µm).

Moreover, as shown in Figure 24 in HSM5 desmosomes were reported to possesses a significant increment in the degree of flexion if compared to HSM5 healthy control (Degree of flexion (°): HSM5 20,01±0,6069, p<0,0001; HSM5_helathy control 14,67±0,8543).

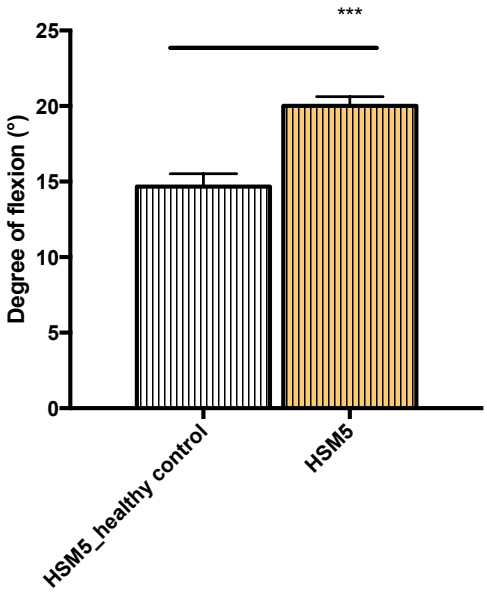

Figure 24. Transmission electron microscopy (TEM) for the determination of the degree of flexion of desmosomes. TEM analysis shows an increment in the degree of flexion of desmosomes in HSM5 if compared to HSM5 healthy control. The study of the degree of flexion of desmosomes was performed on skin biopsies deriving from an ulcerative lesional area of the left armpit of HSM5 and from the same body site of the HSM5 healthy control. Results are expressed as average degree of flexion (°) ± SD of 96 independent measurements. Data analyses were performed with Mann-Whitney *U test* comparing HSM5_healthy control with HSM5; ***p< 0,0001.

A further qualitative evaluation of the images highlighted that in HSM5 the electron dense intracellular plaque seems to be disorganised and majorly expanded if compared to the one observed in the healthy sample possibly suggesting that the arrangement of the intracellular portion of the cytoplasmic plaque is altered hence possibly impacting the functionality of the cell junction.
Next, conventional TEM was assessed to verify whether differences in desmosome morphology also occur in HaCaT *DSP* WT/WT, WT/KI, WT/KO and KI/KO cells. Considering that HaCaT cells are a cell line that grows in a monolayer, the number of complete desmosomes is very low. For this reason, the TEM data are presented only as qualitative observations related to the overall morphology of desmosomes, and quantitative evaluatons are not accessible.

In WT/WT cells, desmosomes were reported to possess a normal phenotype with an average length of 100-150 nm and a regular distribution of the cytoplasmic plaque at both sides of the cellular junction (figure 25 A). In WT/KI and WT/KO clones, desmosomes appeared to present only a slightly altered structure resulting in complexes that are majorly stretched out and showing a slight less deposition of proteins on the intracellular plaque, hence giving origin to thinner but apparently regularly organised structures (Figure 25 B and C).

Several defects in desmosome arrangement were registered in KI/KO clones; indeed, cells presented an unequal deposition of proteins on the intracellular plaque that gives origin to asymmetric structures. Furthermore, in the analysed samples two different subsets of desmosomal populations were identified and include a shorter and thinner one, and a predominant one given by extensively stretched out desmosomes that seems to have a uniform and regularly organised intracellular plaque (Figure 25 D).

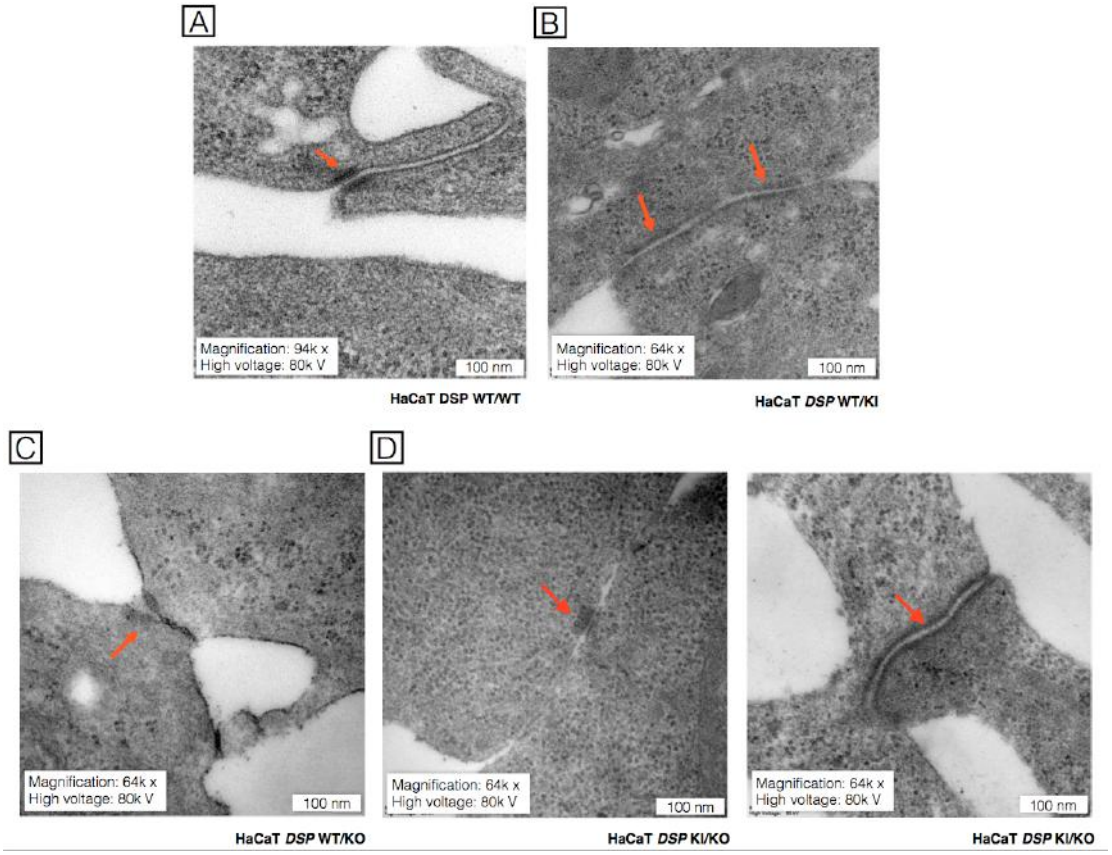

Figure 25. Transmission electron microscopy (TEM) to evaluate the morphology of desmosomes in HaCaT *DSP* clones. Representative images of desmosomes obtained in HaCaT *DSP* WT/WT (A), HaCaT *DSP* WT/KI (B), HaCaT *DSP* WT/KO (C) and HaCaT *DSP* KI/KO (D) clones. Results are reported as qualitative observations related to the overall morphology of desmosomes. Desmosomes are indicated with the red arrow. Image A was acquired at 94k x magnification and 80k V high voltage (scale bar 100 nm), while figure B-C-D were acquired at 64k x magnification and 80k V high voltage (scale bar 100 nm).

However, observations in the *in vitro* genetic model, despite the known limitations, highly suggest that the expression of the sole mutated *DSP* allele (KI/KO cells) affects the morphology of the adhesive junction, while in the case of the heterozygote the desmosome emerges as only slightly altered.

Taken together, these results might suggest that the *DSP* variant might at least partially contribute to the increment in size of desmosomes, though the direct effects of this morphological alteration on desmosome function are yet to be fully understood and need to be unravelled.

4.6 Differentiation and proliferation of keratinocytes

While dealing with disorders involving alterations in desmosomes, it is necessary to avoid associating desmosomal proteins exclusively to mechanical adhesion. Other crucial cellular functions regulated by these junctions, including differentiation and proliferation, should be envisaged.

During terminal differentiation, specific expression profiles of the various desmosomal proteins are activated in a differentiation-stage specific mode in keratinocytes through mechanisms that have been thoroughly described in literature. These differential expression patterns determine specific and dynamic reorganisations of intermediate filaments and actin cytoskeleton in their associations with desmosomes and adherens junctions, respectively (Lechler and Fuchs, 2007; Kottke et al., 2006).

Until recently, DSP was thought to exclusively interact with intermediate filament cytoskeleton. However, recent evidence has shown that the protein, both in the epidermis and in cultured keratinocytes, might also be involved in the reorganization of microtubules (Garrod and Chidgey, 2008). As keratinocytes progressively differentiate, microtubules are subjected to an extensive rearrangement from a widespread and continuous network emanating from the centrosome, to one that is specifically restricted on the cell's periphery that concentrates on desmosomes. It is now evident that DSP plays a central role in this process since it directly binds, through the coil- coiled domain, to the microtubule anchoring protein nein that is therefore recruited to desmosomes (Lechler and Fuchs, 2007).

Immunostaining of K14 and K10 on samples deriving from an ulcerative lesional area of the left armpit of HSM5 and from the same body site of HSM5 healthy control were performed in order to assess the presence of any alterations at the level of keratinocyte differentiation amongst the two samples. As shown in Figure 26, no significant differences in K14 and K10 distributions were detected in the analysed skin biopsies.

Particular attention should be given to K14: in HSM5 healthy control K14 is distinctly localised in the cells of the basal layer directly resting on the basement membrane, while in HSM5 K14 seems to be also partially distributed in the suprabasal layers. This discrepancy is due to technical issues related to the fact that the skin biopsies deriving from HSM5 are old and of poor quality. In addition, the skin biopsy of HSM5 was not perfectly cut at a 90 ° angle and the analysed region presents nuomeorus invaginations at the basal layer-dermal interface. Neverthless, even if results might be subjected to a bias related to technical problems, hence obliging to interpret results very cautiously, images indicate no significant differences in K14 localisation. On the other hand, the staining of K10 indicates a clear distribution of the cytokeratin in the suprabasal layers. The registered distributions of tested cytokeratins corresponds to a physiological condition (Gilaberte et al., 2016; Sanghvi-Shah and Weber, 2017).

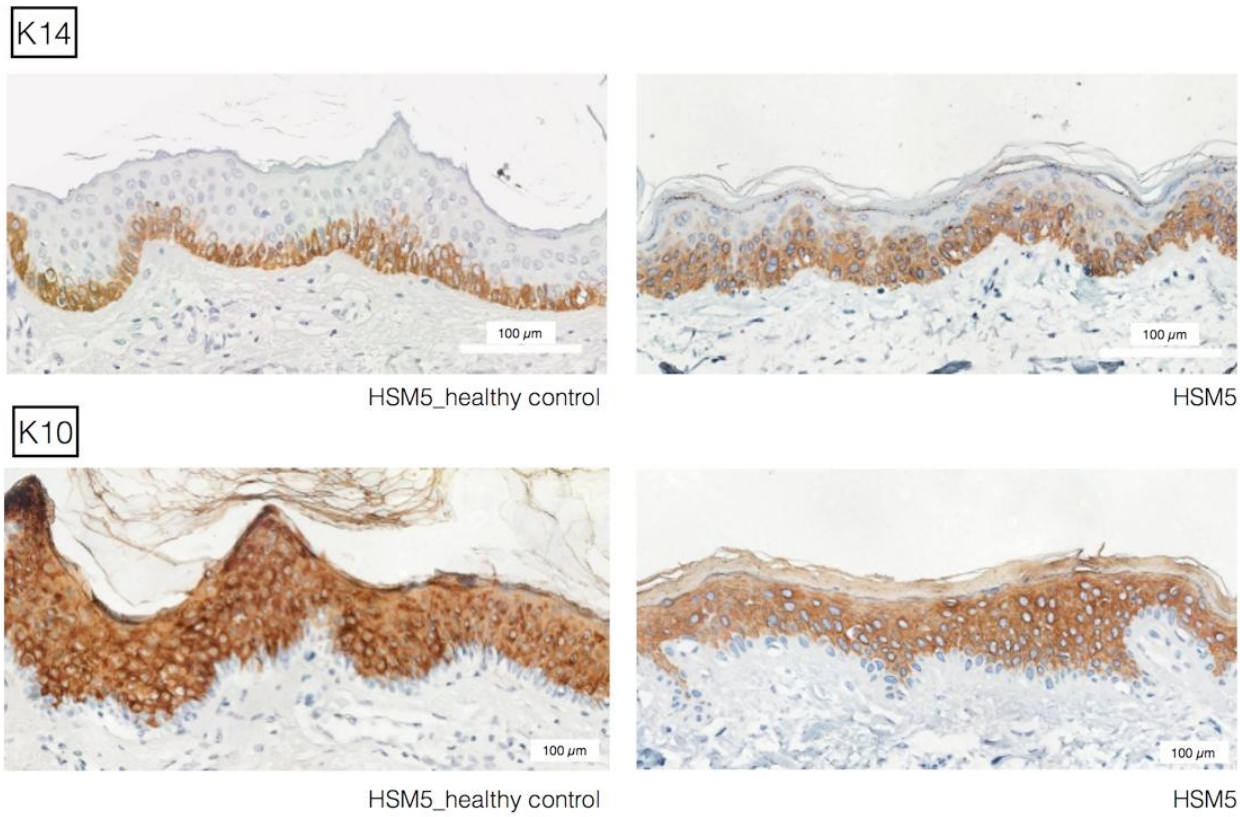

Figure 26. Distribution of K14 and K10 in skin biopsies. Immunostaining of K14 and K10 was performed on skin biopsies deriving from an ulcerative lesional area of the left armpit of HSM5 and from the same body site of a healthy control matched per age and sex (HSM5_healthy control). In both samples K14 is distinctly localised in the cells of the basal layer directly resting on the basement membrane (top), while the staining of K10 indicates a clear distribution of the cytokeratin in the suprabasal layers (bottom). All images were acquired at 60x magnification (scale bar 100 µm).

In vitro studies on HaCaT *DSP* clones aimed at analysing the impact of the variant on cellular differentiation are currently ongoing.

Desmosomes exert a pivotal role also in the regulation of keratinocyte proliferation. Desmosomal cadherins have for long been identified as crucial effectors of this process since they possess a tightly regulated expression pattern in the stratified epithelium, and since cadherin-mediated adhesion in epithelial cells is associated to the activation of MAPK (mitogen-activated protein kinase) and PI3K (phosphatidylinositol 3-kinase) signaling pathways (Saito et al., 2012).
Evidence deriving from hereditary human diseases associated to *DSP* gene indicate that alterations in *DSP* expression results not only in tissue disruption but can also induce changes in cellular proliferation by modulating epithelial sheet formation (Wan et al., 2007). In HaCaT cells treated with a transient RNA interference (RNAi) to down-regulate *DSP*, authors observed a concomitant reduced expression of other desmosomal proteins, increased cell proliferation associated to phospho-ERK1/2 and phospho-Akt levels, and an enhanced progression from G1 to S phase when compared to control cells (Wan et al., 2007).
In order to determine the presence of any alterations at the level of keratinocyte proliferation, immunostaining of Ki67, a well-established proliferation marker, was performed on samples deriving from an ulcerative lesional area of the left armpit of HSM5 and from the same body site of HSM5 healthy control.
Ki67 was chosen to monitor proliferation in skin samples since its levels of expression are strictly associated to cell proliferation and are exclusively detected during the active phases of cell cycle progression (Scholzen and Gerdes, 2000). As shown in Figure 27, no significant variations in Ki67 staining were registered amongst the two samples. Indeed, the signal appears to be primarily localized in a restricted number of cycling basal keratinocytes interspersed in a predominant population of non-cycling cells committed to terminal differentiation and waiting for appropriate signals to induce their migration towards the suprabals layers (Heenen et al., 1998). Also in this case, the fact that in HSM5 sample Ki67+ cells seem to be majourly interspersed also in the suprabasal layers, is due to technical issues related to the fact that the skin biopsies deriving from HSM5 are old and of poor quality. Taking into account these technical bias, it it possible to confirm the presence of no significant differences between analysed samples; nevertheless, results need to be interpreted prudently.

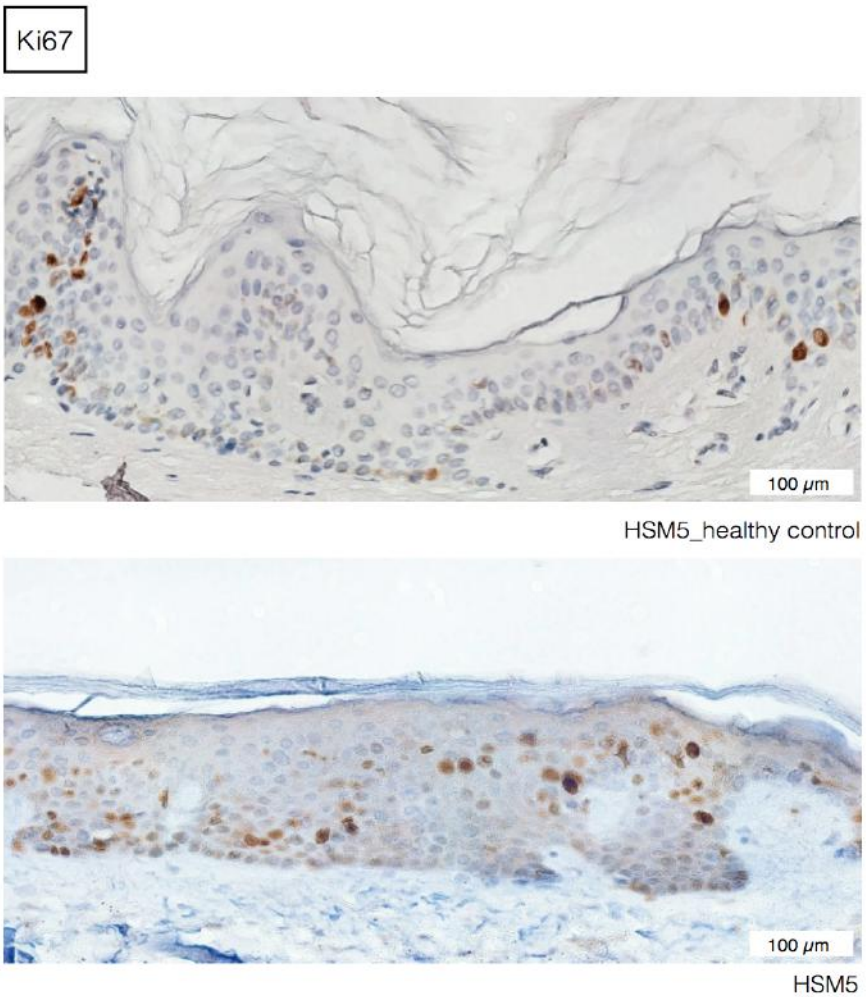

Figure 27. Distribution of Ki67 in skin biopsies. Immunostaining of Ki67 was performed on skin biopsies deriving from an ulcerative lesional area of the left armpit of HSM5 and from the same body site of a healthy control matched per age and sex (HSM5_healthy control). (A) In HSM5 healthy control, Ki67 staining appears to be primarily localized in a restricted number of cycling basal keratinocytes interspersed in a predominant population of non-cycling cells committed to terminal differentiation. (B) In HSM5 Ki67+ cells seem to be more numerous and unevenly distributed also in the suprabasal layers. All images were acquired at 60x magnification (scale bar 100 μm).

In addition, the potential impact of *DSP* variant on cell proliferation was assessed in HaCaT *DSP* WT/WT, WT/KI, WT/KO and KI/KO cells. The progression of proliferation was monitored over time and registered at different time periods (24-48-72 hours). As indicated in Figure 28, no significant changes in MFI of CFSE were observed in none of the tested clones and in none of the selected timings.

These results lead to the assumption that the variant is apparently not able to induce variations in keratinocyte proliferation, thus further sustaining the outcomes observed in skin samples.

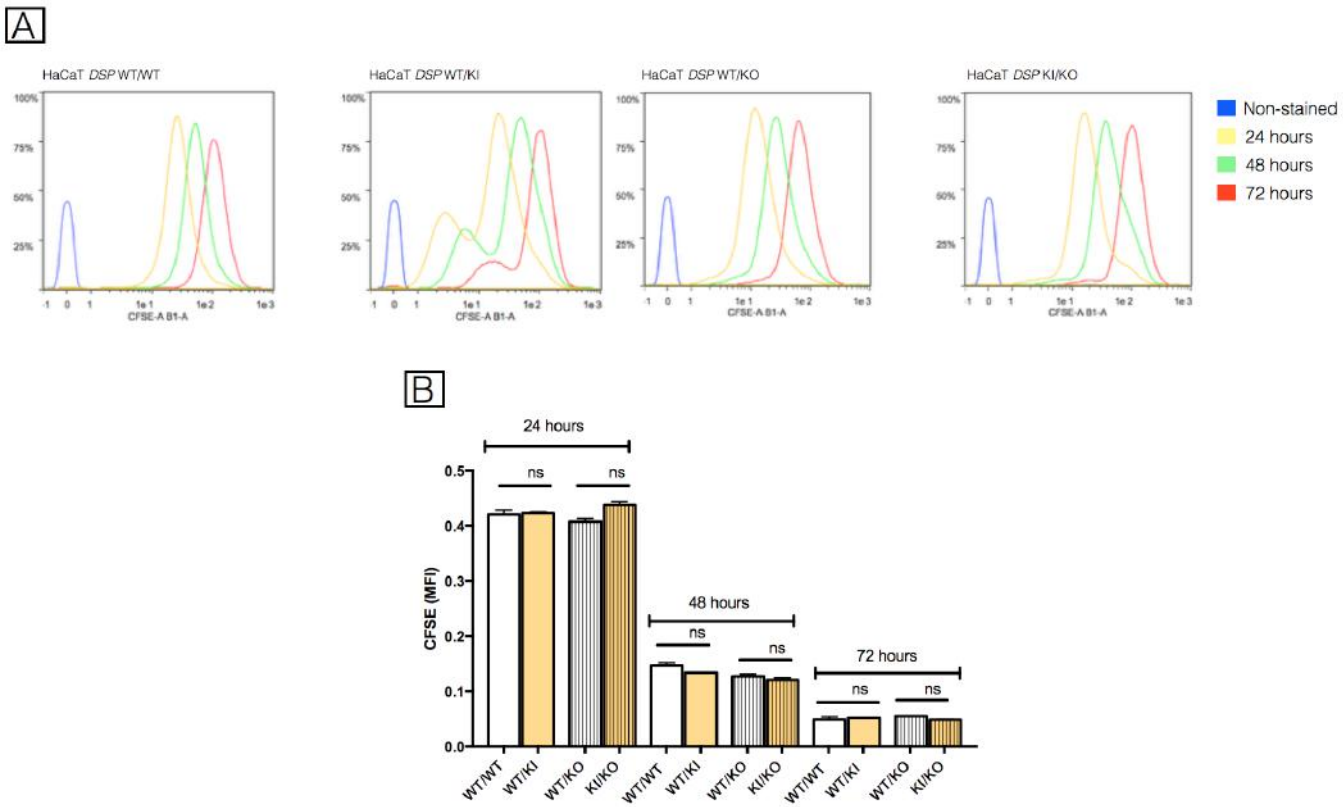

Figure 28. Proliferation assays in HaCaT *DSP* clones. In HaCaT *DSP* clones, proliferation was evaluated at 24, 48 and 72 hours by CFSE assay. (A) Representative images showing the staining with CFSE at the following time intervals: 24 (yellow), 48 (green) and 72 (red) hours. Non-stained cells are shown in blue. (B) MFI of CFSE in HaCaT *DSP* clones at different time intervals. Each value represents the mean ± SD of three independent experiments. Data analyses were performed with Mann-Whitney *U test* by comparing *DSP* WT/WT cells with *DSP* WT/KI cells and WT/KO clones with KI/KO clones; ns: not significant.

Results suggest that although the intracellular distribution DSP and the morphology of desmosomes in the PASH case results to be altered, together these factors do not strictly affect cellular differentiation and proliferation. It is possible to hypothesise that other signalling pathways known to regulate keratinocyte fate and homeostasis by finely modulating the expression of differentiation genes and cytoskeletal remodelling, might compensate for potential functional and structural deficiencies of desmosomes during these processes (McMullan et al., 2003; Dubash and Green, 2011).

4.7 Barrier function of the skin and TEWL

The skin constitutes a primary barrier that creates a definite separation between the body and the environment. The skin barrier functionally resides in the most superficial layer of the epidermis, the stratum corneum consisting of corneocytes interspersed in an abundant extracellular lipid matrix. Barrier functions prevent the excessive water loss through the epidermis (TEWL) and avoids the

permeation of compounds from the environment into the viable epidermal and dermal layers thereby limiting the onset of immune responses (van Smeden and Bouwstra, 2016).

The maintenance of adequate levels of skin hydration, defined by the water content of the stratum corneum, is an aspect that has recently gained renewed attention since it has been seen to mediate crucial physiological characteristics of the skin including barrier function, mechanical properties, drug penetration and desquamation (Berardesca et al., 2018). In chronic skin diseases, including PS and atopic dermatitis, different studies confirmed the presence of an incremented TEWL accompanied by a low water content of the skin due to a defective water retention capacity of the stratum corneum. It has been hypothesised that in skin disorders higher TEWL values associated to low hydration might be due to defects in skin barrier functions and/or to alteration in the keratinisation processes (Berardesca et al., 2018). In addition, one case report presenting a *DSP* mutation that completely truncated the C-terminal region of the protein was charachterised by lack of hair (alopecia), nail loss, and death at 10 days post-partum due to excessive TEWL (Jonkman et al., 2005).

The evaluation of the water flow from the stratum corneum to the environment is conventionally determined by the registration of TEWL values that provide standardised measurements and constitute a non-invasive procedure widely employed for monitoring skin pathologies (Rogiers and EEMCO Group, 2001). HSM5, F_HSM5, M_HSM5 and healthy controls matched per age and sex to each family member were subjected to the analysis. Particular attention was given to the selection of controls since TEWL values are known to conspicuously decrease during aging in a sex-dependent manner (Leveque et al., 1984).

As indicated in Figure 29, significant increments in TEWL (g/m^2h) values were observed in all family members while compared to their respective control on the face (forehead/cheek) (TEWL: HSM5 25,1±0.01, $p<0.05$; HSM5_healthy control 3.867±1.371), (TEWL: M_HSM5 19.83±1.069, $p<0.05$; M_HSM5_healthy control 14.33±2.266) (TEWL: F_HSM5 17.13±4.5, $p<0.05$; F_HSM5_healthy control 9.15±1.542), in the left fingertip (TEWL g/m^2h: HSM5 34.33±1.115, $p<0.05$; HSM5_healthy control 18.05±4.108), (TEWL: M_HSM5 35±2, $p<0.05$; M_HSM5_healthy control 23.22±2.839) (TEWL: F_HSM5 20±1, $p<0.05$; F_HSM5_healthy control 14.47±3.209), while in the right fingertip statistically significant changes were observed only in HSM5 (TEWL: HSM5 29.33±1.528, $p<0.05$; HSM5_healthy control 17.95±1.297), and M_HSM5 (TEWL: M_HSM5 31.87±1.963, $p<0.05$; M_HSM5_healthy control 22.65±3.541).

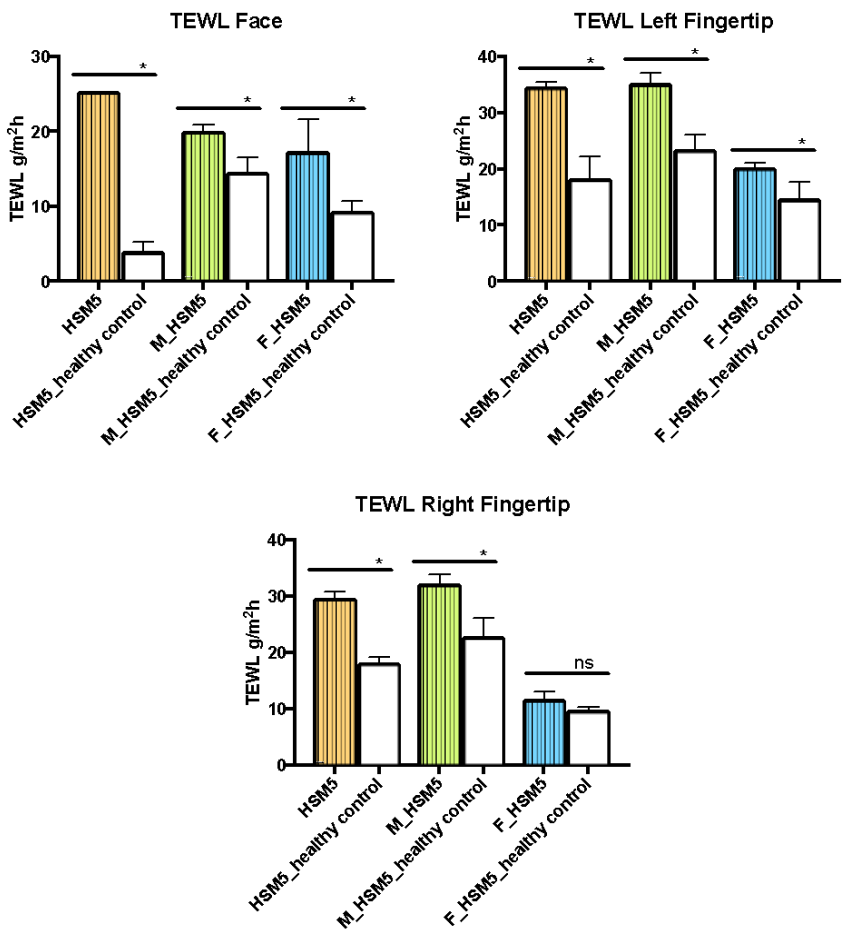

Figure 29. Transepidermal water loss (TEWL) in HSM5, M_HSM5, F_HSM5 and healthy controls. TEWL was performed on HSM5, F_HSM5, M_HSM5 and healthy controls matched per age and sex to each family member. For all analysed individuals, TEWL measurements were acquired on the face (forehead/cheek), on the left fingertip and on the right fingertip. Each value represents the mean ± SD of three independent experiments. Data analyses were performed with Mann-Whitney *U test* comparing each family member to their respective healthy control; ns: not significant; *p<0,05.

These values might indicate that in all family members, both in the patient carrying the variant in homozygosis and in his parents presenting the variant in heterozygosis, alterations in skin barrier function are present, since the occurrence of keratinisation defects were previously excluded in HSM5.

The acquisition of TEWL measurements was also performed on HS cases matched per age and sex to HSM5. As indicated in Figure 30, significant increments in TEWL (g/m^2h) values were observed in HSM5 when compared to HS cases on the left fingertip (TEWL: HSM5 34.33±1.115, $p<0.002$; HS cases 14.04±4.246) and on the right fingertip (TEWL: HSM5 29.33±1.528, $p<0.002$; HS cases 16.9±4.408).

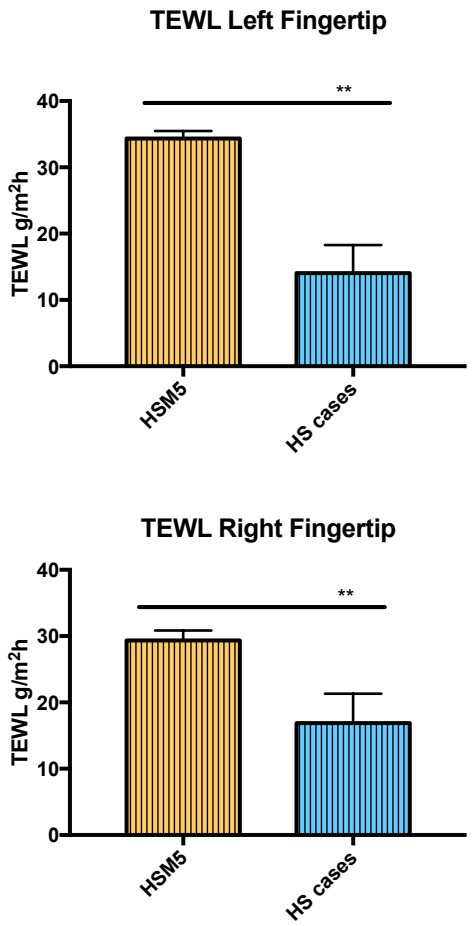

Figure 30. Transepidermal water loss (TEWL) in HSM5 and HS cases. TEWL was performed on HSM5 and on HS cases matched per age and sex to HSM5. TEWL measurements were acquired on the left fingertip and on the right fingertip. Each value represents the mean ± SD of three independent experiments. Data analyses were performed with Mann-Whitney *U test* comparing each family member to their respective healthy control; ns: not significant; **p<0,002.

These results further corroborate the possibility that in HSM5, the identified *DSP* variant, might alter desmosome structure and interfere with the constitution of the epidermal permeability barrier since the epidermis of HSM5 seems to favour the passive evaporation of unbound water through the skin.

The results obtained from the various experimental procedures collectively indicate that the identified *DSP* exonic variant (rs17604693; g.7565494 A>T; c.913A>T, p.Ile305Phe) is a damaging SNV that might strongly impact the functionality of DSP dimer and more broadly of the desmosome.

In silico molecular modelling trajectories highlighted that the DSP dimers carrying the variant in homozygosis and in heterozygosis presents a more stable and compact structure if compared to the wild-type moiety, effect that is greater in the mutated homozygote.

These structural alterations might contribute to an insufficient recruitment of DSP on the desmosomal plaque. Indeed, as indicated in IHC assays DSP shows a cytoplasmic localisation in HSM5 rather than on cell borders as seen in the healthy control. Moreover, both in DSP WT/KI and KI/KO clones, a significant reduction in DSP hyper-adhesive *puncta*/cell were retrieved if compared to controls.

The organisation in characteristic and well conserved electron dense structures is considered as strictly necessary to guarantee the correct organisation and function of mature desmosomes (Garrod and Chidgey, 2008; Hino et al., 1991). In HSM5 desmosomes appeared to be longer and to possess a major degree of flexion if compared to the healthy control. In KI/KO clones, cells presented an unequal deposition of proteins on the intracellular plaque that gave origin to asymmetric structures identified as two different subsets of desmosomal populations that include a shorter and thinner one, and an extensively stretched out one.

No relevant changes in terms of differentiation and proliferation processes were detected in skin biopsies or in cellular clones in presence of the *DSP* variant. On the contrary, significant increments in TEWL values were registered in HSM5 if compared to the healthy control or HS cases matched per age and sex. Analogue increments were observed in M_HSM5 and F_HSM5 if compared to matched healthy controls.

It is possible to speculate that, since proliferation and differentiation issues were excluded both in HSM5 skin biopsies and in cellular clones, the *DSP* SNV presumably alters the mechanical adhesion properties of desmosomes and leads to the disruption of tissue integrity by affecting the properties of the epidermal permeability barrier (Garrod and Chidgey, 2008).

Nevertheless, as suggested by cell biology experiments the variant seems to be dominant since it determines phenotypic changes both when expressed in homozygosis and heterozygosis. In HSM5 the variant is present in homozygosis and the patient reports to be affected by broad and severe skin manifestations together with different associated comorbidities. On the contrary, M_HSM5 and F_HSM5 carrying the SNV in heterozygosis, report to be completely healthy.

In the case of HSM5, it is possible to hypothesize that the effect of the *DSP* variant results to be damaging for two main reasons: firstly, the SNV is present in homozygosis, therefore both alleles carry the variant and no compensating mechanisms aimed at recovering, at least partially, the functionality of DSP protein are available; secondly, the *DSP* variation occurs simultaneously with the auto-inflammatory *NOD2* SNV (rs2066847; c.2938dup; p.Leu1007fsins), thus suggesting that

DSP might act as a modifier gene able to modulate the phenotypic manifestation of *NOD2* in a epistatic manner.

Further corroborating the potential involvement of *DSP* in the pathogenesis of PASH syndrome, are preliminary results derived from WES analysis, confirmed by Sanger sequencing, conducted on PASH patients that we were able to contact thanks to a cooperation with the Dermatology Department of the Fondazione IRCCS Ca' Granda Ospedale Maggiore Policlinico of Milan. Indeed, in one PASH case the same *DSP* SNV retrieved in HSM5 was detected in heterozygosis. In addition, in another PASH patient a rare (MAF<0.05) missense variant occurring in *DSP* gene was identified in heterozygosis. The recognised nucleotide change leads to an amino acid substitution happening in the N-terminal plakin domain of DSP dimer, the same affected region observed in HSM5.

4. RESULTS AND DISCUSSION

Part 2: The case of a Sardinian family

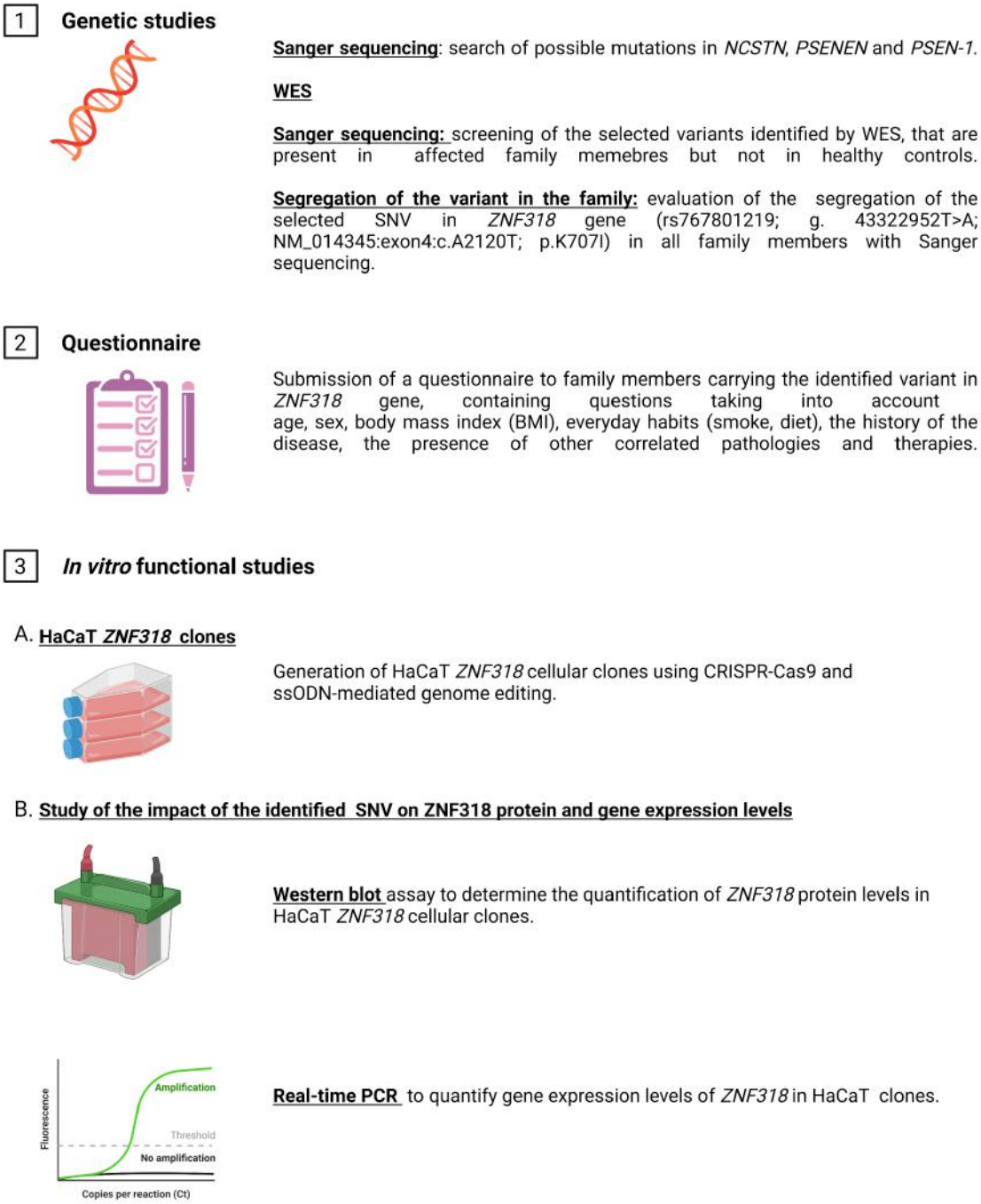

Figure 31. Schematic pipeline of the experimental procedures that were employed to perform genetic and functional studies on a Sardinian family affected by HS.

4.8 Identification of a missense exonic variant in *ZNF318* gene in the affected family members

Thanks to a cooperation with the Dermatology Department of the Fondazione IRCCS Ca' Granda Ospedale Maggiore Policlinico of Milan, we were contacted by a Sardinian family affected by a familial form of HS that never underwent genetic tests. A total of 47 individuals adhered to the study, 11 of which declared to be affected by HS (HS35, HS40, HS53, HS71, HS74, HS80, HS81, HS103, HS108, HS111, HS115), and were then confirmed as HS cases following a telephone interview with a medical doctor. In addition, 4 deceased individuals were reported to have been affected by the disease (Figure 32).

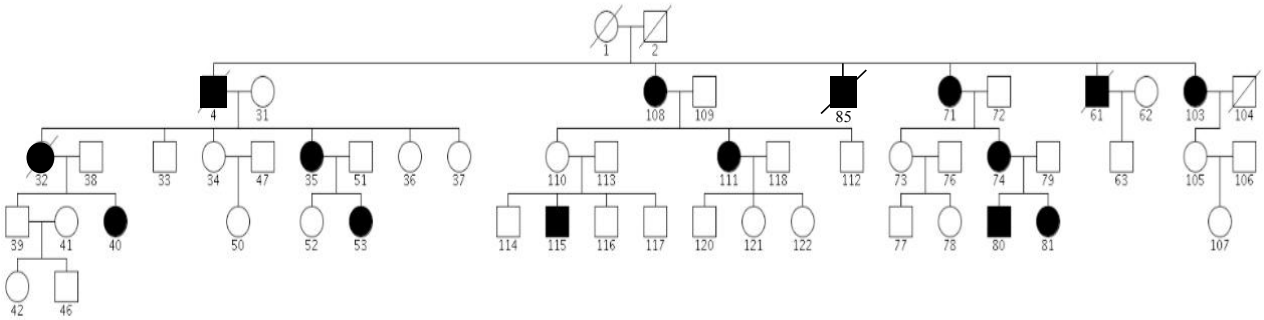

Figure 32. Pedigree of the Sardinian family. 47 individuals adhered to the study, 11 of which declared to be affected by the diseases and 4 of which were reported to have been affected by HS (deceased cases). The disease seems to show an autosomal dominant inheritance since every generation possesses affected members and both genders transmitted the disease to their offsprings. In the family 10 females and 5 males were diagnosed with HS.

Even if the health state of the individuals of the first generation is not known, by observing the pedigree it is possible to speculate that the disorder shows an autosomal dominant-like inheritance since every generation possesses affected members and both genders transmitted the disease to their offsprings. Collectively, in the family 10 females and 5 males were diagnosed with HS. This result highlights an unequal distribution of the disease amongst the two sexes, outcome that is found to be in accordance with literature findings that report a female predominance of the disease (Deckers et al., 2014).

According to literature data that identified a typical pool of mutations occurring in familiar forms of HS found in genes encoding for the various subunits of the γ-secretase complex (Frew et al., 2017), three affected family members (HS71, HS74, HS80) and one healthy control (HS73) were selected and submitted to Sanger sequencing in order to evaluate the presence of mutations in *NCSTN, PSENEN* and *PSEN-1* genes (Figure 33).

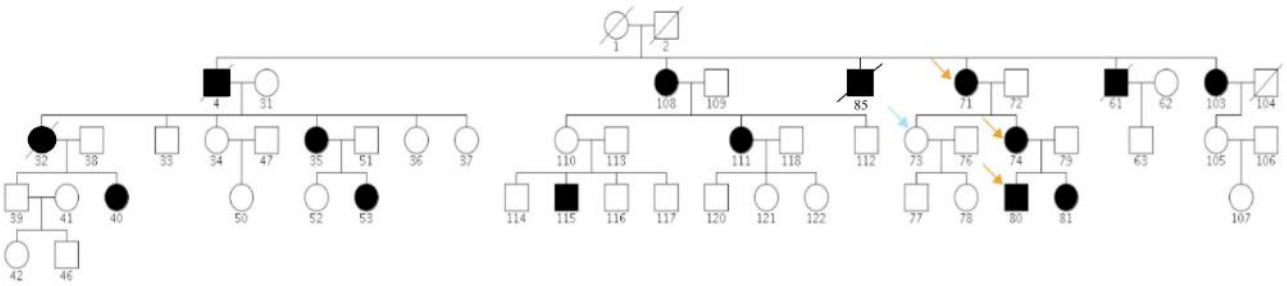

Figure 33. Individuals of the Sardinian family initially submitted Sanger sequencing. Three affected family members (HS71, HS74, HS80) indicated with the orange arrow and one healthy control (HS73) designated with the blue arrow, were initially submitted to Sanger sequencing in order to evaluate the presence of mutations in *NCSTN, PSENEN* and *PSEN-1* genes.

Since no genetic variants in *NCSTN, PSENEN* and *PSEN-1* genes were identified in the analysed cases if compared to the sequence retrieved in the healthy control, WES was performed in order to identify recurrent genetic variants in HS71, HS74 and HS80 cases and not in HS73 healthy control. WES results were processed in order to recover the SNVs that are most likely to be deleterious or pathogenic or functional, by performing a ranking according to the PHRED score with a cut-off of 15, that led to the identification of 29 different exonic variants (Table 8).

Chr	Position	Gene	SNV	Variant effect	HS73	HS71	HS74	HS80
2	g.152346522 G>A	*NEB*	rs78592085	Missense	G/G	G/A	G/A	G/A
2	g.18974279 G>A	*ANKAR*	rs80227981	Missense	G/G	G/A	G/A	G/A
2	g.201846387 C>T	*FAM126B*	rs762955857	Missense	C/C	C/T	C/T	C/T
2	g. 84886244 C>A	*DNAH6*	rs199962095	Missense	C/C	C/A	C/A	C/A
2	g.178528608 T>C	*PDE11A*	rs74357545	Missense	T/T	T/C	T/C	T/C
2	g.167289012 T>A	*SCN7A*	rs148715564	Missense	T/T	T/A	T/A	T/A
2	g. 103039780 G>A	*IL18RAP*	.	Missense	G/G	G/A	G/A	G/A
3	g.66431144 T>A	*LRIG1*	rs140085866	Missense	T/T	T/A	T/A	T/A
4	g.88732968 G>A	*IBSP*	rs141138203	Missense	G/G	G/A	G/A	G/A
4	g. 74275172 G>A	*ALB*	rs148571509	Missense	G/G	G/A	G/A	G/A

5	g.148997780 C>T	*ARHGEF37*	rs567909765	Missense	C/C	C/T	C/T	C/T
6	g.125619955 G>A	*HDDC2*	rs149284773	Structural	G/G	G/A	G/A	G/A
6	g. 43322952 T>A	*ZNF318*	rs767801219	Missense	T/T	T/A	T/A	T/A
6	g.116784650 T>C	*FAM26F*	.	Missense	T/T	T/C	T/C	T/C
8	g. 96064423 G>A	*NDUFAF6*	rs61743028	Missense	G/G	G/A	G/A	G/A
9	g. 79320164 G>C	*PRUNE2*	.	Missense	G/G	G/C	G/C	C/C
9	g. 990638 C>T	*DMRT3*	rs147930723	Missense	C/C	C/T	C/T	C/T
9	g. 977056 C>T	*DMRT3*	.	Missense	C/C	C/T	C/T	C/T
12	g.111956226 T>C	*ATXN2*	rs117851901	Missense	T/T	T/C	T/C	T/C
12	g. 2973517 C>T	*FOXM1*	rs147362692	Missense	C/C	C/T	C/T	C/T
12	g.105520057 T>G	*KIAA1033*	.	Missense	T/T	T/G	T/G	T/G
13	g. 99537338 A>C	*DOCK9*	rs200500566	Missense	A/A	A/C	A/C	A/C
16	g. 58072286 A>C	*MMP15*	rs149358631	Missense	A/A	A/C	A/C	A/C
17	g.18145527 C>T	*LLGL1*	rs150245335	Missense	C/C	C/T	C/T	C/T
17	g. 71431625 C>T	*SDK2*	rs202233721	Missense	C/C	C/T	C/T	C/T
17	g. 26905500 G>A	*SPAG5*	rs143024358	Missense	G/G	G/A	G/A	G/A
19	g.45912489_45 912491delAAG	*CD3EAP*	rs35729377	Inframe deletion	AAG/AAG	AAG/-	AAG/-	AAG/-
20	g. 16496299 G>A	*KIF16B*	rs140237322	Missense	G/G	G/A	G/A	G/A
20	g. 51871502 G>A	*TSHZ2*	rs45479792	Missense	G/G	G/A	G/A	G/A

Table 8. List of the single nucleotide variations (SNV) identified through WES analysis. List of SNV possessing a PHRED>15 identified following WES in HS71, HS74 and HS80 cases and not in HS73 healthy control (orange). For each variant is provided the chromosome, the genomic position including the reference allele and the alternate allele, the name of the gene, the locus accession for the variant type assigned by dbSNP (rs), mutation category and the genotype found in in HS73 healthy control and in HS71, HS74 and HS80 cases. When not available, the rs is indicated with a dot (.).

In order to further screen WES results, Sanger sequencing targeting the identified genes was extended to other three affected family members (HS111, HS53, HS103) (Figure 34).

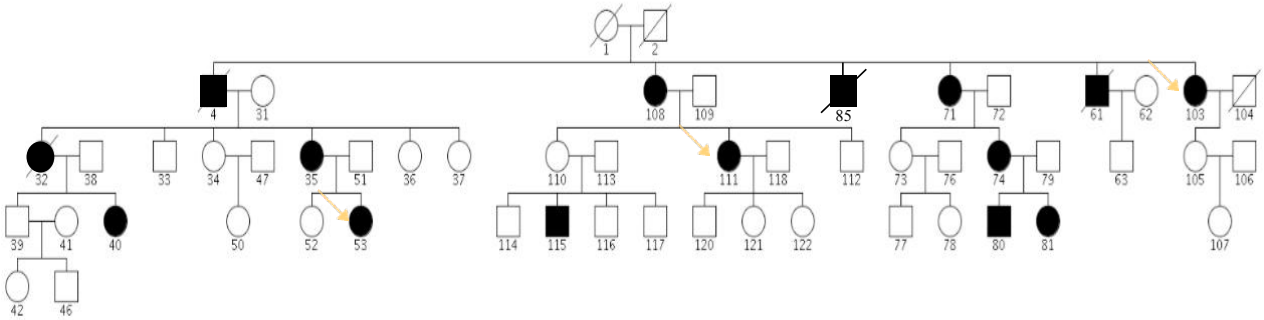

Figure 34. Screening of WES results by Sanger Sequencing. In order to further screen the single nucleotide variations (SNV) identified by WES analysis, Sanger sequencing of target genes was extended to other three affected family members (HS111, HS53, HS103) (orange arrow).

Results allowed the identification of only one gene carrying the variant in all six cases, *ZNF318* (rs767801219; g. 43322952T>A; NM_014345:exon4:c.A2120T; p.K707I), a rare (MAF<0.01) missense SNV that was never been previously correlated to any disease, located on exon 4 of the gene (Table 9).

Chr	Position	Gene	SNV	HS111	HS53	HS103
2	g.152346522 G>A	*NEB*	rs78592085	G/G	G/G	G/A
2	g.18974279 G>A	*ANKAR*	rs80227981	G/G	G/G	G/A
2	g.201846387 C>T	*FAM126B*	rs762955857	C/C	C/C	C/T
2	g. 84886244 C>A	*DNAH6*	rs199962095	C/C	C/C	C/C
2	g.178528608 T>C	*PDE11A*	rs74357545	T/T	T/T	T/C
2	g.167289012 T>A	*SCN7A*	rs148715564	T/T	T/T	T/A
2	g.103039780 G>A	*IL18RAP*	.	G/G	G/G	G/A
3	g.66431144 T>A	*LRIG1*	rs140085866	T/T	T/A	
4	g.88732968 G>A	*IBSP*	rs141138203	G/G	G/G	
4	g. 74275172 G>A	*ALB*	rs148571509	G/G	G/G	G/A
5	g.148997780	*ARHGEF37*	rs567909765	C/C	C/C	C/T

	C>T					
6	g.125619955 G>A	*HDDC2*	rs149284773	G/G	G/G	G/G
6	g. 43322952 T>A	*ZNF318*	rs767801219	T/A	T/A	T/A
6	g.116784650 T>C	*FAM26F*	.	T/T	T/T	T/T
8	g. 96064423 G>A	*NDUFAF6*	rs61743028	G/G	G/A	G/G
9	g. 79320164 G>C	*PRUNE2*	.	G/C	G/G	G/G
9	g. 990638 C>T	*DMRT3*	rs147930723	C/T	C/C	C/T
9	g. 977056 C>T	*DMRT3*	.	C/C	C/T	C/T
12	g.111956226 T>C	*ATXN2*	rs117851901	T/T	T/T	T/C
12	g. 2973517 C>T	*FOXM1*	rs147362692	C/T	C/C	C/C
12	g.105520057 T>G	*KIAA1033*	.	T/T	T/T	T/G
13	g. 99537338 A>C	*DOCK9*	rs200500566	A/A	A/A	A/A
16	g. 58072286 A>C	*MMP15*	rs149358631	A/A	A/A	A/C
17	g.18145527 C>T	*LLGL1*	rs150245335	C/T	C/C	
17	g. 71431625 C>T	*SDK2*	rs202233721	C/C	C/C	C/T
17	g. 26905500 G>A	*SPAG5*	rs143024358	G/A	G/G	G/G
19	g.45912489_ 45912491del AAG	*CD3EAP*	rs35729377	AAG/AAG	AAG/AAG	
20	g. 16496299 G>A	*KIF16B*	rs140237322	G/G	G/A	G/G
20	g. 51871502 G>A	*TSHZ2*	rs45479792	G/G	G/G	G/A

Table 9. List of the single nucleotide variations (SNV) obtained during WES analysis. List of SNV with a PHRED>15 obtained following WES analysis in HS111, HS53 and HS103 cases. For each variant is provided the chromosome, the genomic position including the reference allele and the alternate allele, the name of the gene, the locus accession for the variant type assigned by dbSNP (rs), mutation category and the genotype found in the three affected family members following Sanger sequencing. The only one gene carrying the variant in all six cases is highlighted in orange.

Next, the *ZNF318* variant was evaluated through Sanger sequencing in all the family members who adhered to the study. The SNV was detected in heterozygosis in 17 family members comprising all

of the 11 individuals who initially declared to be affected by HS and in additional 6 individuals (HS110, HS34, HS39, HS52, HS116, HS42) that haven't mentioned to possess any sign of the disease (Figure 35).

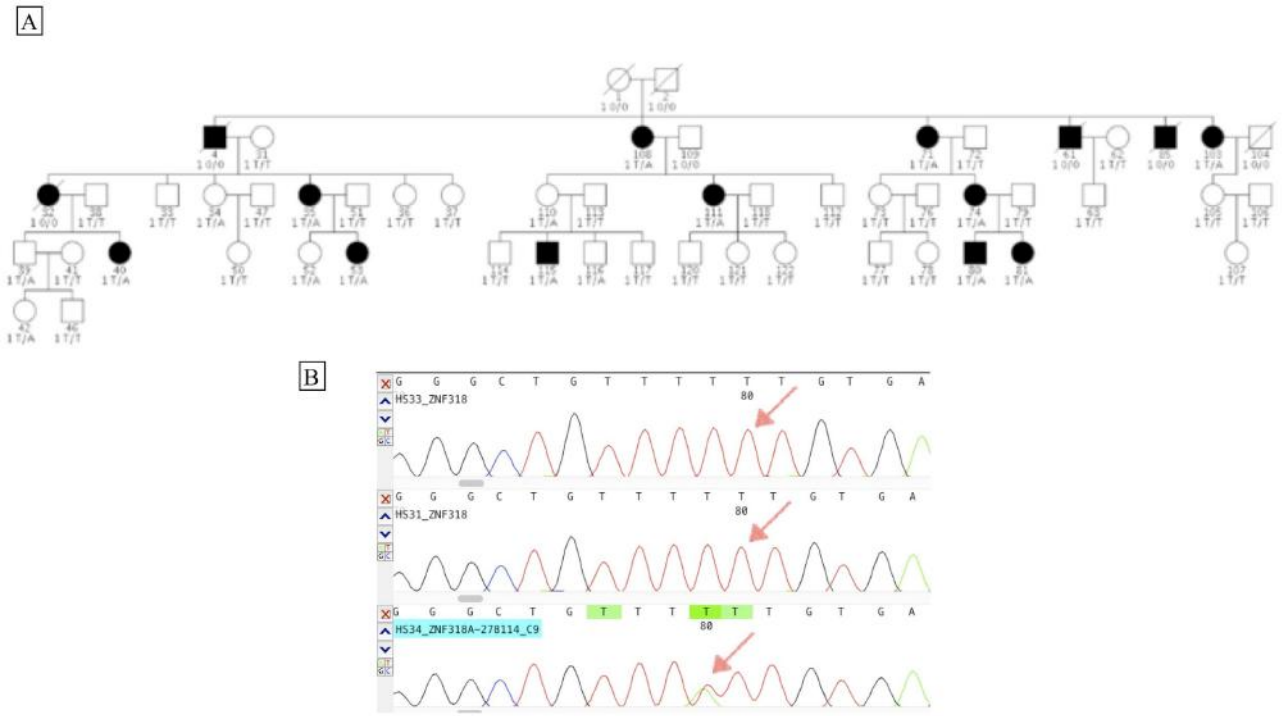

Figure 35. Confirmation of the selected *ZNF318* variant (rs767801219; g.43322952T>A; NM_014345:exon4:c.A2120T; p.K707I) in all family members through Sanger sequencing. (A) Schematic representation of the pedigree of the Sardinian family. Identified genotypes for the selected *ZNF318* variant are reported under each family member. (B) Representative chromatograms deriving from Sanger sequencing of DNA amplification products of *ZNF318* gene. HS33, HS31 and HS34 have all reported to be healthy. HS33 and HS31 carry only wild-type alleles while HS34 is heterozygous for the *ZNF318* variant.

We asked all family members in which the SNV in *ZNF318* gene was detected in heterozygosis whether they were willing to be interviewed by phone. Not all the individuals of interest agreed to be consulted, and those who adhered are 7 of the 11 patients who declared to be affected by HS at the beginning of the study. Recruited individuals were submitted to a questionnaire that takes into account height, weight, sex, age, everyday habits (smoke, diet), the history of the disease, the presence of other correlated pathologies and therapies, aspects that need to be taken seriously into account in order to identify potentially crucial factors that might contribute to unravel putative pathogenic mechanisms at the basis of the onset, progression and severity of HS in the Sardinian family (Table 10).

HS	Age	Sex	Body Mass Index (BMI)	Smoke	Type of Manifestations
35	50	F	27.51	Yes	Abscesses
40	36	F	26.81	No	Cysts
53	24	F	27.55	Yes	Abscesses
74	48	F	22.43	Yes	Abscesses, fistulas, scars
80	24	M	22.2	No	Abscesses and fistulas
81	22	F	20.03	Yes	Abscesses
115	24	M	19.24	Yes	Abscesses and fistulas

HS	Age of onset	Year of diagnosis	First area involved	Trend	Exacerbations in 1 year
35	16	Never diagnosed	Inguinal area + vulva	Stable	1 or 2
40	14 (with menstrual cycle)	Never diagnosed	Inguinal area	Stable	1 or 2
53	13 (with menstrual cycle)	Never diagnosed	Inguinal area	Stable	12
74	12	40	Thigh	Slow progression	30/40
80	16/17	Not diagnosed yet, follow-up in Venice	Thigh	Stable, with an improvement after puberty	3 or 4
81	14	Never diagnosed	Inguinal area	Overall improvement over the last years	1
115	18	22	Axilla	Variable	2

HS	Food that exacerbates HS	Do seasons worsen HS	Worsening during menstrual cycle	Complications	Associated diseases
35	Lactose	Summer	Yes, during menstrual cycle	None	None
40	None	Autumn	Yes, before menstrual cycle	None	None
53	Spicy	No	Yes, before menstrual cycle	Scars	None
74	Lactose, gluten	Winter	Yes, before menstrual cycle	Necrotizing fascitis, scars	Arthritis, arthrosis, chronic inflammation of the cervical spine
80	Gluten, alcohol	Winter		Sever oedema	None
81	Lactose, gluten	Seasonal change	No	None	None
115	None	Summer		Sever oedema and scars. Can't move arms during exacerbations.	None

HS	Currently involved areas	Therapies	Other
35	Inguinal area	Ammonium bituminosulfonate	None
40	Inguinal area, scalp	None	None
53	Inguinal area	None	Stopped oral contraceptive and HS improved
74	axillae, inguinal region, gluteus, tights, face, abdomen, mammary area	Diet, topical antibiotics, topical steroids, oral isotretinoin, hormonal therapy, drainage. Surgical excision	Oral contraceptive worsened HS phenotype
80	Tights, back, cysts on the face	Isotretinoin for acne with success. Macladin 500 mg with benefit. Surgical treatment on the face	Exacerbations during stressful periods. Severe acne during puberty. Cyst on the scalp
81	Inguinal area, axilla	Topical antibiotis with benefits	Exacerbations during stressful periods. Dental abscesses
115	Axillae, inguinal region, gluteus, perineum	Stop smoking, stop deodorant and treated with oral antibiotics. All interventions result without benefits	Exacerbations during stressful periods.

Table 10. Results of the questionnaire submitted to the members of the Sardinian family presenting the detected SNV in *ZNF318* gene in heterozygosis.

Obtained results indicate that smoking is clearly a current habit between the affected members, and that only one of them (HS115) stops during exacerbations. Amongst analysed individuals, the average body mass index (BMI) is of 23.68, and only three cases present a BMI > 25 and therefore can be considered as overweight (HS35, HS40, HS53). Abscesses constitute the most common clinical manifestation observed in cases, while the occurrence of cysts was present but not frequently reported.

Amongst female cases, it is possible to define a connection between HS flaring and menstrual cycle; indeed, most females report a worsening in skin manifestations before menstruation.

Food seems to impact the clinical symptoms; in fact, the intake of lactose and gluten were indicated to worsen the phenotypic manifestations of HS. Specifically, the association between milk consumption and HS exacerbations has been investigated, and takes into account that milk is an

insulinotropic substance that may increase insulin levels and insulin-like growth factor 1 (IGF-1) (Boehncke at al., 2010).

Associations between seasonality and clinical manifestations is very heterogeneous; nevertheless, the transition from one season to another seems to constitute the most critical moment in terms of worsening of HS phenotype.

The age of onset is very similar amongst all cases and approximately coincides with puberty, period in which many declared to be affected by acne vulgaris. Interestingly, only 2 patients were officially diagnosed with HS, event that occurred with a non negligible delay between the initial onset and the establishment of the final diagnosis: 28 years for HS74 and 4 years for HS115.

Considering the affected areas, the inguinal region was the most frequently impacted site during the initial onset of the disease, followed by the thighs and the axillae. Only HS74 and HS115 declared that skin manifestations commonly occur also in atypical areas such as the face, gluteus, back and abdomen. In addition, the majority of cases exhibit a stable trend in the disease's course. Only HS74 is affected by a very severe form of HS, characterized by a slow but progressive worsening accompanied by extremely numerous exacerbations (40 in a year).

Only a few members show complications, collectively represented by oedema and permanent scars.

The collection of information relative to the followed therapeutic strategies was extremely complex since the majority of interviewed individuals declared to resort to self-medication, using topical agents. Indeed, since most of them have not been definitely diagnosed, except for 2 members, none have received neither a proper oral antibiotic therapy nor a topical therapy. Furthermore, stress appears as a very powerful trigger.

As far as the clinical features are concerned, it is possible to conclude that only one member, HS74, possesses a very severe form of HS. HS74 is the only case who declared to have a slow progression of the disease, whereas all the others present a stable trend. HS74 is also the only individual to bear more than two involved areas (axillae, inguinal region, abdomen, breast area, gluteus, tights and face). Furthermore, HS74 resulted as the only case to be affected by other auto-inflammatory diseases including arthritis, arthrosis, and chronic inflammation of the cervical spine. Amongst the identified complications, HS74 lamented also the occurence of granulomas and of dental abscesses.

In conclusion, while analysing the type of clinical manifestations together with the number of exacerbations and the affected body areas, it is possible to define that the Sardinian family is affected by a mild form of HS since the majority of the individuals present a Hurley stage I (5 cases) of the disease, while Hurley II (1 case) and Hurley III (1 case) staging is not frequent.

Overall, results suggest that the identified SNV presents an autosomal dominant inheritance pattern with incomplete penetrance. Indeed, this mode of inheritance might be supported by various

hypotheses that were taken into account. First, it is highly probable that some adult mutated family members have deliberately confirmed not to possess the disease because of the sense of shame and discomfort that commonly lead patients to reject HS. Next, one adult family member (HS39) carrying the missense variant, initially revealed to be completely healthy, but following further investigations, declared to have suffered from a mild form of acne vulgaris during puberty and to be affected by recurrent episodes of cyst formation on the back, suggesting that a failure to report the disease in this case might be associated to misdiagnosis. Notably, none of these mutated individuals are over-weight, a factor that is well known to be a potent trigger in negatively affecting the onset and severity of the disorder (Sabat et al., 2020). Finally, other healthy mutated family members have only passed puberty and HS42 is a child, hence it is possible to speculate that they might manifest HS in the future.
Nonetheless, these outcomes highlight the major limitation of the study, or else that the interpretation of results is biased due the lack of available clinical data.

ZNF318 (NC_000006.12) is a 62514 bp long protein coding gene, mapping on the short arm of chromosome 6 (6p21.1), consisting of 18 exons and encoding for zinc finger 318 (ZNF318), also known as testicular zinc finger (TZF), protein involved in the regulation of the androgen receptor (AR) by acting both as a co-repressor or co-activator in AR transactivation function (Tao et al., 2006a).

Androgen receptor signalling and its role in the skin

The AR is a ligand-activated transcription factor that upon binding with activated androgens, testosterone and dihydrotestosterone, translocates from the cytoplasm to the nucleus. Once in the nucleus, the AR binds as a homodimer to specific DNA sequences, collectively known as androgen-responsive elements, resulting in transcriptional repression or activation of androgen-dependent target genes. The androgen-bound AR complex recruits associated co-regulatory proteins, co-repressors or co-activators, that act by mediating chromatin modifications (Tao et al., 2006a). The signalling cascades induced by AR activation mediates a vast variety of biological functions including male sexual development, besides the development and maintenance of the musculoskeletal, cardiovascular, immune, neural and hematopoietic systems (Davey and Grossmann, 2016).
In the skin and its appendages, AR signalling is known to regulate fundamental functions including the growth and differentiation of sebaceous glands, hair growth, wound healing and epidermal

barrier formation (Del Rosso et al., 2020). The skin is involved both in responding to circulating androgenic pro-hormones, predominantly synthesised in the adrenal glands and in the gonads, and in the *de novo* synthesis of androgens from cholesterol and adrenal precursors with intracine or paracrine activities (Grymowicz et al., 2020). In the skin district, AR receptors are known to be expressed in epidermal and follicular keratinocytes, cells of the dermal papilla, sweat gland cells and to be up-regulated in sebocytes (Fritsch et al., 2001; Xie et al., 2016; Zouboulis, 2009).

Sebaceous glands are considered as key regulators in the maintenance of androgen homeostasis in the skin since crucial enzymes involved in the synthesis, activation and inactivation of androgens are expressed in sebocytes. Primarily the locally synthesised androgens, induce the commitment of AR-expressing immature sebocytes into progressively differentiating lipogenic cells, stimulate the proliferation of sebocytes and promote sebum production (Hirohiko et al., 1992; Imperato-McGinley et al., 1993). Sebum, a mixture of wax esters, cholesterol, fatty acids, cholesterol esters and triacylglycerol, is released by holocrine secretion on the skin's surface where it exerts pivotal functions related to skin homeostasis and innate skin immunity (Inoue et al., 2014). Indeed, in sebaceous gland-deficient mice, a decrement in the hydration levels of the stratum corneum together with enhanced cutaneous inflammation were observed (Wille and Kydonieus, 2003; Georgel at al., 2005). On the contrary, incremented levels of sebum secretion are known to cause various skin disorders including acne (Zouboulis et al., 1998).

Testosterone is known to enhance sebum secretion, while the usage of AR inhibitors results in a decrement in sebogenesis. These aspects might be crucial to consider while dealing with skin diseases characterised by excessive sebum production such as acne, in which treatments with AR blockers lead to a significant clinical improvement (Makrantonaki and Zouboulis, 2007; George et al., 2008).

In hair follicles, the AR is expressed in the mesenchimal-derived cells of the dermal papilla and in the ORS, while it is not found in the bulge or in the hair bulb. Nevertheless, hair cycle progression is exclusively regulated by the binding of androgens, in particular of dihydrotestosterone, to the AR expressed in the dermal papilla. Upon androgenic stimulation, dermal papilla cells secrete various growth factors or extracellular matrix factors that exert both a paracrine effect on hair follicle epithelial cells aimed at promoting cell growth, and an autocrine activity on the dermal papilla itself. Insulin-like growth factor 1 (IGF-1) together with the vascular endothelial growth factor (VEGF), are considered as the main signals responsible for the stimulation of hair growth. On the contrary, inhibitory compounds such as the transforming growth factor beta 2 (TGFβ-2) and Dikkopf 1 (DKK-1), are the main factors involved in hair growth inhibition (Jin et al., 2020; Lolli et al., 2017; Blanpain et al., 2004). The activity of androgens on hair growth strictly depends on the

body localisation of hair follicles; indeed, in the axilla, pubis, chest and face androgens exert a stimulatory effect, while in the scalp the androgenic activity presents an inhibitory impact (Ceruti et al., 2018).

The mechanisms through which androgens might promote wound healing are still not fully characterised; nevertheless, the expression of AR in keratinocytes, fibroblasts and inflammatory cells highly suggest that this signalling route might be involved in the various overlapping phases (homeostasis, inflammation, cell recruitment, matrix remodelling) of wound healing. In C57BL/6 wild-type male mice, testosterone sustains the development of an inflammatory response by directly inducing the production of TNF-α *via* the AR signalling route in macrophages and by reducing both epithelisation and matrix deposition. While in castrated mice or in murine models in which ARs are impaired (e.g. following treatment with flutamide), wounded areas are significantly reduced and are associated to a dampening of inflammatory responses, reduced microphage invasion and increased deposition of matrix (Ashcroft and Mills, 2002; Wang et al.; 2016; Gilliver et al., 2007).

Kao et al., observed that dysfunctions in androgen signalling *via* AR negatively impacts the formation of a functional skin barrier primarily by impairing the constitution of epidermal lamellar bodies. Experiments conducted on pregnant female rats highlighted that the administration of oestrogenic-derived compounds significantly favoured the development of a functional and morphologically normal skin barrier in female and male foetal skin. On the contrary, the administration of dihydrotestosterone to pregnant mice significantly delayed the formation of an intact epidermal barrier. Moreover, observation conducted *in vivo* both on human skin and adult murine models, defined that the conditions regulating skin homeostasis involve extremely similar processes if compared to those responsible in the formation of the foetal skin barrier. Mice affected by hypogonadism displayed faster recovery of the skin barrier when compared to normal animals; furthermore, treatment of mice affected by hypogonadism with testosterone led to the development of similar values to controls. Analogue results were observed in humans affected by hypopituitarism treated with testosterone (Kao et al., 2001).

ZNF318

Two alternatively spliced variants of ZNF318 have been identified and include a longer isoform possessing two zinc-finger motifs of the Cys_2-His_2 type (ZNF318-L) at the C-terminal of the protein and a shorter isoform carrying only one type of Cys_2-His_2 zinc-finger binding domain (ZNF318-S) (Ishizukaet al., 2005). The N-terminal domain (amino acid 1-902) presents a complete sequence identity between the two isoforms and is known to interact with the N-terminal region of the AR.

ZNF318-S and ZNF318-L possess opposite effects on AR-mediated transactivation; indeed, ZNF318-S represses AR-mediated transactivation while ZNF318-L enhances it (Tao et al., 2006a). These two isoforms possess unique mechanisms of mutual regulation since a strict cooperation and crosstalk between them is crucial in order to properly regulate AR-mediated transcription. The two splicing variants act as competitors on the intranuclear events initiated by AR translocation, and literature findings support the assumption that competition with co-activators is a common mechanisms for co-repressors of agonist-bound AR (Tao et al., 2006a). ZNF318-S exerts a suppressive effect that is abrogated following ZNF318-L expression, the two isoforms can associate both in homodimers and heterodimers so that ZNF318-S homodimers act as co-repressors, whereas ZNF318-S/ZNF318-L heterodimers and ZNF318-L homodimers act as co-activators for AR transactivation. It is highly presumable that if one isoform is not functional the entire androgen signalling pathway might be affected (Tao et al., 2006a) (Tao et al., 2006b).
ZNF318 possesses a broad distribution and is found in a vast variety of tissues including male and female tissues, bone marrow and lymphoid tissues, endocrine tissues, lung, brain, adipose and soft tissue, blood and in the skin in which the expression is restricted to keratinocytes and melanocytes (https://www.proteinatlas.org/ENSG00000171467-ZNF318/tissue).

ZNF318 and its impact on AR signalling, constitutes a particularly appealing association that might underline relevant novel aspects related to the pathogenesis of HS. Nonetheless, predicting the effect of the SNV is extremely hard since the identified variant is rare, few references are available and it has never been previously correlated to any disease. Nevertheless, bearing in mind the well established role of androgens in the pathogenesis of HS (Riis et al., 2016), an appealing hypothesis might reside in the fact that the genetic variant could impair the co-repressor activity of ZNF318. Once the repression of androgen-mediated transcription is over, the co-activator isoform guides the androgen pathway, leading to an enhanced expression of target genes. In the hypothesized conditions, cells that are stimulated by circulating androgens will always respond positively. The enhanced and deregulated response to androgens might have diverse implications in the skin, by influencing the activity of the sebaceous glands and sebogenesis, progression of the hair cycle, wound healing and skin barrier function. Moreover, since AR and ZNF318 are widely distributed throughout the entire organism, also the immune system constitutes a potential target. In skin diseases such as acne and psoriasis, abnormal inflammatory responses are sustained by an AR-dependent up-regulation of TNF-α in macrophages that collectively suppress wound healing; therefore, the study of the involvement of AR signalling also in other skin diseases showing a deregulation in inflammatory responses might be of crucial relevance. Indeed, the loss in the co-

repressor activity of ZNF318 might render immune cells overly responsive to circulating androgens therefore potentially exacerbating inflammation (Shi et al., 2021; Lai et al., 2012).
Further corroborating the possibility that alterations in *ZNF318* and AR signalling might constitute a causative event in the pathogenesis of HS in the Sardinian family, resides in the fact that a worsening of HS flaring has been reported before the beginning of the menstrual cycle. Specifically, this period is characterised by high levels of progesterone, a sexual hormone that is known to induce metabolic effects such as hyperinsulinism, event characterised by elevated levels of insulin or IGF-1, known to be linked to androgenic dysregulation (Kalkhoff, 1982). Indeed, insulin and IGF-1 exert a stimulatory effect on 5-α reductase that catalyses the conversion of testosterone into dihydrotestosterone (Melnik and Zouboulis, 2013). Moreover, hyperinsulinism promotes ovarian androgen synthesis independently of gonadotropins and is therefore linked to androgen excess (Unluhizarci et al., 2021). In addition, progesterone produced by adrenal glands is mostly converted into glucocorticoids and circulating androgens (Taraborrelli, 2015).
It is therefore possible that the loss of the co-repressor activity of ZNF318 potentially induced by the identified genetic variant, might be directly linked to a hyper-activation of the androgen signaling route, that concomitantly triggers a higher sensitivity to androgens, particularly relevant in female family members.

Moreover, the variant determines a Lys>Ile amino acid substitution in position 707 and occurs in the N-terminal AR binding region of both zinc finger isoforms. Ile posses an hydrophobic side chain while Lys presents a longer and positively charged side chain, hence the genetic variant determines a change in the length and polarity of the amino acid that might presumably in turn impact the folding and the function of the protein. These considerations are only qualitative, ZNF318 has never been crystallised therefore the assessment of a three-dimensional model aimed at defining the true effect of the amino acid substitution on the protein structure cannot be established.

With the aim of better characterising the consequences of the genetic variant, further investigations were performed in *in vitro* functional studies.

4.9 Generation of *ZNF318* knock-in clones using CRISPR-Cas9 and ssODN-mediated genome editing

In order to determine the effects, contributions and implications of *ZNF318* variant on HS phenotype in the Sardinian family, CRISPR-Cas9 and ssODN-mediated genome editing was used to

obtain HaCaT cells carrying the point mutation of interest (rs767801219; g.43355214 T>A; NM_014345:exon4:c.A2120T; p.K707I).

The generation of a *ZNF318* knock-in clone by insertion of a single-base substitution was achieved using a CRISPR-Cas9 editing system that combines the pSpCas9 endonuclease with a sgRNA and a ssODN, the latter acts as a donor template for DNA repair via the high fidelity HDR mechanism.

The progressive screening through Sanger sequencing of the amplified exon 4 of *ZNF318* deriving from the genomic DNA of genome-edited HaCaT clones, allowed the identification of a knock-in cellular clone carrying the desired base edit in homozygosis (Figure 36). A further validation of the occurrence of the desired genome editing was performed by Sanger sequencing of the cDNA obtained from the retro-transcription of RNA extracted from *ZNF318* KI/KI clone. Results confirmed that the single base substitution determines the desired base change also at the cDNA level (Figure 36).

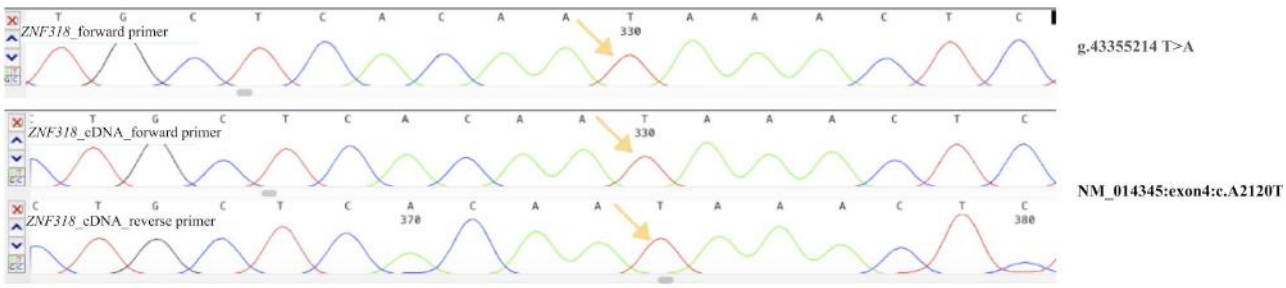

Figure 36. Screening of HaCaT *ZNF318* genome-edited clones. The generation of *ZNF318* clones carrying the point mutation of interest (rs767801219; g.43322952T>A; NM_014345:exon4:c.A2120T; p.K707I) was obtained through CRISPR-Cas9 and ssODN-mediated genome editing in HaCaT cells. Genomic DNA and cDNA deriving from clones were progressively screened through Sanger sequencing that allowed the identification of one cellular lineage of interest, a HaCaT KI/KI clone. Sanger sequencing of genomic DNA highlighted that the clone carries the base edit of interest in homozygosis. Sanger sequencing of cDNA confirmed that the single base substitution determines the desired base change also at the cDNA level.

No clones possessing the genotype found in family members were obtained. Nevertheless, well aware of the limitations of this model, the HaCaT *ZNF318* KI/KI clone was considered as an appropriate candidate to strictly allow the study of the effect of the variant.

4.10 ZNF318 protein levels and *ZNF318* gene expression levels

As shown in figure 37 A, a non-significant trend towards an increment was detected in ZNF318-S and ZNF318-L protein levels if compared to *ZNF318* WT/WT cells.

Obtained results highlighted also a non-significant trend toward an increase in *ZNF318* gene expression in HaCaT *ZNF318* KI/KI clone if compared to *ZNF318* WT/WT cells (figure 37 B).

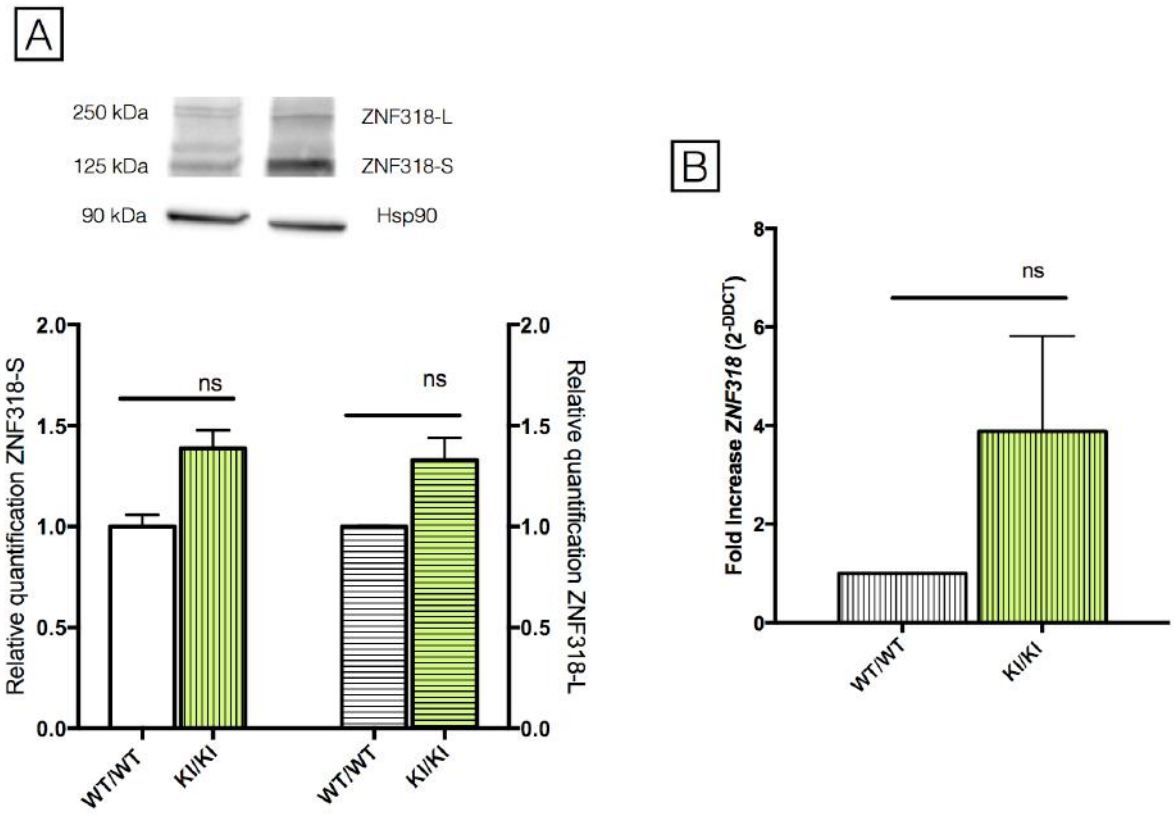

Figure 37. ZNF318 protein levels and *ZNF318* gene expression in HaCaT *ZNF318* clones. (A) Representative Western blot image showing protein levels of ZNF318-S, ZNF318-L and Hsp90, the latter used as the reference protein (top). Quantification of ZNF318-S and ZNF318-L increase normalised to Hsp90 optical density (bottom). (B) Real time quantitative polymerase chain reaction (PCR) and results normalised to *ACTB* expression. Expression of HaCaT *ZNF318* WT/WT clones was normalized to 1. Expression data for three experiments are reported as $2^{-\Delta\Delta Ct}$ average ± SD. Results are representative of three independent experiments. Data analyses were performed with Mann-Whitney *U test* by comparing HaCaT *ZNF318* WT/WT cells with HaCaT *ZNF318* KI/KI cells; ns: not significant.

The ratio between ZNF318 co-activator/co-repressor in keratinocytes is not known. However, it is possible to speculate that augmented gene expression levels of *ZFN318*, might constitute a cellular response aimed at compensating a functional imbalance between the two isoforms. As previously hypothesised, it is presumable that the variant induces an impairment in the co-repressor activity of ZNF318, therefore a major increment in ZNF318-S protein levels might be due to the necessity to restore, at least partially, the lacking activity of the co-repressor component. Not being able to predict the effects of the variant on protein structure, it is not possible to advance further assumptions to coherently explain the obtained preliminary results.

4. RESULTS AND DISCUSSION

Part 3: The case of a Friulian family

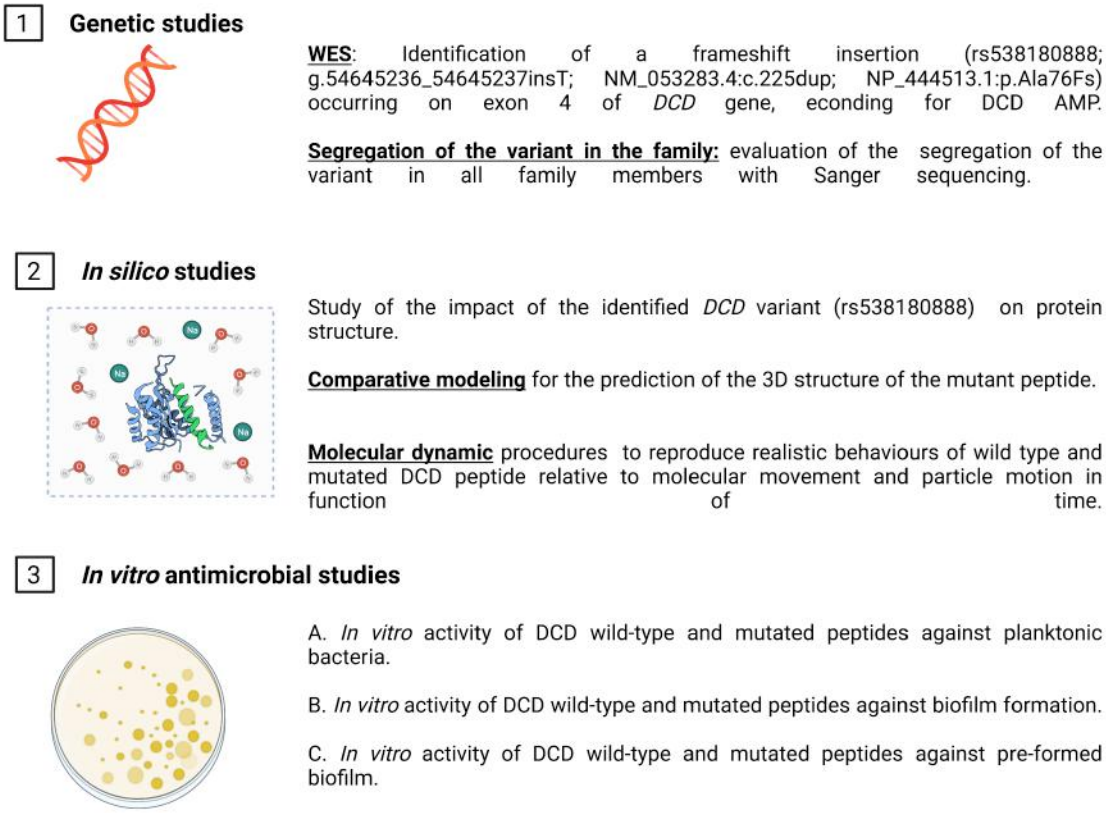

Figure 38. Schematic pipeline of the experimental procedures that were employed to perform genetic and functional studies on the Friulian family affected by HS.

4.11 Identification of a missense exonic variant in *DCD* gene in affected family members

HSM58 is a 50 year old male with a diagnosis of HS and Hurley stage I disease, who was also diagnosed with other comorbidities including celiac disease and dyslipidemia, and to have developed the first clinical signs of HS at 22 years of age. HSM64, the father of HSM58, is a 77 year old man affected by HS, who further reported to be subjected to the onset of relapsing furuncles and to have undergone two surgical treatments for the removal of dermal abscesses during his adolescence. D_HSM58, the daughter of HSM58, is 11 years old and her parents revealed she is starting to manifest relapsing inguinal furuncles.

M_HSM58, the mother of D_HSM58, was also recruited in the study and she reported not to be affected by any known pathology (Figure 39).

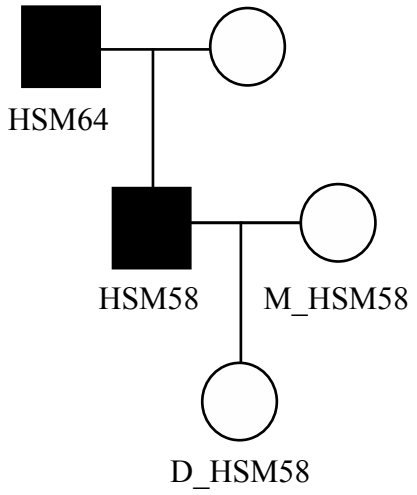

Figure 39. Pedigree of the Friulian family.

None of the recruited individuals were ever subjected to genetic analysis, thus WES was performed in order to identify recurrent genetic variants in HSM58, D_HSM58 and HSM64 and not in M_HSM58 healthy control.

In the overall analysis, a total of 42 different exonic variants were obtained. In order to recover the SNVs that are most likely to be deleterious or pathogenic or functional, first variants were ranked according to the CADD based on the PHRED-like score with a cut-off of 15, next selected genes were screened in order to identify those possessing high levels of expression in the skin, and finally the latter cluster of genes was further selected according to their function in order to retrieve those whose activity can be considered as highly relevant in the context of skin biology and so on HS phenotype. These procedures allowed the identification of six genes (Table 11) and the selected variants were all further confirmed in Sanger sequencing.

Chr	Position	Gene	SNV	Variant effect	M_HSM58	HSM58	D_HSM58	HSM_64
11	g.64832706 C>T	*CDC42BPG*	rs778407688	Missense	C/C	C/T	C/T	C/T
12	g.54645236_54645237ins T	*DCD*	rs538180888	Frameshift insertion	-/-	-/T	-/T	-/T
15	g.43252804 C>T	*TGM5*	rs141299025	Missense	C/C	C/T	C/T	C/T
15	g.83257795 C>T	*BNC1*	rs750398451	Missense	C/C	C/T	C/T	C/T

15	g.99729406_99729407ins C	*LYSMD4*	rs766394415	Frameshift insertion	-/-	-/C	-/C	-/C
19	g.653527delA	*FGF22*	rs773254859	Frameshift deletion	A/A	A/-	A/-	A/-

Table 11. List of the single nucleotide variations (SNV) obtained during WES analysis. List of SNV with a PHRED>15 obtained following WES analysis that were found in HSM58, D_HSM58 and HSM64 and not in M_HSM58 healthy control. For each selected variant is provided the chromosome, the genomic position including the reference allele and the alternate allele, the name of the gene, the locus accession for the variant type assigned by dbSNP (rs), mutation category and the genotype found in in M_HSM58 healthy control and in HSM58, D_HSM58 and HSM64 following Sanger sequencing. Highlighted in orange is the first genetic variant assessed in further studies.

The first genetic variant addressed in the study was the rare (MAF<0.01) frameshift insertion (rs538180888; g.54645236_54645237insT; NM_053283.4:c.225dup; NP_444513.1:p.Ala76Fs) occurring on exon 4 of *DCD* gene. HSM58, and to a lesser extent HSM64, declared to commonly suffer from relapsing suppurating lesions primarily localised on the ingunal and axillary regions, that force them to undergo treatments with antibiotics. Since the selected gene encodes for an AMP, it immediately appeared as an appealing target that might, at least partially, explain a possible mechanism involved in the onset, progression and severity of clinical manifestations in these patients. Our results highlighted that the frameshift insertion is not present in M_HSM58, while is carried in heterozygosis in D_HSM58, HSM64 and HSM58 thus suggesting an autosomal dominant inheritance pattern (Figure 40).

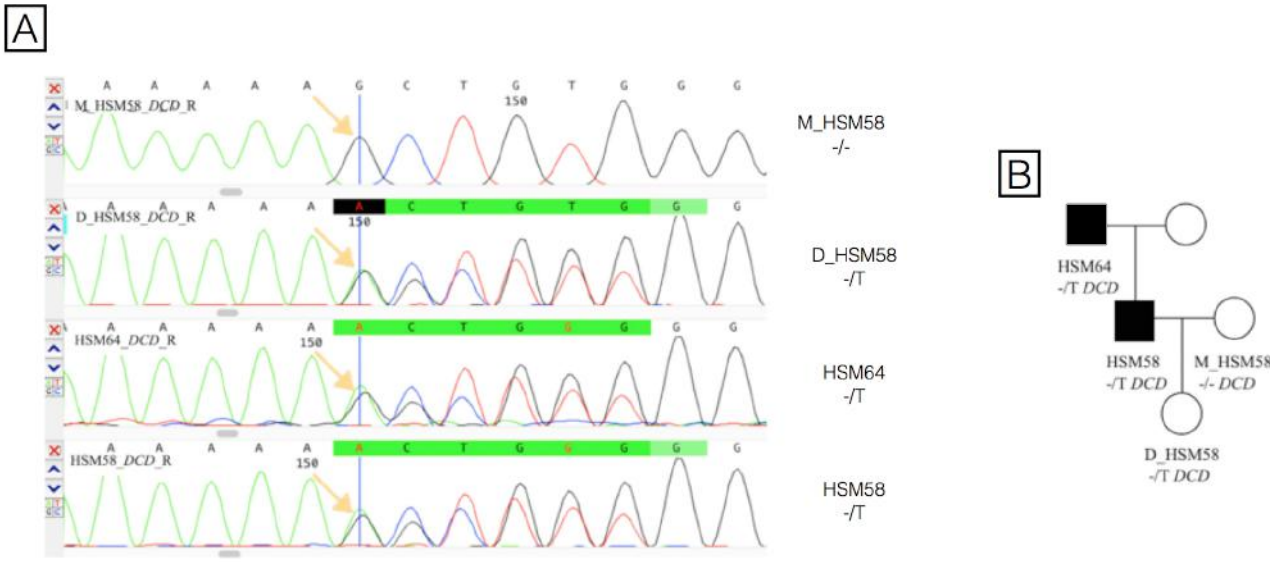

Figure 40. Validation of *DCD* variant in all family members. (A) Sanger sequencing results confirmed that the *DCD* frameshift insertion (rs538180888; g.54645236_54645237insT; NM_053283.4:c.225dup; NP_444513.1:p.Ala76Fs) is

not present in M_HSM58, while is carried in heterozygosis in D_HSM58, HSM64 and HSM58 thus suggesting an autosomal dominant inheritance pattern. (B) Identified genotypes for the selected *DCD* variant are reported under each family member.

DCD (NC_000012.12) is a 3905 bp long protein coding gene, mapping on the long arm of chromosome 12 (12q13.2), consisting of 5 exons and encoding for dermcidin (DCD), an antimicrobial peptide (AMP) first described by Schittek and collaborators (Schittek et al., 2001), possessing no homology to other known AMPs. Their results highlighted that DCD presents specific features: a restricted expression pattern limited to the skin and specifically to the dark mucous cells of the secretory coil of eccrine sweat glands; an intracellular localisation confined in the Golgi network and secretory granules; undergoes activation through proteolytic processing once secreted in eccrine sweat; the active peptides are transported through sweat on the epidermal surface where they contribute to the first line of innate immune responses in the skin by generating a constant barrier that overlies the epithelium (Schittek et al., 2001). Being continually secreted into sweat, DCD has to be considered as a constitutive component of the innate immune defence of the skin acting by modulating epidermal colonisations, rather than as an AMP that responds to inflammation and injuries (Schittek, 2012).

The secreted DCD precursor protein consists of 110 amino acids in which different functional domains can be recognised and comprise (Schittek, 2012): N-terminal signal peptide (amino acid 1-19); a central pro-domain (amino acid 20-62); C-terminal AMP domain (amino acid 63-110) (Figure 41).

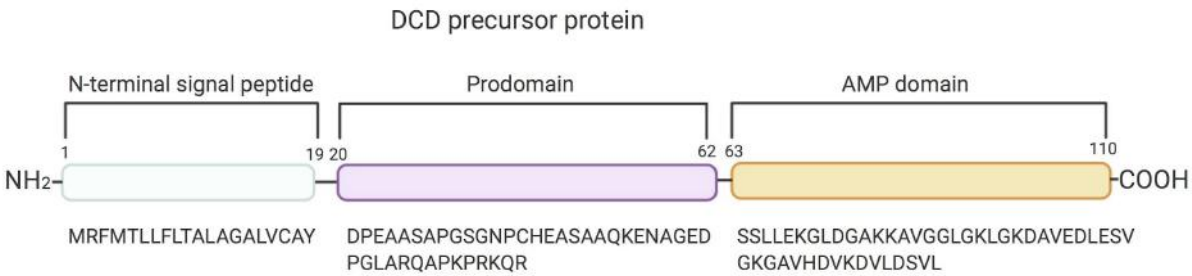

Figure 41. Architectural organisation of DCD precursor protein. Secreted DCD precursor protein consists of 110 amino acids in which three functional domains can be recognised and comprise: a N-terminal signal peptide (amino acid 1-19); a central pro-domain (amino acid 20-62); C-terminal AMP domain (amino acid 63-110).

DCD is secreted into sweat at a constant rate, where the precursor protein is subjected to post-secretory proteolytic processing that ultimately generates N-terminal and C-terminal truncated DCD-derivate active peptides. These active proteins are represented by the anionic DCD-1L

composed by 48 amino acids and DCD-1 comprehending 47 amino acids, and by the cationic SSL-25 comprising 25 amino acids. DCD-1L and DCD-1 only differ in the last amino acid and are the most abundant AMPs found in human sweat exerting well established antimicrobial activities against both Gram-positive (*Staphylococcus aureus, Staphylococcus epidermidis, Staphylococcus lugdunensis, Enterococcus faecalis, Listeria monocytogenes*) and Gram-negative bacteria (*Escherichia coli, Pseudomonas putida, Salmonella typhimurium*), as well as *Candida albicans* (Burian and Schittek, 2015).

DCD-1(L) possesses a L-shaped conformation consisting of three α-helices linked by two flexible turns and, under a broad range of pH values and at high salt concentrations, it presents an amphiphilic structure in which it is possible to recognise a cationic N-terminal region (Ser1-Lys23) and an anionic C-terminal region (Asp24-Leu48) (Burian and Schittek, 2015) (Figure 42).

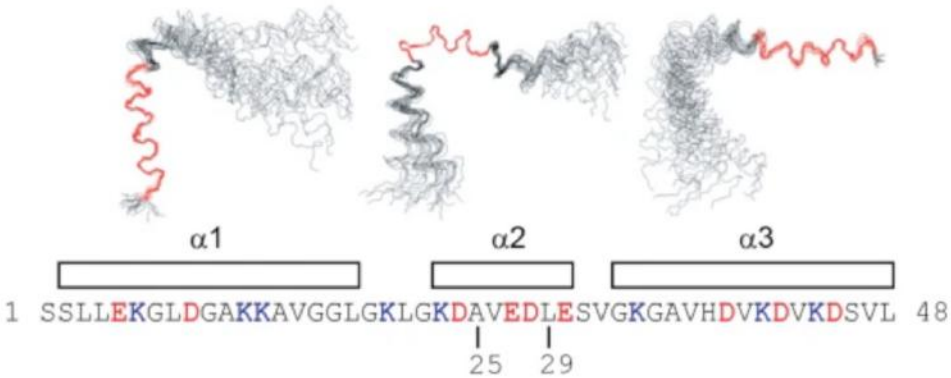

Figure 42. Architectural organisation of active DCD-1(L). The anionic DCD-1L is composed by 48 amino acids and DCD-1 comprehends 47 amino acids. The boundaries of the secondary structures are shown above the sequence of DCD-1(L). In the amino acid sequence, positively charged residues are in blue and negatively charged ones are marked in red. The reported sequence is relative to DCD-1L since DCD-1 lacks in the last residue at the C-terminal of the peptide (Nguyen et al., 2017).

DCD-1(L) antimicrobial activity is thought to happen through a *membrane insertion model* according to which initial electrostatic interactions occurring between the cationic N-terminal domain and the negatively charged bacterial phospholipids, induce the formation of oligomeric complexes that directly insert in the bacterial membrane thus generating ion channels that lead to bacterial death (Burian and Schittek, 2015). Specifically, upon interaction with the bacterial lipid bilayer, Zn^{2+} ions are functional cofactors that promote the oligomerisation of DCD-1(L) monomers by prompting the formation of peptide-lipid or peptide-peptide salt bridges. The clustering of DCD-1(L) peptides on the bacterial surface seems to be strictly mediated by interactions between the C-terminal domain of peptides. Next, DCD-1(L) complexes self-rearrange into progressively higher oligomeric states ultimately resulting in ion channel formation in which the N-terminal domain is

embedded in the membrane hence lining the channel, while the C-terminal region floating on the membrane surface is presumably involved in the stabilisation of the structure by both coordinating the interaction between metal ions and with the negatively charged head group of lipids (Nguyen et al., 2017).

Corroborating the validity of the initial selection of *DCD* as a preliminary target gene to address in the context of the Friulian family, is the fact that in HS a deregulated growth of the skin's microflora together with a dysbiosis-driven aberrant activation of the innate immune system that leads to an excessive inflammatory response, is thought to be partially induced by a marked dysregulation in AMPs production (Ingram et al., 2015; Orenstein et al., 2020).

Furthermore, over- or under- expression of AMPs have been well reported in various dermatologic diseases including atopic dermatitis, psoriasis and chronic leg ulcers, while efforts aiming at the characterisation of the expression profile of AMPs in HS have been made but are currently still very limited (Heilborn et al., 2003).

In a recent study conducted by Coates and collaborators, authors performed transcriptome analysis of lesional and non-lesional areas of HS cases and they observed that many genes associated to sweat gland functions (i.e. *secretoglobins* and *aquaporin 5)*, together with *DCD* and members of the *S100* family of genes presented decreased expression levels in lesional skin, and that these same genes possessed an opposite trend in healing skin portions (Coates et al., 2019). HS chronic non-healing wounds are commonly associated to dysregulations in cytokine and chemokine production, and AMPs expression. Moreover, 50% of HS patients report a secondary involvement of sweat glands following follicular rupture and a change in their sweat habits before the onset of a noticeable lesion, therefore potentially also impacting the activity of those AMPs that are processed once released into sweat (Ring et al., 2017).

In another study conducted by Shanmugan et al., authors identified more than 700 differentially expressed genes in HS skin if compared to healthy controls. Amongst the identified genes, the one exhibiting the greatest fold change in HS skin in respect to control samples was *DCD*, found to be significantly down-regulated. As one would expect, a decrement in the expression of AMPs might explain the increased susceptibility of patients to develop bacterial infections (Shanmugan et al., 2019).

The presence of a typical antimicrobial and sweat-gland gene signature in HS skin might raise novel potential functional links in HS pathogenesis that specifically relies on a tight and complex association between sweat glands and AMPs in wound healing, re-epithelisation processes and major susceptibility to bacterial infections (Coates et al., 2019; Shanmugan et al., 2019).

All these findings further support the selection of *DCD* variant amongst the retrieved genes as a potentially intriguing target involved in the onset and progression of HS in the members of the Friulian family. In this study the impact of the frameshift insertion (rs538180888), occurring on exon 4 of *DCD* gene, was evaluated with the aim of clarifying its potential role on the structure and function of the AMP, and of shedding light on possible novel mechanisms involved in the progression of the disease that might constitute potential targets for the development of tailored therapeutic interventions.

4.12 *In silico* studies: Comparative modelling for the prediction of the 3D structure of DCD mutant peptide

Comparative modelling, also refereed to as homology modelling, constitutes the most widely employed computational approach aimed at predicting the 3D structures of proteins of interest (target) for which no experimentally determined structure is available, based primarily on its alignment to one or more proteins of known structure (templates). Comparative modelling finds also broad applications in designing mutants to test hypothesis relative to the protein's function. Specifically, this methodology relies on the execution of four steps including: (1) retrieving homologous template proteins of known structure; (2) selection of the best template or set of templates by identifying similarities between the target and at least one known template structure; (3) optimizing the multiple sequence alignment (MSA) between target and template protein sequences; (4) building the homology model for the template sequence that resembles as closely as possible the structures of the templates and predicting model errors (Meier and Söding, 2015; Webb and Sali, 2014).

While analysing the wild-type and the mutated DCD targets, the best selected template was given by a structure of DCD-1L from *Homo sapiens* (PBD code 2KSG), sharing 100 % and 60% identity with the wild-type and mutated sequence respectively. Following stereochemical analysis of the amino acid sequence, it was possible to observe that 90% of the amino acid residues were in favourable positions for all models. The Z-score, defined as the energy separation between the native fold and the average of an ensemble of misfolds in the units of the standard deviation of the ensemble (Zhang and Skolnick, 2008), indicated that all models fell within the score range typically found for peptides possessing similar sizes. Moreover, the qualitative model energy analysis distance constrains (QMEAN DisCo) score, showed a global energy of 0.67 for wild-type DCD and a value of 0.63 for mutant DCD (Figure 43).

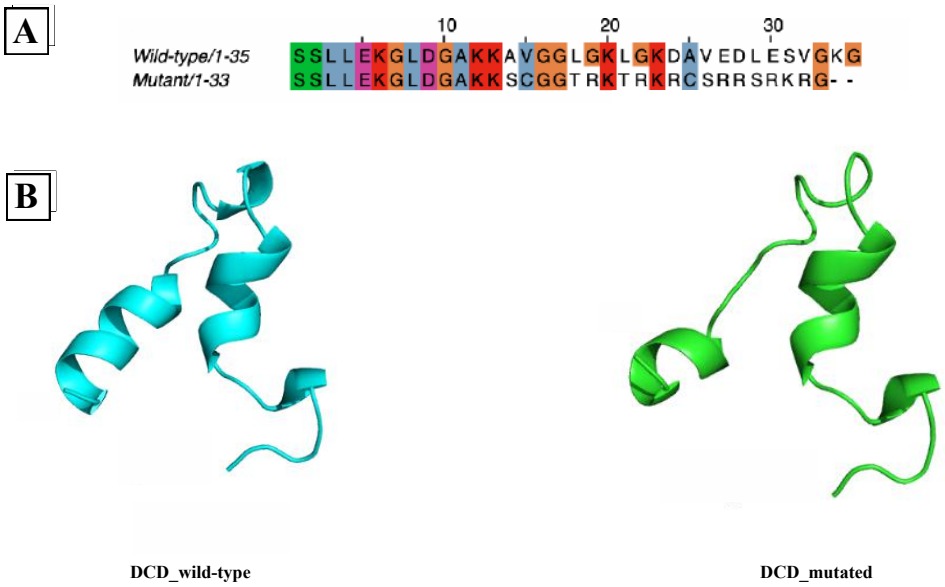

Figure 43. Comparative modelling for the prediction of the 3D structure of DCD mutant. A. Following the selection of the template sequence, the target needs to be aligned to the template structure. B. Next, it is possible to a model for the target DCD_mutated peptide was assessed using information from template DCD_wild-type structures. Molecular dynamic simulations relative to the theoretical 3D models of the wild-type (blue) and mutant (green) DCD peptide.

The identified frameshift variant (rs538180888) disrupts the ORF of *DCD* and results in a 33 amino acid peptide having a completely altered sequence from position 15 to 33 if compared to the wild-type DCD-1L peptide (Figure 44 A). As a consequence, the alteration of the sequence affects both the N-terminal and the C-terminal partitions of the AMP. Indeed, in the mutated sequence it is possible to observe an overall increment in positively charged amino acids and a reduction in the negatively charged ones (Figure 44).

DCD-1(L) Wild-type peptide:

SSLLEKGLDGAKKAVGGLGKLGKDAVEDLESVGKGAVHDVKDVLDSV

DCD-1(L) mutated peptide:

SSLLEKGLDGAKKSCGGTRKTRKRCSRRSRKRG

Figure 44. Sequences of the DCD-1(L) wild-type peptide and of the DCD-1(L) mutated peptide. The identified frameshift insertion in *DCD* gene generates a mutated peptide showing an altered sequence from position 15 to 33 that presents an overall increment in positively charged amino acids and a reduction in the negatively charged ones, and results to be shorter (33 amino acids) when compared to the wild-type DCD-1(L) peptide.

It is possible to speculate that the resulting imbalance in the net charge of the molecule might have severe consequences leading to the loss of its amphiphilic nature, condition seen to be crucial for the antimicrobial mechanism of action of the AMP. Mutated DCD-1(L) might either affect the

electrostatic interactions occurring between the cationic N-terminal domain and the negatively charged bacterial phospholipids, the formation of oligomeric complexes or the formation of the membrane-embedded ion channel. These aspects should be critically investigated in order to determine a potential novel mechanism underlying aberrant inflammatory responses and a marked dysregulation of AMPs with augmented susceptibility to bacterial infections which might further sustain inflammatory processes (Nguyen et al., 2017).

4.13 *In silico* studies: *DCD* (rs538180888) decreases the peptide's stability and compaction, and increases its rigidity

In order to determine the impact of the frameshift variant (rs538180888) on protein structure, MD procedures were performed to reproduce realistic behaviours of both wild-type and mutated DCD peptides, with the aim of retrieving detailed information relative to molecular movement and particle motion in function of time. MD assays were performed for 100 ns in order to study the stability and the conformational changes on DCD structure upon mutation.

RMSD of the backbone atoms is defined as a crucial parameter to evaluate the stabilisation and equilibration of MD trajectories. As shown in figure 45 A, the backbone atoms of wild-type DSP stabilised with an average RMSD at 0.92 nm at 20 ns and did not show any significant change during the analysis, hence suggesting that the modelled protein is stable throughout the simulation. In the case of the mutated DCD peptide, a progressive increment in RMSD levels were observed in the initial phase of the simulation, while after the first 70 ns a stabilisation was registered with average values of 0.85 nm. Collectively, RMSD analysis indicate that the presence of the frameshift insertion in DCD affects protein stability by causing a decreased stability of the AMP.

Root-mean square fluctuation (RMSF) measures the average deviation of an atom or group of atoms over time from a reference structure. As indicated in figure 45 B, while simulating the fluctuation of amino acid residues over time, it is possible to observe that wild-type DCD presents an overall major flexibility when compared to the mutated protein. In addition, the b-factor was determined in order to further investigate flexibility changes amongst the two peptides. B-factor values revealed that the regions possessing the greatest dynamic mobility of the atoms are located at either the N-terminal or C-termianl ends, or in regions without secondary structures (loops), and that wild-type DCD presents a relevantly higher level of flexibility for fluctuation in these regions (Figure 45 C). Collectively, it is possible to conclude that the mutant structure of the peptide is more rigid.

The Rg analysis was employed to determine the level of compaction and the overall dimensions of DCD wild-type and mutated peptide. As indicated in figure 45 D, Rg values in the wild-type protein

did not show a significant stabilisation in the selected time interval, possibly indicating that MD simulations should be performed for times greater than 100 ns to truly define the wild-type's trajectory. The mutant DCD peptide stabilised at an average Rg value of 0.98 nm around 15 ns and was maintained throughout the entire simulation. These results indicate that the wild-type protein tends to acquire a compact structure, while the mutant peptide remains with few significant changes in the position of the mass axis.

SASA is a parameter widely employed for the evaluation of the surface area of the protein accessible to the solvent, and in which high SASA values are indicative of a relative expansion. Results highlighted that the DCD wild-type protein starts with a SASA value of 32 nm^2 that progressively decreases over time reaching a minimum average value of 25 nm^2 at the end of the trajectory. A similar trend was observed in the DCD peptide carrying the frameshift insertion, in which a starting SASA average value of 36 nm^2 gradually decrements reaching an average SASA of 32 nm^2 at the end of the simulation. Results indicate an increment in the accessible surface of the mutant protein, with a predilection at the C-terminus region, if compared to the wild-type AMP (Figure 45 E).

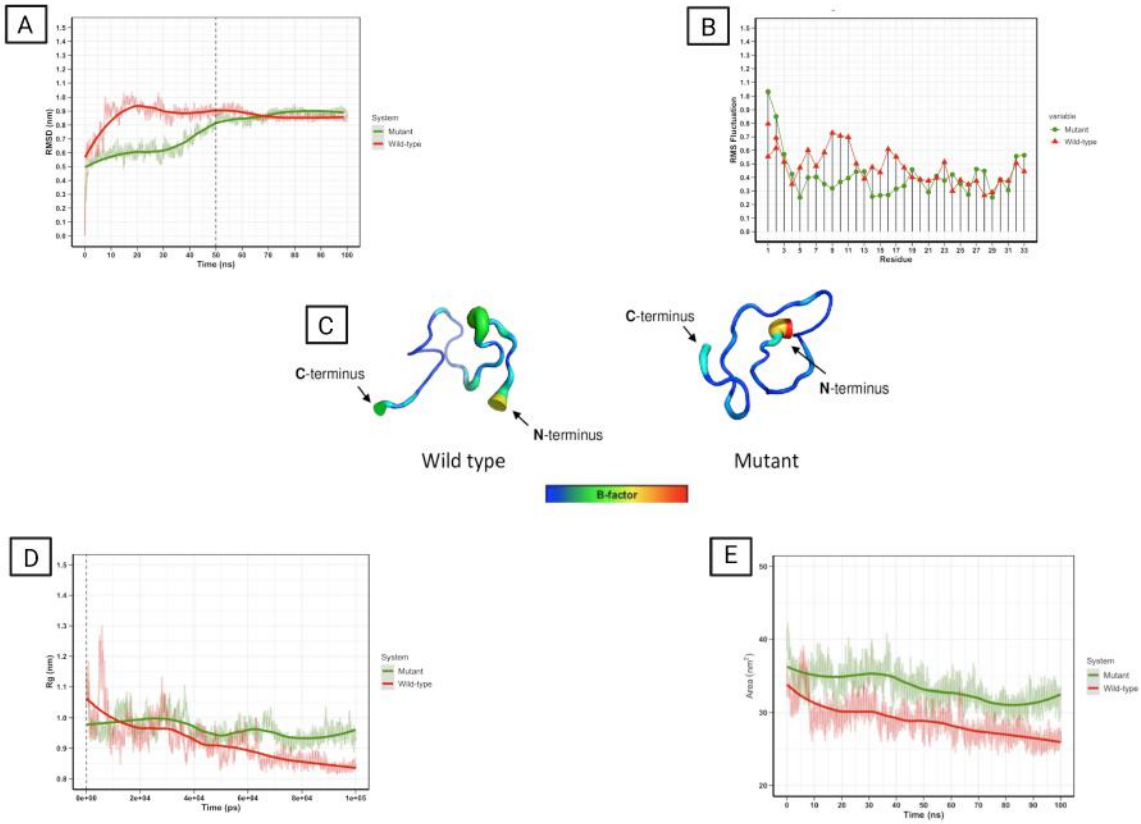

Figure 45. Molecular dynamics of wild type and mutated DCD AMP. (A) Backbone Root-mean square deviation (RMSD) for the backbone atoms of the wild-type DCD peptide (red) and of the DCD peptide carrying the variant in heterozygosis (green) are shown as a function of time (ns). (B) Root-mean square fluctuation (RMSF) of the average deviation/fluctuation of amino acid residues of the wild-type DCD peptide (red) and mutated DCD peptide (green) are shown as a function of the residue's position. (C) B-factor was assessed to further investigate flexibility changes amongst the two peptides. (D) Radius of gyration (Rg) of Cα atoms in the molecular dynamics trajectory for the wild-type DCD peptide (red) and of the mutated DCD peptide (green) are shown as a function of time (ps). (E) Solvent accessible surface area (SASA) of the wild-type DCD peptide (red) and of the mutated DCD peptide (green) are shown as a function of time (ns).

Taken together, these results indicate that the mutant DCD moiety presents a more rigid, less stable and less compact structure that results to be more accessible to solvents, especially in the C-terminal region, if compared to the wild-type DCD AMP.

4.14 Principal component analysis

Principal component analysis (PCA) is a standard mathematical tool used to search for correlations in big data sets, that finds a broad application for the automatic extraction of information from a MD simulation. PCA can be used, combined with physical models of the protein motion, to define objective criteria able to discriminate relevant conformational changes in a protein from the background of atomic fluctuations. This technique is also applicable for the comparison of the motions of two MD trajectories.

Regarding PCA based on the analysis of trajectories of MD simulations, it is possible to describe the conformational dynamics of the peptide through the atomic movements of the structure that are converted into main movements. Figure 46 represents the clusters of conformations along the planes PC1 and PC2. It is possible to observe that the structure of the wild type peptide at 0 and 50 ns showed a wide dispersion area, therefore indicating the presence of considerable variations in conformation and flexibility. Alternatively, movements ranging between 75 and 100 ns presented less dispersed values for both wild type and mutant peptides, hence converging to a more conserved cluster with less variation, but varying in length on the principal components.

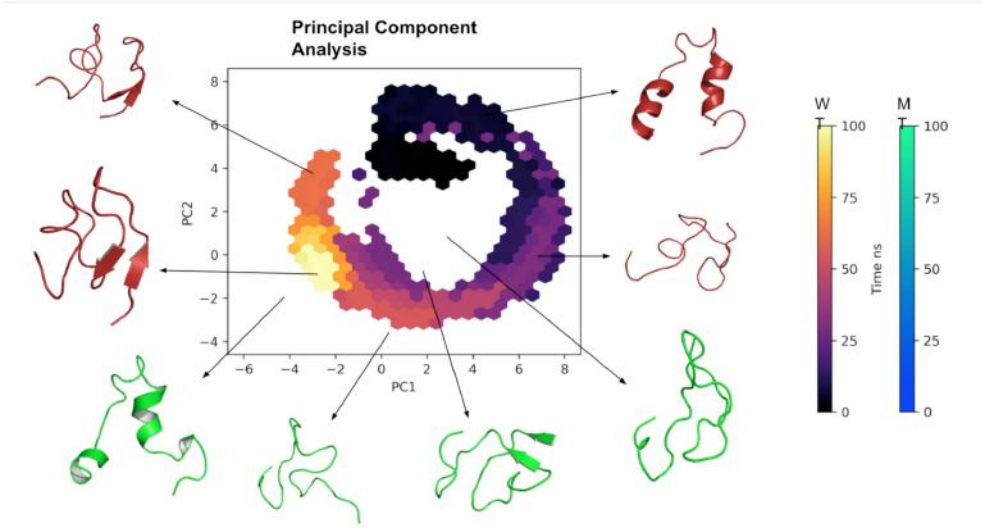

Figure 46. Principle component analysis (PCA). Principle component analysis of 2D clustering of various snapshots of the simulation trajectory based on Cartesian coordinates.

The PCA analysis of the pathways of the peptides showed a clear separation between the wild-type and mutated structures into different components. A larger dynamic shift was registered in the wild-type AMP, therefore further confirming the impact of the frameshift insertion on the structure's stability during the simulation.

4.15 *In vitro* growth inhibition of planktonic bacterial cells by DCD AMPs

Although bacterial infections are considered as a secondary event in the emergence of HS phenotype, a vast variety of microorganisms can be isolated from HS lesions. In addition, the clinical picture of HS clearly resembles the one of an infectious process in which various bacterial specimens deriving from the normal skin flora are responsible for secondary infections in previously sterile compartments and also contribute to initiating and sustaining the inflammatory response in skin regions (Hessam et al., 2016). Moreover, being that HS clinical condition can be largely improved following antibiotic treatment, the role of bacterial infections must be taken into serious account while dealing with HS cases (Langan et al. 2020). Different studies have isolated an array of different bacterial cultures deriving from HS lesions, and results revealed the presence of polymicorbial growth patterns in which *S. aureus*, coagulase-negative Staphylococci (CoNS), including *S. epidermidis* and *S. lugdunensis*, together with mixed anaerobic bacteria and *Corynebacterium spp*. are the dominant types. Even if these bacterial specimens compose the normal human skin flora, they seem to activate a series of pathogen-associated molecular pathways that trigger the immune system in HS cases (Ring et al., 2015).

As shown in Figure 47, the planktonic growth of *S. aureus*, *S. epidermidis*, *S. lugdunensis* was significantly reduced in all tested strains following the treatment with the wild-type DCD peptide (DCD_WT) (% recovered *S. aureus*: DCD_WT 79.093±2.761, p<0.0001; Control 100±4.762) (% recovered *S. epidermidis*: DCD_WT 67.920±1.987, p<0.0001; Control 100±2.891) (% recovered *S. lugdunensis*: DCD_WT 88.543±1.653, p<0.0001; Control 139±4.342) if compared to non-treated (control) bacterial strains. Analogue significant results were registered following the incubation of bacterial strains with DCD-1 dermcidin-derived peptide control (% recovered *S. aureus*: DCD-1 63.762±2.437, p<0.0001; Control 100±4.762) (% recovered *S. epidermidis*: DCD-1 71.387±3.245, p<0.0001; Control 100±2.891) (% recovered *S. lugdunensis*: DCD-1 87.801±2.182, p<0.0001; Control 139±4.342) and DCD-1L dermcidin-derived peptide control (% recovered *S. aureus*: DCD-1L 67.763±1.892, p<0.0001; Control 100±4.762) (% recovered *S. epidermidis*: DCD-1L 66.534±3.725, p<0.0001; Control 100±2.891) (% recovered *S. lugdunensis*: DCD-1L 89.342±1.982, p<0.0001; Control 139±4.342) when compared to the control bacterial strain. On the contrary, no significant results were registered following the treatment of each strain with DCD mutated peptide (DCD_MT) when compared to the control bacterial cells.

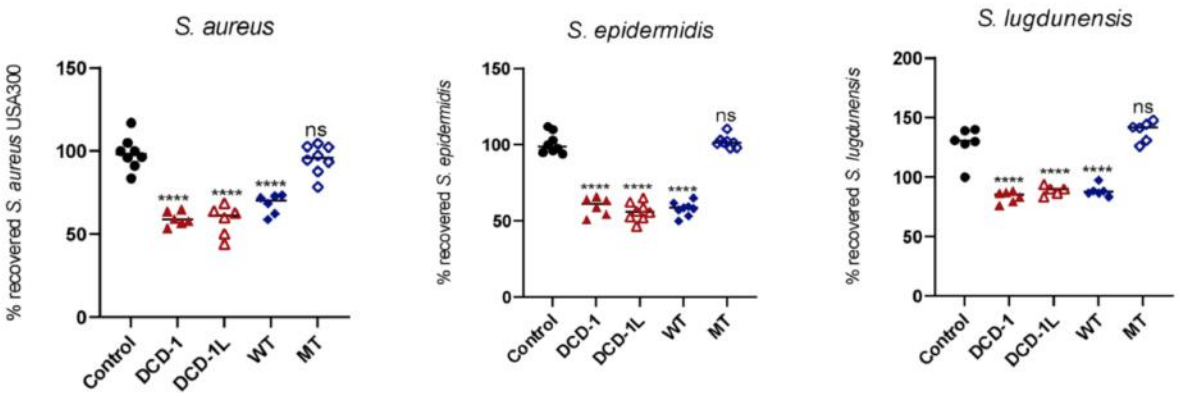

Figure 47. *In vitro* growth inhibition of planktonic cells by DCD AMPs**.** *S. aureus USA300*, *S. epidermidis* or *S. lugdunensis* (1 x 10^8) were incubated with 2 µM human AMPs. After 3 h of incubation, several dilutions of the bacterial suspensions were plated onto TSB agar plates and incubated overnight at 37 °C. The next day bacteria colony-forming units (CFUs) were counted.
Results represent three independent experiments with four technical replicates ± SD. Significant differences to control treatments were analysed by ordinary one-way analysis of variance (ANOVA) followed by Dunnett's multiple comparisons test (**P* < 0.05; ***P* < 0.01; ****P* < 0.001; *****P* < 0.0001)

It is possible to speculate that the resulting imbalance in the net charge of the DCD_MT peptide might have severe consequences leading to the loss of its amphiphilic nature, condition seen to be crucial for the antimicrobial mechanism of action of the AMP.

4.16 *In vitro* activity of DCD against biofilm deposition and eradication

Different bacteria can generate an extracellular matrix, namely biofilm, composed by bacterial aggregations living in a protective extracellular slime matrix containing DNA, proteins and polysaccharides, that collectively act as a protective structure against antimicrobial agents and host defence mechanisms (Ring et al., 10.1111/exd.12793). Biofilm formation is divided into four progressive phases: (1) deposition and attachment of planktonic cells; (2) irreversible attachment accompanied by the deposition of extracellular matrix; (3) biofilm maturation and proliferation; (4) bacterial detachment from biofilm formations and dispersal (Rumbaugh and Sauer, 2020).

Biofilms infections are typically characterised by resistance to antibiotic treatments and by the ability to counteract host-mediated clearance, hence eliciting chronic inflammation, generating persistent infections and causing tissue damage. These properties are perfectly in line with the recurrent nature of HS infections (Ring et al., 2015). Nodules and sinus tracts found in HS cases, are skin formations characterised by a low oxygen tension environment that results to be optimal for bacterial proliferation; indeed, the secondary development of biofilms in these chronic lesions have been reported in various HS cases and possibly indicate that bacterial proliferation and biofilm formation is favoured in already established lesions (Kathju et al., 2012). Different studies highlight that that in samples deriving from chronic lesions, the vast majority were positive for bacterial colonisation and showed biofilm-like structures primarily localised in correspondence of the infundibulum or sinus tracts (Jahns et al., 2014) (Ring, 10.1111/bjd.15007). Biofilm formation represents the most relevant virulence factors associated to *S. aureus* and different CoNS, often isolated form most superficial and deeper partitions of chronic HS lesions (Jahns et al., 2014; Kathju et al., 2012).

For the *in vitro* determination of the activity of DCD_WT and DCD_MT peptides on biofilm deposition and eradication, experiments were conducted on *S. aureus* that is commonly employed as a model in assays focused on biofilm-based studies (Park et al, 2019).

As indicated in Figure 48, DCD_WT peptide significantly inhibits biofilm deposition if compared to non-treated (NT) cells (reduction in biofilm (%): DCD_WT 88,22±10,48, $p<0,05$; NT 102,4±5,66). No significant changes in biofilm formation were registered in *S. aureus* samples incubated with DCD_MT peptide when compared to NT cells.

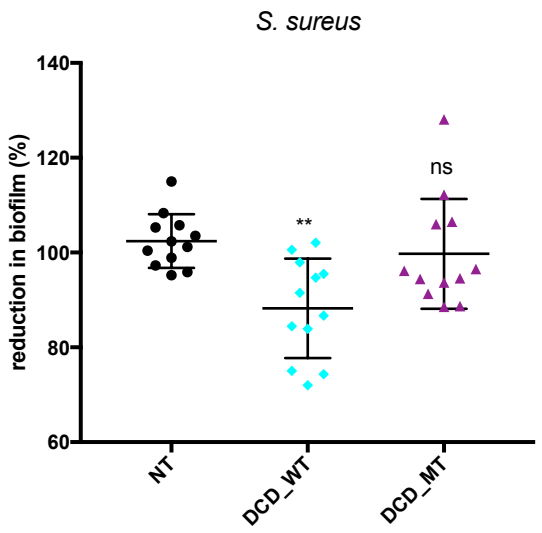

Figure 48. *In vitro* activity of DCD AMPs against biofilm deposition. *S. aureus* (1 x 10^7 CFU/mL) was incubated with 2 µM of human DCD_WT or DCD_MT peptide in BHI medium containing 2% sucrose and plated on 96-multi-well plates for 24 hours. Cells were fixed in methanol and stained with 0,1% crystal violet solution that was solubilised with 95 % ethanol. The absorbance reads were measured at 560 nm using the GloMax® Discover Microplate Reader (Promega). The low cut-off was represented by approximately 3 standard deviations above the absorbance mean of control wells (containing medium alone without bacteria).
Results are represented as three independent experiments with 12 technical replicates ± SD. Significant differences to control treatments were analysed by ordinary one-way analysis of variance (ANOVA) followed by Dunnett's multiple comparisons test (**P* < 0.05; ***P* < 0.01; ****P* < 0.001; *****P* < 0.0001).

These results collectively suggest that the wild-type peptide is efficient in counteracting the deposition and attachment phase of planktonic cells during biofilm formation, while the mutated moiety is not able to exert this antimicrobial function. In this context, it is possible to speculate that the mutated peptide is not able to help prevent local invasion of biofilm-forming microorganisms, therefore rendering patients more susceptible to bacterial infections in chronic lesions.

While analysing the effects of DCD_WT and DCD_MT peptides on pre-formed biofilm, we observed that the bacterial strain was not susceptible to the anti-biofilm activity of either of the tested peptides. Specifically, a non significant trend towards a reduction in the biofilm's biomass was registered following treatment with DCD_WT peptide if compared to NT cells. On the contrary, in respect to NT cells, a significant augmentation in biofilm's growth was observed after the treatment of bacterial cells with DCD_MT peptide (reduction in biofilm (%): DCD_MT 120,4±19,37, p<0,05; NT 101,3 ±11,45) (Figure 49).

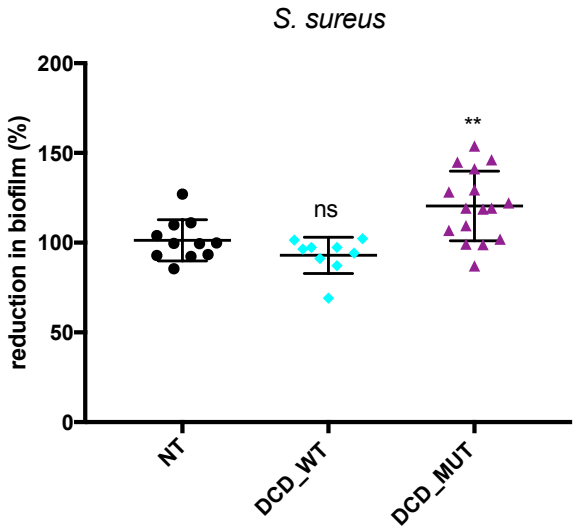

Figure 49. *In vitro* activity of DCD AMPs in biofilm eradication. *S. aureus* (1 x 10^7 CFU/mL) was plated in BHI medium containing 2% sucrose and plated on 96-multi-well plates for 24 hours to allow biofilm forrmation. Next, pre-formed biofilms were incubated with 2 µM of human DCD_WT or DCD_MT peptides for other 24 hours. The next day, cells were fixed in methanol, and stained with 0,1% crystal violet solution that was solubilised with 95 % ethanol. The absorbance reads were measured at 560 nm using the GloMax® Discover Microplate Reader (Promega). The low cut-off was represented by approximately 3 standard deviations above the absorbance mean of control wells (containing medium alone without bacteria).

Results are represented as three independent experiments with 12 technical replicates ± SD. Significant differences to control treatments were analysed by ordinary one-way analysis of variance (ANOVA) followed by Dunnett's multiple comparisons test (**P* < 0.05; ***P* < 0.01; ****P* < 0.001; *****P* < 0.0001).

While evaluating the eradication of pre-formed biofilm, both tested peptides seem not to reduce the biomass of biofilm formations; on the contrary, the mutated form seem to favour the maturation and proliferation of the biofilm. Staphyloccoccal biofilms often express the cationic polysaccharide intercellular adhesin (PIA), compound that mediates intercellular adhesion of adjacent cells and that is also considered as a virulence factor allowing bacterial immune evasion including resistance to antimicrobial peptides and killing by phagocytes (Cerca et al., 2007). PIA has been shown to protect *S. aureus* and *S. epidermidis* form the activity of DCD-1(L) under sweat-like conditions (Schittek, 2012). It is possible to speculate that DCD_WT peptide is not able to exert its function due to the composition of *S. aureus*'s biofilm that, being rich in PIA component, is able to partially evade the antimicrobial activity of the AMP. On the other hand, the augmentation in the levels of biomass formation following the treatment with DCD_MT, might reside in the activation of another resistance mechanism against anti-biofilm peptides. Indeed, the up-regulated production of cationic polysaccharides in the *Staphylococcus spp.* biofilms could prevent the binding of the cationic DCD_MT due to electrostatic repulsion (Hancock et al., 2021).

The results obtained from the various experimental procedures collectively indicate that the identified *DCD* frameshift insertion (rs538180888; g.54645236_54645237insT; NM_053283.4:c.225dup; NP_444513.1:p.Ala76Fs) is a damaging variant that completely disrupts the ORF of *DCD* and results in a 33 amino acid peptide having a completely altered sequence from position 15 to 33 if compared to the wild-type DCD-1(L) peptide. Indeed, in the mutated sequence it is possible to observe an overall increment in positively charged amino acids and a reduction in the negatively charged ones. As a consequence, the alteration of the sequence affects both the N-terminal and the C-terminal partitions of the AMP. In addition, changes in the peptidic sequence renders the protein's structure less stable, more rigid and less compact. Moreover, the mutated peptide is not able to exert a bactericidal effect against planktonic *S. aureus*, *S. epidermidis*, *S. lugdunensis,* it does not counteract the deposition and attachment of planktonic *S. aureus* cells during biofilm formation, and it seems to favour the maturation and proliferation of pre-formed biofilm in *S. aureus*. It is therefore presumable that the structural alterations in the mutated AMP don't allow the exploitation of its antimicrobial mechanisms of action.

Notably, DCD is continually secreted on the skin's surface where it represents a constitutive component of innate immune response aimed at limiting bacterial colonization rather than being involved in inflammation or during responses to injuries (Schittek, 2012). The presence of a non-functional AMP might partially explain the major susceptibility to infections in HSM58 and HSM64.

Nevertheless, being the frameshift variant carried in heterozygosis in D_HSM58, HSM64 and HSM58, experiments are currently being performed in order to quantify the levels of the wild-type and mutated peptide in the affected members of the Friulian family and compare them to healthy controls.

The characterisation of the effect of the identified variant in family members might lay the foundation for the development of personalized treatment options given for instance by the supplementation and activation of natural AMPs, specifically of DCD. In this context, the usage of elastin-derived biometric polypeptides modelled after elastin, could be exploited as an advanced drug delivery system that can promote a controlled delivery of substances of interest in the presence of elastolytic activity. This system is based on smart components that undergo structural and functional changes in response to specific environmental conditions, therefore inducing a specific and localised release of the bioactive domain of the compound previously ligated to the biopolymeric matrix. In the specific case of DCD, the active domain of the wild-type peptide could be embedded into the elastin-derived biometric polypeptide scaffold that might be designed in the form of topical patches; indeed, the contact of patches with the skin is expected to expose the

elastin-derived biometric polypeptides matrix ligated to the DCD bioactive moiety to the activity of proteolytic enzymes present in the sweat that trigger in turn the release of the peptide's active domain directly on the application site (Bandiera et al., 2018).

5. CONCLUSION

The overall purpose of this PhD dissertation was to augment the knowledge of the pathogenic mechanisms at the basis of the onset, progression and severity of HS and of syndromic variants of HS. In this context, the definition of the genetic background of patients, further implemented by functional studies, appeared as a promising strategy in order to ameliorate the diagnosis, the follow-up of patients and to identify specific personalised treatments.

Our study critically highlighted that one of the major issues associated to HS and to syndromic variants is the very limited understanding of the etiopathogenic events involved in these disorders, circumstance that undoubtedly leads to a series of severe consequences including: delayed diagnosis; complication in setting effective therapeutic interventions hence inevitably generating a sense of inadequacy of the physicians; discouragement in patients who suffer from chronic pain, depression, isolation and disfiguring scars which can cause a true disability.

Results also highlighted that the genetic aetiology of these complex disorders is highly heterogeneous, since these diseases can be caused by multiple mutations occurring in a defined set of genes or in multiple genes in various genetic loci. Indeed, disease-susceptibility genes can affect a subset of genetic loci that are collectively common in the analysed population; nevertheless, other variants are individually rare or private to certain families. In this critical context, family-based genetic and genomic studies constitutes a powerful tool for the detection of rare variants, enriched in families, that can provide the identification of several genes and cellular pathways potentially associated to the onset and progression of analysed disorders, additionally prompting the development of tailored and personalised treatments to be administered successfully to selected patients carrying specific mutations. Nevertheless, an important limitation of this approach is linked to the fact that the study is focused on a genetic variant that is private and therefore restricted only to certain families.

1. In the case of a PASH patient, we have identified a missense exonic variant (rs17604693; g.7565494 A>T; c.913A>T; p.Ile305Phe) in homozygosis in exon 7 of *DSP* gene, encoding for desmoplakin (DSP) defined as a crucial component of desmosomes. *In silico* assays confirmed that the SNV renders DSP dimers more compact and stable, while *ex vivo* and *in vitro* studies highlighted that the missense variation might potentially impair the recruitment of DSP on membrane-bound desmosomal structures hence favouring a cytoplasmic distribution, alter the general structure of desmosomes that appear as majorly stretched out and flexed, but seems not to

impact cellular proliferation and differentiation. Additionally, in the PASH case elevated levels of TEWL were registered when compared to healthy controls. Collectively these results possibly indicate that the identified *DSP* SNV is potentially associated to a disruption in skin barrier function rather than being linked to keratinisation or proliferation defects.

2. In the case of the Sardinian family affected by HS, we have identified a rare (MAF<0.01) private mutation in heterozygosis (rs767801219; g. 43322952T>A; NM_014345:exon4:c.A2120T; p.K707I) in exon 4 of *ZNF318* gene in 17 family members comprising all of the 11 individuals who initially declared to be affected by HS and in additional 6 family members that haven't mentioned to possess any sign of the disease. The fact that the variant was also detected in individuals who declared not be affected by HS does not deny the possible causality of the identified SNV in the family; indeed, the trait presents an autosomal dominant inheritance pattern with incomplete penetrance; some adult mutated family members might have deliberately confirmed not to possess the disease because of the sense of shame and discomfort that commonly lead patients to reject HS; in some cases a failure to report the disease is possibly associated to misdiagnosis; some family members have only just passed puberty, suggesting that they haven't manifested HS yet. Even if predicting the effects of the identified SNV is extremely hard since the variant is rare, few references are available, it has never been previously correlated to any disease and it is not currently possible to predict its impact on protein structure, due to the fact that ZNF318 has never been crystallised, we have proposed a possible causative role of the SNV in HS phenotype. It is possible that the variant might impair the co-repressor activity of ZNF318 that causes in turn an AR-mediated enhanced, continuous and deregulated response to circulating androgens. This event might stand at the basis of alterations occurring in sebaceous glands and sebogenesis, progression of the hair cycle, wound healing, skin barrier function and to an abnormal inflammatory responses driven by an AR-dependent up-regulation of TNF-α. Collectively, obtained results further corroborated the crucial impact of hormonal influence in the pathogenesis of HS and allowed to speculate that affected family members, especially females, might benefit from the administration of anti-androgenic hormonal therapies.

3. In the case of a Friulian family affected by HS, we have identified a rare (MAF<0.01) frameshift insertion (rs538180888; g.54645236_54645237insT; NM_053283.4:c.225dup; NP_444513.1:p.Ala76Fs) occurring on exon 4 of *DCD* gene in affected family members. This gene encodes for dermcidin (DCD), an AMP known to exert well defined antimicrobial activities against both Gram-positive and Gram-negative bacteria, as well as against *Candida albicans*. *In silico*

studies revealed that the identified variant renders the mutated peptide more rigid, less stable and less compact in structure, and confers to the AMP an overall positive net charge. We have hypothesised that the resulting structural and charge changes detected in the mutated peptide might directly impact its antimicrobial activity due the loss of the amphiphilic nature of DCD, condition seen to be crucial for the antimicrobial mechanism of action of the AMP. Our hypothesis was confirmed by the fact that mutated DCD is not able to exert a bactericidal effect neither on planktonic *S. aureus*, *S. epidermidis* and *S. lugdunensis*, nor is able to limit biofilm formation or to eradicate pre-formed biofilm by *S. aureus*. Bearing in mind that affected cases lamented the development of recurrent suppurating lesions predominantly in the inguinal and axillary regions, the frameshift variant in *DCD* might partially explain the major susceptibility to bacterial infections observed in cases. The characterisation of the effect of the identified variant in family members might lay the foundation for the development of personalized treatment options given for instance by the supplementation and activation of natural AMPs, specifically of DCD.

Even though in the analysed families, we did not identify alterations in overlapping pathways, our study highlights the crucial importance in performing family-based genetic and genomic studies, further implemented by functional studies, in unravelling potential novel genes and cellular routes involved in the pathogenesis of HS and PASH syndrome. We have confirmed that, while dealing with these disorders, the evaluation of potential disruptions in skin barrier function, hormonal imbalance, and an augmented susceptibility to bacterial infections constitute highly pathogenic mechanisms that need to be initially addressed and further envisaged. Moreover, the direct advantage deriving from the family-based studies lies in the possibility to propose and develop specific therapeutic interventions to be applied to patients carrying specific mutations (Figure 50).

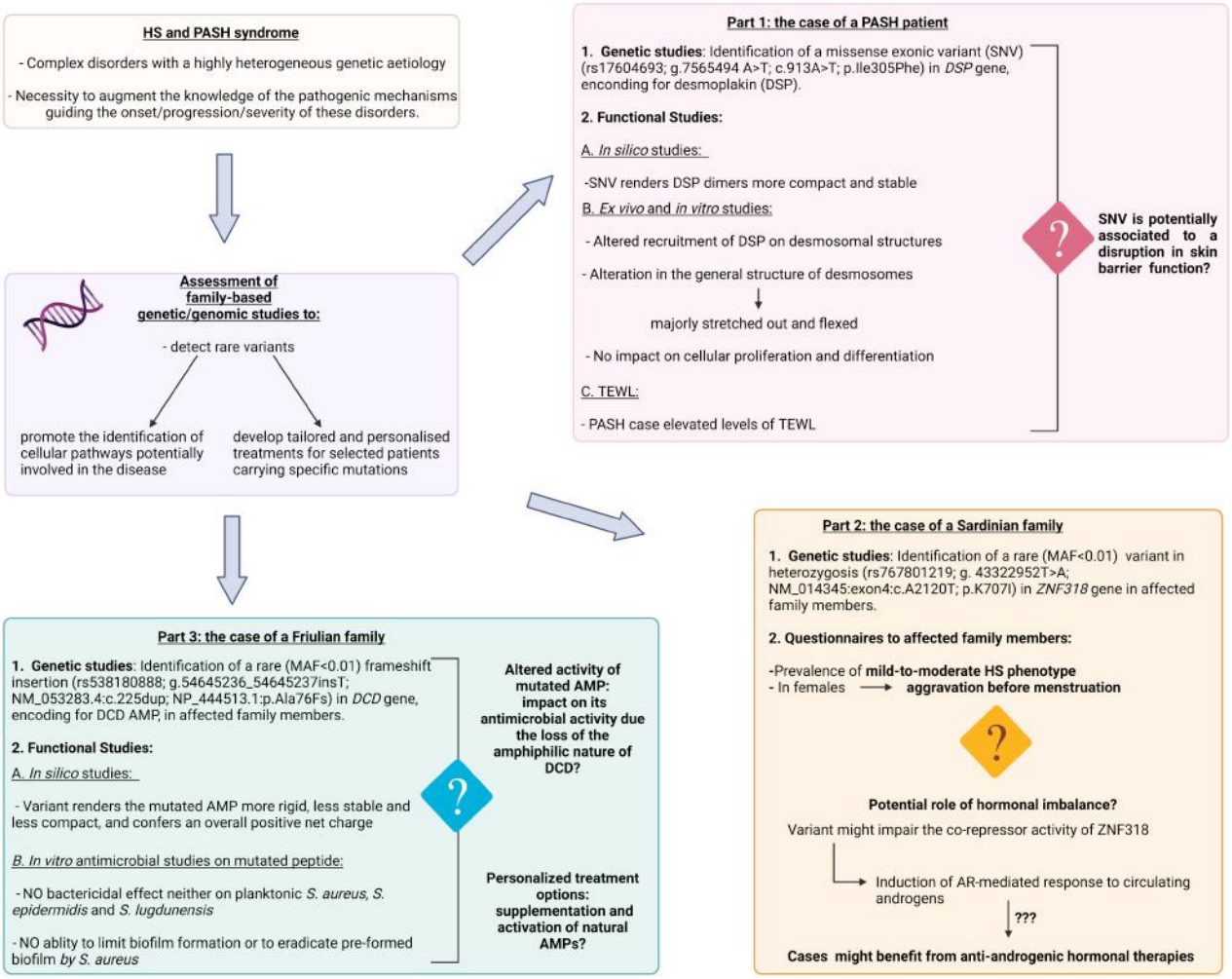

Figure 50. HS and PASH are complex disorders with a highly heterogeneous genetic aetiology. The development of family-based genetic and genomic studies, constitutes a valuable tool for the detection of rare variants, enriched in families, that can provide the identification of several genes and cellular pathways potentially associated to the onset and progression of analysed disorders, additionally prompting the development of tailored and personalised treatments to be administered successfully to selected patients carrying specific mutations. Obtained results critically highlight that while dealing with these complex disorders, the evaluation of potential disruptions in skin barrier function (PASH patient), hormonal imbalance (Sardinian family), and an augmented susceptibility to bacterial infections (Friulian family) constitute highly pathogenic mechanisms that need to be initially addressed and further envisaged.

6. BIBLIOGRAPHY

Abraham MJ, Murtola T, Schulz R, et al. GROMACS: high performance molecular simulations through multi-level parallelisms from laptops to supercomputers. Software X (2015). doi: https://doi.org/10.1016/j.softx.2015.06.001

Agut-Busquet E, Romaní de Gabriel J, Ribera Pibernat M, Gil Duran S, Lozano Molero M, Espinosa A, et al. Association of polymorphisms in the MyD88 gene and susceptibility to severe Hidradenitis suppurativa in a Caucasian population of 101 patients In: *7th European Hidradenitis Suppurativa Foundation (EHSF) Congress.* Rotterdam: John Wiley and Sons Ltd (2018), p. 5–32.

Al.Jassar C, Knowles T, Jeeves M et al. The nonlinear structure of the desmoplakin plakin domain and the effects of cardiomyopathy-linked mutations. *J Mol Biol* (2011) 411(5):1049-61.doi: 10.1016/j.jmb.2011.06.047

Albanesi C, Cavani A and Girolomoni G. IL-17 is produced by nickel-specific T lymphocytes and regulates ICAM-1 expression and chemokine production in human keratinocytes: synergistic or antagonist effects with IFN-gamma and TNF-alpha. *J Immunol* (1999) 162(1):494-502.

Ashcroft GS, Jeong MJ, Ashworth JJ, Hardman M, et al. Tumor necrosis factor-alpha (TNF-α) is a therapeutic target for impaired cutaneous wound healing**.** Wound Repair Regen (2012), 20(1):38-49. doi: 10.1111/j.1524-475X.2011.00748.x.

Ashcroft G and Mills S. Androgen receptor-mediated inhibition of cutaneous wound healing. *J Clin Invest* (2002), 110(5):615-24. doi: 10.1172/JCI15704.

Bandiera A, Passamonti S,Dolci LS and Focarete ML. Composite of elastin-BasedMatrix and Electrospun Poly(L-Lactic Acid) Fibers: a potential smart drug delivery system. *Front Bioeng Biotechnol* (2018). doi: 10.2289/fbioe.2018.00127.

Barth JH and Kealey T. Androgen metabolism by isolated human axillary apocrine glands in hidradenitis suppurativa. Br J Dermatol (1991) 125(4):304-8. doi: 10.1111/j.1365-2133.1991.tb14162.x.

Baylis F and McLeod MM. First-in-human Phase 1 CRISPR Gene Editing Cancer Trials: Are We Ready? *Curr Gene Ther* (2017), 17(4):309-319. doi: 10.2174/1566523217666171121165935.

Benhadou F, van der Zeer HH, Pascual JC, Rigopoulos D, Katoulis A, Liakou AI et al. Pilonidal sinus disease: an intergluteal localization of hidradenitis suppurativa/acne inversa: a cross-sectional study among 2465 patients. *Br J Dermatol* (2019) 181(6):1198-1206. doi: 10.1111/bjd.17927.

Berardesca E, Loden M, Serup J et al. The revised EEMCO guidance for the in vivo measurement of water in the skin**.** *Skin Res Technol* (2018) 24(3):351-358. doi: 10.1111/srt.12599.

Bikle DD. Vitamin D metabolism and function in the skin. *Mol Cell Endocrinol* (2011) 347(1-2):80-9. doi: 10.1016/j.mce.2011.05.017.

Blanpain C, Lowry WE, Pasolli HA, Fuchs E. Canonical notch signaling functions as a commitment switch in the epidermal lineage. *Genes Dev.* (2006), *20*, 3022–3035. doi: 10.1101/gad.1477606.

Blanpain C, Lowry WE, Goeghegan A, Polak L and Fuchs E. Self-renewal, multipotency, and the existence of two cell populations within an epithelial stem cell niche. *Cell* (2004), 118(5):635-48. doi: 10.1016/j.cell.2004.08.012.

Boehncke WH, Katsambas A, ortonne JP and Puig L. EADV preceptorship: advances in dermatology. *J Eur Acad Dermatol Venereol* (2010), 24 Suppl 5:2-24. doi: 10.1111/j.1468-3083.2010.03787.x.

Braun-Falco M, Kovnerystyy O, Lohse P, Ruzicka T. Pyoderma gangrenosum, acne, and suppurative hidradenitis (PASH)--a new autoinflammatory syndrome distinct from PAPA syndrome. *J Am Acad Dermatol* (2012) 66(3):409-15. doi: 10.1016/j.jaad.2010.12.025.

Bray SJ. Notch signalling in context. *Nat. Rev. Mol. Cell Biol*. (2016) *17*, 722–735. doi: 10.1038/nrm.2016.94.

Bruzzese V. Pyoderma gangrenosum, acne conglobata, suppurative hidradenitis, and axial spondyloarthritis: efficacy of anti-tumor necrosis factor α therapy. *J Clin Rheumatol* (2012) 18(8):413-5. doi: 10.1097/RHU.0b013e318278b84c.

Buonomo M, Mansh MD, Thorpe D, Goldfarb N. Development or exacerbation of hidradenitis suppurativa in two transgender men after initiation of testosterone therapy. *Br J Dermatol* (2021). doi: 10.1111/bjd.19812. Online ahead of print.

Burian M and Schittek B. The secrets of dermcidin action**.** *Int J Med Microbiol*. 305(2):283-6. doi: 10.1016/j.ijmm.2014.12.012.

Carroll CM and Li YM. Physiological and pathological roles of the γ-secretase complex. *Brain Res Bull* (2016) 126(Pt 2):199-206. doi:10.1016/j.brainresbull.2016.04.019.

Cerca N, Jefferson KK, Maira-Litràn T, et al. Molecular basis for preferential protective efficacy of antibodies directed to the poorly acetylated form of staphylococcal poly-N-acetyl-beta-(1-6)-glucosamine. Infect Immun (2007), 75(7):3406-13. Doi: 10.1128/IAI.00078-07.

Ceruti JM, Leirós GJ and Balañá ME. Androgens and androgen receptor action in skin and hair follicles. *Mol Cell Endocrinol* (2018), 465:122-133. doi: 10.1016/j.mce.2017.09.009.

Charpentier E, Lavker RM, Acquista E and Cowin P. Plakoglobin suppresses epithelial proliferation and hair growth in vivo**.** *J Cell Biol* (2000),149(2):503-20. doi: 10.1083/jcb.149.2.503.

Chen J, Den Z and Koch PJ. Loss of desmocollin 3 in mice leads to epidermal blistering**.** J Cell Sci (2008), 121(Pt 17):2844-9. doi: 10.1242/jcs.031518.

Chidgey M, Brakebusch C, Gustafsson E, et al. Mice lacking desmocollin 1 show epidermal fragility accompanied by barrier defects and abnormal differentiation. *J Cell Biol* (2001), 155(5):821-32. doi: 10.1083/jcb.200105009.

Chitaev NA and Troyanovsky SM. Direct Ca^{2+}-dependent Heterophilic Interaction between Desmosomal Cadherins, Desmoglein and Desmocollin, Contributes to Cell–Cell Adhesion. *J Cell Biol.* (1997) 138(1): 193–201. doi: 10.1083/jcb.138.1.193.

Clayton RW, Langan EA, Ansell DM, de VosIJHM et al. Neuroendocrinology and neurobiology of sebaceous glands. Biol Reviews (2020). doi: https://doi.org/10.1111/brv.12579.

Coates M, Mariottoni P, Corcoran DL et al. The skin transcriptome in hidradenitis suppurativa uncovers an antimicrobial and sweat gland gene signature which has distinct overlap with wounded skin**.** *PLoS One* (2019) 14(5):e0216249. doi: 10.1371/journal.pone.0216249.

Coi HJ and Weis WI. Purification and Structural Analysis of Desmoplakin. *Methods Enzymol* (2016) 569:197-213. doi: 10.1016/bs.mie.2015.05.006.

Cui S, Guerriero CJ, Szalinski CM, Kinlough CL, Hughey R and Weisz OA. OCRL1 function in renal epithelial membrane traffic. *Am J Physiol Renal Physiol.* (2010), 298(2):F335-45. doi: 10.1152/ajprenal.00453.2009.

Cugno M, Borghi A and Marzano AV. PAPA, PASH and PAPASH Syndromes: Pathophysiology, Presentation and Treatment**.** *Am J Clin Dermatol* (2017) 18(4):555-562. doi: 10.1007/s40257-017-0265-1.

Czech MP. PIP2 and PIP3: complex roles at the cell surface. *Cell* (2000), 100(6):603-6. doi: 10.1016/s0092-8674(00)80696-0.

Damen MSMA, Popa CD, Netea MG, Dinarello CA, Jooste LAB. Interleukin-32 in chronic inflammatory conditions is associated with a higher risk of cardiovascular diseases. Atherosclerosis (2017) 264:83-91. doi: 10.1016/j.atherosclerosis.2017.07.005.

Danby FW, Jemec GBE, Marsch WC, von Laffert M. Preliminary findings suggest hidradenitis suppurativa may be due to defective follicular support. *Br J Dermatol* (2013) 168(5):1034-9. doi: 10.1111/bjd.12233.

Davey RA and Grossmann M. Androgen Receptor Structure, Function and Biology: From Bench to Bedside. *Clin Biochem Rev*. (2016) 37(1): 3–15. PMID: 27057074.

Dekoninck S and Blanpain C. Stem cell dynamics, migration and plasticity during wound healing. *Nat Cell Biol* (2019), **21,** 18–24. doi: https://doi.org/10.1038/s41556-018-0237-6.

De Strooper, B. *et al.* A presenilin-1-dependent γ-secretase-like protease mediates release of notch intracellular domain. *Nature* (1999). doi:10.1038/19083.

Deckers IE, van der Zee HH, Prens EP. Epidemiology of Hidradenitis Suppurativa: Prevalence, Pathogenesis, and Factors Associated with the Development of HS. *Curr Derm Rep* (2014) 54–60. doi:10.1007/s13671-013-0064-8.

Del Rosso JQ, Kircik LH, Stein Gold L, Thiboutot D. Androgens, Androgen Receptors, and the Skin: From the Laboratory to the Clinic With Emphasis on Clinical and Therapeutic Implications. *J Drugs Dermatol* (2020) 19(3):30-35. doi: 10.1111/j.1365-2249.2006.03261.x.

Delva E, Tucker DK, Kowalczyk AP. The desmosome. *Cold Spring Harb Perspect Biol* (2009), 1(2):a002543. doi: 10.1101/cshperspect.a002543.

Dos Santos JB, Figueiredo AR, Ferraz MH, Gomes da Silva, Silveira de Medeiros VL. Cutaneous tuberculosis: epidemiologic, etiopathogenic and clinical aspects - part I. *An Bras Dermatol* (2014) 89(2):219-28. doi:10.1590/abd1806-4841.20142334.

Dubash AD and Green KJ. Desmosomes. *Curr Biol.* (2011) 21(14):R529-31. doi: 10.1016/j.cub.2011.04.035.

Duchatelet S,Miskinyte S, Join-Lambert O et al. First nicastrin mutation in PASH (pyoderma gangrenosum, acne and suppurative hidradenitis) syndrome**.** *Br J Dermatol* (2015) 173(2):610-2. doi: 10.1111/bjd.13668.

Ead JK, Snyder RJ, Wise J, Cuffy C, Jafary H and Fischborn K. Is PASH Syndrome a Biofilm Disease?: A Case Series and Review of the Literature. *Wounds* (2018), 30(8):216-223.

Eckmann L and Karin M. NOD2 and Crohn's disease: loss or gain of function? *Immunity* (2005) 22(6):661-7. doi: 10.1016/j.immuni.2005.06.004.

Edlich RF, Winters KL, Britt LD, Long 3rd WB. Bacterial diseases of the skin. *J Long Term Eff Med Implants* (2005) 15(5):499-510. doi:10.1615/jlongtermeffmedimplants.v15.i5.40.

Elkin K, Daveluy S, Avanaki KM. Hidradenitis suppurativa: Current understanding, diagnostic and surgical challenges, and developments in ultrasound application. *Skin Res Technol.* (2020) 26(1):11-19. doi:https://doi.org/10.1111/srt.12759.

Ellulu M, Patimah I, Khaza'ai H, rahmat A, Abed Y. Obesity and inflammation: the linking mechanism and the complications. Arch Med Sci (2017) 13(4):851-863. doi: 10.5114/aoms.2016.58928.

Ferrero-Milani L, Nielsen OH, Andersen PS, Girardin SE. Chronic inflammation: importance of NOD2 and NALP3 in interleukin-1beta generation**.** Clin Exp Immunol (2007) 147(2):227-35.

Finlay AY and Khan GK. Dermatology Life Quality Index (DLQI)--a simple practical measure for routine clinical use. *Clin Exp Dermatol* (1994) 19(3):210-6. doi: 10.1111/j.1365-2230.1994.tb01167.x.

Fitzsimmons JS, Fitzsimmons EM and Gilbert G. Familial hidradenitis suppurativa: evidence in favour of single gene transmission. *J. Med. Genet.* (1984). doi:10.1136/jmg.21.4.281

Frew JW and Navrazhina K. Into the (gluteal) fold: pilonidal disease and hidradenitis suppurativa - association or continuum? *Br J Dermatol*. (2019) 181(6):1121. doi: 10.1111/bjd.18300.

Frew JW, Hawkes JE, Krueger JG. Topical, systemic and biologic therapies in hidradenitis suppurativa: pathogenic insights by examining therapeutic mechanisms. *Ther Adv Chronic Dis.* (2019) 10:204062231983064. doi:10.1177/2040622319830646.

Frew JW, Vekic DA,Woods J, Cains GD. A systematic review and critical evaluation of reported pathogenic sequence variants in hidradenitis suppurativa. *Br J Dermatol* (2017) 177(4):987-998. doi: 10.1111/bjd.15441.

Fritsch M. Orfanos CE and Zouboulis CC. Sebocytes are the key regulators of androgen homeostasis in human skin. J Invest Dermatol (2001), 116(5):793-800. doi: 10.1046/j.1523-1747.2001.01312.x.

Fuchs, E. Skin stem cells: Rising to the surface. *J Cell Biol.* (2008) *180*, 273–284. doi: 10.1083/jcb.111.6.2807.

Garcovich S, Genovese G, Moltrasio C, Malvaso D, Marzano AV. PASH, PAPASH, PsAPASH, and PASS: The autoinflammatory syndromes of hidradenitis suppurativa. Clinics in Dermatology (2020). https://doi.org/10.1016/j.clindermatol.2020.10.016.

Garg A, Neuren E and Strunk A. Hidradenitis Suppurativa Is Associated with Polycystic Ovary Syndrome: A Population-Based Analysis in the United States. *Journal of Investigative Dermatology* (2018) 138(6):1288-1292. doi: 10.1016/j.jid.2018.01.009.

Garg A, Kirby JS, Lavian J, Lin G and Strunk A. Sex- and Age-Adjusted Population Analysis of Prevalence Estimates for Hidradenitis Suppurativa in the United States. *JAMA Dermatol* (2017), 153(8):760-764. doi: 10.1001/jamadermatol.2017.0201.

Garrod D and Chidgey M. Desmosome structure, composition and function**.** *Biochim Biophys Acta* (2008) 1778(3):572-87. doi: 10.1016/j.bbamem.2007.07.014.

Garrod DR. The assay that defines desmosome hyper-adhesion**.** *J Invest Dermatol* (2013) 133(2):576-7.doi: 10.1038/jid.2012.275.

George R, Clarke S and Thiboutot D. Hormonal therapy for acne. *Semin Cutan Med Surg* (2008), 27(3):188-96. doi: 10.1016/j.sder.2008.06.002.

Georgel P, Crozat K, Lauth X, Makrantonaki E, Seltmann H, et al. A toll-like receptor 2-responsive lipid effector pathway protects mammals against skin infections with gram-positive bacteria. *Infect Immun* (2005), 73(8):4512-21. doi: 10.1128/IAI.73.8.4512-4521.2005.

Giamarellos-Bourboulis E, Platzer M, Karagiannidis I, et al. High Copy Numbers of β-Defensin Cluster on 8p23.1, Confer Genetic Susceptibility, and Modulate the Physical Course of Hidradenitis Suppurativa/Acne Inversa. *J Invest Dermatol*. (2016), 136(8):1592-1598. doi: 10.1016/j.jid.2016.04.021.

Giatrakos S, Huse K, Kanni T, Tzanetakou V, et al. Haplotypes of IL-12Rβ1 impact on the clinical phenotype of hidradenitis suppurativa. *Cytokine* (2013), 62(2):297-301. doi: 10.1016/j.cyto.2013.03.008.

Gilaberte Y, Prieto-Torres L, Pastushenko I, Juarranz Á. Anatomy and Function of the Skin. In *Nanoscience in Dermatology* (2016) pp. 1–14. ISBN 978-0-12-802926-8. doi: https://doi.org/10.1016/B978-0-12-802926-8.00001-X.

Gilliver S, Ruckshanthi J, Atkinson S., et al. Androgens influence expression of matrix proteins and proteolytic factors during cutaneous wound healing. *Lab Invest* (2007) 87, 871–881. doi: https://doi.org/10.1038/labinvest.3700627.

Godsel LM, Sherry NH, Amargo EV et al. Desmoplakin assembly dynamics in four dimensions: multiple phases differentially regulated by intermediate filaments and actin**.** *J Cell Biol* (2005) 171(6):1045-59. doi: 10.1083/jcb.200510038.

Gottlieb J, Mandragne M, Garair C, Sbidian E et al. PAPASH, PsAPASH and PASS autoinflammatory syndromes: phenotypic heterogeneity, common biological signature and response to immunosuppressive regimens**.** Br J Dermatol (2019) 181(4):866-869. doi: 10.1111/bjd.18003.

Gratton R, Tricarico PM, Moltrasio M, Lima Estevao de Oliveira AS, Brandao L, Marzano AV et al. Pleiotropic role of Notch signaling in human skin diseases. *Int J Mol Sci* (2020) 21(12):4214.doi: 10.3390/ijms21124214.

Green KJ. The relationship between intermediate filaments and microfilaments before and during the formation of desmosomes and adherens-type junctions in mouse epidermal keratinocytes. J Cell Biol. (1987) 104(5): 1389–1402. doi: 10.1083/jcb.104.5.1389.

Grymowicz M, Rudnicka E, Podfigurna A, et al. Hormonal effects on hair follicles. *Int J Mol Sci*. (2020). doi: 10.3390/ijms21155342.

Gudjonsson JE, Tsoi LC, Ma F, Billi AC, et al. Contribution of plasma cells and B cells to hidradenitis suppurativa pathogenesis. *JCI Insight.* (2020), 5(19):e139930. doi: 10.1172/jci.insight.139930.

Guet-Rivellet H, Jais JP, Ungeheuer NM et al. The Microbiological Landscape of Anaerobic Infections in Hidradenitis Suppurativa: A Prospective Metagenomic Study. *Clin Infect Dis* (2017) 65(2):282-291. doi: 10.1093/cid/cix285.

Haapasalo A and Kovacs DM. The many substrates of presenilin/γ-secretase. *J Alzheimers Dis* (2011), 25(1):3-28. doi: 10.3233/JAD-2011-101065.

Hampe J, Grebe J, Nikolaus S, Solberg C et al. Association of NOD2 (CARD 15) genotype with clinical course of Crohn's disease: a cohort study. *Lancet* (2002) 359(9318):1661-5. doi: 10.1016/S0140-6736(02)08590-2.

Hancock REW, Alford MA and Haney EF. Antibiofilm activity of host defence peptides: complexity provides opportunities. *Nat Rev Microbiol* (2021). doi:https://doi.org/10.1038/s41579-021-00585-w.

Hana A, Booken D, Henrich C, Gratchev A et al. Functional significance of non-neuronal acetylcholine in skin epithelia. *Life Sci* (2007) 80(24-25):2214-20. doi: 10.1016/j.lfs.2007.02.007.

Heenen M, Thiriar S, Noël C, Galand P. Ki-67 immunostaining of normal human epidermis: comparison with 3H-thymidine labelling and PCNA immunostaining**.** *Dermatology* (1998) 197(2):123-6. doi: 10.1159/000017982.

Heilborn JD, Nilsson MF, Kratz G et al. The cathelicidin anti-microbial peptide LL-37 is involved in re-epithelialization of human skin wounds and is lacking in chronic ulcer epithelium**.** *J Invest Dermatol* (2003) 120(3):379-89. doi: 10.1046/j.1523-1747.2003.12069.x.

Hess B, Kutzner C, van der Spoel D and Lindahl E. GROMACS 4: algorithms for Highly Efficient, Load-Balanced, and Scalable Molecular Simulation. *Chem Theory Comput.* (2008). doi.org/10.1021/ct700301q.

Hessam S, Sand M, Georgas D, Anders A and Bechara FG. Microbial Profile and Antimicrobial Susceptibility of Bacteria Found in Inflammatory Hidradenitis Suppurativa Lesions. *Skin Pharmacol Physiol* (2016), 29:161-167. doi: doi.org/10.1159/000446812.

Heymann MC and Rosen-Wolff A. Contribution of the inflammasomes to autoinflammatory diseases and recent mouse models as research tools. *Clin Immunol* (2013) 147(3):175-84. doi: 10.1016/j.clim.2013.01.006.

Higgins R, Pink A, Hunger R, Yawalkar N and Navarini AA. Generalized Comedones, Acne, and Hidradenitis Suppurativa in a Patient with an *FGFR2* Missense Mutation. *Front. Med.* (2017). doi: https://doi.org/10.3389/fmed.2017.00016.

Hino H, Kobavasi T, Asboe-Hansen G. Size of desmosomes and hemidesmosomes in normal human epidermis**.** *Acta Derm Venereol* (1981) 61(4):279-84.

Hirohiko A, Zouboulis CC and Constantin OE. Control of Human Sebocyte Proliferation In Vitro by Testosterone and 5-Alpha-Dihydrotestosterone Is Dependent on the Localization of the Sebaceous Glands. *The Journal of Investgative Dermatology* (1992). doi: https://doi.org/10.1111/1523-1747.ep12616181.

Holthöfer B, Windhoffer R, Troyanovsky S and Leube RE. Structure and function of desmosomes. *Int Rev of Cytol* (2007). doi: https://doi.org/10.1016/S0074-7696(07)64003-0.

Hunger RE, Surovy Am, Hassan AS, Braathen LR, Yawalkar N. Toll-like receptor 2 is highly expressed in lesions of acne inversa and colocalizes with C-type lectin receptor. Br J Dermatol (2008) 158(4):691-7. doi: 10.1111/j.1365-2133.2007.08425.x.

Ingram JR, Woo PK, Chua SL, Ormerod AD, Desai N, Kai AC et al. Interventions for hidradenitis suppurativa. *Cochrane Database Syst Rev* (2015) 2015(10):CD010081. doi: 10.1002/14651858.CD010081.pub2.

Ingram JR. The genetics of Hidradenitis Suppurativa. *Dermatol Clin* (2016) 34(1):23-8. doi: 10.1016/j.det.2015.07.002.

Ingram RA and Piguet V. Phenotypic heterogeneity in hidradenitis suppurativa (acne inversa): classification is an essential step toward personalized therapy. *J Invest Dermatol* (2013), 133(6):1453-6. doi: 10.1038/jid.2012.476.

Inoue T, Miki Y, Kakuo S, Hachiya A, et al. Expression of steroidogenic enzymes in human sebaceous glands. *J Endocrinol* (2014), 222(3):301-12. doi: 10.1530/JOE-14-0323. Epub 2014 Jun 17.

Imperato-McGinley J, Gautier T, Cai LQ, Yee B, Epstein J and Pochi P. The androgen control of sebum production. Studies of subjects with dihydrotestosterone deficiency and complete androgen insensitivity. *The Journal of Clinical Endocrinology and Metabolisms* (1993). doi: 10.1210/jcem.76.2.8381804.

Ishizuka M, Kawate H, TakayanagiR, Ohshima H, Tao RH, Hagiwara H. A zinc finger protein TZF is a novel corepressor of androgen receptor**.** *Biochem Biophys Res Commun* (2005) 331(4):1025-31. doi: 10.1016/j.bbrc.2005.04.024.

Jafari SMS, Hunger RE and Schlapbach C. Hidradenitis Suppurativa: Current Understanding of Pathogenic Mechanisms and Suggestion for Treatment Algorithm. *Front Med (Lausanne)* (2020), 7:68. doi: 10.3389/fmed.2020.00068.eCollection 2020.

Jahns AC, Kallasli H, Nosek D, et al. Microbiology of hidradenitis suppurativa (acne inversa): a histological study of 27 patients. *APM* (2014). Doi: https://doi.org/10.1111/apm.12220.

Jahoda CAB and Reynolds AJ. Hair follicle dermal sheath cells: unsung participants in wound healing. *The Lancet* (2001). doi:https://doi.org/10.1016/ S0140-6736(01)06532-1.

James GA, Swogger E, Wolcott R, deLancey E, et al. Biofilms in chronic wounds. *Wound Repair Regen* (2008), 16(1):37-44. doi: 10.1111/j.1524-475X.2007.00321.x.

Jemec GB.The symptomatology of hidradenitis suppurativa in women. *Br J Dermatol* (1988)119(3):345-50. doi: 10.1111/j.1365-2133.1988.tb03227.x.

Jiang F and Doudna JA. CRISPR-Cas9 Structures and Mechanisms. *Annu Rev Biophys* (2017), 46:505-529. doi: 10.1146/annurev-biophys-062215-010822.

Jin M, Chen YL, He X, Hou Y, Chan Z and Zeng R. Amelioration of Androgenetic Alopecia by Algal Oligosaccharides Prepared by Deep-Sea Bacterium Biodegradation. *Front Microbiol*. (2020). doi: https://doi.org/10.3389/fmicb.2020.567060

Jinek M, Chylinski K, Fonfara I, Hauer M, Doudna JA and Charpentier E. A Programmable Dual-RNA–Guided DNA Endonuclease in Adaptive Bacterial Immunity. *Science* (2012). doi: 10.1126/science.1225829.

Jonkman MF, Psmooji AMG, Pasmans SGMA van den Berg MP, et al. Loss of desmoplakin tail causes lethal acantholytic epidermolysis bullosa. Cell Press (2005). doi: 10.1086/496901.

Joshi RS. The inner root sheath and the men associated with it eponymically. *Int J Trichology* (2011), 3(1):57-62. doi: 10.4103/0974-7753.82119.

Kalkhoff RK. Metabolic effects of progesterone. *American Journal of Obstetrics and Gynecology* (1982). doi:10.1016/s0002-9378(16)32480-2.

Kalliolias G and Ivashkiv L. TNF biology, pathogenic mechanisms and emerging therapeutic strategies. *Nat Rev Rheumatol* (2016), 12, 49–62. doi: https://doi.org/10.1038/nrrheum.2015.169

Kamp S, Fiehn AM, Stenderup K, Rasada C et al. Hidradenitis suppurativa: a disease of the absent sebaceous gland? Sebaceous gland number and volume are significantly reduced in uninvolved hair follicles from patients with hidradenitis suppurativa. *Br J Dermatol* (2011),164(5):1017-22. doi: 10.1111/j.1365-2133.2011.10224.x.

Kao JS, Mao-Quang M, Crumrine D, et al. Testosterone Perturbs Epidermal Permeability Barrier Homeostasis. *Journal of Investigative Dermatology* (2001). doi: 10.1046/j.1523-1747.2001.01281.x.

Kathju S, Lasko LA, Stoodley P. Considering hidradenitis suppurativa as a bacterial biofilm. *FEMS Immunol Med Microbiol* (2012) 65:385–389. https://doi.org/10.1111/j.1574-695X.2012.00946.x.

Kimball AB, Kerdel F, Adams, D, Mrowietz U, Gelfand JM et al. Adalinumab for the treatment of moderate to severe hidradenitis suppurativa. *Ann Intern Med.* (2012) 157:846-W306. doi: 10.7326/0003-4819-157-12-201212180-00004.

Konig A, Lehmann C and Happle R. Cigarette smoking as a triggering factor of Hidradenitis suppurativa. *Dermatology* (1999) 198(3):261-4.doi: 10.1159/000018126.

Kosukcu C, Taskiran EZ, Batu ED, et al. Whole exome sequencing in unclassified autoinflammatory diseases: more monogenic diseases in the pipeline? *Rheumatology (Oxford)* (2021), 60(2):607-616. doi: 10.1093/rheumatology/keaa165.

Kottke MD, Delva E and Kowalczyk AP. The desmosome: cell science lessons from human diseases. *Journal of Cell Science* (2006) 119: 797-806; doi: 10.1242/jcs.02888.

Kuipers BJH and Gruppen H. Prediction of Molar Extinction Coefficients of Proteins and Peptides Using UV Absorption of the Constituent Amino Acids at 214 nm To Enable Quantitative Reverse Phase High-Performance Liquid Chromatography−Mass Spectrometry Analysis. *J. Agric. Food Chem.* (2007). doi: 10.1021/jf070337l.

Kummer JA, Broekhuizen R, Everett H Agostini L et al. Inflammasome components NALP 1 and 3 show distinct but separate expression profiles in human tissues suggesting a site-specific role in the inflammatory response. *J Histochem Cytochem* (2007) 55(5):443-52. doi: 10.1369/jhc.6A7101.2006.

Kurinna S, Schäfer M, Ostano P *et al.* A novel Nrf2-miR-29-desmocollin-2 axis regulates desmosome function in keratinocytes. *Nat Commun* (2014) 5, 5099 doi: https://doi.org/10.1038/ncomms609.

Kurzen H, Moll I, Schafer S, et al. Compositionally different desmosomes in the various compartments of the human hair follicle. *Differentiation* (1998), 63(5):295-304. doi: 10.1046/j.1432-0436.1998.6350295.x.

Lai JJ, Lai KP, Chuang KH, Chang P Yu, IC, Lin WJ, Chang C. Monocyte/macrophage androgen receptor suppresses cutaneous wound healing in mice by enhancing local TNF-alpha expression. J *Clin Invest* (2009) 119(12):3739-51. doi: 10.1172/JCI39335.

Lai JJ, Chang P, Lai KP, Chen L and Chang C.T he role of androgen and androgen receptor in skin-related disorders. *Arch Dermatol Res* (2012), 304(7):499-510. doi: 10.1007/s00403-012-1265-x.

Lazic T, Li Q, Frank M, Uitto J, Zhou LH. Extending the phenotypic spectrum of keratitis-ichthyosis-deafness syndrome: report of a patient with GJB2 (G12R) Connexin 26 mutation and unusual clinical findings. *Pediatr Dermatol.* (2012), 29(3):349-57. doi: 10.1111/j.1525-1470.2011.01425.x.

Lechler T and Fuchs E. Desmoplakin: an unexpected regulator of microtubule organization in the epidermis. *J Cell Biol* (2007) 176(2): 147–154. doi: 10.1083/jcb.200609109.

Leuenberger M, Berner J, Di Lucca J, Fischer et al. PASS Syndrome: An IL-1-Driven Autoinflammatory Disease**.** *Dermatology* (2016) 232(2):254-8. doi: 10.1159/000443648.

Leveque JL, Corcuff P, de Rigal J, Agache P. In vivo studies of the evolution of physical properties of the human skin with age**.** *Int J Dermatol* (1984) 23(5):322-9. doi: 10.1111/j.1365-4362.1984.tb04061.x.

Li A, Peng Y, Taiclet LM, Tanzi RE. *Analysis of hidradenitis suppurativa–linked mutations in four genes and the effects of PSEN1-P242LfsX11 on cytokine and chemokine expression in macrophages*). Hum Mol Genet (2019) 28(7):1173-1182. doi: 10.1093/hmg/ddy414.

Li H, Yang Y, Hong W, et al. Applications of genome editing technology in the targeted therapy of human diseases: mechanisms, advances and prospects. *Sig Transduct Target Ther* (2020), 5, 1. doi: https://doi.org/10.1038/s41392-019-0089-y.

Li Y, Leung ELH, Pan H, Yao X, et al. Identification of potential genetic causal variants for rheumatoid arthritis by whole-exome sequencing. *Oncotarget* (2017), 2017 Nov 22;8(67):111119-111129. doi: 10.18632/oncotarget.22630

Lieber MR, Gu J, Lu H, Shimazaki N and Tsai AG. Nonhomologous DNA end joining (NHEJ) and chromosomal translocations in humans. Subcell Biochem (2010), 50:279-96. doi: 10.1007/978-90-481-3471-7_14.

Lindhardt Saunte DM and Jemec GBE. Hidradenitis Suppurativa: Advances in Diagnosis and Treatment. *JAMA* (2017) 318(20):2019-2032. doi: 10.1001/jama.2017.16691.

Liu M, Davis JW, Idler KB, Mostafa NM, Okun MM and Waring JF. Genetic analysis of NCSTN for potential association with hidradenitis suppurativa in familial and nonfamilial patients.

Br J Dermatol. (2016),175(2):414-6. doi: 10.1111/bjd.14482.

Lolli F, Pallotti F, Rossi A, Fortuna MC, et al. Androgenetic alopecia: a review. *Endocrine* (2017), 57(1):9-17. doi: 10.1007/s12020-017-1280-y.

Lowe MM, naik HB, Clancy S, Pauli M, et al. Immunopathogenesis of hidradenitis suppurativa and response to anti-TNF-α therapy. *JCI Insight*. (2020), 5(19):e139932. doi: 10.1172/jci.insight.139932.

Lucke T, Choudhry R, Thom R, Selmer IS, Burden AD and Hodgins MB. Upregulation of connexin 26 is a feature of keratinocyte differentiation in hyperproliferative epidermis, vaginal epithelium, and buccal epithelium. *J Invest Dermatol.* (1999), 112(3):354-61. doi: 10.1046/j.1523-1747.1999.00512.x.

Luo R, Chong W, Wei Q, et al. Whole-exome sequencing identifies somatic mutations and intratumor heterogeneity in inflammatory breast cancer. *npj Breast Cancer* (2021). doi: https://doi.org/10.1038/s41523-021-00278-w.

Maestrini E, Korge BP, Ocaña-Sierra J, Calzolari E et al. A Missense Mutation in Connexin26, D66H, Causes Mutilating Keratoderma with Sensorineural Deafness (Vohwinkel's Syndrome) in Three Unrelated Families. *Human Molecular Genetics (1999),* 1237–1243. doi: 10.1093/hmg/8.7.1237.

Makrantonaki E and Zouboulis CC. Testosterone metabolism to 5alpha-dihydrotestosterone and synthesis of sebaceous lipids is regulated by the peroxisome proliferator-activated receptor ligand linoleic acid in human sebocytes. *Br J Dermatol* (2007), 156(3):428-32. doi: 10.1111/j.1365-2133.2006.07671.x.

Marraffini LA. CRISPR-Cas immunity in prokaryotes. *Nature* (2015), 526, 55–61. doi: https://doi.org/10.1038/nature15386.

Marzano AV, Ceccherini I, Gattorno M, Fanoni D et al. Association of pyoderma gangrenosum, acne, and suppurative hidradenitis (PASH) shares genetic and cytokine profiles with other autoinflammatory diseases. Medicine (Baltimore) (2014) 3(27):e187.doi: 10.1097/MD.0000000000000187.

Marzano AV, Trevisan C, Gattorno M, Ceccherini I, De Simone C, Crosti C. Pyogenic arthritis, pyoderma gangrenosum, acne, and hidradenitis suppurativa (PAPASH): a new autoinflammatory syndrome associated with a novel mutation of the PSTPIP1 gene**.** JAMA Dermatol (2013) 149(6):762-4. doi: 10.1001/jamadermatol.2013.2907.

Marzuillo P, Piccolo V, Mascolo M, Apicella A, Argenziano G, Della Vecchia N, Guarino S and Miraglia Del Giudice E. Patients affected by dent disease 2 could be predisposed to hidradenitis suppurativa. *Eur Acad Dermatol Venereol* (2018), 32(8):e309-e311. doi: 10.1111/jdv.14860.

Mc Aleer MA, Pohler E, Smith FJ, Wilson NJ et al. Severe dermatitis, multiple allergies, and metabolic wasting syndrome caused by a novel mutation in the N-terminal plakin domain of desmoplakin. *J Allergy Clin Immunol* (2015) 136(5):1268-76. doi: 10.1016/j.jaci.2015.05.002.

McMullan R, Lax S, Robertson H et al. Keratinocyte differentiation is regulated by the Rho and ROCK signaling pathway. *Curr Biol* (2003) 13(24):2185-9. doi: 10.1016/j.cub.2003.11.050.

Meier A and Söding J. Automatic Prediction of Protein 3D Structures by Probabilistic Multi-template Homology Modeling. *Plos Computational Biology* (2015). doi:https://doi.org/10.1371/journal.pcbi.1004343.

Melnik BC. Role of FGFR2-signaling in the pathogenesis of acne. *Dermatoendocrinol*. (2009), 1(3):141-56. doi: 10.4161/derm.1.3.8474.

Melnik BC and Zouboulis CC. Potential role of FoxO1 and mTORC1 in the pathogenesis of Western diet-induced acne. *Experimental Dermatology* (2013). doi:10.1111/exd.12142.

Merk HF. Barrier skin. *Krutmann J and Merk HF (eds) Environment and Skin*. (2018) Springer Cham. doi: htrps://doi.org/10.1007/978-3-319-43102-4_1.

Montero-Vilchez T, Segura-Fernández-Nogueras MV, Pérez-Rodríguez I, Soler-Gongora M, Martinez-Lopez A, et al. Skin Barrier Function in Psoriasis and Atopic Dermatitis: Transepidermal Water Loss and Temperature as Useful Tools to Assess Disease Severity. *J.Clin.Med.* (2021), *10*(2), 359. doi: https://doi.org/10.3390/jcm10020359.

Montgomery JR, White TW, Martin BL Turner ML and Holland SM. A novel connexin 26 gene mutation associated with features of the keratitis-ichthyosis-deafness syndrome and the follicular occlusion triad. *J Am Acad Dermatol*. (2004), 51(3):377-82. doi: 10.1016/j.jaad.2003.12.042.

Morgan BE. The dermal papilla: an instructive niche for epithelial stem and progenitor cells in development and regeneration of the hair follicle. *Cold Spring harb Perspect Med*. (2014), 4(7): a015180. doi: 10.1101/cshperspect.a015180.

Mortimer PS, Dawber RP, Gales MA, Moore RA. Mediation of hidradenitis suppurativa by androgens. Br Med J (Clin Res Ed) (1986) 292(6515):245-8. doi: 10.1136/bmj.292.6515.245.

Mojumdar EH, Pham QD, Topgaard D *et al.* Skin hydration: interplay between molecular dynamics, structure and water uptake in the stratum corneum. *Sci Rep* (2017). doi: https://doi.org/10.1038/s41598-017-15921-5.

Naik HB, Nassif A, Ramesh MS, Schultz G et al.Are Bacteria Infectious Pathogens in Hidradenitis Suppurativa? Debate at the Symposium for Hidradenitis Suppurativa Advances Meeting, November 2017. *J Invest Dermatol* (2018) 139(1):13-16. doi: 10.1016/j.jid.2018.09.036.

Napolitano M, Megna M, Timoshchuck EA, Patruno C, Balato N, Fabbrocini G, Monfrecola G. Hidradenitis suppurativa: from pathogenesis to diagnosis and treatment. *Clin Cosmet Investig Dermatol. (2017) 10:105-115.* doi:10.2147/CCID.S111019.

Negroni A, Pierdomenico M, Cucchiara S, Strontai L. NOD2 and inflammation: current insights. *J Inflamm Res* (2018**)** 11:49-60. doi: 10.2147/JIR.S137606.

Nguyen VS, Tan KW, Ramesh K. *et al.* Structural basis for the bacterial membrane insertion of dermcidin peptide, DCD-1L. *Sci Rep* (2017) 7, 13923. doi: https://doi.org/10.1038/s41598-017-13600-z.

Nikolakis G, Join-Lambert O, Karagiannidis I et al. Bacteriology of hidradenitis suppurativa/acne inversa: A review. *J Am Acad Dermatol* (2015) 73(5 Suppl 1):S12-8. doi: 10.1016/j.jaad.2015.07.041.

Nomura T. Hidradenitis Suppurativa as a Potential Subtype of Autoinflammatory Keratinization Disease. *Front Immunol* (2020), 11:847. doi: 10.3389/fimmu.2020.00847.eCollection 2020.

Norgett E, Hatsell SJ, Carvajal-Huerta L, Ruiz Cabezas JC, et al. Recessive mutation in desmoplakin disrupts desmoplakin–intermediate filament interactions and causes dilated cardiomyopathy, woolly hair and keratoderma. *Human Molecular Genetics* (2000). doi: https://doi.org/10.1093/hmg/9.18.2761.

Nussenzweig P and Maraffini LA. Molecular Mechanisms of CRISPR-Cas Immunity in Bacteria. Annu Rev Genet (2020), 54:93-120. doi: 10.1146/annurev-genet-022120-112523.

Orenstein LAV, Kguyen TV, Damiani G, Sayed C, Jemec GBE, Hamzavi. Medical and Surgical Management of Hidradenitis Suppurativa: A Review of International Treatment Guidelines and Implementation in General Dermatology Practice. *Dermatology* (2020) 236(5):393-412. doi: 10.1159/000507323.

Oostenbrink C, Villa A, Mark AE and Van Gunsteren WF. A biomolecular force field based on the free enthalpy of hydration and solvation: The GROMOS force-field parameter sets 53A5 and 53A6. *Journal of Computational Chemistry* (2004). doi.org/10.1002/jcc.20090.

Ousterout D, Kabadi A, Thakore P, et al. Multiplex CRISPR/Cas9-based genome editing for correction of dystrophin mutations that cause Duchenne muscular dystrophy. *Nat Commun* (2015),6, 6244 (2015). doi:https://doi.org/10.1038/ncomms7244.

Paller AS, Czarnowicki T, Renert-Yuval Y, Holland K et al. The spectrum of manifestations in desmoplakin gene (DSP) spectrin repeat 6 domain mutations: Immunophenotyping and response to ustekinumab**.** *J Am Acad Dermatol* (2018) 78(3):498-505.e2. doi: 10.1016/j.jaad.2017.10.026.

Pan Y, Lin MH, Tian X, Cheng HT, Gridley T, Shen J, Kopan R.gamma-secretase functions through Notch signaling to maintain skin appendages but is not required for their patterning or initial morphogenesis. *Dev Cell* (2004) 7(5):731-43. doi: 10.1016/j.devcel.2004.09.014.

Park SC, Lee MY, Kim JY, et al. Anti-Biofilm Effects of Synthetic Antimicrobial Peptides Against Drug-Resistant *Pseudomonas aeruginosa* and *Staphylococcus aureus* Planktonic Cells and Biofilm. *Molecules* (2019), 24(24):4560. doi: 10.3390/molecules24244560.

Pickar-Oliver A and Gersbach CA. The next generation of CRISPR–Cas technologies and applications. *Nat Rev Mol Cell Biol* (2019), 20, 490–507. doi: https://doi.org/10.1038/s41580-019-0131-5.

Pink A, Anzengruber F, Navarini AA. Acne and hidradenitis suppurativa.*Br J Dermatol.* (2018) 178(3):619-631. doi: 10.1111/bjd.16231.

Pink AE, Simpson MA, Desai N, Dafou D et al. Mutations in the γ-secretase genes NCSTN, PSENEN, and PSEN1 underlie rare forms of hidradenitis suppurativa (acne inversa). *J Invest Dermatol* (2012), 132(10):2459-2461. doi: 10.1038/jid.2012.162.

Prabhakara R, Harro JM, Leid JG, Harris M and Shirtliff ME. Murine immune response to a chronic Staphylococcus aureus biofilm infection. *Infect Immun* (2011), 79(4):1789-96. doi: 10.1128/IAI.01386-10.

Qingyang L, Fang H, Dang E and Wang G. The role of ceramides in skin homeostasis and inflammatory skin diseases. *J Derm Sci* (2019). doi:https://doi.org/10.1016/jdermsci.2019.12.002).

Rabionet R, Gasparini P, Estevill X. Molecular genetics of hearing impairment due to mutations in gap junction genes encoding beta connexins. Human Mutation (2000). doi: 10.1002/1098-1004(200009)16:3<190::AID-HUMU2>3.0.CO;2-I.

Radek KA, Elias PM, Taupenot L, Mahata KS, O'Connor DT, Gallo RL. Neuroendocrine nicotinic receptor activation increases susceptibility to bacterial infections by suppressing antimicrobial peptide production. *Cell Host Microbe* (2010) 7(4):277-89. doi: 10.1016/j.chom.2010.03.009.

Rangarajan A, Talora C, Okuyama R, Nicolas M, Mammucari C, et al. Notch signaling is a direct determinant of keratinocyte growth arrest and entry into differentiation. *EMBO J*. (2001) *20*, 3427–3436. doi: 10.1093/emboj/20.13.3427.

Rawla P, Thandra KC, Limaiem F. Lymphogranuloma venereum. StatPearlsPublishing (2020) doi: https://www.ncbi.nlm.nih.gov/books/NBK537362/

Richard G. Connexins: a connection with the skin. *Experimental Dermatology* (2001). doi:https://doi.org/10.1034/j.1600-0625.2000.009002077.x).

Ring HC, Theut Riis P, Zarchi K, et al. Prodromal symptoms in hidradenitis suppurativa. *Clin Exp Dermatol* (2017) 42(3):261-265. doi: 10.1111/ced.13025.

Ring HC, Mikkelsen PR, Miller IM, Jenssen H, et al. The bacteriology of hidradenitis suppurativa: a systematic review. *Experimental Dermatology* (2015). doi: 10.1111/exd.12793.

Riordan SM, Heruth DP, Zhang LQ, et al. Application of CRISPR/Cas9 for biomedical discoveries. *Cell Biosci* (2015), 5, 33. doi: https://doi.org/10.1186/s13578-015-0027-9.

Riss PT, Ring HC Themstrup L, Jemec GB. The Role of Androgens and Estrogens in Hidradenitis Suppurativa - A Systematic Review. *Acta Dermatovenerol Croat* (2016) 24(4):239-249.

Rogiers V and EEMCO Group. EEMCO guidance for the assessment of transepidermal water loss in cosmetic sciences. Skin Pharmacol Appl Skin Physiol (2001) 14(2):117-28. doi: 10.1159/000056341.

Rumbaugh KP and Sauer K. Biofilm dispersion. *Nat Rev Microbiol*. (2020),18, 571–586. doi:https://doi.org/10.1038/s41579-020-0385-0.

Sabat, R., Jemec, G.B.E., Matusiak, Kimball AB, Prens E, Wolk K. Hidradenitis suppurativa. *Nat Rev Dis Primers* (2020) 12;6(1):18. https://doi.org/10.1038/s41572-020-0149-1.

Saito M, Tucker DK, Kohlhorst D, Niessen CM, Kowalczyk AP. Classical and desmosomal cadherins at a glance. *J Cell Sci.* (2012) 125(11): 2547–2552. doi: 10.1242/jcs.066654.

Sakuma T, Nishikawa A, Kume S, et al. Multiplex genome engineering in human cells using all-in-one CRISPR/Cas9 vector system. *Sci Rep* (2014),4, 5400 (2014). doi:https://doi.org/10.1038/srep05400

Sanghvi-Shah R and Weber GF. Intermediate Filaments at the Junction of Mechanotransduction, Migration, and Development. *Front Cell Dev Biol* (2017) 5:81. doi: 10.3389/fcell.2017.00081.

Saraceno R, Babino G, Chiricozzi A, Zangrilli A, Chimenti S. PsAPASH: a new syndrome associated with hidradenitis suppurativa with response to tumor necrosis factor inhibition**.** *J Am Acad Dermatol* (2015). 72(1):e42-4.doi: 10.1016/j.jaad.2014.10.002.

Sartorius K, Lapins J, Emtestam L, Jemec GBE. Suggestions for uniform outcome variables when reporting treatment effects in hidradenitis suppurativa. Br J Dermatol (2003) 149(1):211-3. doi: 10.1046/j.1365-2133.2003.05390.x.

Saunte DM, Boer J, Stratigos A, Szepietowski JC, Hamzavi I, Kim KH et al. Diagnostic delay in hidradenitis suppurativa is a global problem. *Br J Dermatol* (2015) 173(6):1546-9. doi:10.1111/bjd.14038.

Savva A, Kanni T, Damoraki G, Kotsaki A, et al. Impact of Toll-like receptor-4 and tumour necrosis factor gene polymorphisms in patients with hidradenitis suppurativa. *Br J Dermatol* (2013), Feb;168(2):311-7. doi: 10.1111/bjd.12105.

Schittek B, Hipfel R, Sauer B *et al.* Dermcidin: a novel human antibiotic peptide secreted by sweat glands. *Nat Immunol* (2001) 2, 1133–1137. doi: https://doi.org/10.1038/ni732.

Schittek B. The multiple facets of dermcidin in cell survival and host defense**.** *J Innate Immun* (2012) 4(4):349-60. doi: 10.1159/000336844.

Schleusener J, Salazar A, von Hagen J, Lademann J and Darvin ME. Retaining Skin Barrier Function Properties of the Stratum Corneum with Components of the Natural Moisturizing Factor—A Randomized, Placebo-Controlled Double-Blind In Vivo Study. *Molecules* (2021) *26*(6), 1649. doi: https://doi.org/10.3390/molecules26061649.

Schnitzler F, Friedrich M, Wolf C, Angelberger M et al. The NOD2 p.Leu1007fsX1008 mutation (rs2066847) is a stronger predictor of the clinical course of Crohn's disease than the FOXO3A intron variant rs12212067**.** *PLoS One.* (2014) 9(11):e108503. doi: 10.1371/journal.pone.0108503.

Scholzen T and Gerdes J. The Ki-67 protein: from the known and the unknown**.** *J Cell Physiol* (2000) 182(3):311-22. doi: 10.1002/(SICI)1097-4652(200003)182:3<311::AID-JCP1>3.0.CO;2-9.

Schroder K, Hertzgog PJ, Ravasi T, Hume DAInterferon-gamma: an overview of signals, mechanisms and functions. J leukoc Biol (2004) 75(2):163-89. doi: 10.1189/jlb.0603252.

Scnappauf O, Chae JJ, Kastner DL, Aksentijevich I. The Pyrin Inflammasome in Health and Disease**.** *Front Immunol* (2019) 10:1745. doi: 10.3389/fimmu.2019.01745.eCollection 2019.

Seyed Jafari MS, Hunger RE, Schlapbach C. Hidradenitis Suppurativa: Current Understanding of Pathogenic Mechanisms and Suggestion for Treatment Algorithm. *Front Med (Lausanne)* (2020) 4;7:68. doi:10.3389/fmed.2020.00068.

Seyed Jafari MS, Knüsel E, Cazzaniga S, Hunger RE. A Retrospective Cohort Study on Patients with Hidradenitis Suppurativa. *Dermatology* (2018) 234:71–78. doi: https://doi.org/10.1159/000488344.

Shanmugam VK, Meher Zaman N, McNish S, Hant FN. Review of Current Immunologic Therapies for Hidradenitis Suppurativa. *Int J Rheumatol* (2017)2017:8018192.doi: 10.1155/2017/8018192.

Shanmugan VK, Jone D, McNish S, Bendall ML and Crandall KA. Transcriptome patterns in hidradenitis suppurativa: support for the role of antimicrobial peptides and interferon pathways in disease pathogenesis. *Clinical and Experimental Dermatology* (2019). doi: 10.1111/ced.13959

Shi H, Cheer K, Simanainen U, Lesmana B, Ma D, et al. The contradictory role of androgens in cutaneous and major burn wound healing. *Burns & Trauma* (2021) https://doi.org/10.1093/burnst/tkaa046.

Shridas P and Tannock LR. Role of serum amyloid A in atherosclerosis. Curr Opin Lipidol (2019) 30(4):320-325.doi: 10.1097/MOL.0000000000000616.

Siebel C and Lendahl U. Notch Signaling in Development, Tissue Homeostasis, and Disease. *Physiol. Rev.* 2017 *97*, 1235–1294. doi: 10.1152/physrev.00005.2017.

Sklyarova T, Bonné S, D'Hooge P, et al. Plakophilin-3-deficient mice develop hair coat abnormalities and are prone to cutaneous inflammation. *J Invest Dermatol* (2008), 128(6):1375-85. doi: 10.1038/sj.jid.5701189.

Tao RH, Kawate H, Ohnaka K et al. Opposite effects of alternative TZF spliced variants on androgen receptor. *Biochem Biophys Res Commun* (2006a) 341(2):515-21. doi: 10.1016/j.bbrc.2005.12.213.

Tao RH, Kawate H, Wu Y, Ohnaka K, Ishizuka M et al. Testicular zinc finger protein recruits histone deacetylase 2 and suppresses the transactivation function and intranuclear foci formation of agonist-bound androgen receptor competitively with TIF2**.** *Mol Cell Endocrinol* (2006) 247(1-2):150-65. doi: 10.1016/j.mce.2005.12.052.

Taraborrelli S. Physiology, production and action of progesterone. *AOGS.* (2015). doi:10.1111/aogs.12771.

Tricarico PM, Boniotto M, Genovese G, Zouboulis CC, Marzano AV, crovella S. An Integrated Approach to Unravel Hidradenitis Suppurativa Etiopathogenesis. *Front Immunol* (2019) 10:892.doi: 10.3389/fimmu.2019.00892.

Tzanetakou V, Kanni T, Giatrakou S, Katoulis A, Papadavid E, Netea MG et al. Safety and Efficacy of Anakinra in Severe Hidradenitis SuppurativaA Randomized Clinical Trial**.** *JAMA Dermatol.* (2016) 152(1):52-59. doi:10.1001/jamadermatol.2015.3903.

Uddin F, Rudin CM and Sen T. CRISPR gene therapy: applications, limitations, and implications for the future. Front Oncol. (2020). doi: https://doi.org/10.3389/fonc.2020.01387.

Unluhizarci K, Karaca Z and Kelestimur F. Role of insulin and insulin resistance in androgen excess disorders. *World J Diabetes* (2021), 12(5):616-629. doi: 10.4239/wjd.v12.i5.616.

Valour F, Sénéchal A, Dupieux C, Karsenty J, Lustig S, Breton P et al. Actinomycosis: etiology, clinical features, diagnosis, treatment, and management**.** Infect Drug Resist (2014) 7:183-97. doi: 10.2147/IDR.S39601.

van der Zee HH, Horvath B, Jemec GBE, Prens EP. The Association between Hidradenitis Suppurativa and Crohn's Disease: in Search of the Missing Pathogenic Link. J Invest Dermatol (2016) 136(9):1747-1748. doi: https://doi.org/10.1016/j.jid.2016.05.102.

van der Zeer HH and Jemec GBE. New insights into the diagnosis of hidradenitis suppurativa: Clinical presentations and phenotypes. *J Am Acad Dermatol* (2015) 73(5 Suppl 1):S23-6. doi: 10.1016/j.jaad.2015.07.047.

van Smeden J and Bouwstra JA. Stratum Corneum Lipids: Their Role for the Skin Barrier Function in Healthy Subjects and Atopic Dermatitis Patients**.** *Curr Probl Dermatol* (2016) 49:8-26. doi: 10.1159/000441540.

Van Straalen KR, Prens EP, Willemsen G, Boomsma DI, van der Zee HH. Contribution of Genetics to the Susceptibility to Hidradenitis Suppurativa in a Large, Cross-sectional Dutch Twin Cohort. *JAMA Dermatol* (2020) 156(12):1359-1362. doi:10.1001/jamadermatol.2020.3630.

Veijouye SJ, Yari A, Heidari F, Sajedi N, Moghani FG and Nobakht. Bulge region as a putative hair follicle stem cells niche: a brief review. *Iran J Public Health* (2017),46(9):1167-1175.

Vasioukhin V, Bowers E, Bauer C. *et al.* Desmoplakin is essential in epidermal sheet formation.*Nat Cell Biol* (2001) 3**,** 1076–1085. doi: https://doi.org/10.1038/ncb1201-1076.

Vekic, D. A., Frew, J. & Cains, G. D. Hidradenitis suppurativa, a review of pathogenesis, associations and management. Part 1. *Australas J Dermatol.* (2018) 59, 267–277. doi: 10.1111/ajd.12770.

Vidal VPI, Chaboissier MC, Lützkendorf S et al. Sox9 is essential for outer root sheath differentiation and the formation of the hair stem cell compartment. *Curr Biol.* (2005), 15(15):1340-51.doi: 10.1016/j.cub.2005.06.064.

Vossen ARJV, van der Zee HH, Prens EP. Hidradenitis Suppurativa: A Systematic Review Integrating Inflammatory Pathways Into a Cohesive Pathogenic Model. *Front Immunol* (2018) 14;9:2965. https://doi.org/10.3389/fimmu.2018.02965.

Walsh J, Muruve D and Power C. Inflammasomes in the CNS. *Nat Rev Neurosci* (2014) 15, 84–97. doi:https://doi.org/10.1038/nrn3638.

Wan H, South AP, Hart IR. Increased keratinocyte proliferation initiated through downregulation of desmoplakin by RNA interference**.** *Exp Cell Res* (2007) 313(11):2336-44. doi: 10.1016/j.yexcr.2007.01.010.

Wang Y, Simanainen U, Cheer K, Suarez FG, et al. Androgen actions in mouse wound healing: Minimal in vivo effects of local antiandrogen delivery. *International Journal of Tissue Repair and Regeneration* (2016). doi: https://doi.org./10.1111/wrr.12420

Wang B, Liu XM, Liu ZN, Wang Y et al. Human hair follicle-derived mesenchymal stem cells: Isolation, expansion, and differentiation. *World J Stem Cells (2020),* 12(6):462-470. doi: 10.4252/wjsc.v12.i6.462.

Water PJ. Degradation of mutant proteins, underlying "loss of function" phenotypes, plays a major role in genetic disease. *Curr Issues Mol Biol* (2001) 3(3):57-65.

Watt FM, Estrach S and Ambler CA. Epidermal Notch signalling: differentiation, cancer and adhesion. *Curr Opin Cell Biol* (2008) 20(2):171-9. doi: 10.1016/j.ceb.2008.01.010.

Watt FM. Mammalian skin cell biology: At the interface between laboratory and clinic. *Science* (2014) 346(6212):937-40. doi: 10.1126/science.1253734.

Webb B and Sali A. Comparative protein structure modeling using MODELLER. *Current Protocols* (2014). doi: 10.1002/0471250953.bi0506s47

Wiedenheft B, Sternberg S and Doudna J. RNA-guided genetic silencing systems in bacteria and archaea. *Nature* (2012), 482, 331–338. doi:https://doi.org/10.1038/nature10886.

Wieczorek M and Waleka I. Hidradenitis suppurativa - known and unknown disease. *Reumatologia* (2018) 56(6):337-339.doi: 10.5114/reum.2018.80709.

Wikramanayake TC, Stojadinovic O and Tomic-Canic M. Epidermal Differentiation in Barrier Maintenance and Wound Healing. *Adv Wound Care* (New Rochelle) (2014) 3(3):272-280. doi: 10.1089/wound.2013.0503.

Wille JJ and Kydonieus A. Palmitoleic Acid Isomer (C16:1Δ6) in Human Skin Sebum Is Effective against Gram-Positive Bacteria. *Skin Pharmacol Physiol* (2003). doi:10.1159/000069757.

Wilson VG. Growth and differentiation of HaCaT keratinocytes**.** *Methods Mol Biol* (2014) 1195:33-41. doi: 10.1007/7651_2013_42.

Witte-Handel E,Wolk K, Tsaousi A, Irmer L et al. The IL-1 Pathway Is Hyperactive in Hidradenitis Suppurativa and Contributes to Skin Infiltration and Destruction. J Invest Dermatol (2019) 139(6):1294-1305. doi: 10.1016/j.jid.2018.11.018.

Wolk K, Warszawska K, Hoeflich C, Witte E et al. Deficiency of IL-22 contributes to a chronic inflammatory disease: pathogenetic mechanisms in acne inversa. *J Immunol* (2011) 186(2):1228-39. doi: 10.4049/jimmunol.0903907.

Won Oh WJ, Kloepper J, Langan EAA, Kim Y, Yeo J et al. Guide to Studying Human Hair Follicle Cycling In Vivo. *J Invest Dermatol* (2016), 136(1):34-44. doi: 10.1038/JID.2015.354.

Wu SS, Li QC, Yin CQ, Xue W and Song CQ. Advances in CRISPR/Cas-based Gene Therapy in Human Genetic Diseases. *Theranostics* (2020), 10(10):4374-4382. doi: 10.7150/thno.43360.eCollection 2020.

Xiao X, He Y, Li, C, Zhang X, Xu H and Wang B. Nicastrin mutations in familial acne inversa impact keratinocyte proliferation and differentiation through the Notch and phosphoinositide 3-kinase/AKT signalling pathways. *Br J Dermatol.* (2016), 174(3):522-32. doi: 10.1111/bjd.14223.

Xie L, Yang R, Liu S. et al. TR3 is preferentially expressed by bulge epithelial stem cells in human hair follicles. *Lab Invest* (2016)96, 81–88 (2016). doi:https://doi.org/10.1038/labinvest.2015.125

Yermakovich D, Sivitskaya L, Vaikhanaskaya T , et al. Novel desmoplakin mutations in familial Carvajal syndrome. *Acta Myol* (2018), 37(4):263-266.

Yousef H, Alhajj M, Sharma S. Anatomy, Skin (Integument), Epidermis. StatPearlsPublishing (2020) doi:https://www.ncbi.nlm.nih.gov/books/NBK470464/).

Yu JW, Fernandes-Alnemri T, Datta P, Wu J, Juliana C, Solorzano L et al. Pyrin activates the ASC pyroptosome in response to engagement by autoinflammatory PSTPIP1 mutants**.** *Mol Cell* (2007) 28(2):214-27. doi: 10.1016/j.molcel.2007.08.029 .

Yu KR, Natanson H and Dunbar CE. Gene Editing of Human Hematopoietic Stem and Progenitor Cells: Promise and Potential Hurdles. *Hum Gene Ther* (2016), 27(10):729-740. doi: 10.1089/hum.2016.107.

Zagaria O, Ruggiero A, Fabbrocini G, Gallo L, Romanelli M and Marasca C. Wound care, adalimumab, and multidisciplinary approach in a patient affected by PASH syndrome. *Int Wound J* (2020), 17(5):1528-1531. doi: 10.1111/iwj.13403.

Zafar K, Sedeek KE, Rao GS, Khan Z, et al. Genome Editing Technologies for Rice Improvement: Progress, Prospects, and Safety Concerns. *Front genome Ed.* (2020). doi: https://doi.org/10.3389/fgeed.2020.00005.

Zanger P, Holzer J, Schleucher R, Scherbaum H, Schittek B and Gabrysch S. Severity of Staphylococcus aureus infection of the skin is associated with inducibility of human beta-defensin 3 but not human beta-defensin 2. Infect Immun. (2010), 78(7):3112-7. doi: 10.1128/IAI.00078.

Zhang X, Li Y, Xu H, Zhang YW. The γ-secretase complex: from structure to function. *Front Cell Neurosci* (2014). 8:427. doi: 10.3389/fncel.2014.00427.

Zhang L and Skolnick J. What should the Z-score of native protein structure be) Protein Science (2008). doi: 10.1002/pro.5560070515.

Zouboulis CC. Sebaceous gland receptors. *Dermato-Endocrinology* (2009). doi: 10.4161/der.1.2.7804.

Zouboulis CC, Tzellos T, Kyrgidis A, Jemec GBE, Bechara FG et al. Development and validation of the International Hidradenitis Suppurativa Severity Score System (IHS4), a novel dynamic scoring system to assess HS severity. *Br J Dermatol* (2017) 177(5):1401-1409. doi: 10.1111/bjd.15748.

Zouboulis CC, Xia L, Akamatsu H, Seltmann H, et al. The Human Sebocyte Culture Model Provides New Insights into Development and Management of Seborrhoea and Acne. Dermatology (1998). doi:10.1159/000017861.